REPORT NO. FAA-RD-76-94

DEVELOPMENT OF PREDICTIVE WAKE VORTEX TRANSPORT MODEL FOR TERMINAL AREA WAKE VORTEX AVOIDANCE

M. R. Brashears
A. D. Zalay
L. C. Chou
K. R. Shrider

Lockheed Missles & Space Company, Inc.
Huntsville Research & Engineering Center
4800 Bradford Drive
Huntsville AL 35807

MAY 1976
FINAL REPORT

Prepared for

U.S. DEPARTMENT OF TRANSPORTATION
FEDERAL AVIATION ADMINISTRATION
Systems Research and Development Service
Washington DC 20590

NOTICE

This document is disseminated under the sponsorship of the Department of Transportation in the interest of information exchange. The United States Government assumes no liability for its contents or use thereof.

NOTICE

The United States Government does not endorse products or manufacturers. Trade or manufacturers' names appear herein solely because they are considered essential to the object of this report.

TECHNICAL REPORT STANDARD TITLE PAGE

1. Report No.	2. Government Accession No.	3. Recipient's Catalog No.
FAA-RD-76-94		

4. Title and Subtitle	5. Report Date
DEVELOPMENT OF PREDICTIVE WAKE VORTEX TRANSPORT MODEL FOR TERMINAL AREA WAKE VORTEX AVOIDANCE	May 1976
	6. Performing Organization Code

7. Author(s)	8. Performing Organization Report No.
M. R. Brashears, A. D. Zalay, L. C. Chou, and K. R. Shrider	LMSC-HREC TR D496597 DOT-TSC-FAA-76-15

9. Performing Organization Name and Address	10. Work Unit No.
Lockheed Missiles & Space Company, Inc.* Huntsville Research & Engineering Center 4800 Bradford Drive Huntsville AL 35807	FA605/R6122
	11. Contract or Grant No. DOT-TSC-988
	13. Type of Report and Period Covered Final Report February-October 1975
12. Sponsoring Agency Name and Address U.S. Department of Transportation Federal Aviation Administration Systems Research and Development Service Washington DC 20590	14. Sponsoring Agency Code FA-505

15. Supplementary Notes

*Under contract to: U.S. Department of Transportation
Transportation Systems Center
Kendall Square
Cambridge, MA 02142

16. Abstract

The wake vortex transport program has been expanded to include viscous effects and the influence of initial roll-up, atmospheric turbulence, and wind shear on the persistence and motion of wake vortices in terminal areas. Analysis of wake characteristics has shown that changes in the spanwise loading due to flaps increase the initial sink rate, decrease the separation, and initiates the circulation decay process earlier. Buoyancy due to jet exhaust entrainment and ambient stratification retards vortex spreading and increases descent. Atmospheric turbulence and shear promote a more rapid decay reducing the late-time descent and spread rates of vortices. Vortex tilting has been related to an interaction involving the wind shear, ground plane, and the vorticity detrainment process.

Recognition of the effects of tilting, spanwise loading, vorticity detrainment, burst/sink instabilities, and atmospheric conditions has resulted in an analytic wake transport and decay model with increased accuracy and improved predictive capabilities.

17. Key Words	18. Distribution Statement
Wind Shear Aircraft Wakes Wake Vortices Atmospheric Effects Trailing Vortex Transport	DOCUMENT IS AVAILABLE TO THE U.S. PUBLIC THROUGH THE NATIONAL TECHNICAL INFORMATION SERVICE, SPRINGFIELD, VIRGINIA 22161

19. Security Classif. (of this report)	20. Security Classif. (of this page)	21. No. of Pages	22. Price
Unclassified	Unclassified	232	

Form DOT F 1700.7 (8-69)

PREFACE

This document represents the final report of Contract DOT-TSC-988 and covers the period 11 February to 10 October 1975. The study was performed by personnel at the Lockheed Missiles & Space Company, Inc., Huntsville Research & Engineering Center, Huntsville, Alabama, under the direction of Dr. M. R. Brashears.

The authors are especially grateful to Dr. J. N. Hallock, TSC Contracting Officer's Technical Monitor, for his technical contributions and able assistance during the performance of this contract.

METRIC CONVERSION FACTORS

Approximate Conversions to Metric Measures

Symbol	When You Know	Multiply by	To Find	Symbol
		LENGTH		
in	inches	2.5	centimeters	cm
ft	feet	30	centimeters	cm
yd	yards	0.9	meters	m
mi	miles	1.6	kilometers	km
		AREA		
in^2	square inches	6.5	square centimeters	cm^2
ft^2	square feet	0.09	square meters	m^2
yd^2	square yards	0.8	square meters	m^2
mi^2	square miles	2.6	square kilometers	km^2
	acres	0.4	hectares	ha
		MASS (weight)		
oz	ounces	28	grams	g
lb	pounds	0.45	kilograms	kg
	short tons (2000 lb)	0.9	tonnes	t
		VOLUME		
tsp	teaspoons	5	milliliters	ml
Tbsp	tablespoons	15	milliliters	ml
fl oz	fluid ounces	30	milliliters	ml
c	cups	0.24	liters	l
pt	pints	0.47	liters	l
qt	quarts	0.95	liters	l
gal	gallons	3.8	liters	l
ft^3	cubic feet	0.03	cubic meters	m^3
yd^3	cubic yards	0.76	cubic meters	m^3
		TEMPERATURE (exact)		
°F	Fahrenheit temperature	5/9 (after subtracting 32)	Celsius temperature	°C

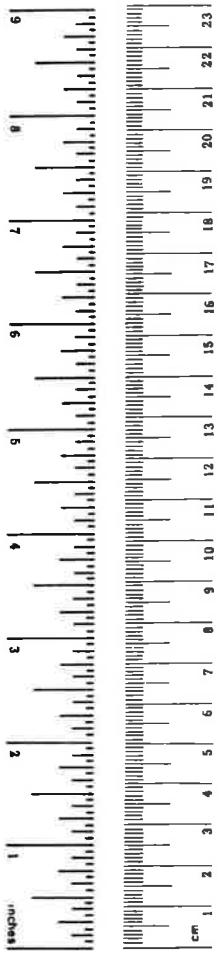

Approximate Conversions from Metric Measures

Symbol	When You Know	Multiply by	To Find	Symbol
		LENGTH		
mm	millimeters	0.04	inches	in
cm	centimeters	0.4	inches	in
m	meters	3.3	feet	ft
m	meters	1.1	yards	yd
km	kilometers	0.6	miles	mi
		AREA		
cm^2	square centimeters	0.16	square inches	in^2
m^2	square meters	1.2	square yards	yd^2
km^2	square kilometers	0.4	square miles	mi^2
ha	hectares (10,000 m^2)	2.5	acres	
		MASS (weight)		
g	grams	0.035	ounces	oz
kg	kilograms	2.2	pounds	lb
t	tonnes (1000 kg)	1.1	short tons	
		VOLUME		
ml	milliliters	0.03	fluid ounces	fl oz
l	liters	2.1	pints	pt
l	liters	1.06	quarts	qt
l	liters	0.26	gallons	gal
m^3	cubic meters	35	cubic feet	ft^3
m^3	cubic meters	1.3	cubic yards	yd^3
		TEMPERATURE (exact)		
°C	Celsius temperature	9/5 (then add 32)	Fahrenheit temperature	°F

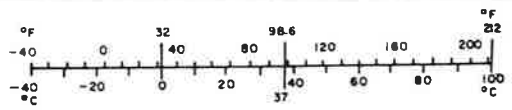

CONTENTS

LIST OF FIGURES

LIST OF TABLES

NOMENCLATURE

Symbol	Description
A, A_1, A_2	area of vortex cell within limiting streamline, ft^2
A_u, A_v, A_w	frictional velocity constant
AR	aspect ratio of wing
a	constant, 1.339
a_1	constant, Γ/ν_T
a_2	constant, $r(0)/\bar{c}$
b	aircraft wingspan, ft
b'	instantaneous separation of vortex pair, ft
C_L	lift coefficient
C_ℓ	sectional lift coefficient
C_P	specific heat at constant pressure, Btu/lb-^oR unless noted otherwise
C_t	temperature generated turbulent kinetic energy, cm^2/sec^3
C_u	shear generated, turbulent kinetic energy, cm^2/sec^3
c	wing chord, ft
$\bar{c}$	mean wing chord, ft
d	atmospheric boundary layer thickness, ft
e	eccentricity of vortex cell, $Pb'/2A$
g	gravitational acceleration, 32.17 ft/sec^2 unless noted otherwise

Symbol	Description
H	heat flux, cal/sec
h	height above ground plane, ft
h_I	turbulence height parameter, ft
h/ℓ'	Monin-Obukhov length scale
h_w	wind shear height parameter, ft
K	spanwise loading coefficient
K_1	wind shear parameter, 1/sec
k	turbulent mixing constant
L_1, L_2, L_3	constants, with units sec, sec/cm$^{2/3}$, and dimensionless, respectively
L_u, L_v, L_w	turbulence integral scale length
ℓ	mixing length, ft
P, P_1, P_2	vortex cell perimeter, ft
q	rms turbulence level, ft/sec
R, R_1, R_2	distance from origin, ft
Ri	Richardson number
Ri_{20}	Richardson number at 20 ft altitude above ground
r	vortex core radius, ft
T	temperature, $^{\circ}$R unless noted otherwise
T_1	wind shear parameter, $1/(0.4\ \partial\bar{u}/\partial h)$, sec
T_ℓ	time to linking, sec
t	time, sec
t^*	dimensionless vorticity detrainment period

Symbol	Description
U_∞	freestream velocity, ft/sec
u, v, w	velocity in x, y, z direction, ft/sec
$\bar{u}$	horizontal mean wind speed, ft/sec, unless noted otherwise
$\bar{u}_{20}$	horizontal mean wind speed at 20 ft altitude above ground, ft/sec
u^*	friction velocity, ft/sec, unless noted otherwise
u_o^*	friction velocity at ground level, ft/sec
u'_n	normal velocity fluctuation across vortex cell boundary, ft/sec
V_A	characteristic airspeed, $0.3264\,\bar{u}_{20}$, ft/sec
V_∞	vortex induced velocity, ft/sec
Y_1	wind profile function, $(u_*/h)\,\bar{u}_{20}$
y_1	interior end of vortex sheet, ft
Y_2	wind shear profile function, $f(h/\ell')$
y_2	outboard end of vortex sheet, ft
Y_3	wind shear profile function, $g(h/\ell')$
$\bar{y}_{12}$	center of vortex sheet, $(y_1 + y_2)/2$, ft
Z_o	roughness length, ft
Γ	circulation, ft^2/sec
Δ	difference
ϵ	ratio of vortex height to 1/2 separation distance

Symbol	Description
ϵ_1	dissipation of turbulent kinetic energy, cm^2/sec
η	variable, y/b
η_1	universal vortex lifetime function
κ	Von Karman constant, 0.4
λ	buoyancy parameter, $1-\rho/\rho_o$
ν	kinematic viscosity, ft^2/sec
ν_T	turbulent eddy viscosity, ft^2/sec
ξ	vorticity, 1/sec
ξ'	fluctuating vorticity, 1/sec
$\overline{\xi}$	mean vorticity, 1/sec
ρ	density within vortex cell, $slug/ft^3$
ρ_o	atmospheric density, $slug/ft^3$ unless noted otherwise
σ	dimensionless wind shear parameter
$\sigma_u, \sigma_v, \sigma_w$	standard deviation of turbulence, ft/sec
τ	shear stress, $gm/sec^2\text{-}cm$
τ_1	characteristic vortex instability time
Φ_u, Φ_v, Φ_w	turbulence power spectra
Φ_{uw}	turbulence cospectrum
ϕ	velocity potential
Ω	turbulent spatial frequency in the x direction, rad/ft

1. INTRODUCTION

Wake vortex encounters present a potential threat to aircraft operations. Statistics compiled by the National Transportation Safety Board and by the U. S. Air Force Inspection Safety Center show that in the past decade over 200 accidents have been attributed to wake vortex hazards (Refs. 1 and 2). Indications are that these and other possible vortex-related accidents could have been avoided and their effects lessened considerably had the pilots and flight control personnel known of the existence, location and intensity of hazardous wake vortex conditions. In order to establish safe aircraft operations with minimum queueing delays, a Wake Vortex Avoidance System (WVAS) is being developed by the Department of Transportation as part of a long range effort for providing terminal area wake avoidance along with minimum aircraft spacings.

An important aspect of the Wake Vortex Avoidance System is the capability for predicting the position of the wake vortex as a function of space and time. To determine whether or not a wake vortex hazard exists at a terminal area, the vortex transport and decay process must be understood in sufficient detail so that the motion and breakdown of the vortex can be predicted within the flight corridor. Under previous research programs, a Predictive Wake Vortex Transport Model has been developed by Lockheed-Huntsville to meet the needs of the DOT Wake Vortex Avoidance System (Refs. 3 through 9). The results of these programs have shown that the primary transport phenomena including the influence of wind, wind shear, ground plane, and buoyancy can be successfully incorporated into an analytic wake transport model. The wake transport model has been substantially verified by comparing the predicted tracks with the measured vortex tracks recorded during DOT flyby tests. However, the analysis has also identified a number of additional wake transport and decay effects such as wake tilting, vortex dissipation and detrainment

which can be important in defining wake vortex phenomena. Preliminary results indicated that these more complex wake transport and decay effects can have an important impact on the terminal area wake vortex hazard and should therefore be included in the Predictive Wake Vortex Transport Model. This provided the motivation for the present study.

The Predictive Wake Vortex Transport Model has been developed and refined at Lockheed-Huntsville over a period of four years. The development of the Predictive Model is summarized below:

- "Wake Vortex Avoidance System," FAA-RD-72-108, (LMSC-HREC D306226), December 1972.

A simple version of the Predictive Model was developed for use in a conceptual wake vortex avoidance system.

- "Analysis of Predicted Aircraft Wake Vortex Transport and Comparison with Experiment," FAA-RD-74-74. I and II, April 1974.

The sensitivity of the Predictive Model to potential errors in input parameters was evaluated. Theoretical ground wind signatures were compared with experimental results obtained during proof-of-concept tests at the National Aviation Facilities Experimental Center (NAFEC) in October and November 1972. Close agreement was shown between predicted and measured ground-wind vortex signatures. The resolution of the Predictive Model was further investigated by comparing theoretical vortex trajectories with NAFEC photographic observations.

- "Wake Vortex Transport Considerations and Meteorological Data Analysis," LMSC-HREC TR D390424, November 1974.

The Predictive Model was broadened to include buoyancy. The scope of the atmospheric characterization was enlarged to consider potential temperature, wind shear, Richardson number, eddy dissipation characteristics,

Pasquill class, and different wind profiles. Computer routines were developed to perform the necessary signal conditioning, statistical analysis, and probability density calculations to extract the relevant atmospheric parameters from the digitized output of on-site meteorological sensor arrays,

- "Analysis of Wake Vortex Measurements," LMSC-HREC TR D496558, September 1975.

The Predictive Wake Vortex Transport Model was updated so that detailed on-site meteorological measurements could be interpreted and utilized to predict more accurately the vortex transport and decay characteristics. Ground wind wake vortex signatures and wind profile measurements were processed and analyzed from the DOT/JFK wake vortex test program.

Under the present research program the Predictive Model was expanded to include viscous effects and the influence of initial roll-up, atmospheric turbulence, wind shear, and buoyancy on the motion of wake vortices in terminal areas. Specific objectives of this research effort included:

1. Broadening the Predictive Model to account for non-elliptical spanwise loading effects including multiple vortex wakes
2. Refinement of the buoyancy model developed earlier in Ref. 7 to account for ground plane, wind shear, and buoyancy due to jet engine exhaust entrainment
3. Incorporation of a vortex lifetime criteria into the Predictive Model
4. Incorporation of circulation decay mechanisms into the Predictive Model
5. Expansion of the meteorological characterization so that the relevant atmospheric parameters can be computed more accurately
6. Analysis of the effect of asymmetric vortex parameters on wake vortex transport.

The development of a more accurate Predictive Model was sought by incorporating the above capabilities into the original vortex transport theory.

The following report summarizes the results of the investigation. In Section 2 the theoretical basis for the expanded Predictive Wake Vortex Transport Model are developed including a review, critical assessment of modification (when necessary) of existing theoretical models regarding vortex formation, vortex motion, vortex lifetime, and meteorological effects. The basis for specific vortex transport mechanisms are described as developed for the current Predictive Model. Comparison of the updated theoretical model with observed wake vortex trajectories is presented in Section 3, including a discussion of the dominant trends and an assessment of improved predictive capabilities.

2. DEVELOPMENT OF PREDICTIVE VORTEX TRANSPORT MODEL

Efforts have been made to update the Predictive Wake Vortex Transport Model developed by Lockheed-Huntsville for DOT-TSC in order to include additional vortex transport and decay effects including the influence of spanwise loading, buoyancy, viscous decay and other meteorological parameters. A description of the updated predictive program is presented in the following sections including a discussion of the underlying physical phenomena and a derivation of the analytic model.

2.1 VORTEX FORMATION

Initial versions of the Predictive Model (Refs. 3 through 9) computed the initial wake vortex characteristics assuming an elliptically loaded airfoil. Analysis of the predicted and experimentally observed wake vortex trajectories indicated that the theoretical model consistently underestimated the initial vortex descent rate by approximately 10% (Ref. 9). It was conjectured that non-elliptical spanwise loading effects could account for this consistent source of error. Under the present research program, efforts have been made to include the influence of aircraft lift characteristics, including the effects of flaps, on the motion of wake vortices. The Donaldson-Betz rollup technique was investigated as a means of determining the location and strength of the multiple wake vortices. Evaluation of the multiple wake trajectories using the Donaldson-Betz rollup technique showed that the wake transport could be modeled more appropriately from momentum conservation arguments. In the following discussion the basic Donaldson-Betz rollup technique is reviewed, its capabilities and limitations are discussed, and a simplified rollup method is developed for the purposes of the Predictive Model.

Accurate representation of the wake vortex hazard in terminal area operations requires a fundamental knowledge of the initial wake vortex parameters including circulation, separation and core radius which must be determined from the aircraft characteristics. As a result of the nonuniform spanwise loading distribution, a finite aspect ratio wing generates a vortex sheet which rolls up into a vortex pair. The classical rollup process recognized first by Lanchester (Ref. 10) and quantified later by Prandtl and Betz (Refs. 11 and 12) is shown in Figs. 2-1. A number of different approaches have been followed for computing the actual rollup process including energy and momentum conservation arguments (Ref. 13), point vortex rollup schemes (Refs. 14 through 19) and Betz invariant procedures (Refs. 20 through 30). For the purposes of modeling wake vortex hazards, wake vortex simulations have been carried out at Lockheed-Huntsville involving many of the vortex rollup techniques cited above.

Experience has shown that simple expressions based on momentum conservation are useful for computing the initial wake vortex strength and spacing parameter for moderate aspect ratio aircraft in the clean configuration. However, the model cannot handle flap or near wake rollup effects.

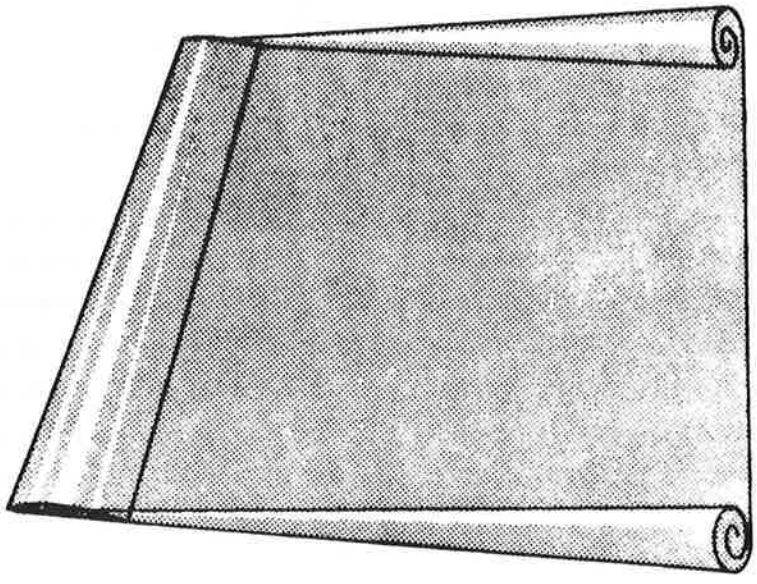

Fig. 2-1 - Vortex Sheet Behind a Finite Aspect Ratio Wing

Finite element deformed wake calculations utilizing available lifting surface programs have modeled both flap and near wake rollup effects but the results appear to be sensitive to both the step and the mesh size and consume considerable time. Betz rollup formulation developed by Donaldson et al. have also been used at Lockheed-Huntsville for computing wake vortex phenomena associated with aircraft in the terminal environment including flap effects.

Donaldson et al. (Refs. 28, 29 and 30) have shown that a wing can generate multiple vortices, as a result of the flaps carrying an appreciable portion of the load. By utilizing the "Betz invariants" Donaldson has developed a technique to calculate the strength and location of the various vortices shed from each side of the wing by assuming the vortices roll up independently of each other. To determine a technique for providing allowances in the predictive model for flap effects, the technique developed by Donaldson has been incorporated into the Predictive Model to examine the trajectory of multiple vortices and to compare it with earlier analysis of NAFEC test data (Refs. 4, 5, 6 and 9).

The rolled-up wake vortices behind a wing with arbitrary lift distribution have been calculated in accordance with Donaldson's recipe (see Ref. 30) where both "tip" and "interior" vortices are determined by their strengths and locations. Donaldson's assumption is that the nature of the initial roll-up is inviscid, thus, it is stipulated that the roll-up satisfied the three Betz invariants:

$$-\int_{y}^{b/2} \frac{d\Gamma(\eta)}{d\eta}\, d\eta = \int_{o}^{r} \frac{d\Gamma(\rho)}{d\rho}\, d\rho = \Gamma_o(y) \tag{2.1}$$

$$\int_{y}^{b/2} \eta \frac{d\Gamma(\eta)}{d\eta}\, d\eta = \bar{y}(y) \int_{y}^{b/2} \frac{d\Gamma(\eta)}{d\eta}\, d\eta \tag{2.2}$$

$$-\int_{y}^{b/2} \frac{d\Gamma(\eta)}{d\eta} \left[y - \bar{y}(y) \right]^2 d\eta = \int_{o}^{r} \rho^2 \frac{d\Gamma}{d\rho}\, d\rho \tag{2.3}$$

These three equations, representing the conservation of circulation, impulse and moment of impulse, relate the final rollup configuration to the initial flat vortex sheet without knowing the detailed rollup process. The approximation is that the cores are circular and both the initial and final states are inviscid and two dimensional in nature.

The rollup geometry is illustrated in Fig. 2-2 for the case of a "tip" vortex on an elliptically loaded wing.

For the "interior" vortex calculation, the three Betz invariants are written, between two arbitrary points A and B, as prescribed in Fig. 2-3.

$$-\int_{y_1}^{y_2} \frac{d\Gamma}{dy}\, dy = \int_{o}^{r_B} \frac{d\Gamma'_B}{dr}\, dr \tag{2.4}$$

$$\bar{y}_{12} \int_{y_1}^{y_2} \frac{d\Gamma}{dy}\, dy = \int_{y_1}^{y_2} y \frac{d\Gamma}{dy}\, dy \tag{2.5}$$

$$-\int_{y_1}^{y_2} \frac{d\Gamma}{dy} (y - \bar{y}_{12})^2\, dy = \int_{o}^{r_B} r^2 \frac{d\Gamma'_B}{dr}\, dr \tag{2.6}$$

From Eqs. (2.4), (2.5) and (2.6), Donaldson manipulates the simple recipe to yield

$$\bar{y}_{12} \int_{y_1}^{y_2} \frac{d\Gamma}{dy}\, dy = \int_{y_1}^{y_2} y \frac{d\Gamma}{dy}\, dy \tag{2.7}$$

$$r_B = y_2 - \bar{y}_{12} = \bar{y}_{12} - y_1 \tag{2.8}$$

$$\Gamma'_B(r_B) = \Gamma(y_1) - \Gamma(y_2) = \Gamma_1 - \Gamma_2 \tag{2.9}$$

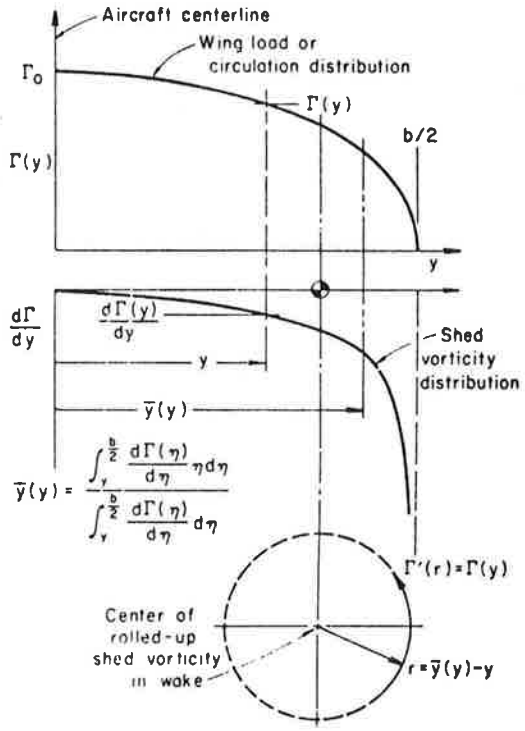

Fig. 2-2 - The Roll-Up Relation of a Tip Vortex (Ref. 30)

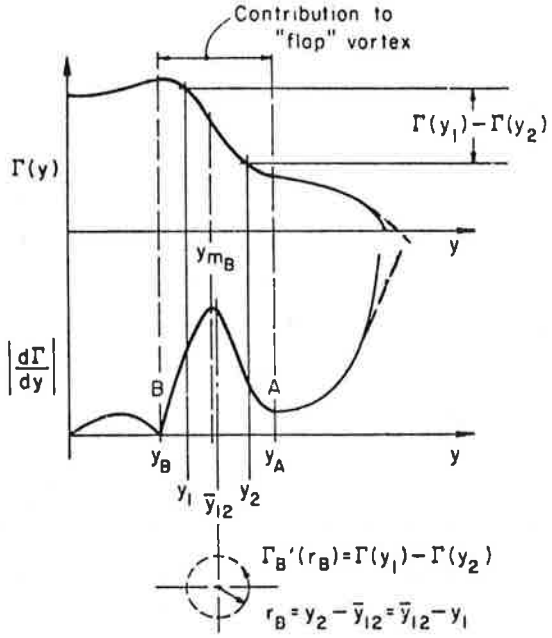

Figs. 2-3 - The Roll-Up Relation of "Interior" Vortices (Ref. 30)

These equations are equivalent to solving the integral equation

$$\bar{y}_{12} \int_{y_1}^{y_2} \frac{d\Gamma}{dy}\, dy = \int_{y_1}^{y_2} y \frac{d\Gamma}{dy}\, dy \tag{2.10}$$

subject to the constraint

$$\bar{y}_{12} = \frac{y_1 + y_2}{2} \tag{2.11}$$

Since Eqs. (2.7) and (2.8) contain three unknowns, the definition of the rollup process is indeterminate. In physical terms, the following questions remain unsolved;

1. Where does roll-up originate or what portion of the sheet forms the center of an "interior" vortex?
2. Where does the vortex sheet trailed from the wing divide itself into tip and "interior" vortices?

Donaldson et al, answer the first question by taking the origin of roll-up to be where $|d\Gamma/dy|$ is maximum. Their second answer is that each interior vortex is rolled up between two minima in $|d\Gamma/dy|$.

An algorithm has been coded and developed to integrate the equations given above subject to the rollup constraints postulated by Donaldson et al. Results obtained by the Lockheed-Huntsville multiple vortex code are presented in Figs. 2-4 and 2-5. For the spanwise loading distribution shown in Fig. 2-4, the Lockheed-Huntsville program yields the following initial multiple vortex locations and strengths:

	Γ, ft^2/sec	y_{12}, ft
Inboard flap vortex	1200	30
Outboard flap vortex	1725	65
Tip vortex	2350	95

Figure 2-5 shows the resulting trajectory of each vortex for the above multiple vortex wake. In this sample, no wind was included in the calculation to allow analysis of the relative orbits of the individual vortices.

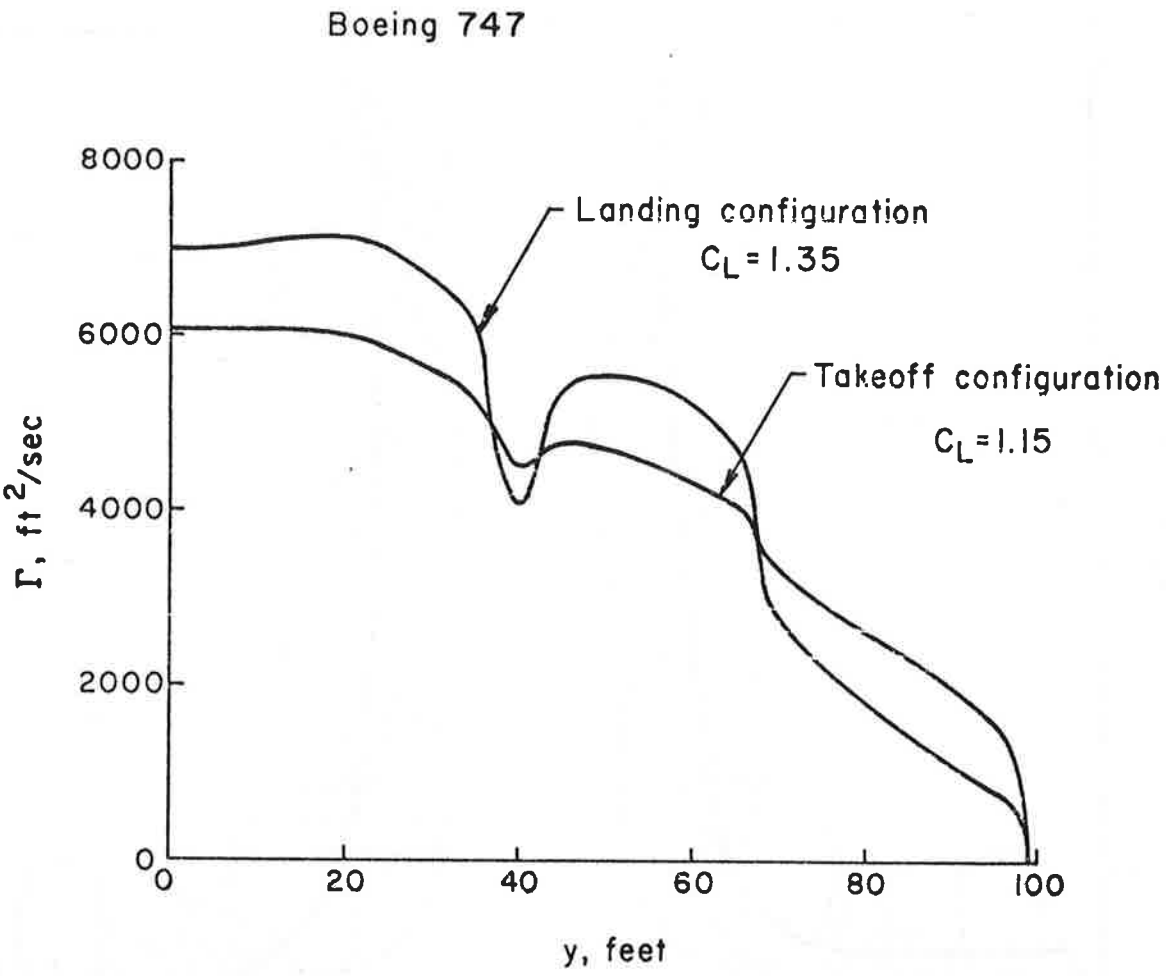

Fig. 2-4 - Wing Load Distribution on the 747 Aircraft from Lifting Surface Theory (Ref. 30)

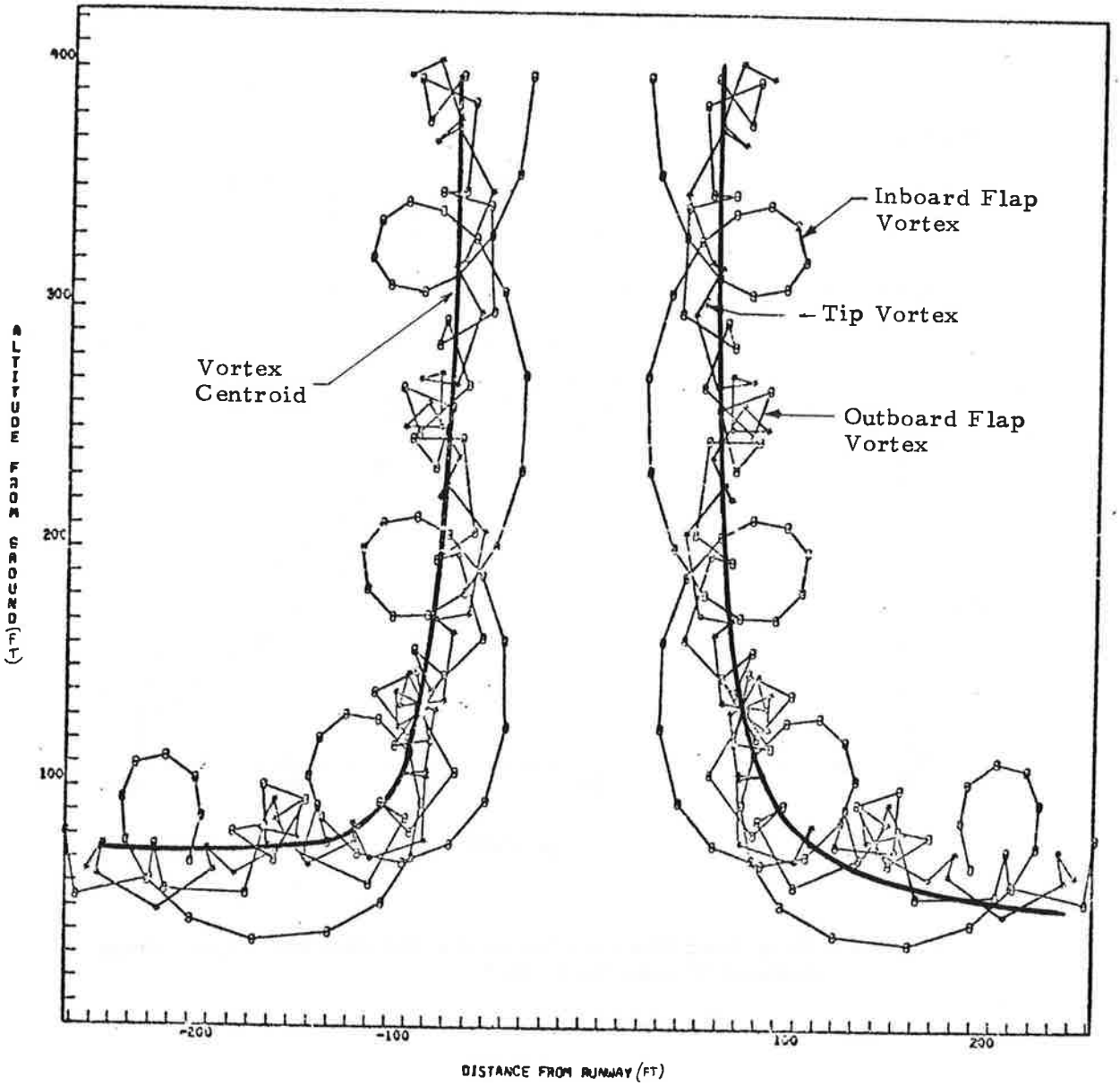

Fig. 2-5 - Multiple Vortex Trajectory Computed for a B-747 Aircraft in Landing Configuration

For the zero wind vortex descent case shown in the figure, the centroid of the multiple vortices is indicated by the heavy solid line. Note that the multiple vortices, consisting of the tip and inboard and outboard flap vortex filaments, rotate and translate with the centroid in an epicyclic manner. For identifying the hazardous wake vortex volume, the results in Fig. 2-5 show that the Donaldson-Betz rollup technique prescribes the initial vortex location and strength for the multiple vortex trajectory calculations. It is also noted that the centroid of the multiple vortex wake gives an indication of the general location of the vortex system.

While the previous figures demonstrate the capabilities of the modified Betz rollup model, there are certain limitations inherent in the Donaldson-Betz model. Efforts at Lockheed-Huntsville to apply the modified Betz rollup technique to predict terminal area wake motion has run into problems because of three difficulties:

1. To start the rollup calculations accurate definition of the airfoil spanwise loading distribution is necessary, the type of information which is difficult to obtain theoretically since the spanwise loading distributions computed for flapped airfoils by lifting surface programs do not agree well with experimental measurements.
2. Circulation strength and location of the multiple vortices appear to vary with the details of the rollup procedure.
3. Actual vortex wake measurements indicate a merging of the multiple vortex wake which is neglected in the inviscid rollup model.

Errors in the spanwise loading distribution computed theoretically for flapped airfoils can be seen in Fig. 2-6. Note the different spanwise loading curves observed and computed from theory. In this case, if the modified Betz rollup recipe is applied to the loading curve derived from the lifting surface code a much stronger flap vortex and a much weaker tip vortex is predicted than occurs.

A lack of accurate definition of the spanwise loading distributions hinders the practical application of the modified Betz technique to wake vortex prediction. Recent calculations by Aeronautical Research Associates of Princeton, Inc., of the vortex wake hazards of commercial aircraft have shown only

moderate agreement between measured and computed vortex profiles for flapped airfoils (Ref. 29).

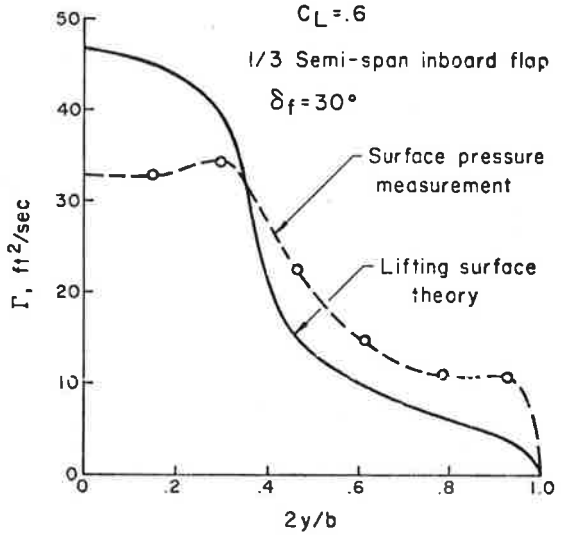

Fig. 2-6 - Lift Distribution on a Flapped Wing as Determined from Lifting Surface Theory and Surface Pressure Taps (Ref. 19)

Although the above rollup process is an extension of the Betz invariant principle, it introduces two more constraints. In order to make the system a well-posed boundary value problem, the Donaldson formulation postulates that the "interior" vortex begins to roll up about the points where $|d\Gamma/dy|$ is maximum. Also, the extent of the rolled up region is determined to be that segment of the sheet which lies between local minima. Note that these two assumptions are not necessary in the original Betz model because the basic model is valid only for a uniform strength vortex sheet (elliptical loading) and only one maximum of $|d\Gamma/dy|$ occurs which is at the tip. In the Betz model, roll up always proceeds from the tip inboard. Unfortunately, for the more general case, the choice of rollup point and direction determines the location and strength of the individual vortices. Thus, the modified Betz rollup model is very sensitive to the manner in which the wing is segmented and is not entirely satisfactory for predicting multiple vortex parameters. A comparison of vortex spacing, $\overline{y}$, and vortex strength, Γ, computed by Donaldson and by Lockheed-Huntsville following the Donaldson recipe is presented in Table

2-1. Differences in spacing and strength are attributed to the manner in which the elements were rolled up.

TABLE 2-1

DONALDSON-BETZ ROLLUP CALCULATIONS

Configuration	Donaldson's Result		Lockheed-Huntsville Results	
	$\bar{y}$ (ft)	Γ (ft^2/sec)	$\bar{y}$ (ft)	Γ (ft^2/sec)
DC-7, Flap Vortex	34.2	1843	34.47	1576
DC-7, Tip Vortex	56.5	500	56.35	330
C-141, Flap Vortex	49.6	2784	51.52	2093
C-141, Tip Vortex	76.4	1350	77.8	1042

In addition to the difficulties cited above, the modified Betz rollup technique does not account for viscous vortex merging effects. From the analysis of NAFEC test data (Ref. 7) it is apparent that multiple vortices are not observed at extended downstream distances. This implies that the assumption of independent roll up of the various vortices is not realistic since all of the vortices ultimately merge.

Inviscid rollup techniques, represented by the Donaldson-Betz method, predict multiple vortices which persist far downstream as sketched in Fig. 2-7. However, experimental measurements indicate that the multiple vortices behind flapped lifting surfaces merge into a single vortex pair within 13 to 32 spans downstream as shown in Fig. 2-8. Thus, the modified Betz model must be broadened by considering additional viscous effects.

Recognizing the strength and limitations of the Donaldson-Betz rollup recipe, an effort has been made to develop an alternate vortex rollup model for the Predictive Wake Vortex Transport code which takes into account non-elliptical spanwise loadings. The computed multiple vortex trajectories cited earlier have shown that the translation of the centroid or the trailing vortex wake provides a good measure of the motion of the complete system. Furthermore, experimental measurements (Ref. 23) have demonstrated that multiple vortices behind flapped lifting surfaces merge into a single vortex pair within 32 spans

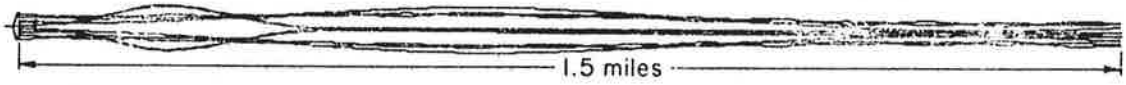

Top View

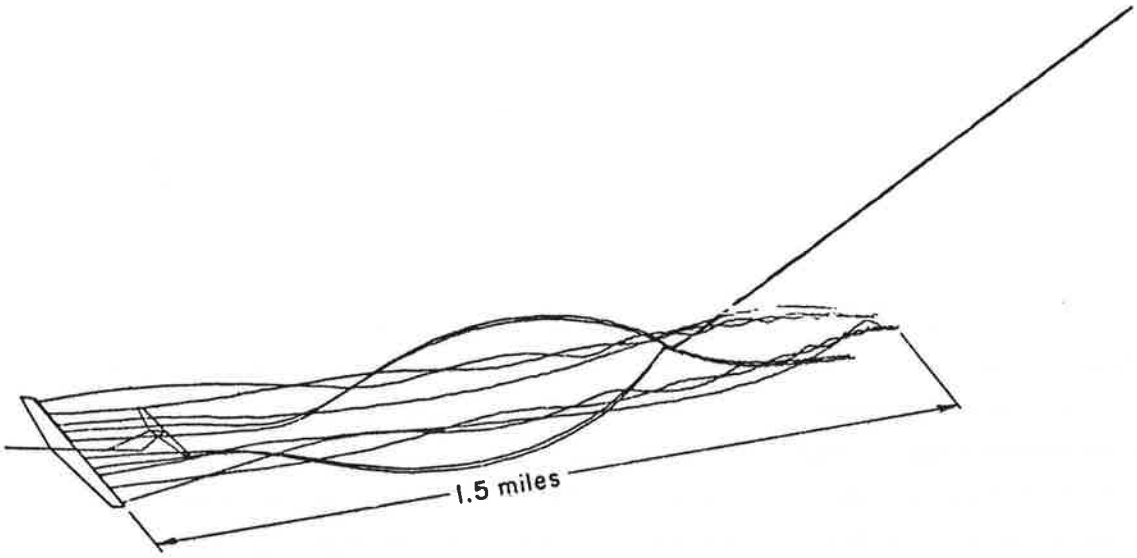

Oblique View

Fig. 2-7 - Vortex Roll-Up Computed for a B-747 in Landing by the Donaldson-Betz Method (Ref. 30)

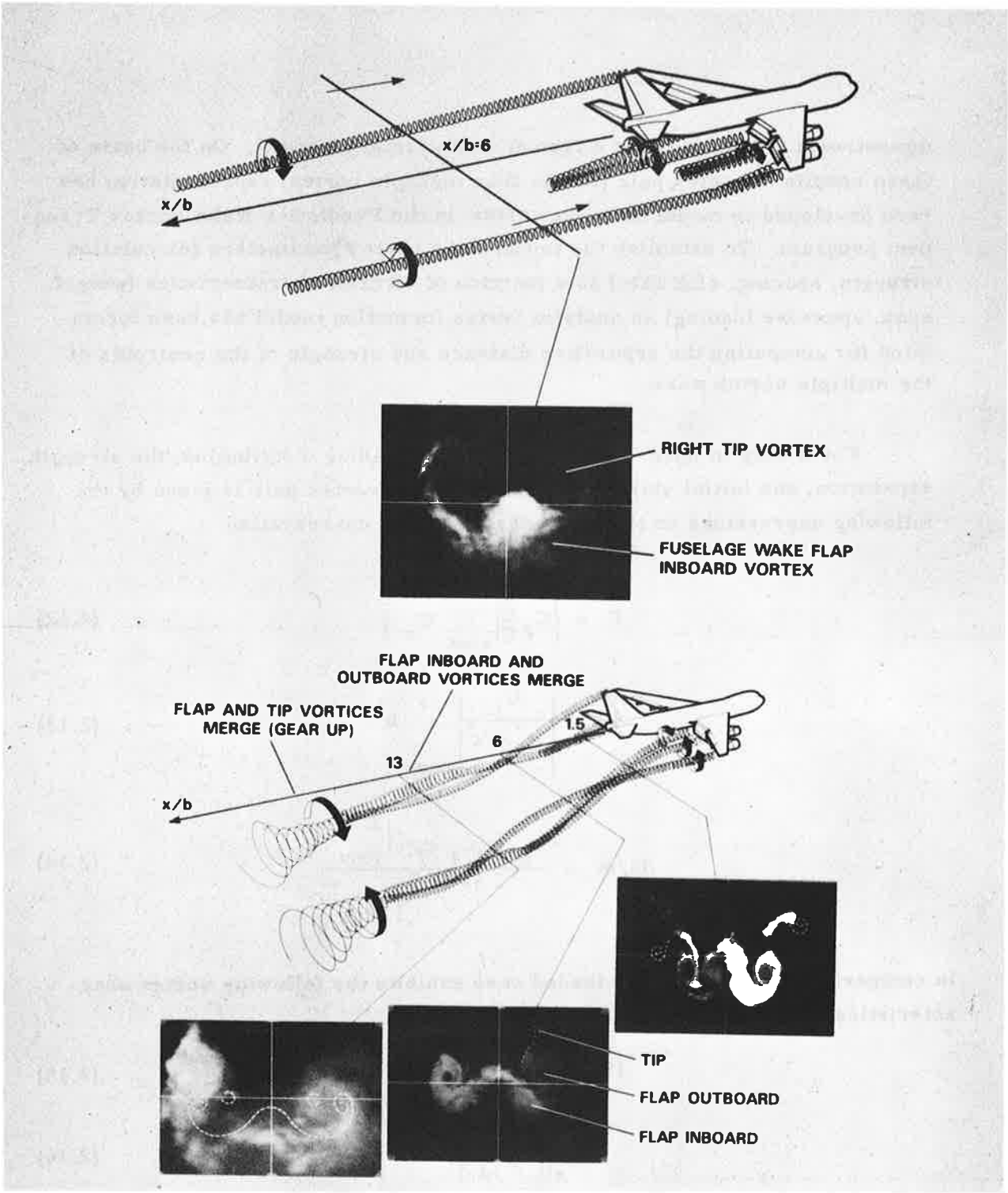

Fig. 2-8 - Observed Wake Geometry for a B-747 in Landing Configuration (Ref. 23)

downstream (18 seconds for a typical commercial aircraft). On the basis of these results, a vortex pair (rather than multiple vortex) representation has been developed to model the wake vortex in the Predictive Wake Vortex Transport program. To establish the initial wake vortex parameters (circulation strength, spacing, sink rate) as a function of aircraft characteristics (weight, span, spanwise loading) an analytic vortex formation model has been formulated for computing the separation distance and strength of the centroids of the multiple vortex wake.

For a wing of span b with an arbitrary loading distribution, the strength, separation, and initial sink rate of the rolled up vortex pair is given by the following expressions on the basis of momentum conservation

$$\Gamma = \left| C_\ell \frac{c}{\bar{c}} \right|_{root} U_\infty \frac{\bar{c}}{2} \tag{2.12}$$

$$b' = \left| \frac{C_L}{C_\ell \, c/\bar{c}} \right|_{root} b \tag{2.13}$$

$$dh/dt = \frac{-U_\infty \bar{c} \left| C_\ell \, c/\bar{c} \right|^2_{root}}{4\pi \, b \, C_L} \tag{2.14}$$

In comparison, the elliptically loaded case exhibits the following vortex characteristics:

$$\Gamma_{ell} = \frac{2}{\pi} C_L \bar{c} \, U_\infty \tag{2.15}$$

$$b'_{ell} = \frac{\pi}{4} b \tag{2.16}$$

$$dh/dt_{ell} = -4\bar{c} \, \frac{C_L U_\infty}{\pi^3 b} \tag{2.17}$$

On the basis of Eq. (2.14), the vortex sink rate for a wing having an arbitrary spanwise loading distribution is given by

$$dh/dt = \frac{-C_L U_\infty}{4\pi K^2 AR} \tag{2.18}$$

where

$$K = \frac{C_L}{|C_\ell c/\bar{c}|_{root}}$$

which is a measure of the spanwise loading and $AR = b/\bar{c}$. For an elliptical loading $K = \pi/4$. However, for wings with inboard flaps the root sections tend to be more heavily loaded; K is less, and hence the vortex sink rate is higher.

Equation (2.18) has been incorporated into the Predictive Wake Vortex Transport Program and trajectories have been calculated using different values of K to reflect flap effects.

2.2 VORTEX MOTION

An important aspect of the Wake Vortex Avoidance System is the capability for predicting the position of the wake vortex hazard as a function of space and time. Research at DOT-TSC and Lockheed-Huntsville (Refs. 3 through 9) on vortex wakes in the terminal environment has shown that in most of the cases ambient winds transport the vortex out of the flight corridor rapidly so that the normal operational aircraft separation distances could be decreased. The maximum spacing requirements for landing and takeoff operations occur under light crosswind conditions when the lateral velocity of the vortex (relative to the air) is opposed by an equal and opposite crosswind velocity so that the upwind vortex "stalls" in the flight corridor. From operational considerations this light wind situation is particularly troublesome since a wake vortex could persist for some period of time. It is perhaps not surprising then that most of the wake vortex encounter accidents have occurred when the cross wind was less than 5 knots (Ref. 1). These results indicate

that wake transport is a key parameter in the definition of a wake vortex avoidance system.

Earlier versions of the Predictive Model (Ref. 3 through 9) have shown that wind shear and buoyancy can influence wake vortex transport at terminal areas. Vortex tilting mechanisms were postulated to account for consistent sources of error between predicted and observed late-time wake vortex behavior. In the present program, efforts were made to expand the Predictive Model and to quantify the effects of wind shear, buoyancy, circulation decay, and ground plane proximity on wake vortex transport.

The motion of the rolled up vortex pair is affected through the following mechanisms:

1. Advection by the ambient wind
2. Translation by mutual and self-induction
3. Translation due to outside forces.

A synergistic effect can take place when two or more of the above mechanisms interact. For example, the vertical gradient of the ambient wind, wind shear, can affect the vorticity field of the wake thereby: (1) altering the cross-sectional area of the wake vortex cell, and (2) creating a separated wind shear buoyancy layer. Previous studies at Lockheed-Huntsville (Ref. 9) have shown that the size of the downwind cell shrinks as the ground plane is approached and the degree of asymmetry is a strong function of the wind shear. It was postulated that this effect could lead to changes in the wake transport characteristics. To quantify these effects in more detail, a general Predictive Wake Vortex Transport Model has been developed.

A sketch of the wake geometry of the Predictive Vortex Model is presented in Fig. 2-9. Asymmetric behavior of the buoyancy as well as circulation containing cells are accounted for this comprehensive simulation. For the vortex model sketched in Fig. 2-9, the transport equations including

buoyancy, ground plane, and vortex tilting effects have been formulated. Transport of the wake vortex by the wind is handled independently as a simple coordinate translation.

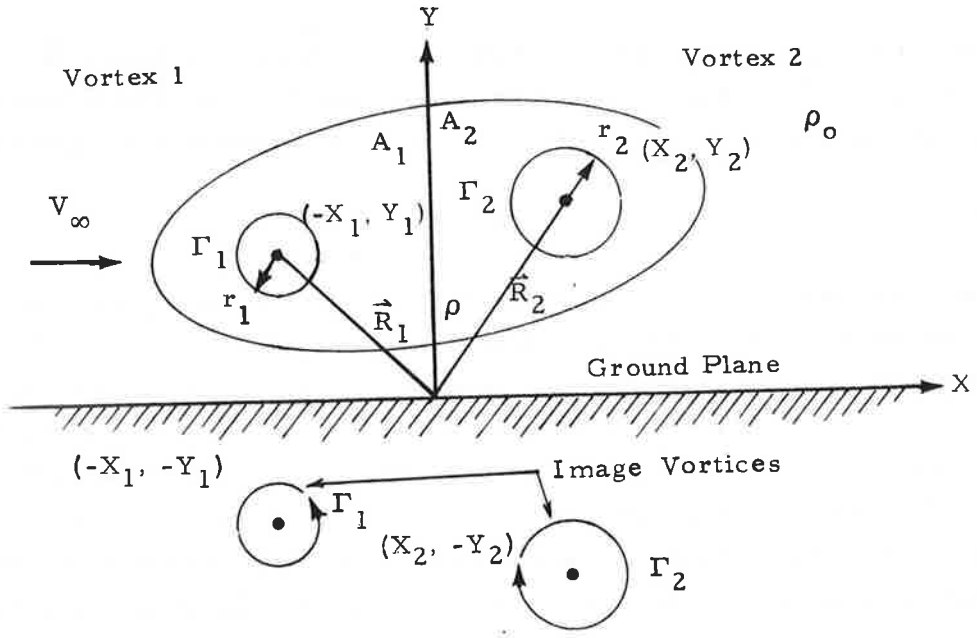

$(-X_1, Y_1)$ (X_2, Y_2) $(-X_1, -Y_1)$ $(X_2, -Y_2)$	location of vortices (center of vorticity-containing region)
r_1, r_2	core radius of vortices (radius of vorticity-containing region)
A_1, A_2	area of vortex cell (area of buoyancy-containing region)
ρ	density of air within vortex pair
ρ_o	ambient density
Γ_1, Γ_2	circulation of vortex pair

Fig. 2-9 - Geometry of the Predictive Wake Vortex Transport Model

An exact equation for the two-dimensional drift of a horizontal, inviscid, incompressible buoyant vortex in a uniform flow subject to gravity may be derived in vector notation as (see Appendix A)

$$(\dot{\vec{R}} - \vec{V}_\infty) \times \vec{\Gamma} - \lambda A (\ddot{\vec{R}} - \vec{\nabla}\Phi) - (2-\lambda)\pi r^2 \ddot{\vec{R}} = 0 \tag{2.19}$$

where $\vec{R}$ is the position vector of the vortex centroid, $\dot{\vec{R}}$ is the velocity, $\ddot{\vec{R}}$ is the acceleration, $\vec{V}_\infty$ is the uniform flow velocity and Φ is the gravitational potential. The parameter λ is called the buoyancy index which is defined as

$$\lambda = 1 - \frac{\rho}{\rho_o} \tag{2.20}$$

in which ρ is the density of the fluid inside the vortex core and ρ_o is the density of the surrounding atmosphere. The first term in Eq. (2.19) is the lift force on the vortex due to the Kutta-Joukowski condition. The buoyancy force on the vortex is represented by the second term. The last term in the equation is the inertial force due to the vortex hydrodynamic mass. Equation (2.19) reduces to Costen's buoyancy equations (Ref. 31) when the vortex mass is neglected and the buoyancy carrying area is limited to the inner viscous core region which was used in earlier wake vortex transport calculations (Ref. 9).

Using the coordinate system shown in Fig. 2 - 9 we can write

$$\begin{gathered}
\vec{R}_1 = -X_1 i + Y_1 j, \quad \vec{R}_2 = X_2 \vec{i} + Y_2 \vec{j} \\
\vec{V}_\infty = V_\infty(x)\, \vec{i} + V_\infty(y)\, \vec{j} \\
\vec{\Gamma}_1 = -\vec{k}\Gamma_1, \quad \vec{\Gamma}_2 = \vec{k}\Gamma_2 \\
\Phi = -gy
\end{gathered} \tag{2.21}$$

where i, j, and k are the unit vectors in the x, y and z directions, respectively. Substituting the above expressions into Eq. (2.19), the equations of motion for the vortex pair reduce to

$$(\dot{Y}_1 - V_\infty(Y_1))\Gamma_1 - \lambda_1 A_1 \ddot{X}_1 - (2-\lambda_1)\pi r_1^2 \ddot{X}_1 = 0 \qquad (2.22)$$

$$(\dot{X}_1 + V_\infty(-X_1))\Gamma_1 + \lambda_1 A_1 \ddot{Y}_1 + \lambda_1 A_1 g + (2-\lambda_1)\pi r_1^2 \ddot{Y}_1 = 0 \qquad (2.23)$$

$$(\dot{Y}_2 - V_\infty(Y_2))\Gamma_2 - \lambda_2 A_2 \ddot{X}_2 - (2-\lambda_2)\pi r_2^2 \ddot{X}_2 = 0 \qquad (2.24)$$

$$(\dot{X}_2 - V_\infty(X_2))\Gamma_2 + \lambda_2 A_2 \ddot{Y}_2 + \lambda_2 A_2 g + (2-\lambda_2)\pi r_2^2 \ddot{Y}_2 = 0 \qquad (2.25)$$

where the subscripts 1 and 2 refer to the two vortices.

Applying the Biot-Savart law to compute the mutual and self-induction effects due to the vortex pair and its image, the velocities are given by the following equations.

$$V_\infty(-X_1) = \frac{\Gamma_1}{4\pi Y_1} + \frac{\Gamma_2}{2\pi}\frac{Y_1+Y_2}{(Y_1+Y_2)^2+(X_1+X_2)^2} + \frac{\Gamma_2}{2\pi}\frac{Y_2-Y_1}{(Y_2-Y_1)^2+(X_1+X_2)^2} \qquad (2.26)$$

$$V_\infty(Y_1) = \frac{\Gamma_2(X_1+X_2)}{2\pi}\left[\frac{1}{(Y_1+Y_2)^2+(X_1+X_2)^2} - \frac{1}{(Y_2-Y_1)^2+(X_1+X_2)^2}\right] \qquad (2.27)$$

$$V_\infty(X_2) = \frac{\Gamma_2}{4\pi Y_2} - \frac{\Gamma_1}{2\pi}\frac{Y_1+Y_2}{(Y_1+Y_2)^2+(X_1+X_2)^2} - \frac{\Gamma_1}{2\pi}\frac{Y_2-Y_1}{(Y_2-Y_1)^2+(X_1+X_2)^2} \qquad (2.28)$$

$$V_\infty(Y_2) = \frac{\Gamma_1(X_1+X_2)}{2\pi}\left[\frac{1}{(Y_1+Y_2)^2+(X_1+X_2)^2} - \frac{1}{(Y_2-Y_1)^2+(X_1+X_2)^2}\right] \qquad (2.29)$$

The initial boundary conditions for uniform descent and no wake tilting are given by

$$X_1(0) = X_2(0) = b'/2$$

$$Y_1(0) = Y_2(0)$$

$$\Gamma_1(0) = \Gamma_2(0)$$

$$A_1(0) = A_2(0) = 11.42(b'/2)^2/2$$

$$\ddot{X}_1(0) = \ddot{X}_2(0) = 0 \qquad (2.30)$$

$$\ddot{Y}_1(0) = \ddot{Y}_2(0) = 0$$

Equations (2.22) through (2.30) represent an extension of the predictive model developed earlier (Ref. 7) for describing terminal area vortex transport behavior. Additional flexibility is present in the above model to consider vortex tilting and asymmetric vortex decay and transport effects. For example, buoyancy of the vortex influences the wake motion through the λA term and different buoyant forces can promote different sink rates. Vorticity detrainment influences the circulation of each cell through changes in Γ and mismatches in Γ can lead to tilting.

While the above transport equations are based on an inviscid point vortex model, the effects of viscosity and turbulent mixing are handled indirectly by variations in wake cell size, shape, and circulation. It is assumed that the wake characteristics such as vortex strength, cell size and shape are independent from the transport process and are a function of the vortex height above the groundplane, wind shear and ambient turbulence level. Thus, the wake descent is specified by Eqs. (2.22) through (2.30) with the circulation, buoyancy and cell area parameters (Γ, λ and A) determined from other considerations. As noted earlier, the influence of the uniform ambient wind is handled as a simple coordinate translation and therefore does not appear explicitly in the above equations of motion.

To account for the effects of cell size and shape on vortex transport, the wake vortex streamlines obtained earlier in Refs. 9 and 32 have been integrated with a planimeter to obtain the characteristic wake vortex perimeters and cell areas. For the general case of a vortex pair descending toward the ground in a given linear wind shear profile, $K_1 = \partial u/\partial h$, the shape and size of the wake vortex cell can be determined uniquely from the dimensionless

height and wind shear parameter, $\epsilon = 2h/b'$ and $\sigma = \pi K_1 b'^2/2\Gamma$, respectively. Potential flow calculations have shown that as the vortex wake approaches the groundplane, the downwind cell shrinks more rapidly than the upwind cell. The result is an asymmetric configuration which is shown in Fig. 2-10.

The influence of groundplane proximity and wind shear on the wake vortex cell geometry is summarized in Table 2-2, and the dominant trends are shown in Figs. 2-11 and 2-12. Note the sharp decrease in the vortex cell area and the large increase in the vortex cell perimeter to area ratio for $\epsilon \leq 1.5$. Significantly, the groundplane wake vortex interaction altitude, $\epsilon \sim 1.5$, corresponds to the altitude at the middle to near marker for commercial aircraft during landing operations. The increase in the perimeter of the wake vortex cell, despite the decrease in the cell area, is a result of the lateral deformation and stretching of the vortex cell. As shown in Fig. 2-10, very close to the ground the upwind cell cross section is considerably flattened out from the conventional quasi-elliptical cross-section. It is also interesting to note that a reversal occurs in the upwind vortex cell area for $\sigma = 0$, 1, and 2, respectively. From the $\sigma = 0$ to $\sigma = 1$ case the total cross-sectional area is reduced slightly, ~20%, but the upwind cell contains a larger fraction of the total cross sectional area, i.e., it increases from 50 to 88% of the total area at $\epsilon = \infty$. For higher σs, the reduction in total cross-sectional area overrides the redistribution of the wake vortex cross-sectional area from the downwind to the upwind cell. The results given above provide the vortex cell area and shape parameters which are required in the Predictive Wake Vortex Transport Model to compute the wake descent.

2.3 VORTEX DECAY AND BREAKUP

Wake vortex decay and breakup play an important role in establishing the extent of vortex induced aircraft hazards. For example, when the vortex stalls in the flight corridor, it is generally the viscous and nonlinear wake decay processes which finally alleviate the potential hazard. Efforts have been made to model the observed decay and breakup phenomena of wake vortices as a step in improving the theoretical Predictive Model.

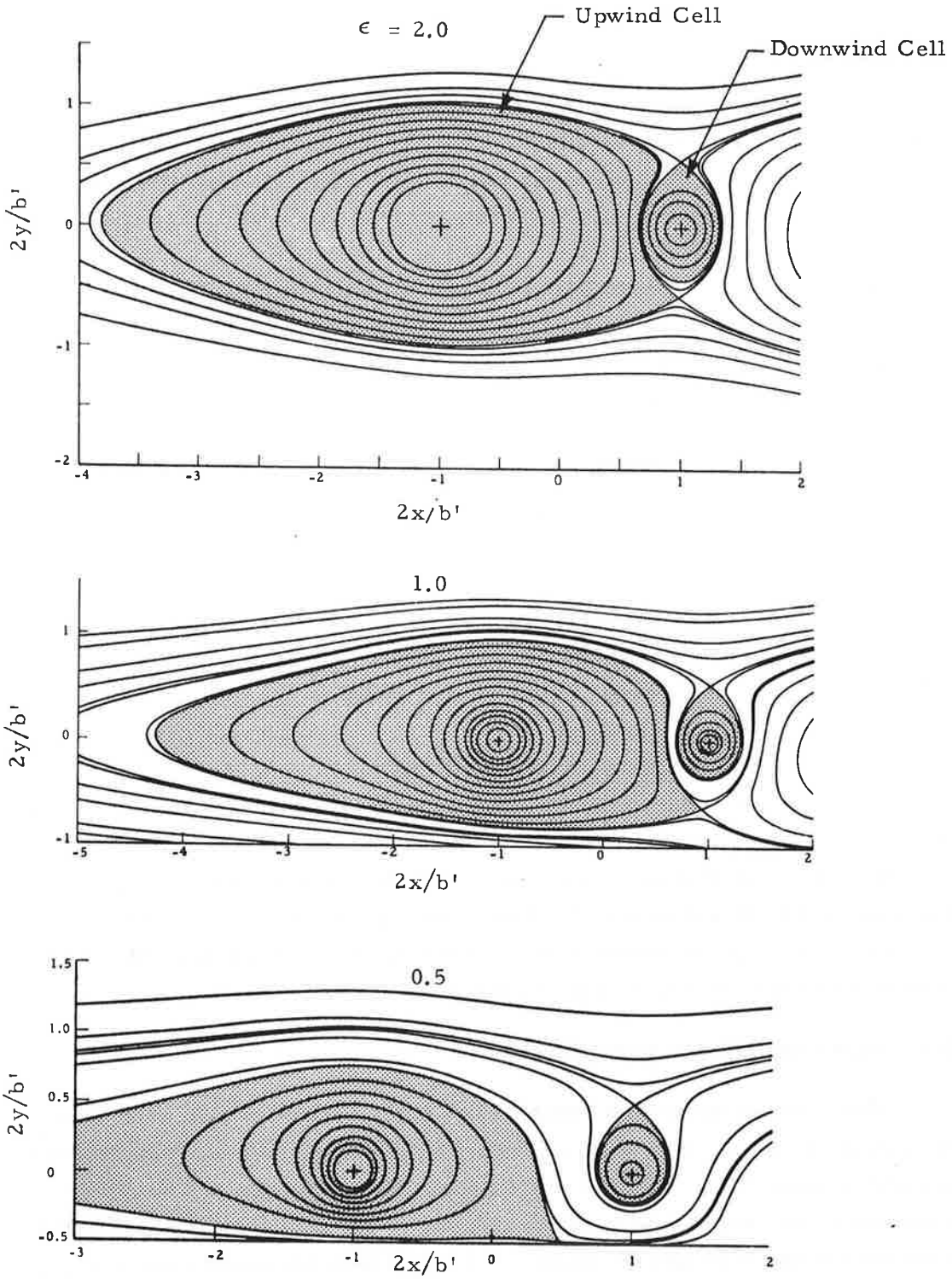

Fig. 2-10 - Effect of Ground Plane Height, $\epsilon = 2h/b'$, on Wake Vortex Cell Streamlines in the Presence of Wind Shear $\sigma = \pi K_1 (b')^2/2\Gamma = 3.0$ (Ref. 9, Wind Direction Left to Right)

TABLE 2-2

EFFECT OF WIND SHEAR AND GROUND PLANE ON WAKE VORTEX CELL CHARACTERISTICS

ϵ	σ	$\frac{4A_1}{b'^2}$	$\frac{4A_2}{b'^2}$	$\frac{2P_1}{b'}$	$\frac{2P_2}{b'}$	$\frac{P_1 b'}{2A_1}$	$\frac{P_2 b'}{2A_2}$
∞	0	5.7	5.7	9.4	9.4	1.6	1.6
∞	1	8.4	1.1	11.1	4.5	1.3	4.1
∞	2	8.0	1.0	11.6	3.4	1.5	3.4
∞	3	7.5	0.6	11.4	2.7	1.5	4.5
5	1	7.9	1.3	11.0	4.4	1.4	3.4
5	2	7.8	0.7	11.5	3.1	1.5	4.4
5	3	7.7	0.5	12.0	2.6	1.6	5.2
2	1	7.5	1.0	10.0	4.0	1.3	4.0
2	2	7.5	0.6	11.0	2.8	1.5	4.7
2	3	7.4	0.4	13.0	2.4	1.8	6.0
1	1	5.1	0.9	8.5	3.6	1.7	4.0
1	2	5.0	0.5	9.4	2.8	1.9	5.6
1	3	5.0	0.3	11.0	2.3	2.2	7.7
0.5	1	3.1	0.6	6.9	3.0	2.2	5.0
0.5	2	3.3	0.4	8.2	2.3	2.5	5.8
0.5	3	3.7	0.2	9.5	1.9	2.6	9.5

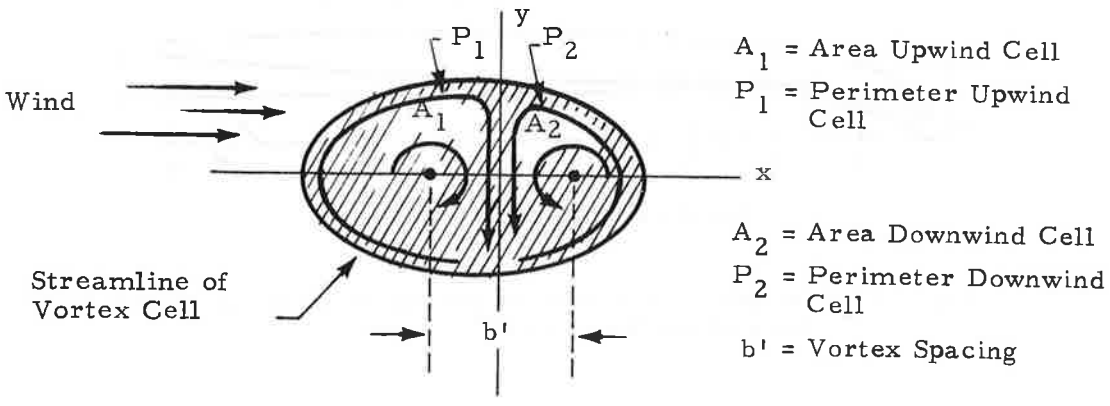

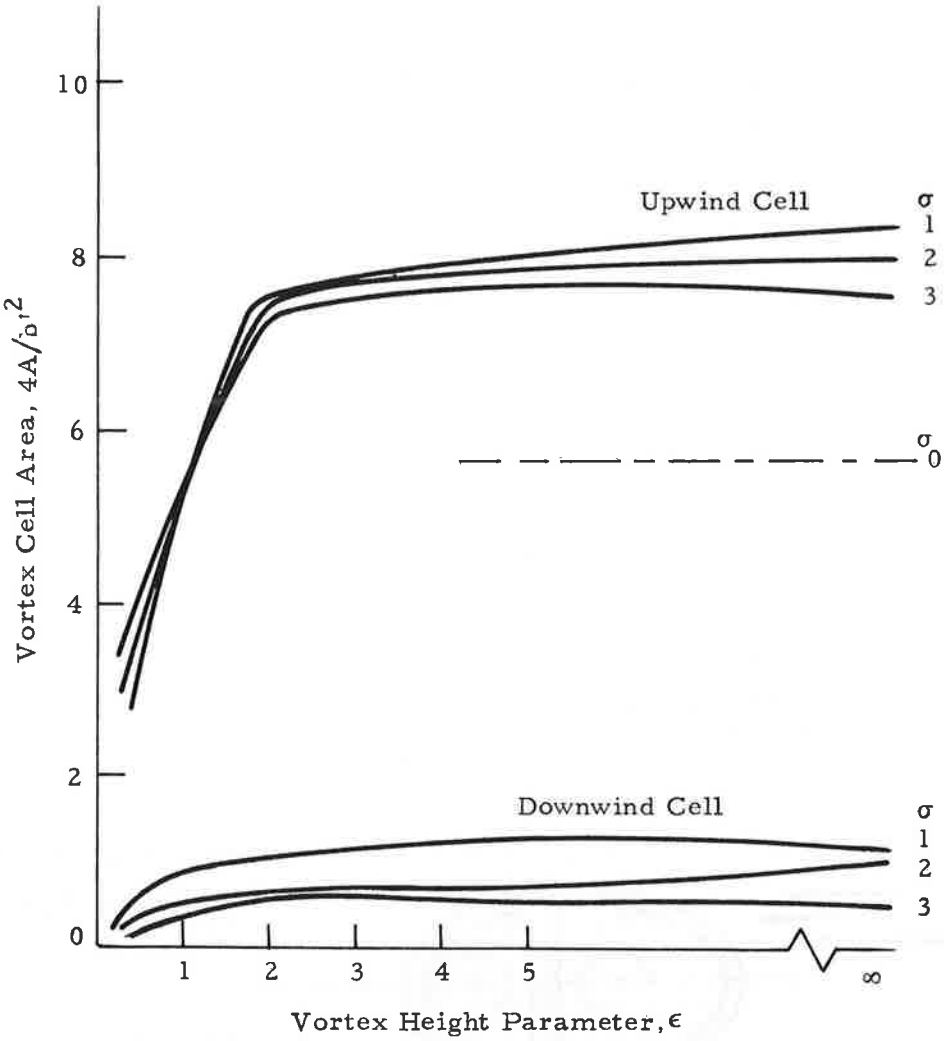

Fig. 2-11 - Influence of Vortex Height and Wind Shear on the Area of the Vortex Cell

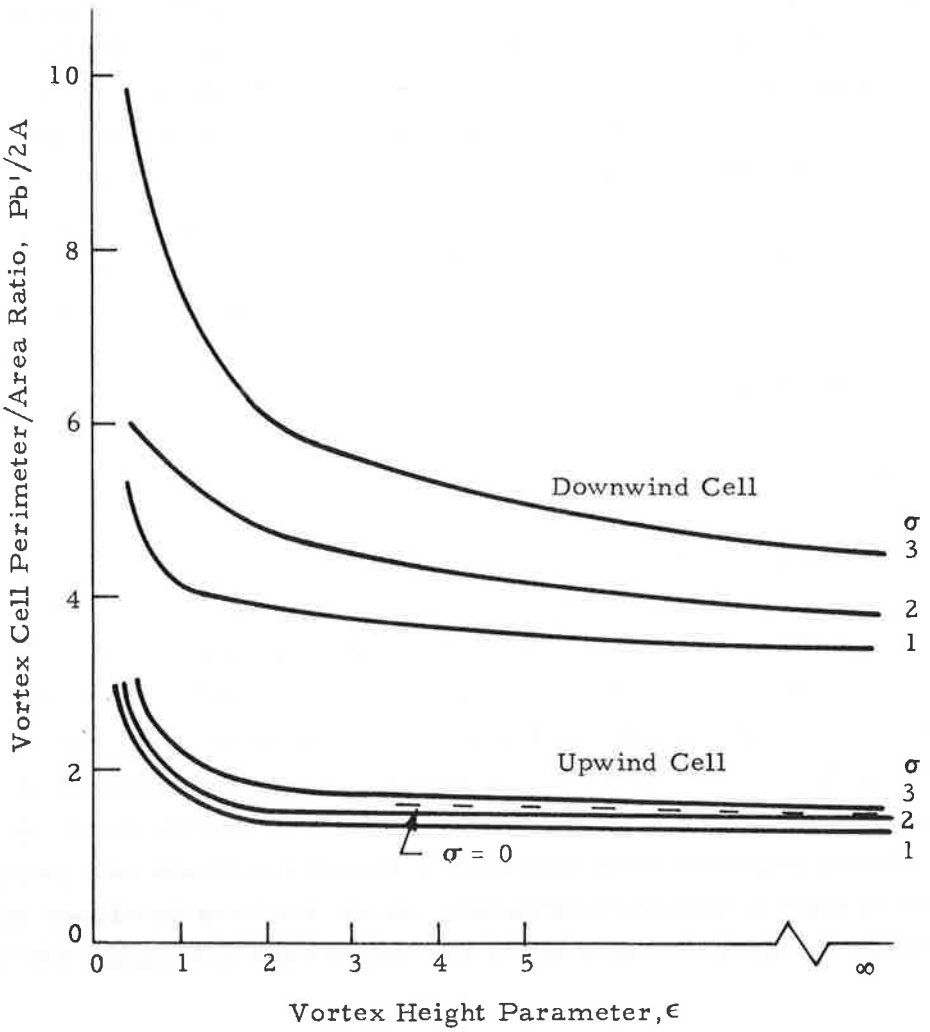

Fig. 2-12 - Influence of Vortex Height and Wind Shear on the Perimeter/ Area Ratio of the Vortex Cell

Analysis of particular measurements (Ref. 33) has identified three dominant vortex decay and breakdown mechanisms: (1) turbulent diffusion; (2) sinusoidal linking instability; and (3) vortex breakdown. These vortex decay and breakdown mechanisms have been incorporated into the Predictive Wake Vortex Transport Model.

The effect of turbulent diffusion on vortex decay has been considered by a number of investigators following the classical viscous vortex solution of Lamb with a turbulent eddy viscosity, ν_T, replacing the original laminar kinematic viscosity coefficient, ν. A number of different values have been proposed for ν_T, and experimental measurements indicate that the kinematic viscosity is a function of vortex circulation strength as shown in Fig. 2-13 (Ref. 34). However, experimental results also show that the turbulent eddy viscosity coefficient is a function of downstream distance (Fig. 2-14) so that decay rates other than $t^{-1/2}$ are possible. In order to model this effect, variable mixing length models have been proposed (Refs. 34 and 35) which can account for any type of turbulent decay rate.

The turbulent kinematic viscosity models cited above are useful in estimating the early-time vortex core diffusion. However, at late times vorticity is transported out of the vortex cell as shown by flow visualization studies (Ref. 36) and sketched in Fig. 2-15 (Ref. 32). The flow of vorticity out of the vortex cell decreases the circulation of the quasi-elliptical cell and leaves behind a secondary wake. Recall that in the Lamb turbulent diffusion model vorticity is redistributed through core growth but the total circulation of the system is fixed. However, the vorticity detrainment model suggests that vorticity is left behind in the wake which contributes zero moment so that the total circulation of the descending vortex cell decreases. In order to model this important decay mechanism a vorticity detrainment theory has been developed and incorporated into the Lockheed-Huntsville Predictive Vortex Transport Model.

During the initial stage sketched in Fig. 2-15 the core radius grows due to turbulent diffusion as predicted from Reynolds number similarity and Lamb's turbulent vortex model

$$r(t) = (r^2(0) + 5.04\, t \nu_T)^{1/2} \qquad (2.31)$$

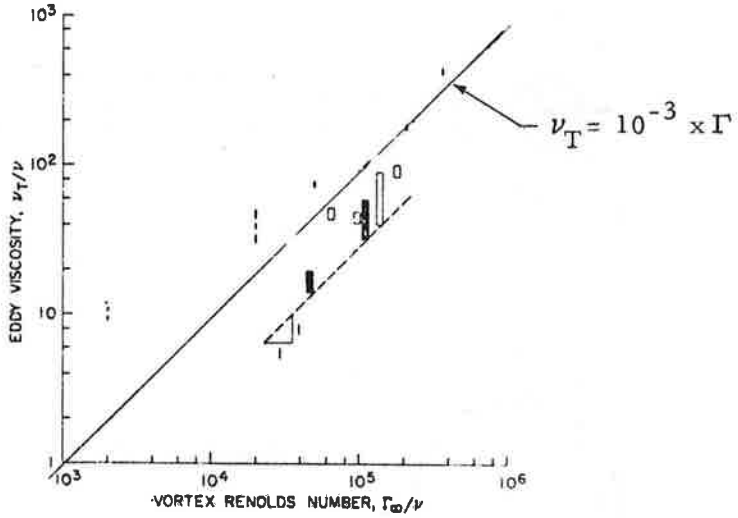

Fig 2-13 - Comparison of Experimental Eddy Viscosity Data (Ref. 34)

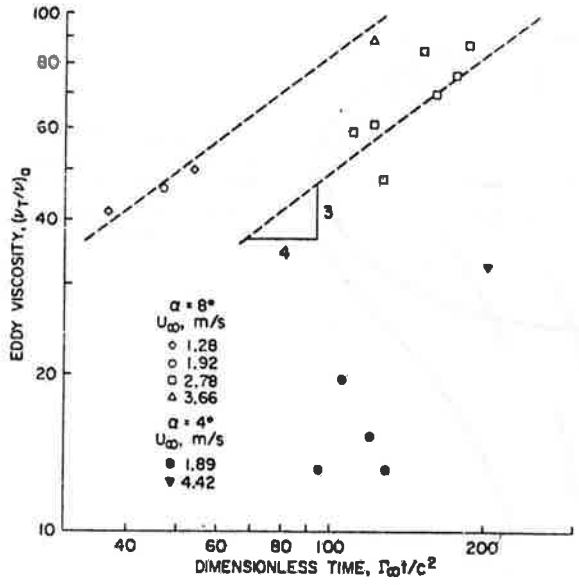

Fig. 2-14 - Time Dependence of Eddy Viscosity Determined from Experimental Data (Ref. 34)

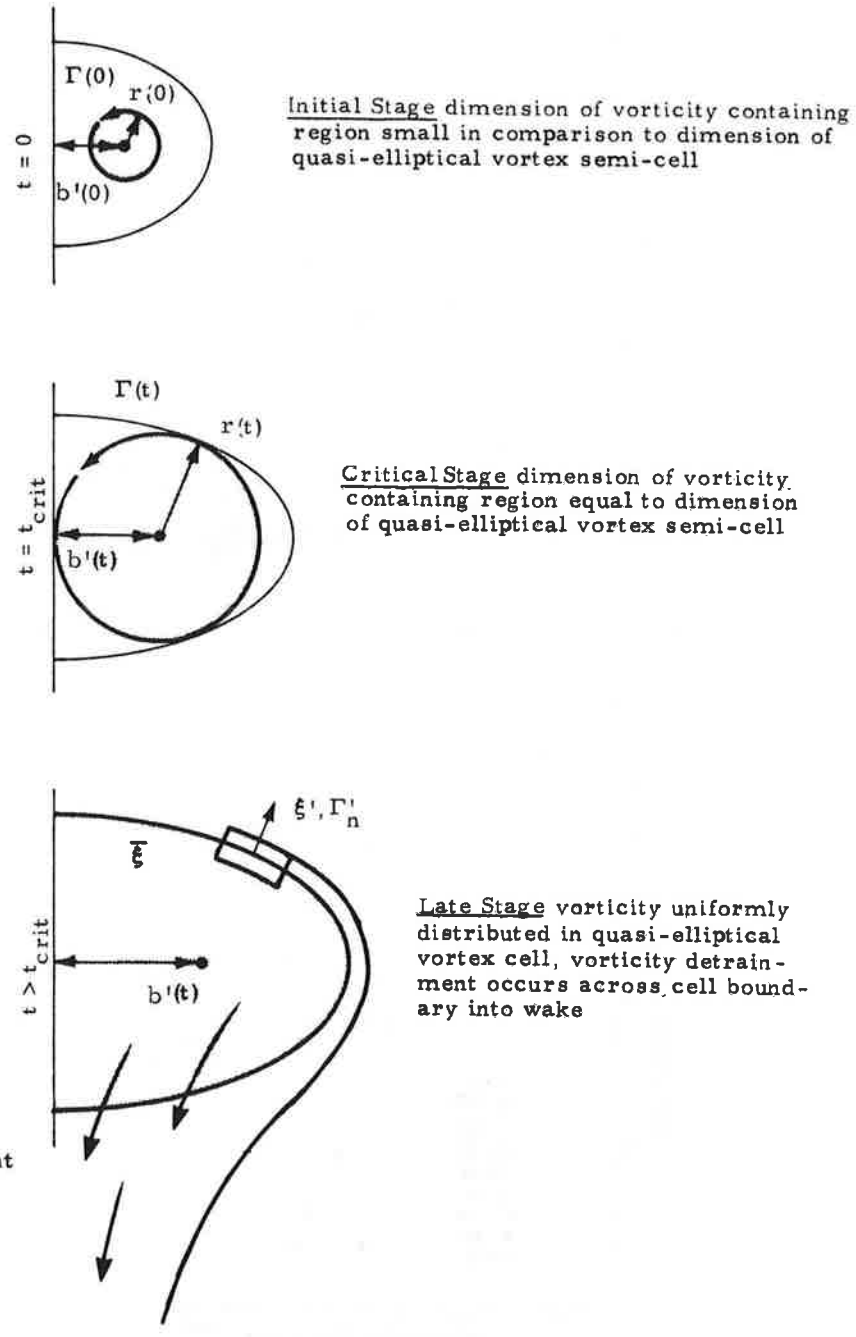

Fig. 2-15 - Sketch of Vortex Core Growth — Vorticity Left Behind in Secondary Wake (Ref. 32)

where ν_T is a function of Γ as shown earlier. It is realistic to assume that little or no vorticity detrainment occurs out of the quasi-elliptical vortex cross section when the viscous core radius is less than the vortex spacing parameter as sketched in Fig. 2-15. In terms of the total circulation strength, the criteria are

$$\Gamma(t) = \Gamma(0) \quad \text{if} \quad r(t) < \frac{b'(t)}{2} \tag{2.32}$$

where $r(t)$ is given in Eq. (2.31).

A vorticity detrainment model using the results of the second order closure analysis has been derived in Ref. 30 for the case of a vortex pair with a circular cross-sectional area descending in the absence of wind shear and ground plane proximity. The vorticity detrainment model for a wake vortex of arbitrary cross-sectional geometry and spacing is derived as follows on the basis of the familiar mixing length theory which includes wind shear and ground plane effects.

For the case where vorticity is present throughout the quasi-elliptic cross sectional area (the Late Stage in Fig. 2-15) it is reasonable to assume that vorticity transport occurs out of the vortex cell. If a fluctuation of vorticity, ξ', and velocity u_n', exists across the boundary of the quasi-elliptical vortex cell, the time rate of change of circulation is given by

$$d\Gamma/dt = -\oint \overline{u_n' \xi'}\, ds \tag{2.33}$$

where the line integral is taken around half of the cell as shown in Fig. 2-15.

Assuming that the fluctuations across the boundary are insensitive to position (Ref. 30),

$$d\Gamma/dt = -P \overline{\langle u_n' \xi' \rangle} \tag{2.34}$$

where $\langle\ \rangle$ denotes the average value of $\overline{u_n' \xi'}$ around the perimeter P sketched in Table 2-2.

For turbulent shear flows, vorticity and momentum transport can be described by the familiar mixing length theory (Eq. 3.3.17, Ref. 37)

$$\overline{u_n' \xi'} \sim - q\ell \frac{\partial \bar{\xi}}{\partial n} \tag{2.35}$$

where q is the rms turbulence level, ℓ is the mixing length, and $\partial\bar{\xi}/\partial n$ is the mean normal vorticity gradient. The above equation can be further reduced assuming

$$\frac{\partial \bar{\xi}}{\partial n} \sim \frac{-\bar{\xi}}{b'/2} = \frac{-\Gamma}{b'/2}$$

$$\ell \sim b'/2$$

so that

$$\overline{u'\xi'} = k\, q\, \Gamma/A \tag{2.36}$$

where k is a constant and A is the area of the vortex cell. Substituting Eqs. (2.36) into (2.34) the circulation equation becomes

$$d\Gamma/dt = - k\, q\, e \frac{\Gamma}{b'/2} \tag{2.37}$$

where e is a measure of the "eccentricity" of the vortex cell, $e = Pb'/2A$ which was tabulated earlier in Fig. 2-12 . For $k\, e = 0.41$, Eq. (2.37) is identical to the expression derived by Donaldson (Eq. (5.24)), Ref. 30 using the second order closure model.

In order to evaluate the above expression, it can be assumed that volume loss is equivalent to vorticity loss (Ref. 30)

$$\Gamma(0)\, b'(0) = \Gamma(t)\, b'(t) \tag{2.38}$$

implying that vorticity which is transported across the cell boundary is either cancelled or left behind in the wake. Applying this boundary condition to Eq. (2.37), and holding the vortex geometry e fixed with time the solution is given by

$$\Gamma(t) = \Gamma(0) \left\{ \frac{k\, q\, e\, t}{b'(0)/2} + 1 \right\}^{-1} \tag{2.39}$$

In terms of the vorticity detrainment model developed earlier, the Late Stage growth of the vortex core is prescribed by Eq. (2.39).

To summarize the complete model, for a vortex with a fixed arbitrary cross-sectional geometry, vorticity detrainment occurs based on the following criteria:

$$\Gamma(t) = \Gamma(0) \quad \text{if} \quad \frac{b'(t)}{2} > (r^2(0) + 5.04\ \nu_T t)^{1/2} \tag{2.40}$$

$$\Gamma(t) = \Gamma(0)\left\{\frac{k\ q\ et}{b'(0)/2} + 1\right\}^{-1} \quad \text{if} \quad \frac{b'(t)}{2} \leq (r^2(0) + 5.04\ \nu_T t)^{1/2} \tag{2.41}$$

The circulation equation shown above describes the effect of turbulent diffusion on the overall vortex growth and decay process. The influence of ground proximity and turbulence is handled through the parameters b', ν_T, q and e. For the more general case of a vortex pair whose cross-sectional geometry, e, also changes as a function of time, it is necessary to integrate Eq. (2.37) directly as a function of time during the vortex transport process.

In addition to the turbulent decay mechanism, linking and bursting instabilities are often responsible for the wake vortex breakup. As shown by Crow (Ref. 38) mutual and self-induction effects can cause the vortex to undergo a sinusoidal instability when outside perturbations such as atmospheric turbulence disturb the relative location of the vortex pair. The sinusoidal modes produce a periodic linking of the vortex pair followed by a rapid decay or bursting of the ring-shaped segments. When the relative effect of atmospheric turbulence on the linking instability is taken into account, a universal vortex lifetime function can be derived (Refs. 32 and 39) of the following form

$$\eta_1 = 0.00271\ \frac{\tau_1^{3/4}}{e^{2.49\tau_1}} \tag{2.42}$$

$$\eta_1 = \epsilon_1 (b')^4/\Gamma^3$$

$$\tau_1 = T_\ell\ \Gamma/2\pi\,(b')^2$$

where the circulation strength and spacing of the vortex pair are Γ and b', the turbulent dissipation ϵ_1, and the time to vortex linking is T_ℓ.

The universal vortex lifetime model presented above demonstrates reasonable agreement with the vortex linking time observed for light aircraft in weakly turbulent weather conditions as shown in Fig. 2-16. In order to extend the universal vortex lifetime concept to more turbulent conditions and different aircraft classes, an empirical model has been developed which is depicted in Fig. 2-17.

For the purposes of the present study, a simple relationship has been selected to predict vortex lifetime as a function of turbulent dissipation rate,

$$T_\ell = \frac{L_1}{L_2 \epsilon_1^{1/3} + L_3} \tag{2.43}$$

where the L's are constants which are a function of the vortex strength and spacing of the trailing vortex pair. It is recognized that ground plane proximity alters the basic vortex link instability so that looping occurs with the image vortices and this area is the subject of continuing investigation. It is anticipated that future wake measurements conducted by Lockheed-Huntsville and others under the DOT-TSC program studying wake decay near the ground will be used to verify the above simplified model.* Until additional results are obtained, the vortex lifetime relationship given in Eq. (2.43) and shown in Fig. 2-17 with L_1 = 120 sec, L_2 = 1 sec/cm$^{2/3}$, L_3 = 1 will be utilized in the Predictive Wake Vortex Transport Model to determine the maximum lifetime of the wake hazard as a function of ambient atmospheric conditions. A distinction is not made in the selected lifetime model between different aircraft types since the predicted variations in vortex lifetimes between heavy and light commercial transports is on the order of 10%, which is less than the typical scatter in the observed vortex lifetime (see Fig. 2-16).

*During the writing of this report, results have been published indicating that the above vortex lifetime is shortened by approximately 10% when ground plane proximity is included in the analysis (Tombach, I. H., S. C. Crow, and E. R. Bate, Jr., "Investigation of Vortex Wake Stability Near the Ground," AFOSR TR-75-1501, 31 July 1975).

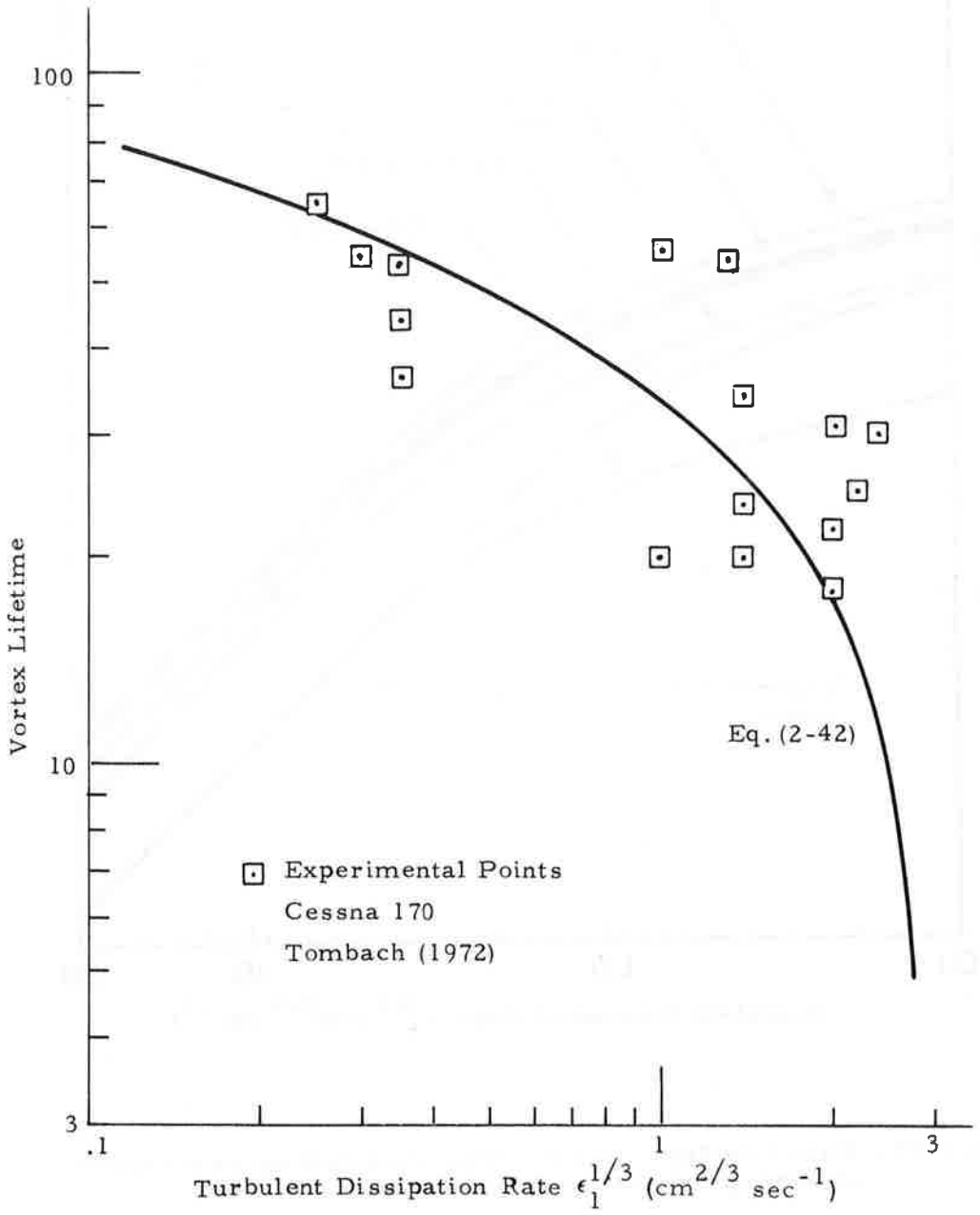

Fig. 2-16 - Comparison of Predicted and Observed Time-to-Linking (Ref. 32)

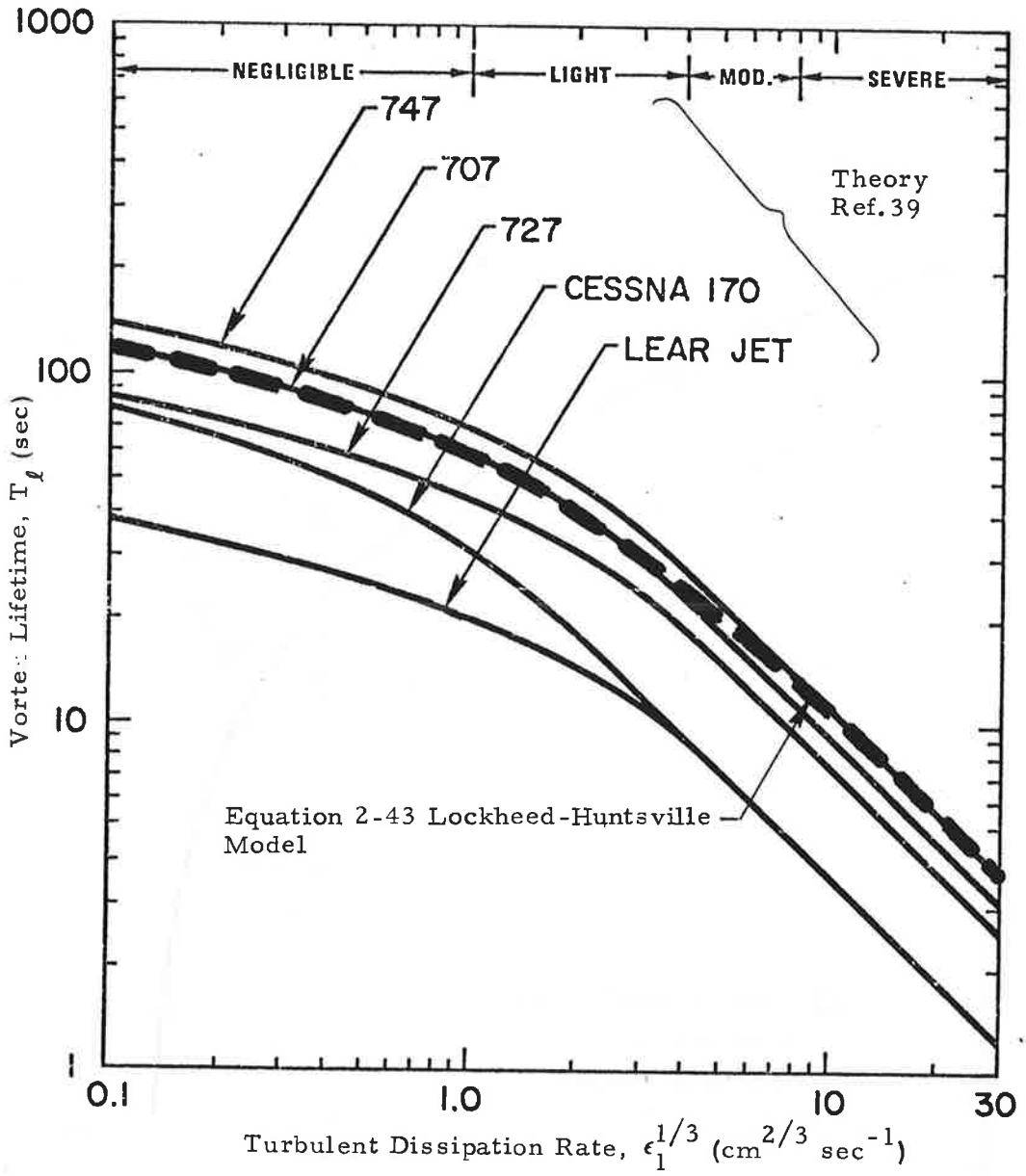

Fig. 2-17 - Wake Life Span Due to Vortex Pair Linking as a Function of Atmospheric Dissipation Rate (Ref. 39)

2.4 METEOROLOGICAL CONSIDERATIONS

Atmospheric conditions play an important role in defining terminal area wake conditions. As demonstrated earlier in Section 2.3, vortex lifetime is a function of the local atmospheric turbulence characteristics. In addition, vorticity detrainment and hence a decrease in circulation strength is prompted by atmospheric turbulence. Of course, the ambient winds can also carry the vortex out of the terminal area flight corridor or cause it to "stall" near the runway. On the basis of these effects, it is evident that the accurate simulation of the motion of wake vortices in a terminal area environment via the Predictive Wake Vortex Transport Model requires accurate forecasting of the ambient meteorological conditions. In previous work at Lockheed-Huntsville (Refs. 7 and 9) a meteorological characterization has been developed for wake vortex transport utilizing the measurements provided by the DOT-TSC ground wind propeller anemometer and MET tower sensor arrays at JFK International Airport. Under the present research effort, the meteorological model has been updated using the analytic and probabilistic descriptions of low altitude mean wind and turbulence given in Ref. 40. A meteorological model has been developed which can utilize available DOT-TSC or NOAA ground wind observations to specify the wind and turbulence profile necessary for predicting terminal area wake vortex transport. The following is a summary of the meteorological model developed for the Predictive Wake Vortex Transport Model.

2.4.1 Mean Wind Profile

$$\bar{u} = \bar{u}_{20}\, Y_1 \left[\ell n\left(\frac{h}{Z_o} + 1\right) + Y_2 - \left(\frac{h_w}{d}\right) Y_3 \right] \qquad (2.44)$$

which is selected from Ref. 40, where the elements are defined as follows:

$\bar{u}_{20}$ = horizontal mean wind speed at 20 ft

h = specified height in ft

d = atmospheric boundary layer thickness = $2000\, u_{*_o}$ in ft

Z_o = roughness length

$$h_w = \begin{cases} h & \text{if } h < d \\ d & \text{if } h \geq d \end{cases}$$

$$Y_1 = \frac{u_*/\kappa}{\bar{V}_{20}}$$

$$Y_2 = f\,(h/\ell')$$

$$Y_3 = g\,(h/\ell')$$

and where u_* and κ are the friction velocity and the von Karman constant, respectively.

For the sake of convenience, the wind profile (and Richardson number) is referenced to the measurements at the 20 ft level above the ground since the NOAA surface wind speed observations are available at this height. However, the selected wind shear model is general and any selected reference height within the boundary layer is acceptable. The functions Y_1, Y_2 and Y_3 are given in Figs. 2-18, 2-19 and 2-20 where h/ℓ' is the Monin-Obukhov similarity parameter. The functional relationship of h/ℓ' versus Ri_{20} is given in Fig. 2-21. For a detailed derivation of Eq. (2.44) the reader is directed to Ref. 40.

In combination with available meteorological measurements, the above equation is used as the fundamental meteorological wind profile for modeling advective vortex wake behavior in the natural environment. Equation (2.44) has been incorporated into the Predictive Wake Vortex Transport Model. Sample results from this model showing the wind profiles versus altitude at various Richardson numbers are presented in Fig. 2-22. A 15 ft/sec wind speed at the 20 ft level is shown in Fig. 22 which is representative of the daytime mean wind speed observed during the JFK vortex monitoring tests in the spring of 1975. The results indicate that as the positive Ri_{20} increases, the wind speed increases; while as the negative Ri_{20} decreases the wind speed reduces slightly. This is attributed to the buoyancy force increasing the momentum along the vertical direction. The computed wind profiles are similar to the results of Ref. 40, and sensitivity of the selected wind profile to the measured Richardson number can be noted from Fig. 2-22.

In addition to the mean wind profile, the vertical gradient of the wind, a wind shear, is also essential to the modeling of vortex transport

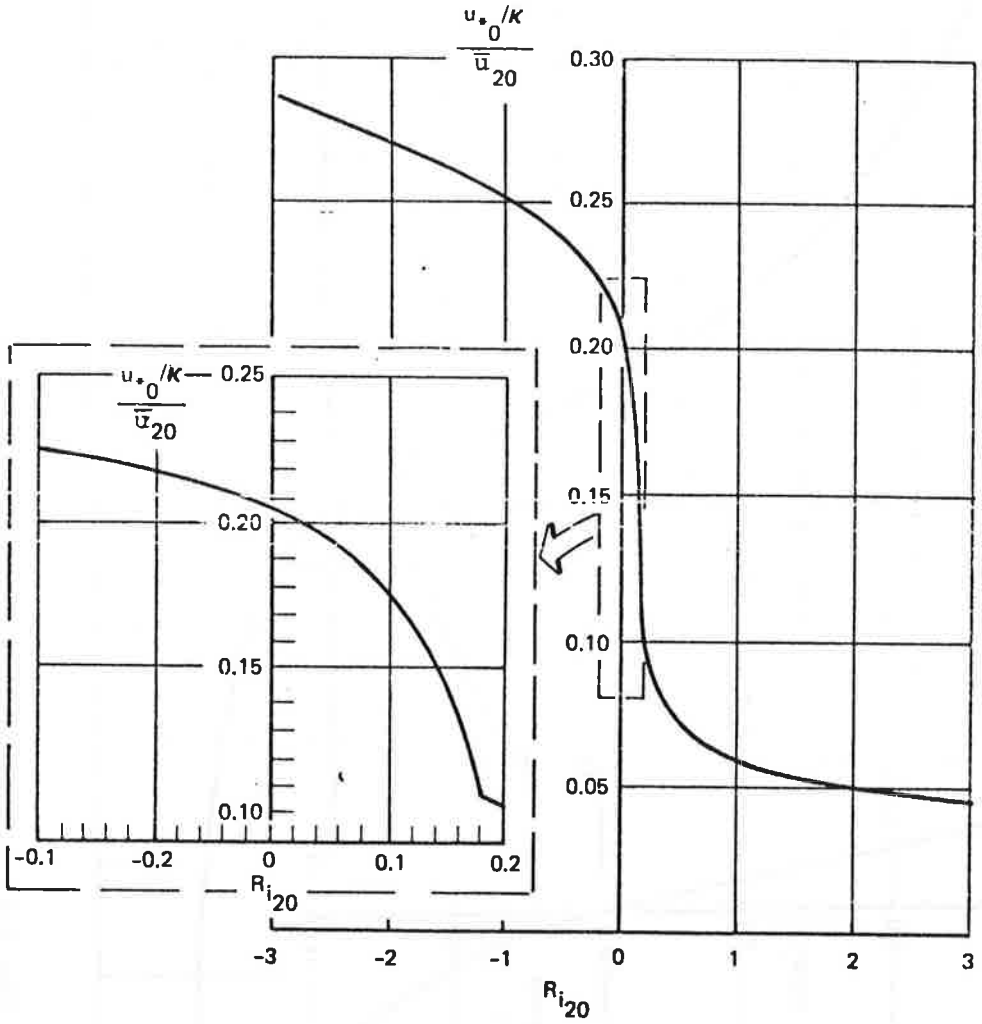

Fig. 2-18 - Mean Wind Proportionality Constant, Y_1 (Ref. 40)

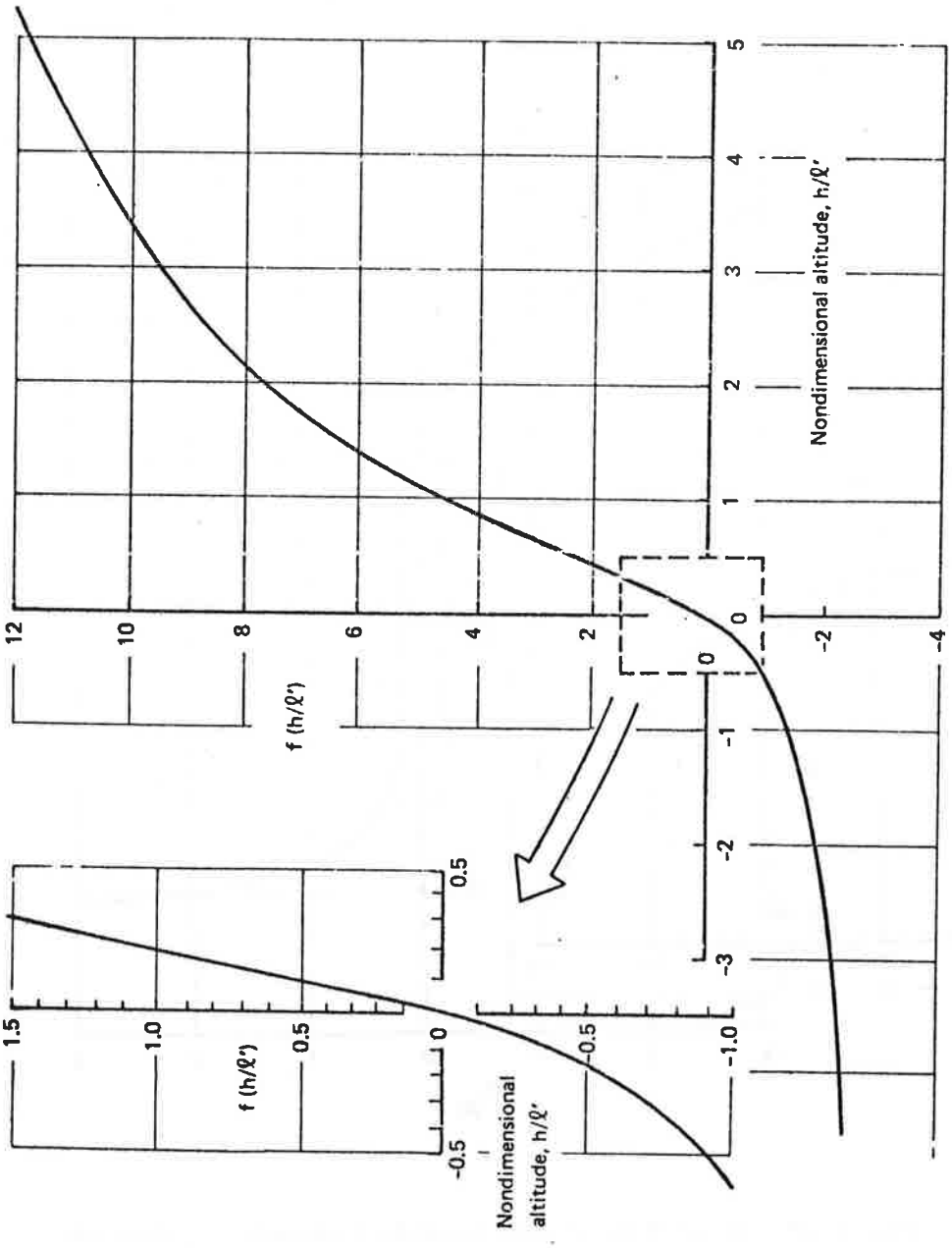

Fig. 2-19 - Contribution of Non-Neutral Stability to Mean Wind, Y_2 (Ref. 40)

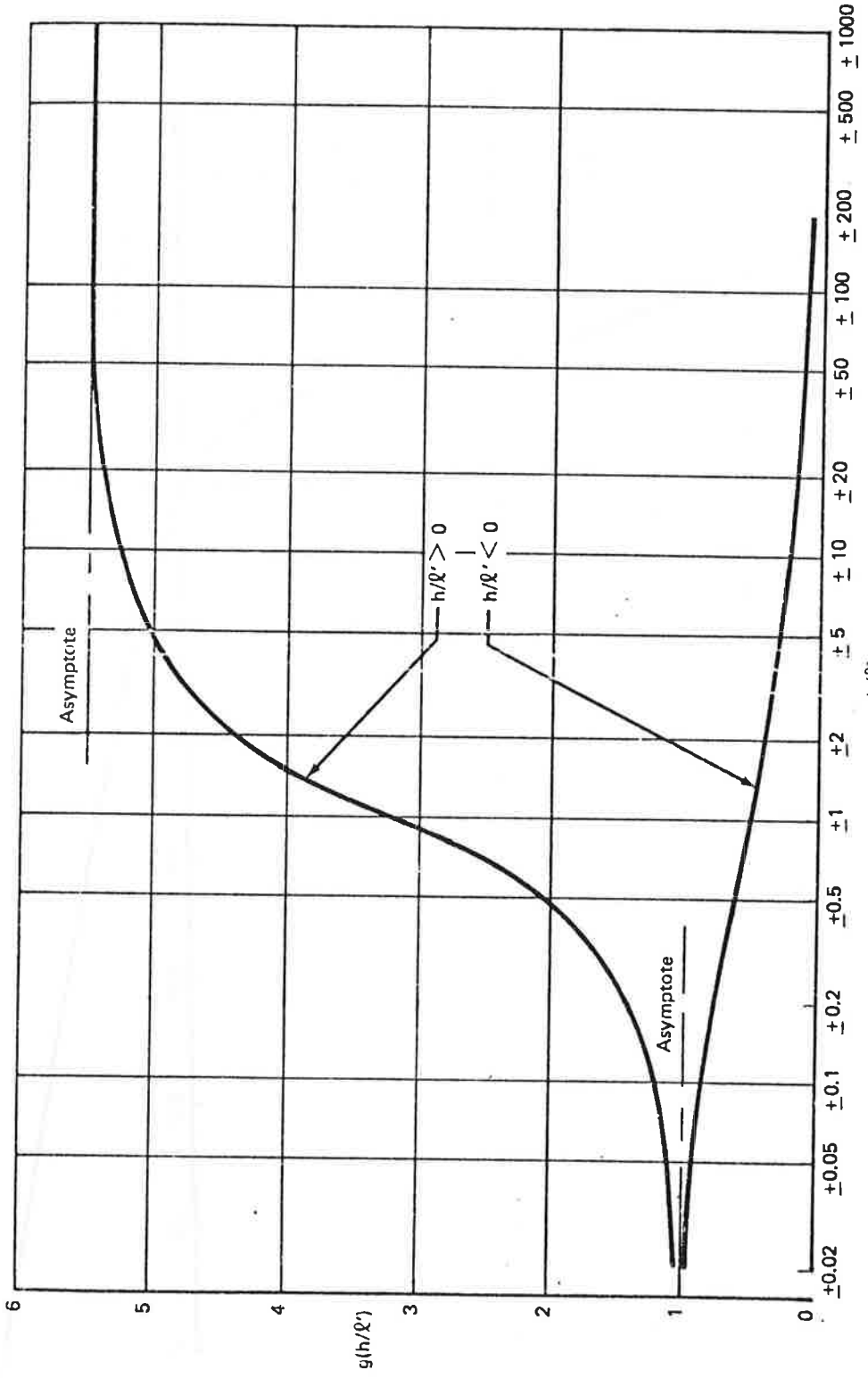

Fig. 2-20 - Variable Shear Stress Correction to Wind Profile, Y_3 (Ref. 40)

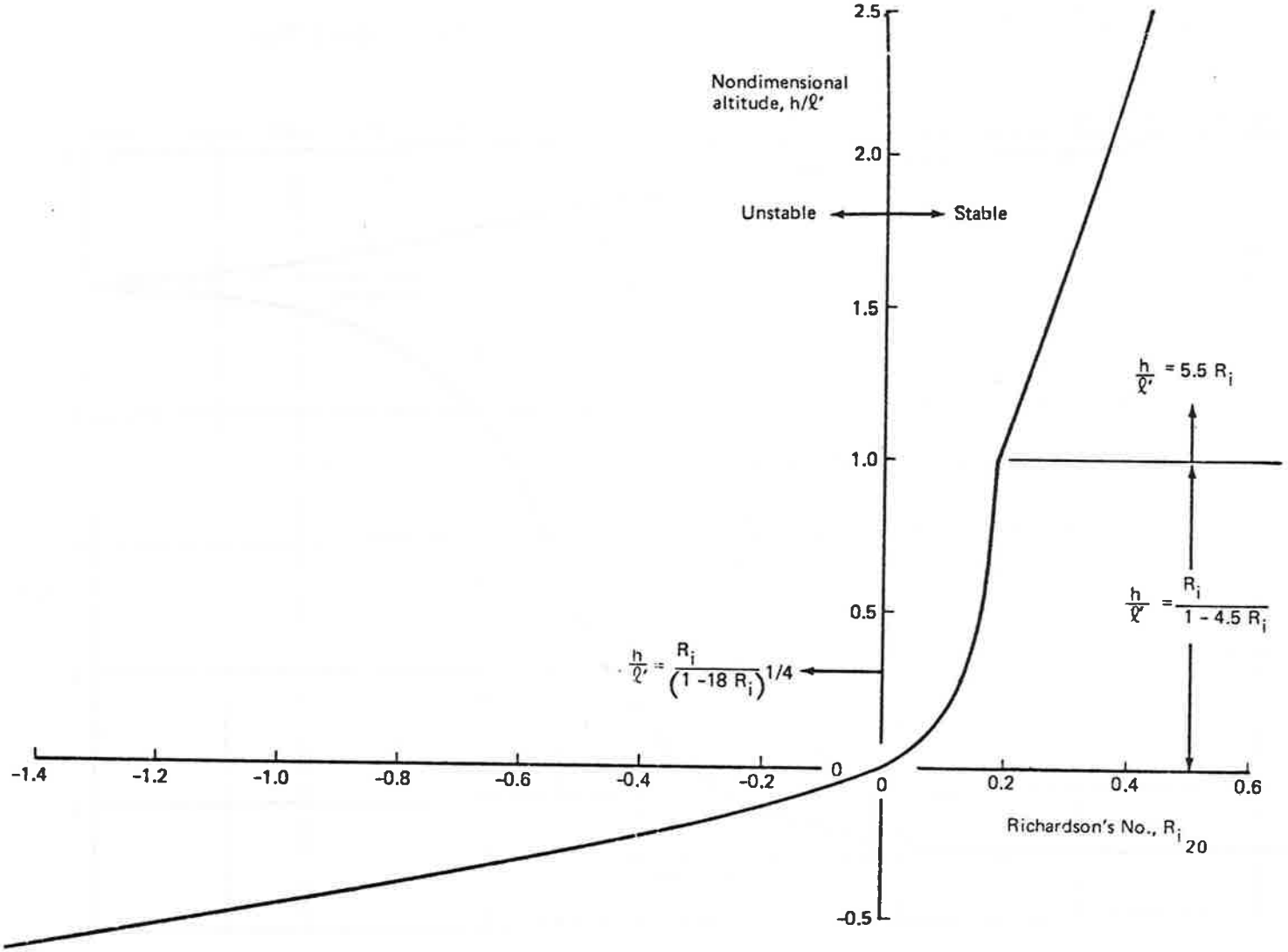

Fig. 2-21 - Low Altitude Richardson Number Profile (Ref. 40)

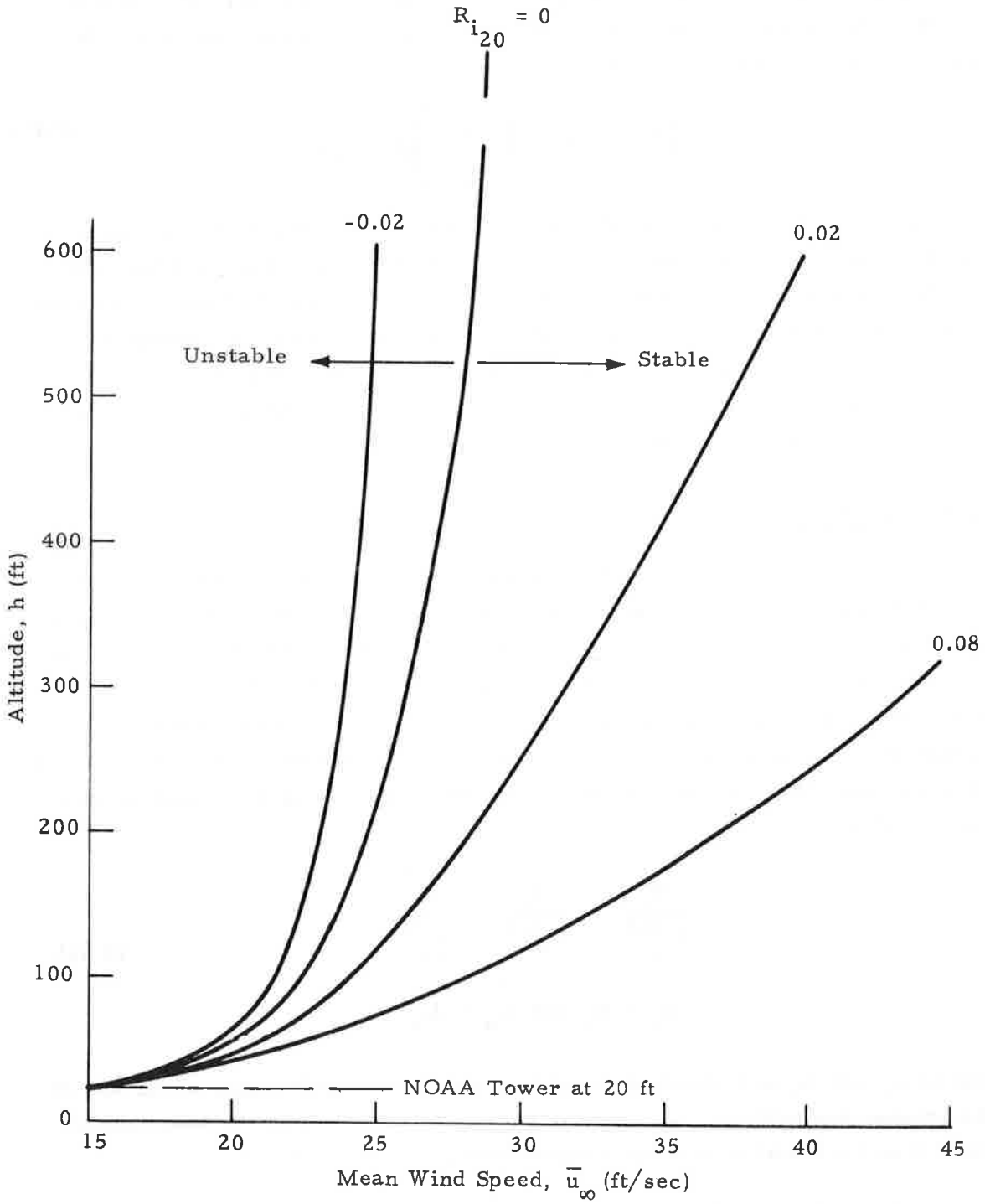

Fig. 2-22 - Example of Predicted Horizontal Mean Wind Profile as a Function of Richardson Number

and decay phenomena. Differentiating the previous expression (Eq. (2.44), for $R_i \sim 0$, the mean shear profile in terms of the functions tabulated in Figs. 2-18 and 2-20 is given by

$$\frac{\partial \bar{u}}{\partial h} = 0.4\, \bar{u}_{20} \left(\frac{u_{*_o}/\kappa}{\bar{u}_{20}} \right) \left(1 - \frac{h_w}{d} \right) Y_3 \tag{2.45}$$

The above expressions, Eqs. (2.33) and (2.45), summarize the mean wind and wind shear profile incorporated into the Predictive Wake Vortex Transport Model. The sensitivity of the selected wind profile to the Richardson number has been illustrated earlier in Fig. 2-22. However, it is recognized that complete verification of the selected wind profile requires comparison with observed wind measurements for a range of reference heights, velocities, roughness lengths, and Richardson numbers.

2.4.2 Turbulence

Ambient turbulence is a particularly important wake transport and decay parameter. As noted earlier in Refs. 32 and 33, vortex linking and bursting show a very strong correlation with atmospheric turbulence and winds. For the purpose of the Predictive Wake Vortex Transport Model, von Karman turbulence spectrum has been chosen to model the natural atmospheric wind shear and turbulence profiles. In the isotropic von Karman turbulence model, it is assumed that the spectra have different integral scales for each component so that

$$\frac{\sigma_u^2}{L_u^{2/3}} = \frac{\sigma_v^2}{L_u^{2/3}} = \frac{\sigma_w^2}{L_w^{2/3}} \tag{2.46}$$

$$\sigma_u = \sigma_v \text{ and } L_u = L_v$$

where σ_i and L_i are standard deviations and the integral scales along u, v, w directions, respectively; and u, v and w are the velocities in the longitudinal lateral and vertical directions, respectively.

On the basis of Ref. 43 it is postulated that the standard deviations follow the empirical form

$$\frac{\sigma_u}{\sigma_w} = \frac{\sigma_v}{\sigma_w} = \left\{ \begin{array}{ll} \dfrac{1}{\left(0.1777 + 0.823\ \dfrac{h}{h_I}\right)^{0.4}} & , \quad h < h_I \\ 1 & , \quad h \geq h_I \end{array} \right\} \tag{2.47}$$

with $h_I = 1000$ ft.

The variance of the vertical component of turbulence is given as

$$\frac{\sigma_w}{u_*} = f\left(\frac{h}{\ell'}\right) \tag{2.48}$$

and is prescribed in Fig. 2-23. Note that σ_w decreases as h/ℓ' increases and $h/\ell' = 1.22$ corresponds to the critical Richardson number, $R_{i_{20}} \cong 0.14$.

The vertical integral scale is given as

$$L_w = \left\{ \begin{array}{ll} h & , \quad h < h_I \\ h_I & , \quad h \geq h_I \end{array} \right. \tag{2.49}$$

and the analysis is limited to the planetary boundary layers, $h < h_I$ with

$$L_u = L_v = L_w \left(\frac{\sigma_u}{\sigma_w}\right)^3 \tag{2.50}$$

Figure 2-24 describes the variances at various altitudes and Fig. 2-25 describes the integral scales.

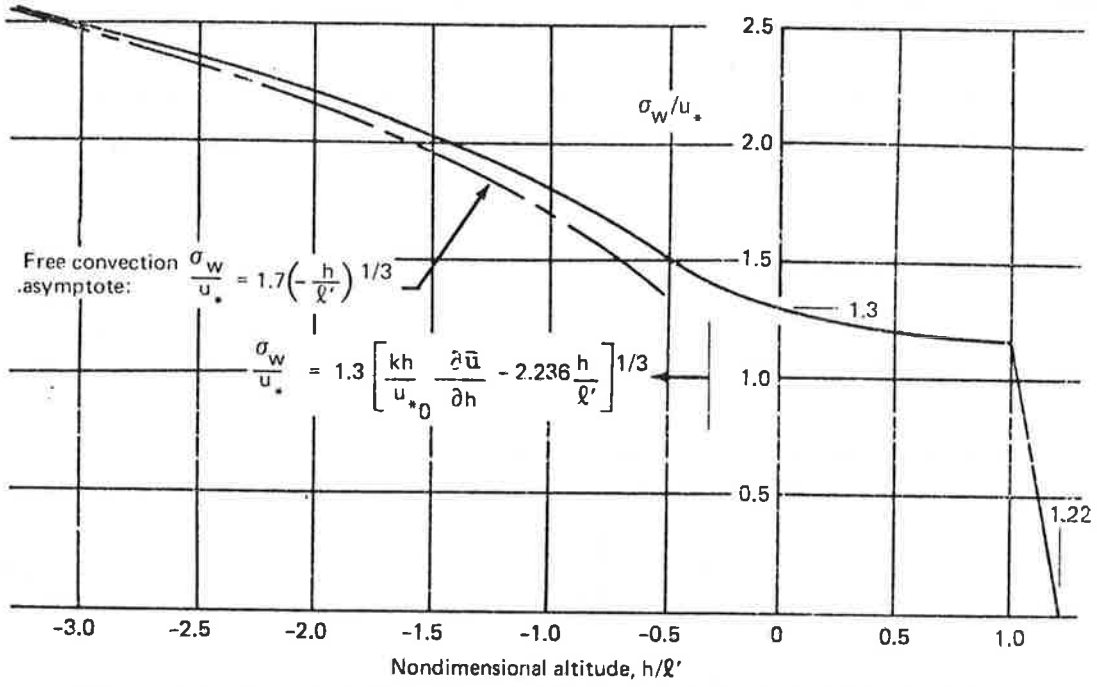

Fig. 2-23 - σ_w/u_* Variation with Stability (Ref. 40)

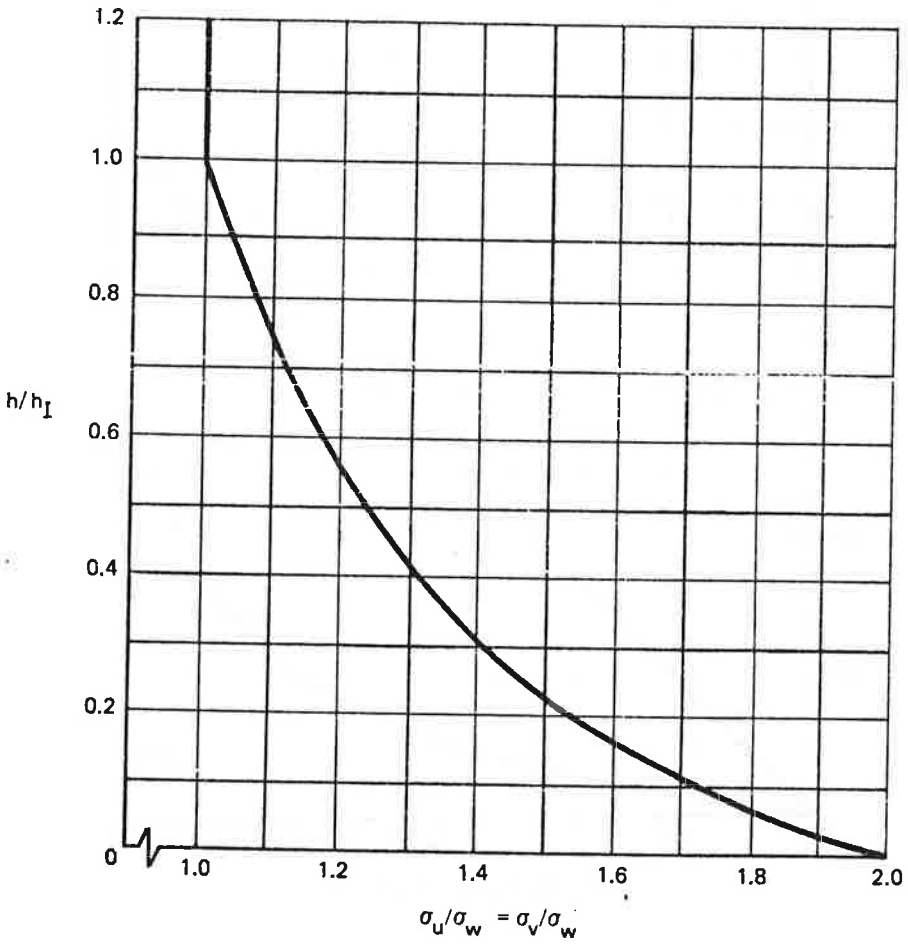

Fig. 2-24 - Selected Description for Variances of Horizontal Turbulence Components (Ref. 40)

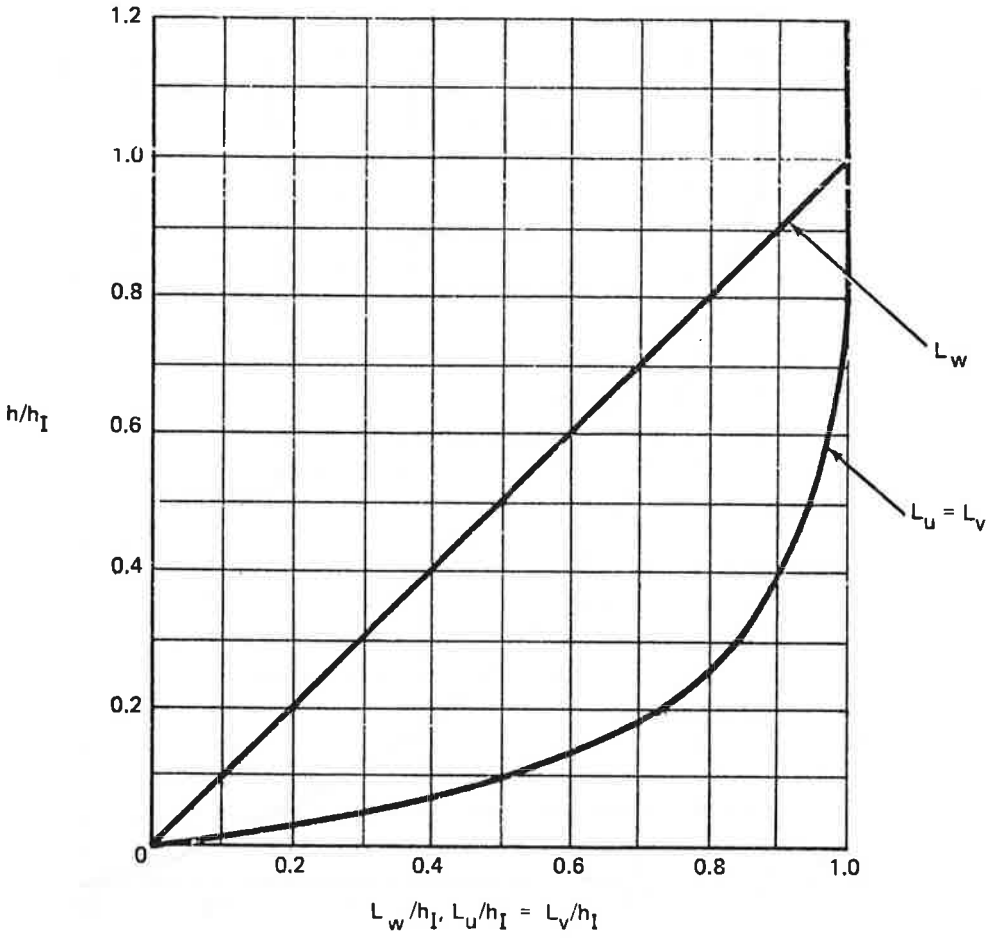

Fig. 2-25 - Selected Integral Scale Description (Ref. 40)

The power spectra for the turbulence field is specified by

$$\Phi_u = \frac{\sigma_u^2 L_u}{\pi} \frac{1}{\left[1 + (a L_u \Omega_1)^2\right]^{5/6}} \tag{2.51}$$

$$\Phi_v = \frac{\sigma_v^2 L_v}{2\pi} \frac{1 + (8/3)\ (a\Omega_1 L_v)^2}{\left[1 + (a L_v\ \Omega_1)^2\right]^{11/6}} \tag{2.52}$$

$$\Phi_w = \Phi_v \qquad a = 1.339 \tag{2.53}$$

where Ω_1 is the component of the spatial frequency in the u direction.

The cospectrum is given by

$$\Phi_{uw}(\Omega_1) = \frac{u_*^2 V_A}{2(1/T_1)} \frac{\sqrt{\left[\frac{\pi}{\sigma_u^2 L_u} \Phi_u(\Omega_1)\right]\left[\frac{2\pi}{\sigma_w^2 L_w} \Phi_w(\Omega_1)\right]}}{\left\{1 + \ell n\left[\frac{2V_A}{\left(\frac{1}{T_1}\right) L_u}\right]\right\}\left[1 + \left(\frac{V_A \Omega_1}{1/T_1}\right)^2\right]^{1/2}} \tag{2.54}$$

where $\frac{1}{T_1} = 0.4 \frac{\partial \bar{u}}{\partial h}$, $\partial\bar{u}/\partial h$ was described earlier in Eq. (2.45), and $V_A = 0.3264\ \bar{u}_{20}$ which is a characteristics airspeed (described in Ref. 40).

The power spectra specified in equations (2.51) through (2.53) are a measure of the turbulent energy $\bar{u}'^2$ and $\bar{v}'^2$ and $\bar{w}'^2$ while the cospectrum, given by Eq. (2.54), is an approximate measure of the shear stress. Although not used in the current Predictive Model, they are included for future possible uses. It can be shown that when the density fluctuations are neglected (Ref. 43) the local shear stress is the integral of the cospectrum over the total frequency range.

$$\frac{\tau}{\rho} = u_*^2 = -\overline{u'w'} = -\int_{-\infty}^{\infty} \Phi_{uw}(\Omega_1)\, d\Omega_1 \qquad (2.55)$$

The cospectrum is plotted as a function of spatial frequency in Fig. 2-26. Note that the cospectrum is not sensitive to altitude within the atmospheric boundary layer and the variations in the cospectrum occur mainly at low spatial frequencies.

In order to update and to expand the capabilities of the Predictive Wake Vortex Transport Model; the comprehensive atmospheric wind, wind shear, and turbulence characteristics presented in Eqs. (2.44) through (2.55) have been incorporated into the analytic model. Sensitivity of the wake transport to these atmospheric variables as well as other effects is considered in the following section.

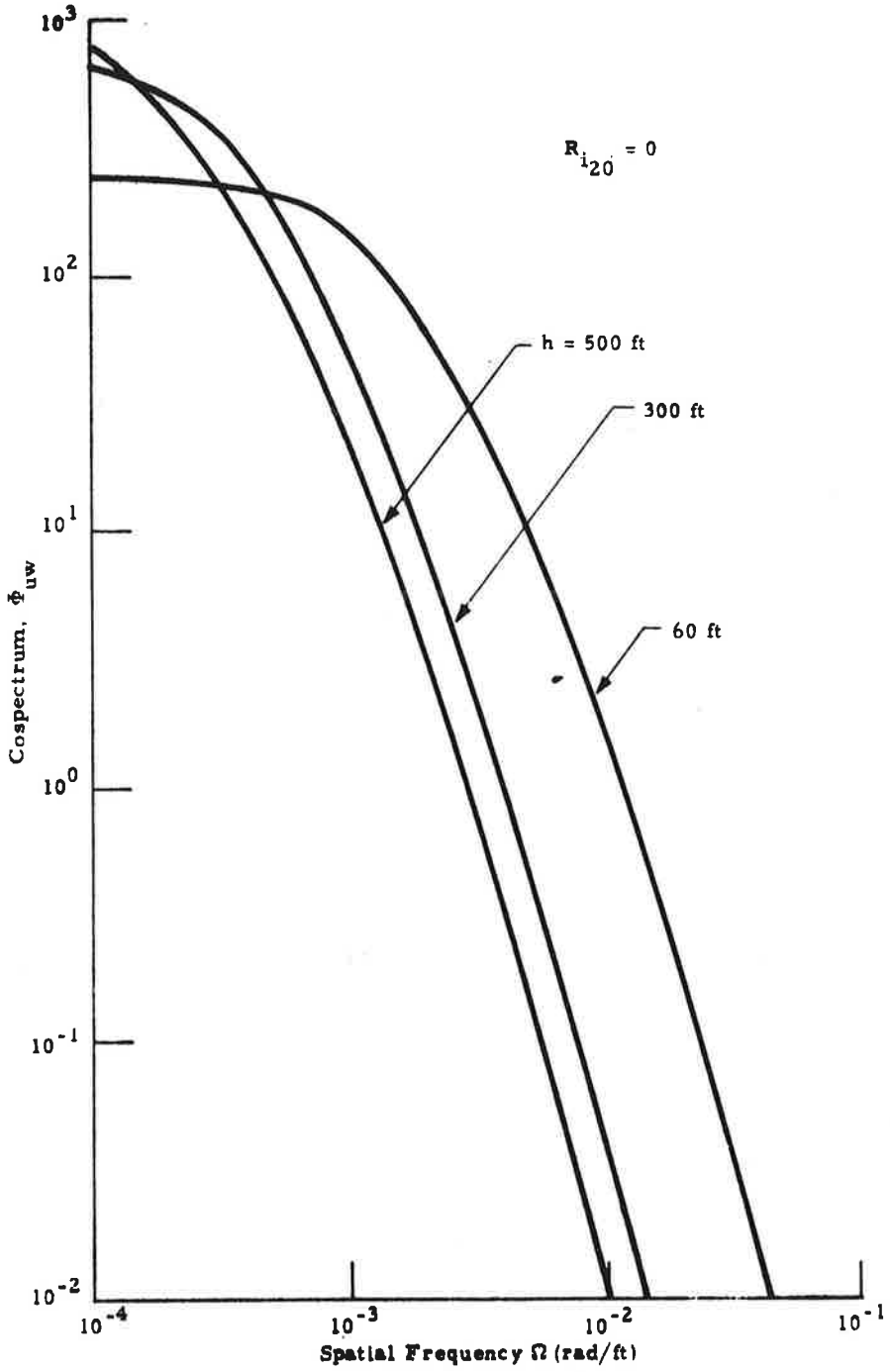

Fig. 2-26 - Cospectrum Shape (Ref. 40)

3. COMPARISON OF PREDICTED AND OBSERVED VORTEX TRACKS

In addition to incorporating candidate groundwind shear turbulence, and vortex lifetime models into the Lockheed-Huntsville Predictive Wake Vortex Transport Model, as summarized in Section 2, efforts have been made to assess the impact of each of the model updates by comparing the predicted vortex tracks with available experimental measurements. The influence of spanwise loading, buoyancy, vorticity detrainment, vortex lifetime, and wake tilting on vortex transport and decay is considered in this section. Wherever possible, the updated theoretical model has been verified by comparison with actual observed vortex tracks. As an alternative, in cases where the influence of specific parameters could not be isolated from the experimental data base, efforts have been made to establish the range of variations predicted by the theoretical model to assess their significance.

3.1 METEOROLOGICAL CONSIDERATIONS

In order to compare the Predictive Model with observed vortex trajectories, it is necessary to define the ambient meteorological conditions accurately as an input to the calculations. Thus, an important consideration of the Predictive Wake Vortex Transport Model is how well it predicts the actual wind and turbulence profiles. In the following discussion, comparison is made between the theoretical meteorological model developed in Section 2.4 and available measurements from JFK International Airport.

Since turbulence covers all wavelengths in the spectral analysis, and some suppression occurs due to ground proximity for the longer wavelengths of turbulent motion, it is important to decide what wavelength is suitable for wake vortex prediction. Our assumption is that the turbulence is in the inertial subrange of eddy sizes. According to Kolmogorov's similarity hypothesis it

suggests that all properties of turbulence are described by the turbulent diffusivity coefficient ϵ_1. Thus, the measurement of ϵ_1 becomes quite useful for our vortex predicting system. During wake vortex tests at JFK International Airport, FAA aircraft N9093P conducted wind speed, temperature and turbulent diffusivity measurements during take-off, level flight, and ILS landing maneuvers using onboard instrumentation. The turbulent diffusivity coefficient and temperature profile as measured from the sounding aircraft during take-off is presented in Fig. 3-1. The corresponding winds aloft observed during this flight from time 0946 to 1013 are presented in Fig. 3-2. The ground wind given by the control tower for this same time period was 10 knots (on the basis of the 20 ft NOAA surface wind measurements) as shown by the dashed line near the bottom of the figure.

To compare the theoretical model of the mean wind profile with experimental data, the theoretical model must first be able to compute the Richardson number and the mean wind speed near the ground. The gradient Richardson number is defined as (Ref. 40)

$$Ri = \frac{g}{T} \frac{(\partial T/\partial h + g/C_p)}{(\partial u/\partial h)^2} \tag{3.1}$$

where

T = absolute temperature, ^{o}R
C_p = specific heat at constant pressure = 0.24 Btu/lbm-^{o}R
g = gravitational constant = 32.17 ft/sec^2
$\bar{u}$ = horizontal mean wind speed, ft/sec

On the basis of Eq. (3.1), the Richardson number has been computed for the 20 ft level for a sample wake vortex test (JFK 4/22/74/F-1) where FAA MET sounding measurements were made of the temperature (and turbulent diffusivity). The observed temperature and turbulent diffusivity profiles are shown in Fig. 3-1. For this case, the Richardson number is determined to be $Ri_{20} = -0.0005$. Using the above Richardson number and the observed NOAA surface wind speed at 20 ft altitude, the theoretical wind shear profile derived in Section 2.4 can be applied. The predicted wind profile and experimental tower measurements are compared in Fig. 3-2.

Location: New York, JFK
Date: 22 April 1974
Flight No.: F-1
Time: 0933

Takeoff Climb Data FAA
MET Sounding Aircraft
Wake Vortex Tests

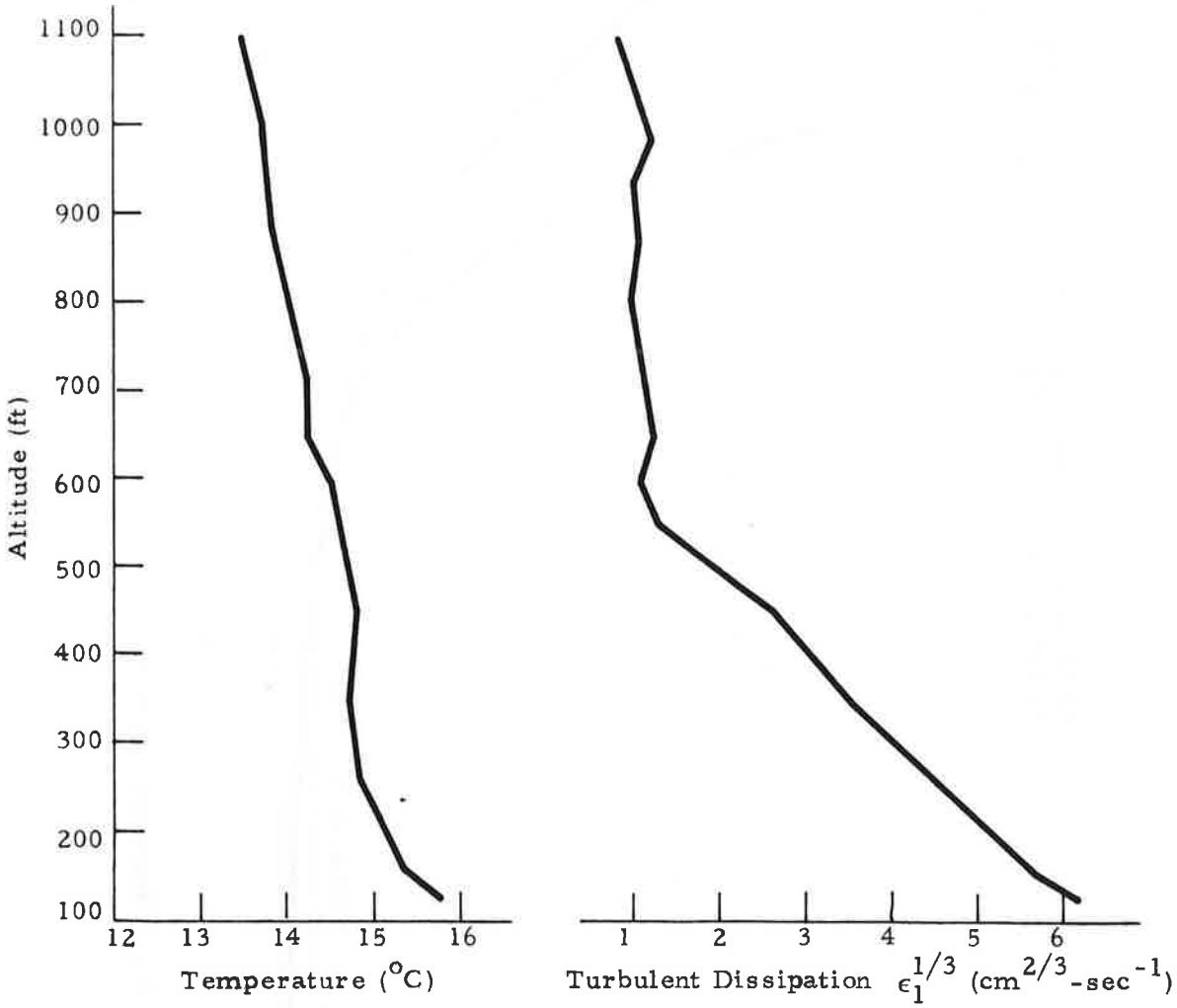

Fig. 3-1 - Meteorological Measurements Obtained by DOT-TSC at JFK

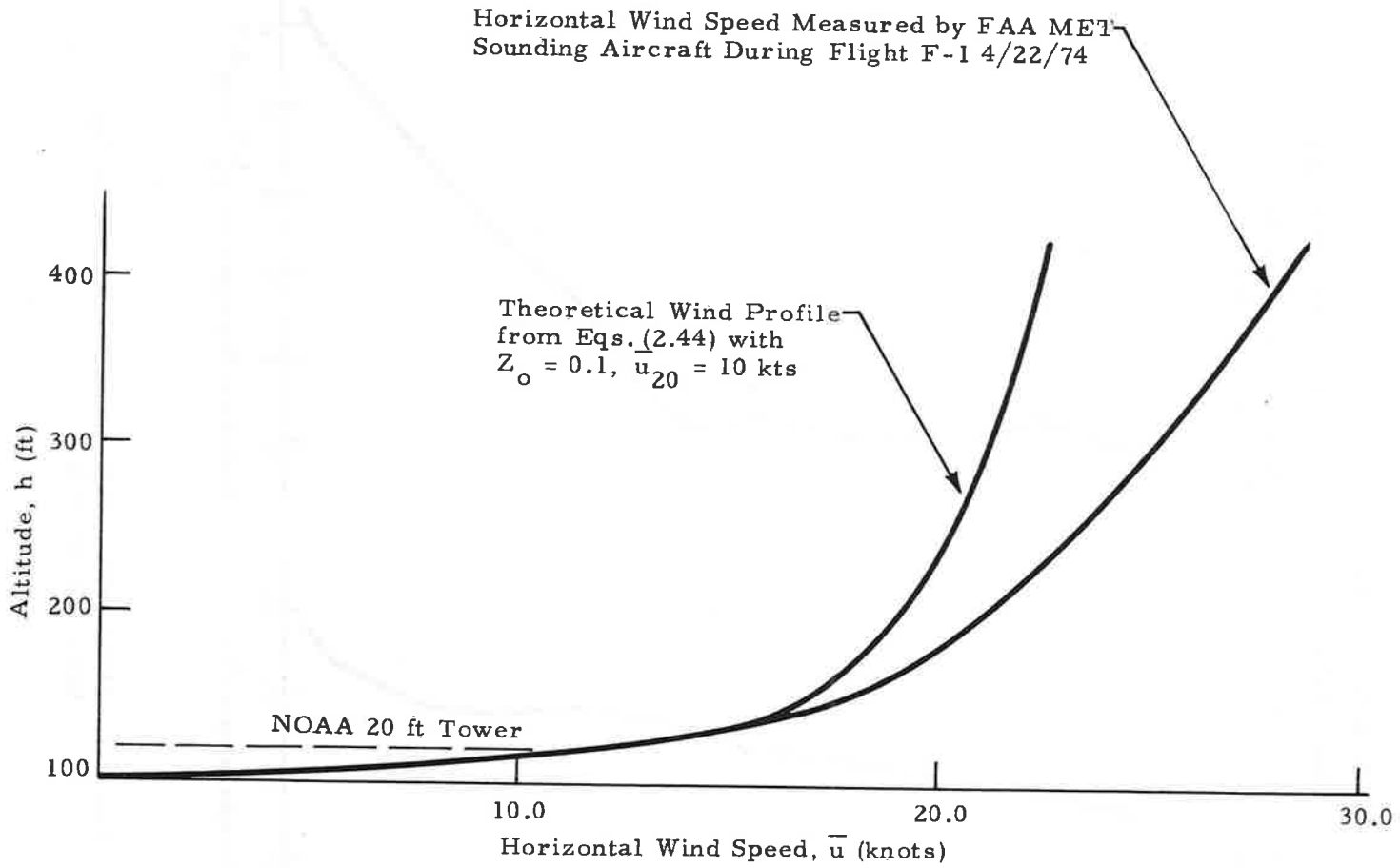

Fig. 3-2 - Observed and Predicted Mean Wind Profile for JFK International Airport

As shown by the curves in Fig. 3-2, the analytic wind shear profile determined from the Richardson number and the observed NOAA 20 ft surface wind spped correlates well with the actual wind shear measurements over the range $h>0$ to 150 ft where hazardous wake vortex encounters can occur (Ref. 1). At altitudes above 150 ft, the theoretical model tends to underestimate the magnitude of the wind field which is attributed to the low selected reference altitude (20 ft). The use of a high altitude reference wind speed would improve the correlation above 150 ft but the penalty would be reduced accuracy in the low altitude range. For wake vortex monitoring, the altitude range of interest is 50 to 200 ft so that a reference altitude within this range would be more suitable.

For this particular JFK wind shear survey, it is also possible to compare the turbulence profile predicted by the theoretical model developed in Section 2.4 using the 20 ft level Richardson number and mean wind speed as input parameters with the measured vertical turbulence profile. The turbulent kinetic energy in equilibrium can be approximated by the following equation (see Ref. 42)

$$\epsilon_l = C_u + C_t \tag{3.2}$$

where

$C_u = u_*^2 \, \partial\bar{u}/\partial h$ = velocity structure coefficient of turbulence = production of mechanical energy through wind shear

$C_t = gH/C_p \rho_o T$ = temperature structure coefficient of turbulence = production of energy through kinetic energy transport

Definitions of the terms in Eq. (3.2) are:

ϵ_l = turbulent dissipation rate, cm^2/sec^3
$\bar{u}$ = horizontal wind speed, cm/sec
u_* = friction velocity, cm/sec
H = heat flux, positive upward, cal/sec
T = absolute temperature, ^oK
ρ_o = atmospheric density, gm/cm^3

C_p = specific heat of constant pressure, cal/gm^{o}K
g = gravitational constant, cm/sec^2

Restricting the analysis to the nearly neutral case, i.e., $Ri_{20} \cong 0$ and $C_T \ll C_u$, it is found that

$$\epsilon_1 = u_*^2 \, \partial\overline{u}/\partial h \tag{3.3}$$

Both ϵ_1 and $\partial\overline{u}/\partial h$ are available from experimental data, so that the frictional velocity u_* can be determined. Equation (3.3) is valid close to the ground where all terms in the turbulent energy equation vanish (see Ref. 40, p. 208).

Near the surface layer, the variances are related to the frictional velocity by

$$\sigma_{u,v,w} = A_{u,v,w} \, u_* \tag{3.4}$$

In the nearly neutral air, Lumley and Panofsky suggest that (see Ref. 43):

$$A_u = 2.5$$
$$A_v = 2.5$$
$$A_w = 1.3$$

Based on the raw data of Fig. 3-1 and the wind shear profile of Fig. 3-2, the observed and predicted turbulence parameters are as follows:

Altitude (ft)	$\partial\overline{u}/\partial h$ (sec^{-1})	$\epsilon_1^{1/3}$ ($cm^{2/3}$-sec^{-1})	u_*/u_{*_o} (Theory)	u_*/u_{*_o} (Measured)	σ_u	σ_w
20	0.374	5.7	1.00	1.00	2.00	1.04
100	0.100	5.2	1.46	0.96	2.92	1.52
200	0.069	4.0	0.83	0.92	2.40	1.25
300	0.056	3.0	0.91	0.89	1.32	0.95

where the theoretical value of u_*/u_{*_o} is defined as

$$u_* = u_{*_o} (1 - h/d) \tag{3.5}$$

The above table shows that the frictional velocity computed from the theoretical model agrees with the observed frictional velocity in the altitude range 200 ft and above. Near the ground, at altitudes less than 100 ft, the nonisotropic turbulence field is not modeled as well.

As demonstrated for the case considered above, the theoretical wind shear and turbulence profile incorporated into the Predictive Model correlates reasonably well with the observed wind shear and turbulence profile.

3.2 INFLUENCE OF SPANWISE LOADING

The Predictive Wake Vortex Transport Model has been updated to include the effects of spanwise loadings as summarized in Eq. (2.18). Initial wake vortex sink rates are presented in Table 3-1 as computed by the Lockheed-Huntsville predictive model. In computing the vortex descent velocities for Table 3-1, the spanwise loading coefficient K was obtained from lifting surface calculations given in Ref. 29. The lift coefficient and airspeed in Table 3-1 were taken from typical NAFEC flight test measurements. Note that for the cases tabulated in Table 3-1, the value of K determined from the vortex lattice calculations is generally less than the theoretical value $K = \pi/4$ found for elliptically loaded wings. Thus, the flap effect model predicts consistently higher sink rates and smaller spacings than the simple elliptical representation. The last column in Table 3-1 indicates the time after vortex formation at which vorticity detrainment is initiated and the constant vortex sink rate model is no longer valid. This time will be considered in more detail later in Section 3.4.

To demonstrate the effect of spanwise loading variations on the wake vortex descent, sample calculations have been carried out using the elliptic and non-elliptic values for K in the Predictive Wake Vortex Transport Model

TABLE 3-1

INFLUENCE OF SPANWISE LOADING ON THE INITIAL VORTEX PARAMETERS

Aircraft	Config.	U_∞ (ft/sec)	C_L	K	b' (ft)	-dh/dt (ft/sec)	t^* (sec)
B747	TO	274	1.02	0.74	145	5.8	195
AR = 6.96	H	372	0.66	0.80	157	4.4	282
b = 196 ft	L	245	1.23	0.70	137	7.0	153
L-1011	TO	279	1.07	0.78	121	5.6	169
AR = 6.95	TA	267	1.20	0.74	114	6.7	134
b = 155 ft	L	241	1.51	0.71	110	8.3	104
DC-10	TO	257	1.21	0.63	98	9.2	83
AR = 6.95	TA	243	1.20	0.62	96	8.9	85
b = 155 ft	L	230	1.37	0.62	96	9.6	78
B-727	TO	216	1.59	0.70	76	7.8	77
AR = 7.20	H	346	0.60	0.67	73	5.1	112
b = 108 ft	L	211	1.64	0.67	73	8.5	67

Notes: HC – holding cruise configuration
L – landing configuration
TO – take-off configuration
TA – take-off approach configuration

*Detrainment

as shown in Figs. 3-3 through 3-7. For each case, the spanwise loading coefficient K has been computed from the aircraft lift coefficient based on the recorded NAFEC aircraft weight and airspeed and the lifting surface calculations given in Ref. 29. Comparing the vortex trajectories computed from elliptical loading assumptions and from the generalized model developed in Section 2.1, it is evident that the inclusion of flap effects produces a more accurate prediction. The recognition of non-elliptical loading effects results in faster descent rates which compare more favorably with available experimental measurements. Additional cases are presented in Appendix B.

The observed and predicted wake vortex trajectories are given in Appendix B for the same NAFEC B-747 runs analyzed earlier in Ref. 9 assuming an elliptical spanwise loading. A spanwise loading coefficient of $K = 0.6$ has been used for all of the calculations in Appendix B. It represents the minimum value of K anticipated during B-747 landing maneuvers and yields the maximum initial vortex descent rate and minimum vortex separation (the opposite of the elliptical loading case $K = 0.785$, which predicts the minimum descent rate and maximum vortex separation). Thus, the calculations in Appendix B and the previously published B-747 trajectories in Ref. 9 show the extreme effects of spanwise loading on vortex motion.

Comparing the present results in Appendix B with the previously published results from Ref. 9, (which have not been reproduced in this report for sake of brevity) it is found that the faster vortex descent rates corresponding to the non-elliptical loading case agree more closely with the observed wake vortex motion. However, for some of the cases the computed vortex descent based on $K = 0.6$ overpredicts the vortex sink rate. A spanwise loading coefficient of $K = 0.7$, approximately 90% of the elliptical coefficient, appears to fit the observed B-747 vortex trajectories more consistently.

3.3 INFLUENCE OF BUOYANCY

Considerable attention has been focused in the past on the influence of buoyancy on the wake transport and decay process. Density mismatch in the

• Experiment NAFEC B-747

——— Theory (No tilting, buoyancy or viscous core effects)

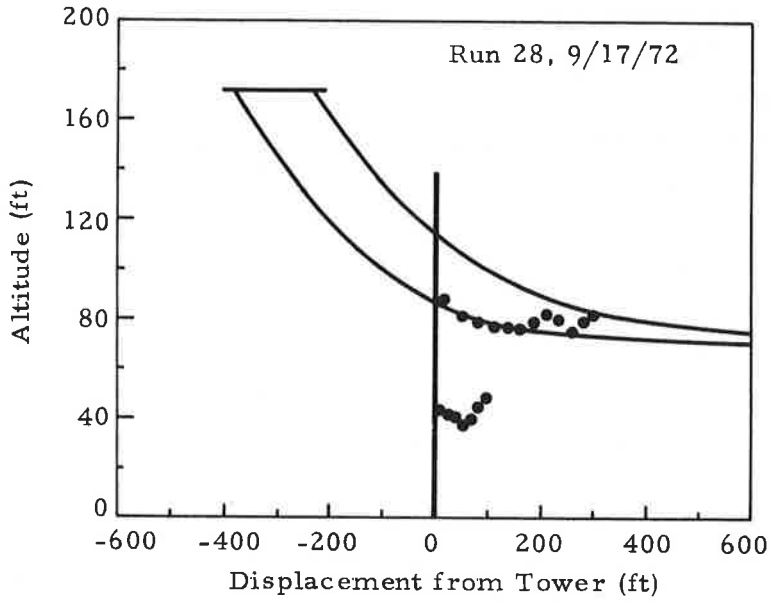

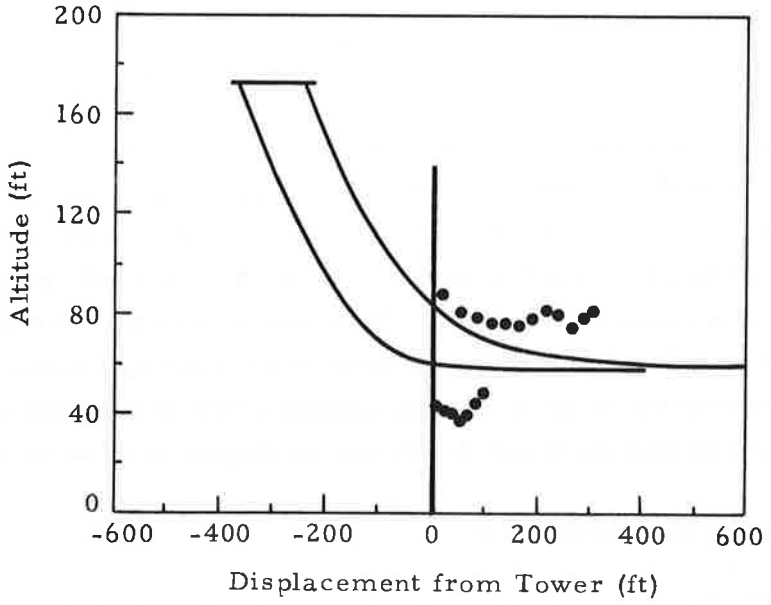

Fig. 3-3 - Predictive Wake Vortex Transport Code with Elliptic Loading, Top K = $\pi/4$, and with Flap Effects, Bottom K = 0.63 – Run 28

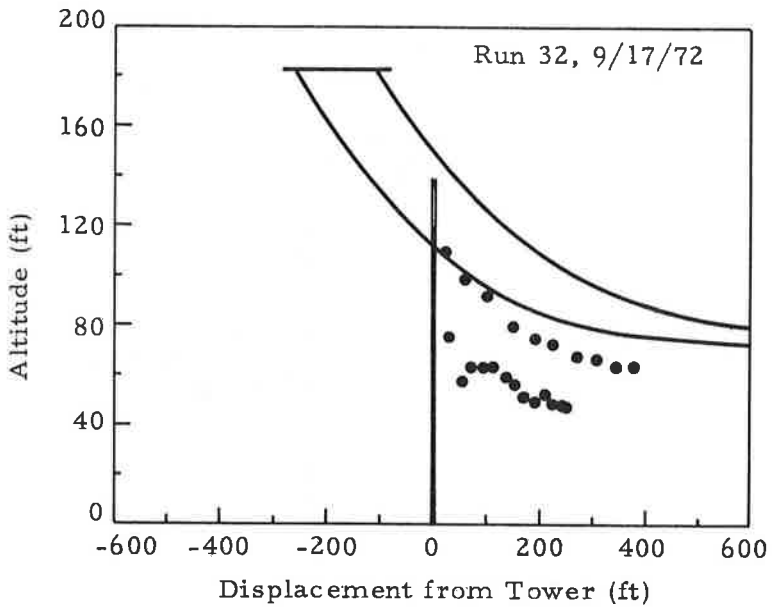

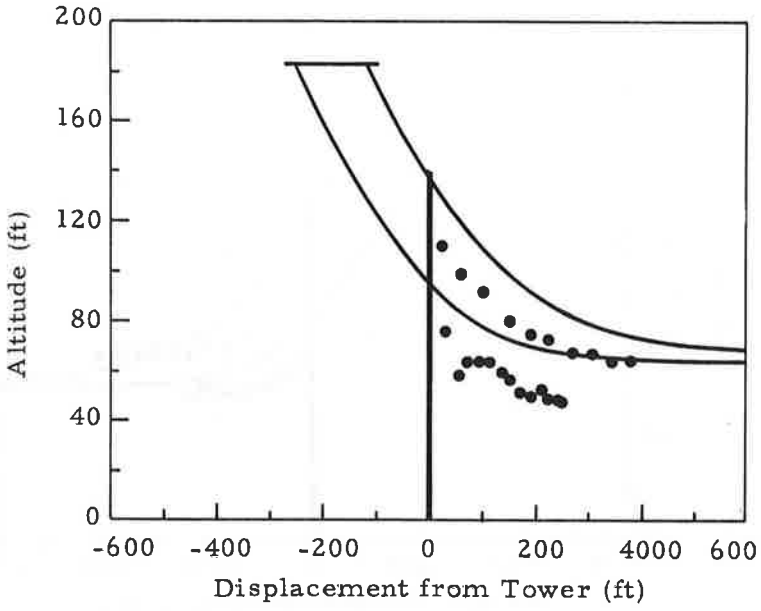

Fig. 3-4 - Predictive Wake Vortex Transport Code with Elliptic Loading, Top K = $\pi/4$ with Flap Effects, Bottom K = 0.69 – Run 32

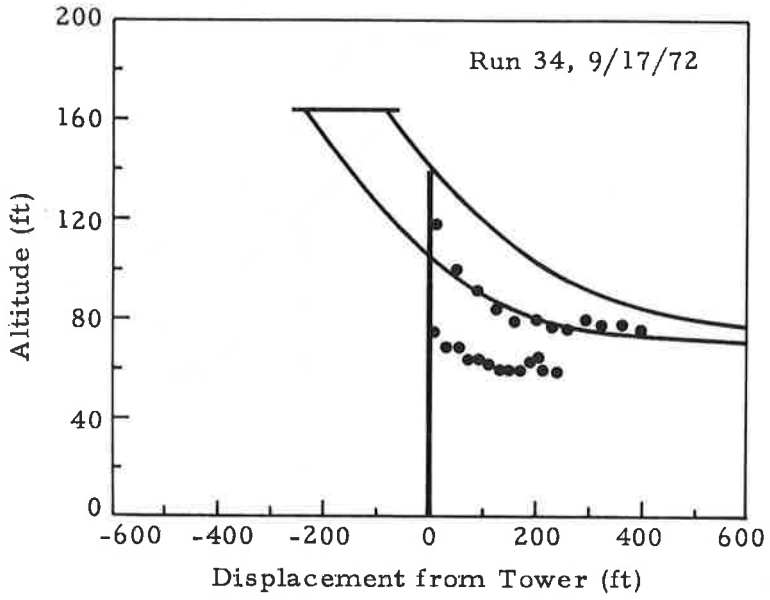

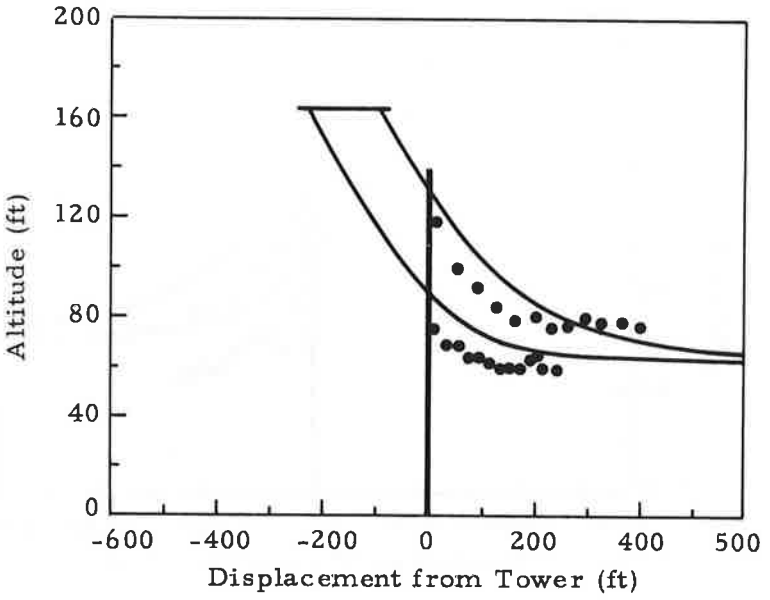

Fig. 3-5 - Predictive Wake Vortex Transport Code with Elliptic Loading, Top K = $\pi/4$, and with Flap Effects, Bottom K = 0.69 – Run 34

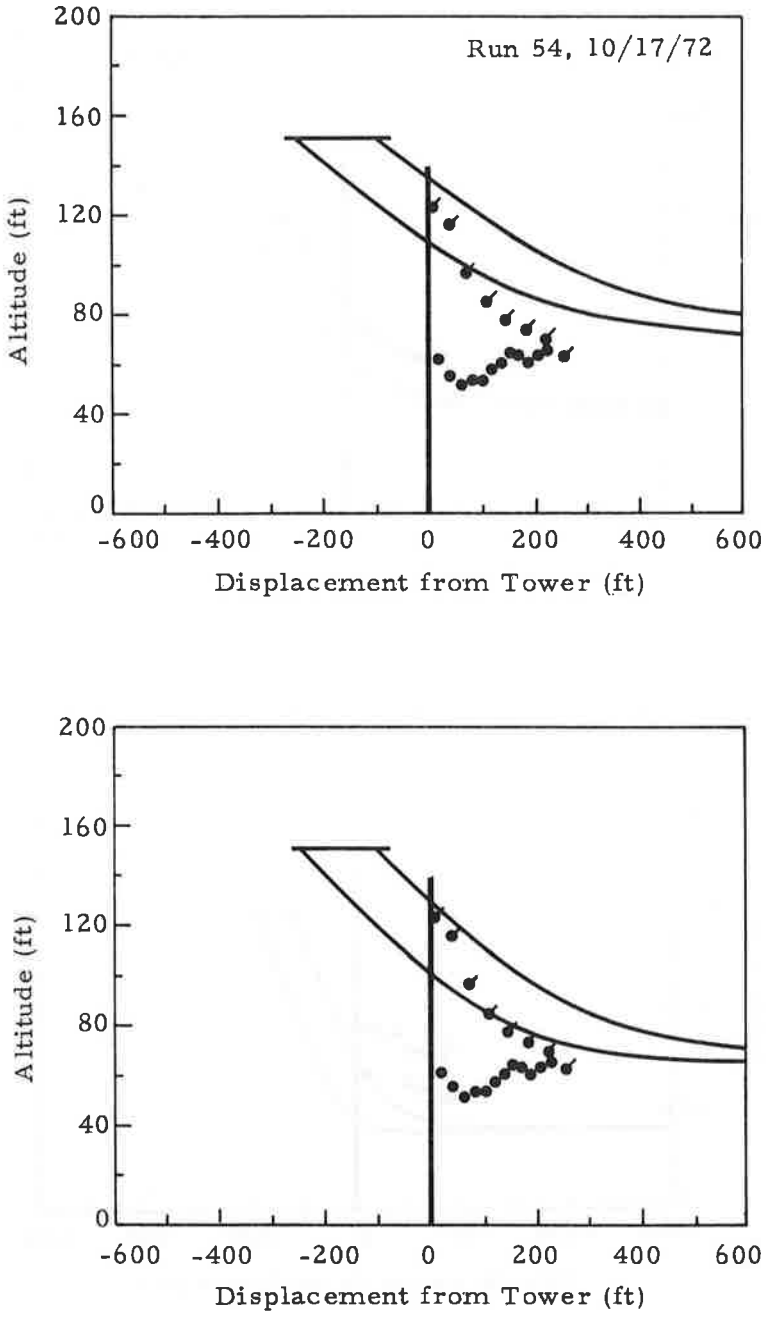

Fig. 3-6 - Predictive Wake Vortex Transport Code with Elliptic Loading, Top K = $\pi/4$, and with Flap Effects, Bottom K = 0.72 – Run 54

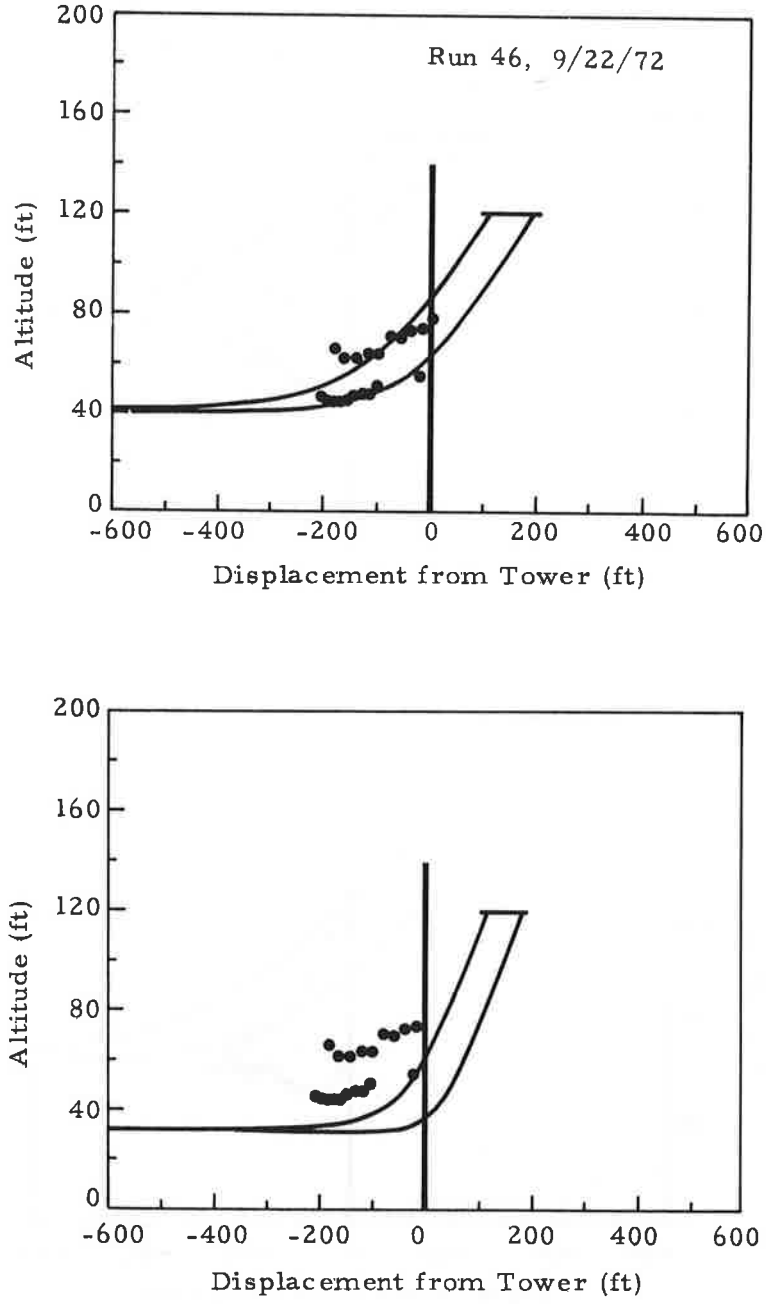

Fig. 3-7 - Predictive Wake Vortex Transport Code with Elliptic Loading, Top K = $\pi/4$ with Flap Effects, Bottom K = 0.62 — Run 46

vortex cell can be caused by two factors: (1) descent of the vortex pair into a stratified environment, and (2) entrainment of exhaust gases from jet engines. Indications are that ambient stratification is a relatively weak effect while jet exhaust entrainment in conjunction with strong stratification can lead to a significant slow down of the natural vortex descent process.

It is useful to compute the characteristic time required to cancel the downward momentum of the vortex pair by upward buoyancy due to ambient stratification, exhaust ingestion, and due to both effects. The characteristic time can be shown to be given by (Appendix C):

$$t = \frac{T\Gamma b'}{\Delta T g A} \tag{3.6}$$

where Γ, b', and A are the strength, spacing and total cell area of the vortex wake and ΔT is the temperature difference attributed to ambient stratification, jet exhaust entrainment, or both effects.

Measurements by Tombach (Ref. 44) have shown that the average temperature difference observed in the vortex due to stratification is $\Delta T \sim 0.5^{\circ}C$. This is for a light twin-engine private aircraft. However, similar results are anticipated for larger commercial aircraft since the trailing vortex pair is geometrically identical. It is the ambient lapse rate rather than generating aircraft parameters which are considered to be significant in atmospheric buoyancy effects (Ref. 32).

Little information is available on the vortex-jet entrainment process. However, calculations by Hoshizaki et al. (Ref. 45) suggests that $\Delta T \sim 1.0^{\circ}C$ for aircraft with engines mounted near the centerline of the vortex so that entrainment of exhaust gases can provide as much as twice the density mismatch as stratification alone. Substituting these typical values of ΔT into Eq. (3.6), the characteristic time required for buoyancy effects to cancel the downward momentum of the vortex pair for a B-747 and a B-727 aircraft ranges from 73 to 360 seconds as shown in Table 3-2.

TABLE 3-2

CHARACTERISTIC TIME REQUIRED FOR BUOYANCY EFFECTS TO CANCEL THE DOWNWARD MOMENTUM OF THE VORTEX PAIR

Aircraft	Config.	C_L	t_1 (sec)	t_2 (sec)	t_3 (sec)
B-747	HC	0.79	217	108	73
	L	1.23	310	165	96
	TO	1.10	267	133	89
B-727	HC	0.58	215	107	72
	L	1.59	320	160	95
	TO	1.59	560	280	188

t_1 = buoyancy due to stratification

t_2 = buoyancy due to exhaust entrainment

t_3 = buoyancy due to both stratification and exhaust entrainment

HC = holding configuration

L = landing configuration

TO = takeoff configuration

From these calculations it can be noted that on the order of 300 seconds is required for stratification to stop the wake descent. The results suggest that ambient stratification, alone, is not a dominant factor in the terminal area wake vortex transport process. Similar conclusions have been drawn by Crow (Ref. 46) who notes that the typical ratio of accelerations due to stratification and circulation is in the range 0.1 to 0.2. However, if both stratification and jet entrainment are active, then Table 3-2 shows that wake descent can be cancelled within 100 seconds, a short enough time period to influence terminal area wake vortices. For this reason, buoyancy in ground plane effects have been incorporated in the Predictive Vortex Wake Transport Model.

On the basis of the general terminal area wake vortex transport model developed in Section 2.2, it is seen that buoyancy affects the vortex transport and decay process through the buoyant force term λA where λ and A are the density parameter and area of the vortex cell, respectively. Calculations have been carried out with the Predictive Wake Vortex Transport Model for a range of vortex parameters to evaluate the influence of buoyancy on terminal area wake vortex characteristics.

It is appropriate to define the buoyancy-containing area of the wake vortex as the quasi-elliptical oval determined from the vortex stream function. Physically, the semi-elliptical streamline connecting the front and rear stagnation point of the vortex encloses the region of fluid which translates with the wake vortex. Hence, not only the inner viscous core but also the whole oval cross-sectional area can contribute to the buoyancy of the wake vortex. This is in contrast to the original Costen model (Ref. 31) and the previous version of the Predictive Wake Vortex Transport Program (Ref. 9) where it was assumed that only the viscous core radius, r, defines the buoyant area ($A = \pi r^2$). In the updated Predictive Model the characteristic area of each vortex cell is computed as a function of the initial vortex separation distance, b' and the ground plane height and wind shear parameter, $A = (b'/2)^2 f(\epsilon, \sigma)$, according to the discussion presented earlier in Section 2.2.

A density mismatch between the vortex and the ambient atmosphere, or a nonzero value of λ, can result from ambient stratification, jet exhaust entrainment, or both effects. In the previous discussion it was shown that jet exhaust entrainment appears to have a stronger influence than ambient stratification on wake vortex buoyancy, therefore jet exhaust entrainment is considered in more detail. Assuming all of the kinetic energy of the jet exhaust is deposited in the oval vortex wake region, the temperature rise is given by (Appendix D)

$$\Delta T = \frac{b\,\bar{c}\,(TSFC)\,q'\,U_\infty\,C_L}{7200\,\tau\,A\,C_p\,g} \tag{3.7}$$

where b, $\bar{c}$, TSFC, U_∞, C_L and τ are the wingspan, mean chord, thrust specific fuel consumption, airspeed, lift coefficient and lift-to-drag ratio of the aircraft, respectively; A is the total cross-sectional area of the vortex wake, C_p is the heat capacity of the air at constant pressure, q' is the thermal energy released per pound of fuel, and g is the gravitational constant. The temperature rise given above influences the density parameter according to the relationship (Appendix C)

$$\lambda = \frac{\Delta T}{T_o + \Delta T} \tag{3.8}$$

where T_o is the ambient temperature.

To demonstrate the capability of the above model, it is useful to consider as a sample case a B-747 in landing configuration with b = 196 ft, $\bar{c}$ = 27.3 ft, TSFC ~ 0.9 lb fuel/hr/lb thrust, q = 18,000 Btu/lb, U_∞ = 272 ft/sec, C_L = 1.25, τ = 3, A = 11.42 $(\pi b/8)^2$ = 67585 ft^2, and C_p = 0.24 Btu/lb$^\circ$R. For the above parameters the predicted temperature rise and density parameter due to jet exhaust entrainment as given by Eqs. (3.7) and (3.8) are ΔT = 1.4°C and λ = 0.005, respectively. Actually, not all of the jet exhaust may become entrained in the vortex but ambient stratification may increase the buoyancy so that λ will range from 0 to 0.005 for the B-747 aircraft.

The influence of jet exhaust entrainment on the wake hazard transport is illustrated in Figs. 3-8 and 3-9 for the B-747 in landing. The wake transport has been computed from the updated predictive model (Eqs. (2.22) through (2.29)) for different density parameters. Note that in the absence of buoyancy, for λ = 0, the xy descent trajectory is symmetric, i.e., the transport is initiated at t = 0 sec with x = 77 ft and y = 200 ft and ends at t = 50 sec with x = 200 ft and y = 77 ft. However, with buoyant jet exhaust entrainment considered, the vortex does not follow a symmetric pattern and descends closer to the ground. The final altitude for $t \geq 50$ seconds is x = 55 ft which is 30% lower than the non-buoyant case. Comparing the buoyant and non-buoyant descent, it is noted that as a result of jet exhaust ingestion:

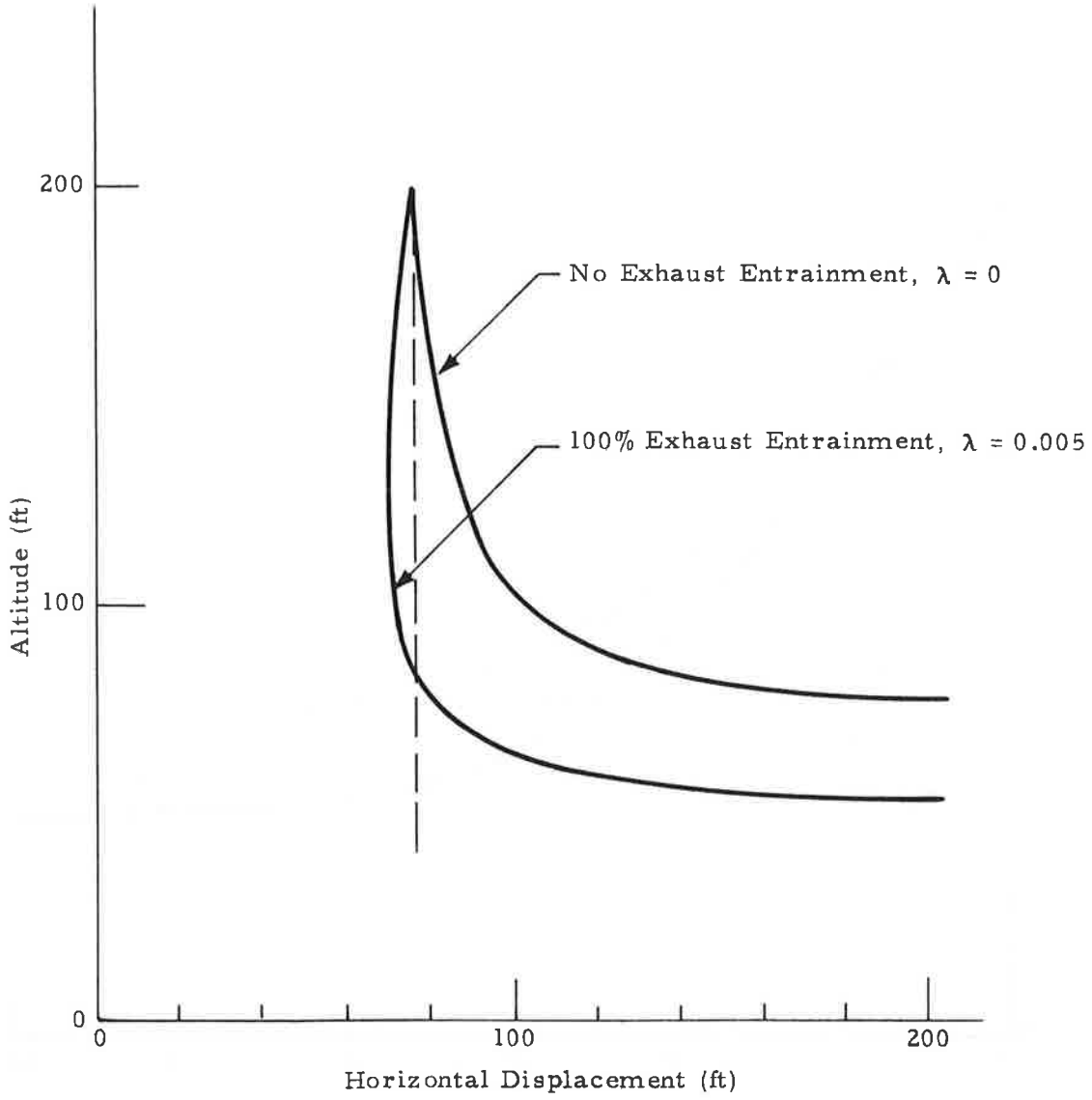

Fig. 3-8 - Influence of Jet Exhaust Entrainment on Vortex Altitude and Lateral Displacement for a B-747 Aircraft in Landing

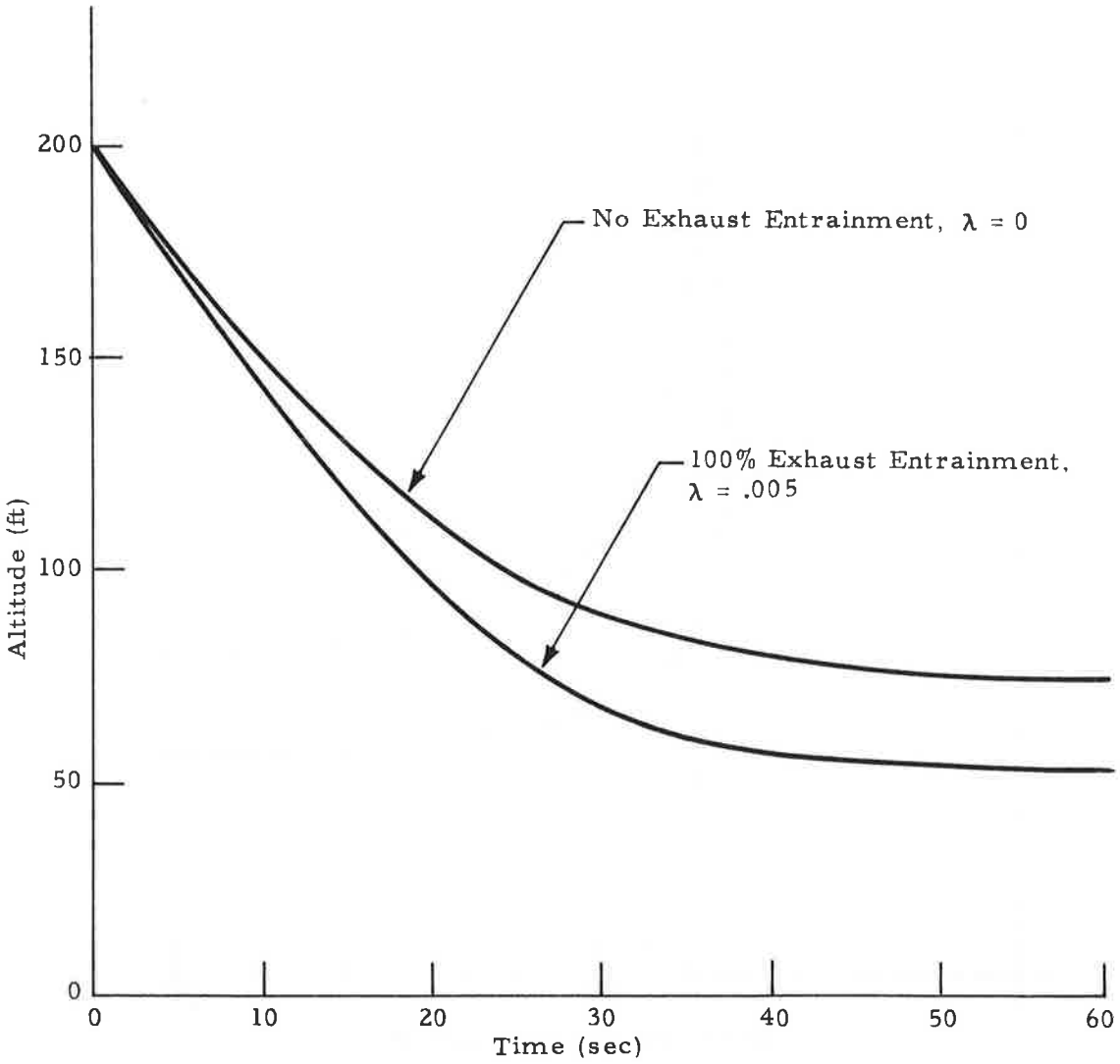

Fig. 3-9 - Influence of Jet Exhaust Entrainment on Vortex Descent for a B-747 Aircraft in Landing

1. The vortex pair tends to sink without appreciable spreading.
2. The wake vortex approaches closer to the ground.

Limited experimental measurements have been made to identify the effect of jet engine thrust on wake vortex transport. In some of the NAFEC tests, wake vortex surveys were conducted with the outboard port or starboard engines set at idle during simulated landing approaches. The results of these tests are tabulated below for those fly-bys where the relative position of the port and starboard vortex could be discerned (Ref. 9).

TABLE 3-3

INFLUENCE OF ENGINE THRUST SETTING ON WAKE VORTEX DESCENT

Aircraft Type	NAFEC Run No.	Altitude of Vortex from Wing Tip with Idle Outboard Engine with Respect to the Other Vortex	Vortex on Idle Engine Side
B-747	56	Same	Downwind
B-747	57	Lower	Downwind
B-747	58	Lower	Downwind
B-747	59	Higher	Upwind
B-747	60	Lower	Upwind
B-707	6	Higher	Upwind
B-707	7	Lower	Downwind
B-707	8	Lower	Downwind
B-707	9	Lower	Downwind
B-707	16	Same	Upwind
B-707	18	Lower	Upwind
B-707	40	Lower	Downwind
B-707	41	Lower	Downwind

In Table 3-3, the trailing vortex from the wing with the outboard engine idle is generally at a lower altitude than the vortex from the opposite wing tip (where the engine thrust settings are normal). However, the wake vortex from the wing with the outboard engine idle is also the downwind vortex in a majority of the cases and, as discussed later in Section 3.6, moderate to strong wind shear causes the downwind vortex to sink. Thus, it is difficult to discriminate between the effects of buoyancy due to jet engine exhaust entrainment from other vortex transport considerations in the available data base. The vigorous evaluation of the influence of buoyancy in the Predictive Model requires additional experimental measurements for correlation.

3.4 INFLUENCE OF VORTICITY DETRAINMENT

Detrainment of vorticity from the concentrated vortex wake is an important decay mechanism which can have a significant effect on the definition and transport of the wake vortex. As sketched earlier in Fig. 2-15, vorticity detrainment occurs when the viscous core radius of the vortex, r(t), becomes equal in magnitude to the semi-major axis, b'(t)/2 of the quasi-elliptical vortex cell. Assuming the viscous core grows due to turbulent diffusion and the separation of the vortices is a constant, the time required for the core radius to equal the radius of the vortex cell is given by the following expression

$$t = \frac{(b'(t)/2)^2 - r^2(0)}{5.04\ \nu_T} \tag{3.9}$$

where r(0) is the initial core radius and ν_T is the turbulent eddy kinematic viscosity. This expression can be reduced further using Eq. (2.12) and the empirical expressions relating the eddy kinematic viscosity coefficient and initial vortex core radius, $a_1 = \nu_T/\Gamma$ and $a_2 = r(0)/\bar{c}$ to obtain the result

$$t = \frac{K^3 b\ AR}{10.08\ a_1\ C_L\ U_\infty}\left[1 - \left(\frac{2a_2}{K\ AR}\right)^2\right] \tag{3.10}$$

In deriving Eq. (3.10) from Eq. (3.9) it is assumed that the vortex is out of ground effect so that the vortex spacing parameter b' is constant, with time. The parameter a_1 is approximately 10^{-3} based on model tests (Ref. 47) and is an order of magnitude smaller for flight test measurements where the effects of atmospheric turbulence are present (Ref. 48). The initial vortex core radius parameter, a_2, is a function of aircraft characteristics. For example, measurements conducted in the wake of the C-5A indicate that $a_2 \sim 0.1$ and 0.2 for the flap-up and flap-down flight configurations, respectively (Ref. 48). For the DC-9, a_2 also ranges from 0.1 to 0.2 but appears to be independent of flap setting (Ref. 49).

The relationship given by Eq. (3.10) demonstrates that the constant initial wake vortex sink rate given earlier in Eq. (2.18) is valid up to a time t which is determined largely from aircraft parameters. The onset of the wake vortex slow down process has been calculated from Eq. (3.10) for representative aircraft assuming the constants $a_1 = 10^{-3}$, and $a_2 = 0.1$ in the hold and $a_2 = 0.2$ in the approach, takeoff, and landing configurations. The results are presented in the last column in Table 3-1 shown earlier. A significant variation can be noted in the predicted onset of the wake decay process which ranges from approximately 100 to 300 seconds in the holding configurations for the aircraft considered. These calculations suggest that a slow down in the vortex descent rate due to vortex decay can be a relevant parameter, particularly for low aspect ratio aircraft. Similar results can be inferred from model wake decay measurements (Ref. 50).

To further reduce the expression given in Eq. (3.10), the characteristic vorticity detrainment time can be defined in terms of a dimensionless parameter, t^*, as follows

$$t^* = t \frac{C_L U_\infty}{b AR} \tag{3.11}$$

Combining Eqs. (3.10) and (3.11) it is found that

$$t^* = \frac{K^3}{10.08\, a_1} \left[1 - \left(\frac{2a_2}{K AR} \right)^2 \right] \tag{3.12}$$

Note that for typical commercial airliners during landing $a_2 \sim 0.2$, $K \sim 0.7$, $AR \sim 7$ so that the second term in Eq. (3.12) is negligible. Thus, the characteristic detrainment time is given by

$$t^* \sim \frac{K^3}{10.08\, a_1} \tag{3.13}$$

The final expression derived above is surprising. It shows that the onset of vorticity detrainment is governed primarily by one parameter, the spanwise loading coefficient K. For elliptically loaded wings $K = \pi/4$ so

that $t^* = 0.048/a_1$. However, when the aircraft has its flaps deployed, as during approach or landing, then typically K = 0.7 and $t^* = 0.034/a_1$. Thus, different airplane configurations can exhibit different wake vortex detrainment characteristics depending on their flap geometry. Note that the most rapid vortex decay would be achieved if the wing loading were concentrated inboard so that $K \rightarrow 0$.

Once the vorticity detrainment has been initialized, circulation decays with time according to Eqs. (2.40) and (2.41) derived earlier. Comparison between the theoretical model and available vortex decay measurements is presented in Fig. 3-10. Significant scatter can be noted in the experimental data but the analytic vorticity detrainment model agrees well with the experimental trends. The dashed line in the figure refers to the maximum decay rate possible by vortex "aging" techniques such as spoilers, splines, etc., where the viscous core diameter is increased to match the vortex cell radius immediately during roll-up. In this case the circulation decay is initiated at t = 0 and the vortex strength is dissipated much more rapidly.

Decrease in the circulation of the trailing vortex due to vorticity detrainment influences the descent of the vortex pair. The vorticity detrainment model developed above has been incorporated into the Predictive Wake Vortex Transport Model. Vortex trajectories illustrating the effect of circulation decay are presented in Fig. 3-11 for the B-747 landing wake parameters given earlier in Fig. 3-10.

As shown in Fig. 3-11, the effect of vorticity detrainment is to slow the descent of the wake vortex at late times. Experimental vortex measurements out of ground effect show the same general trend indicated by the theoretical model, a slowdown of the vortex descent rate at late times (Refs. 48 and 49).

3.5 INFLUENCE OF VORTEX LIFETIME

Breakup of the coherent vortex wake due to sinusoidal link and/or burst instabilities is important in terms of defining the wake vortex at terminal

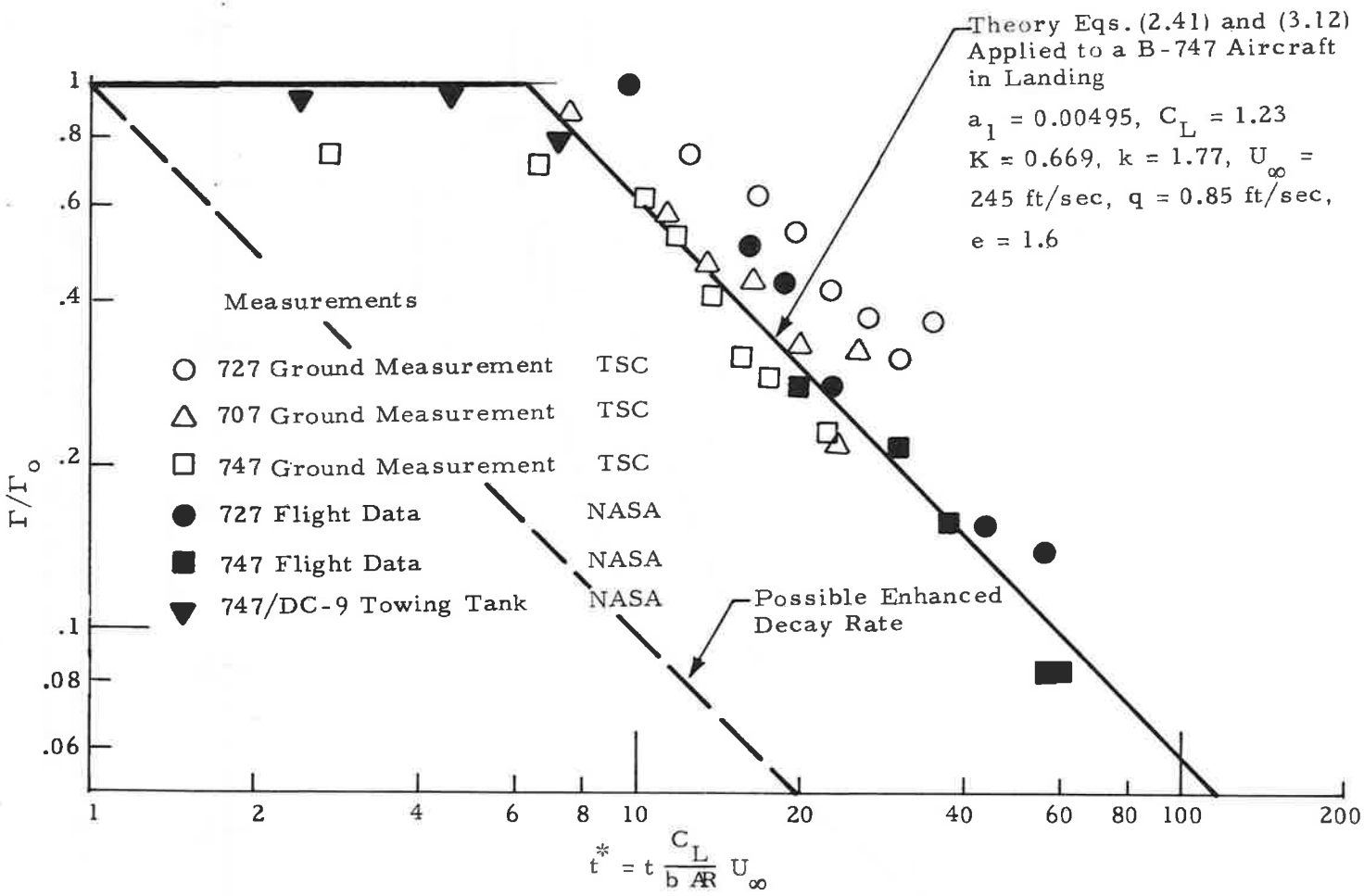

Fig. 3-10 - Wake Strength Decay for Landing Aircraft as a Function of Dimensionless Time (Ref. 51)

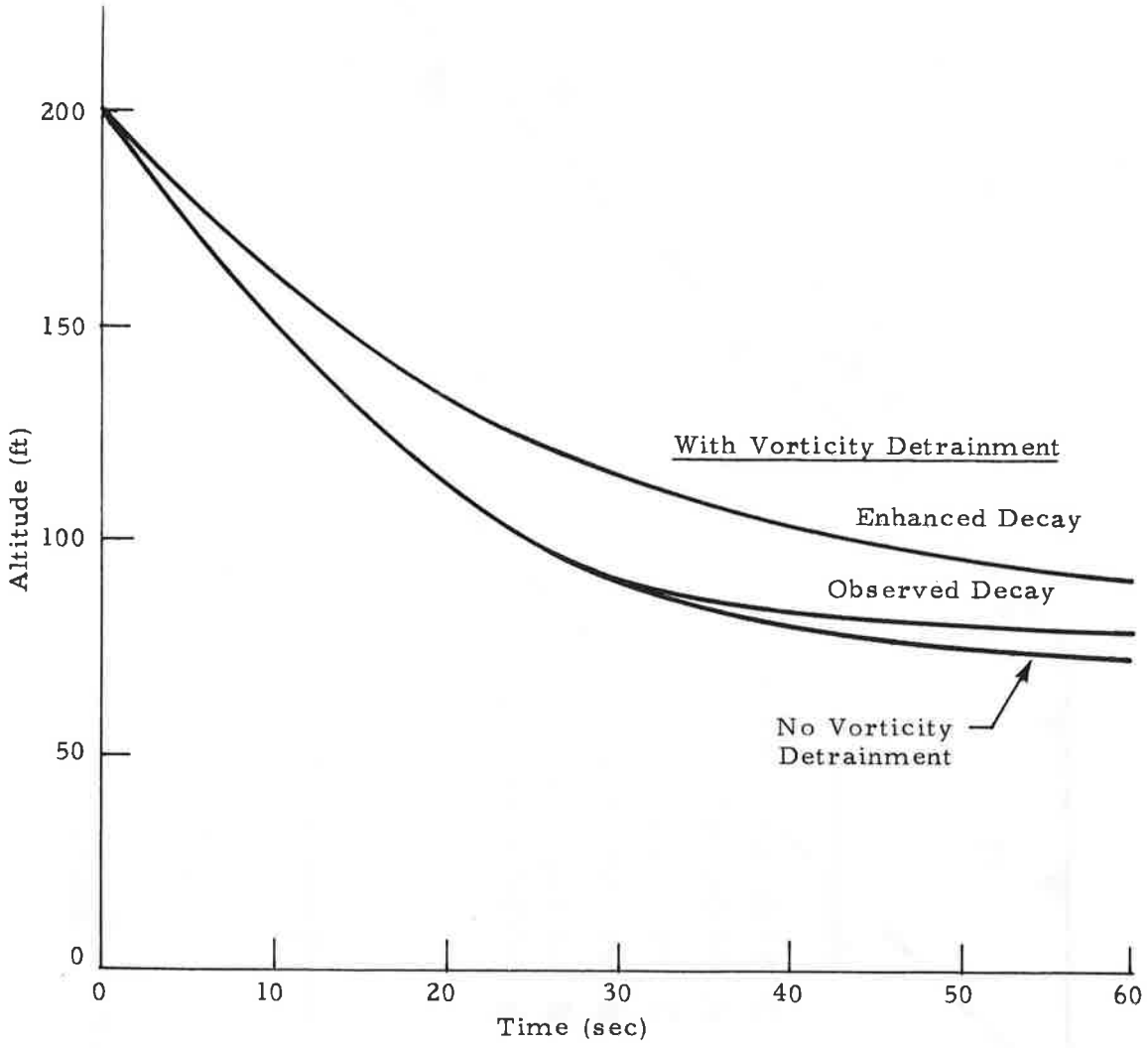

Fig. 3-11 - Influence of Vorticity Detrainment on Wake Vortex Transport for a B-747 Aircraft in Landing

areas. If the vortex remains "stalled" in the flight corridor, a safe aircraft separation distance is directly related to the vortex lifetime. For this reason, an analytic vortex lifetime model has been incorporated into the Predictive Wake Vortex Transport Model.

The wake vortex lifetime model developed earlier in Section 2.3 has been applied to a representative aircraft fly-by shown in Fig. 3-12. The measured port and starboard vortex positions are shown by the P's and S's and the corresponding predicted vortex positions are shown by the X's and *'s. The dashed lines in Fig. 3-12 indicate the vortex lifetime predicted by Eq. (2.43) for low, moderate, and severe turbulence conditions as well as for the turbulence conditions measured for the fly-by. Note that depending upon the turbulence conditions, $\epsilon_1^{1/3}$ = 0.1, 1.0 and 10 $cm^{2/3}$ sec^{-1}, the vortex transport ceases at t = 11, 60 and 108 sec, respectively.

Based on the observed wind shear and temperature profile, the turbulent eddy diffusivity for this run is determined to be $\epsilon_1^{1/3}$ = 0.581 using the equations developed in Section 2.4. Thus, the predicted vortex lifetime is t = 76 sec which is the point where the predicted vortex trajectory ends. In comparison, the experimental measurements indicated that the port vortex was visible up to t ~ 25 sec. The vortex lifetime curve of McGowan (Ref. 52) predicts a three minute vortex lifetime based on the observed ground wind speed for the fly-by ($\bar{u}_{20}$ = 2.27 ft/sec). From the type of comparisons made above, it is noted that the Predictive Model generates vortex lifetime forecasts which agree qualitatively with available measurements and empirical guidelines. However, an assessment of vortex lifetime including detailed correlation of predicted versus observed vortex lifetime requires a more comprehensive data base than is currently available.

3.6 WAKE TILTING EFFECTS

Tilting of the trailing vortex pair with respect to the ground plane is often observed at late times when the vortex wake is at low altitudes. Experimental measurements indicate that upstream or downstream tilting of the vortex can occur depending upon atmospheric conditions. Mechanisms which have been proposed to relate tilting to wind shear include a secondary

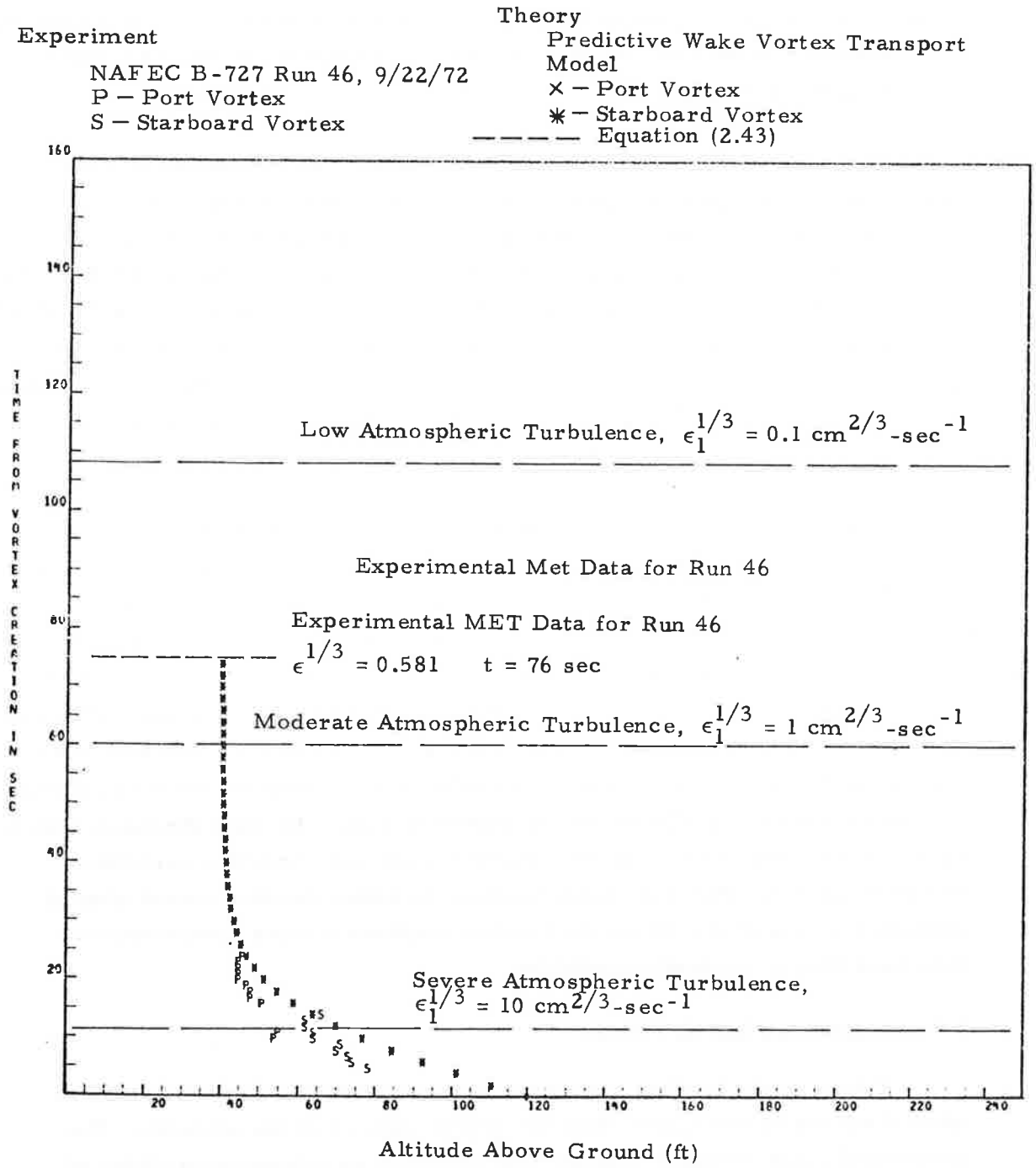

Fig. 3-12 - Influence of Vortex Lifetime on Wake Vortex Trajectory

ground vortex model (Ref. 53) and a stagnation point mismatch model (Ref. 9) as sketched in Fig. 3-13.

When the wind shear is represented by parallel lines of discrete vortices and the trailing vortex pair is allowed to interact with the atmospheric shear layers, a secondary ground vortex is formed due to the stretching and deformation of the atmospheric vorticity field. The ground vortex, opposite in sign to the adjacent trailing vortex filament, causes the vortex pair to tilt (Fig. 3-13a). This tilting mechanism has been investigated in Ref. 4 and has been incorporated into the Predictive Wake Vortex Transport Model to account for the downwind vortex rising with respect to the downwind vortex.

In addition to the free-vortex shear layer interaction noted above, the wake vortex streamlines become asymmetric as they descend toward the ground plane in the presence of wind shear. The upstream cell stretches longitudinally while the downstream cell shrinks in size. When the vortex is very close to the ground, the stagnation point of the upstream cell attaches to the ground but the stagnation point of the downstream cell does not, so that the two stagnation points lie on different streamlines. As shown in Fig. 3-13b, this situation results in the stagnation point of the downstream cell being higher than the stagnation point of the upstream cell. It has been hypothesized that the vortex tilts upwind due to this effect (Ref. 9). Comparison with measurements has shown that the vortex pair does in fact tilt upwind in the presence of light shear (and downstream in the presence of strong shear) tending to verify this hypothesis.

While the stagnation point mismatch and secondary ground vortex are relevant vortex tilting mechanisms, asymmetric vortex cell behavior can also lead to wake tilting effects. Wake tilting due to asymmetric vortex cell characteristics is illustrated by the sketch in Fig. 3-13c. In the presence of strong wind shear, the upwind cell of the vortex is larger than the downwind cell. From the general buoyancy, ground plane, and vorticity detrainment model derived earlier in Section 2, it follows that the two unequal vortex cells will have different inertial masses, buoyancy forces, and vorticity detrainment rates. Depending upon the mismatch in the mass, buoyancy, and circulation of the two cells, the wake vortex can tilt upwind or downwind. Since the

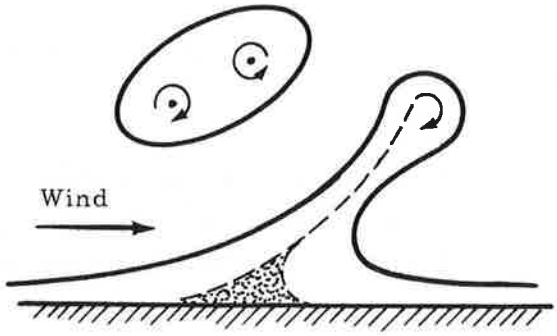

a. Secondary Ground Vortex

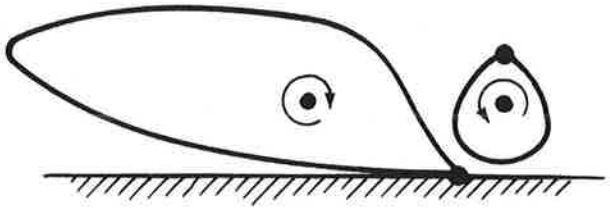

b. Stagnation Point Mismatch

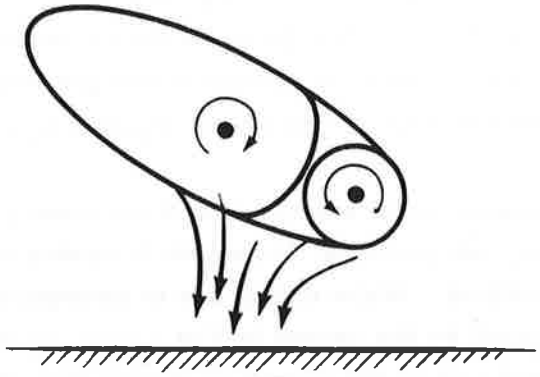

c. Asymmetric Buoyancy and Circulation Distribution

Fig. 3-13 - Vortex Tilting Mechanisms

wind shear parameter, σ, determines the shape and size of the respective vortex cells, wind shear is an important parameter in defining the wake tilting phenomena.

It is useful to consider the effect of wind shear on wake tilting. Previous research at Lockheed-Huntsville (Ref. 9) analyzing experimental NAFEC flight test measurements has established a predominate downwind tilting trend (i.e., the downwind vortex is at a lower altitude than the upwind vortex) for strong wind shear, $\sigma > 0.4$. The dimensionless wind shear parameter, σ, can be expressed as

$$\sigma = \pi K_1 K^3 AR\, b/C_L U_\infty \tag{3.14}$$

where K_1 is the atmospheric wind shear parameter, $K_1 = \partial u/\partial h$, and K, AR, b, C_L and U_∞ are the aircraft spanwise loading coefficient, aspect ratio, wing span, lift coefficient, and airspeed, respectively. For instance, for a B-707 in landing configuration K = 0.6, AR = 6.9, b = 142 ft, C_L = 1.15, U_∞ = 245 ft/sec so that $\sigma = 2.3\, K_1$. It is found that for downwind tilting K_1 must be greater than 0.17 for a landing B-707. However, the atmospheric wind shear parameter K is generally in the range 0 to 0.18 sec^{-1}, where the latter value corresponds to a 10 kt/100 ft shear which may be hazardous for certain aircraft operations. Occasionally, the wind shear can also have a small negative value indicating a reversal in the atmospheric boundary layer.

Measurements are available for the wind shear observed during the NAFEC B-707 flight tests. The observed wind shear perpendicular to the aircraft flight path between the 23 and 140 foot levels recorded by weather instrumentation during 63 fly-bys is presented in Figs. 3-14 and 3-15. As shown in Fig. 3-14, the measured values of K_1 range from 0.23 to -0.03. The frequency distribution in Fig. 3-15 indicates that the mean value of K_1 is 0.06.

On the basis of Fig. 3-15 and Eq. (3.14), it is noted that for the B-707 fly-bys the dimensionless wind shear parameter, σ, is generally less than 0.4

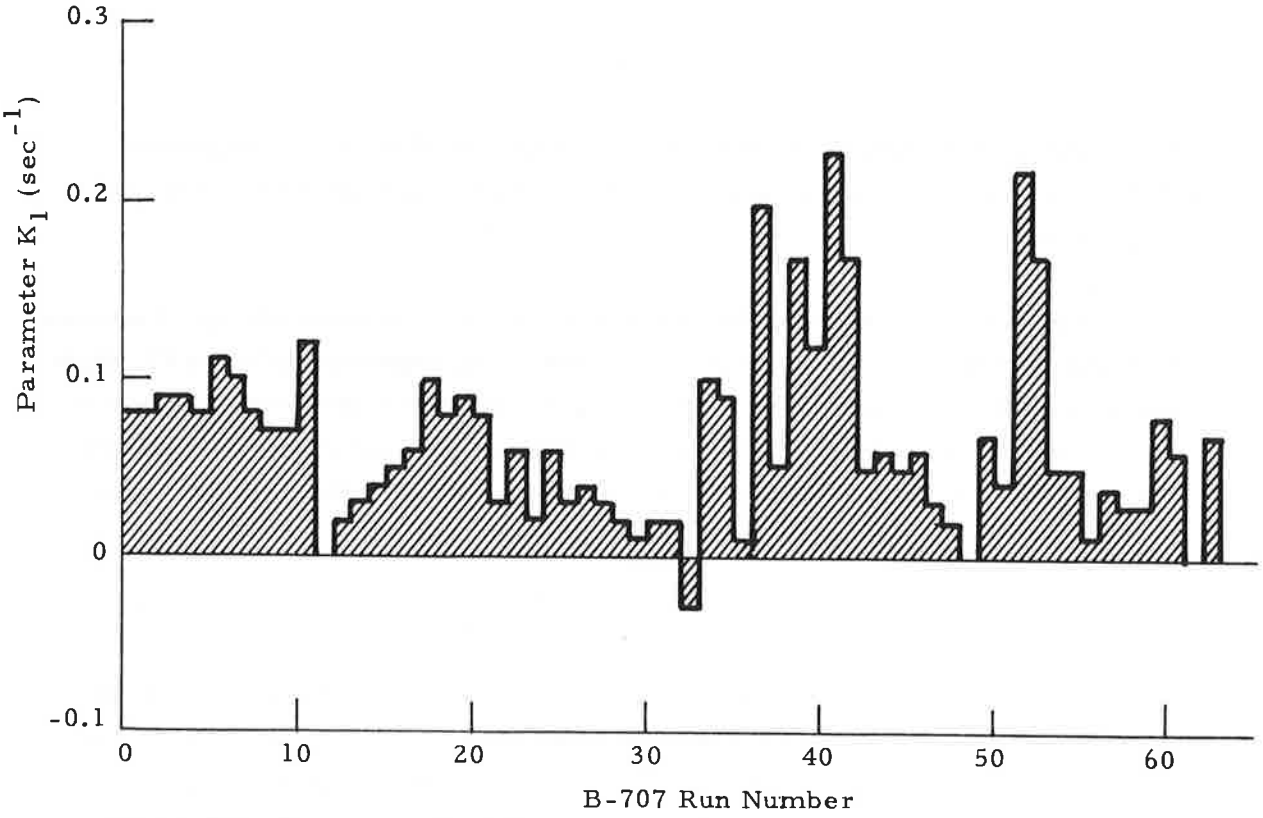

Fig. 3-14 - Observed Wind Shear Parameter Perpendicular to the Aircraft Flight Path Between the 23 and 140-Foot Levels for FAA NAFEC B-707 Flyby Tests Conducted on 10/18/72 and 11/1/72

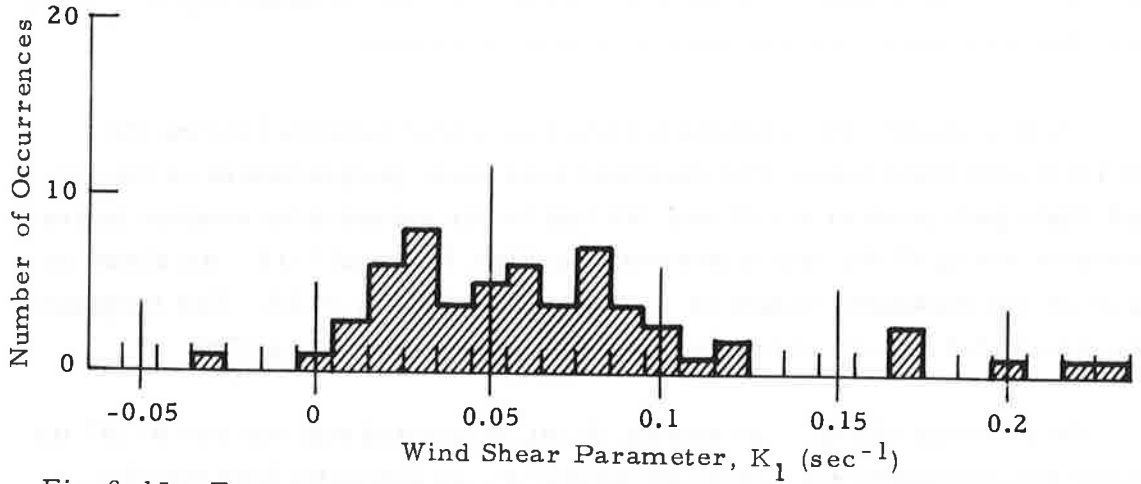

Fig. 3-15 - Frequency Distribution of Wind Shear Parameter for FAA NAFEC B-707 Flyby Tests Conducted on 10/18/72 and 11/1/72

and an upwind tilting trend is predicted, i.e., the upwind vortex is lower than the downwind vortex. However, for some of the cases $\sigma > 0.4$ since $K_1 >$ .17 and a downwind tilting is anticipated. Analysis of those NAFEC B-707 fly-bys where both the wind shear parameter and the wake vortex tilting are available indicates that the upwind vortex rises 73% of the time (B-707 Runs 2, 3, 4, 7, 8, 9, 13, 17, 34, 43 and 46) while the downwind vortex rises 26% of the time (B-707 Runs 15, 25, 26 and 32). However, for Runs 7, 8 and 9 the outboard engines on the downwind wing were set at idle. When these fly-bys are eliminated from the data base, the upwind vortex rising phenomenon is still dominant. This is not consistent with the previous σ tilt criteria and suggests that other wind shear vortex transport interactions may be occurring.

Since some level of wind shear can occur for most terminal area operations, it is useful to calculate the effects of wind shear on the transport and decay of vortices near the ground. From the vortex streamline calculations cited earlier (Figs. 2-11 and 2-12), it is noted that the upstream vortex cell is larger than the downwind cell in the presence of wind shear. When the streamline calculations are used as a basis to define the asymmetric quasi-elliptical cross section of the descending vortex, it is possible to compute the vorticity detrainment from the vortex value according to the general vorticity detrainment model derived earlier in Section 2. The results of the calculations are shown in Figs. 3-16, 3-17 and 3-18.

The influence of vorticity detrainment on the circulation strength of the trailing vortex for a B-747 in landing is presented in Fig. 3-16 where the parameter kq is a measure of the vorticity transport from the wake and is the product of the turbulent mixing constant, k, and the rms turbulence level, q, of the vortex wake. With no atmospheric turbulence (kq = 0) the circulation strength of both the upwind and downwind trailing vortices is constant as a function of time. However, under moderate turbulence (kq = 0.5), the strength of the trailing vortex pair is dissipated as a function of time. The downwind vortex detrains vorticity faster by virtue of its reduced cross-sectional area so that a mismatch in circulation occurs. The corresponding vortex trajectory for this case is shown in Figs. 3-17 and 3-18.

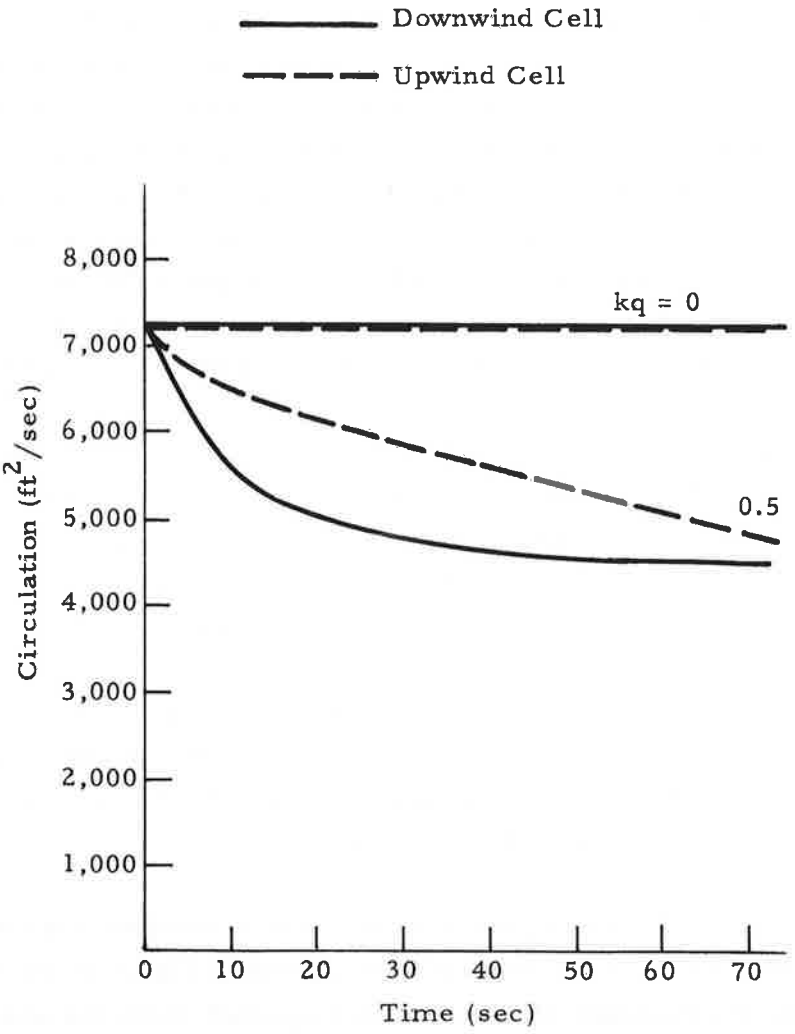

Fig. 3-16 - Influence of Vorticity Detrainment on Circulation Strength of Trailing Vortex Pair for a B-747 in Landing Configuration; $C_L = 1.21$, $K = 0.6$, $\sigma = 1.0$

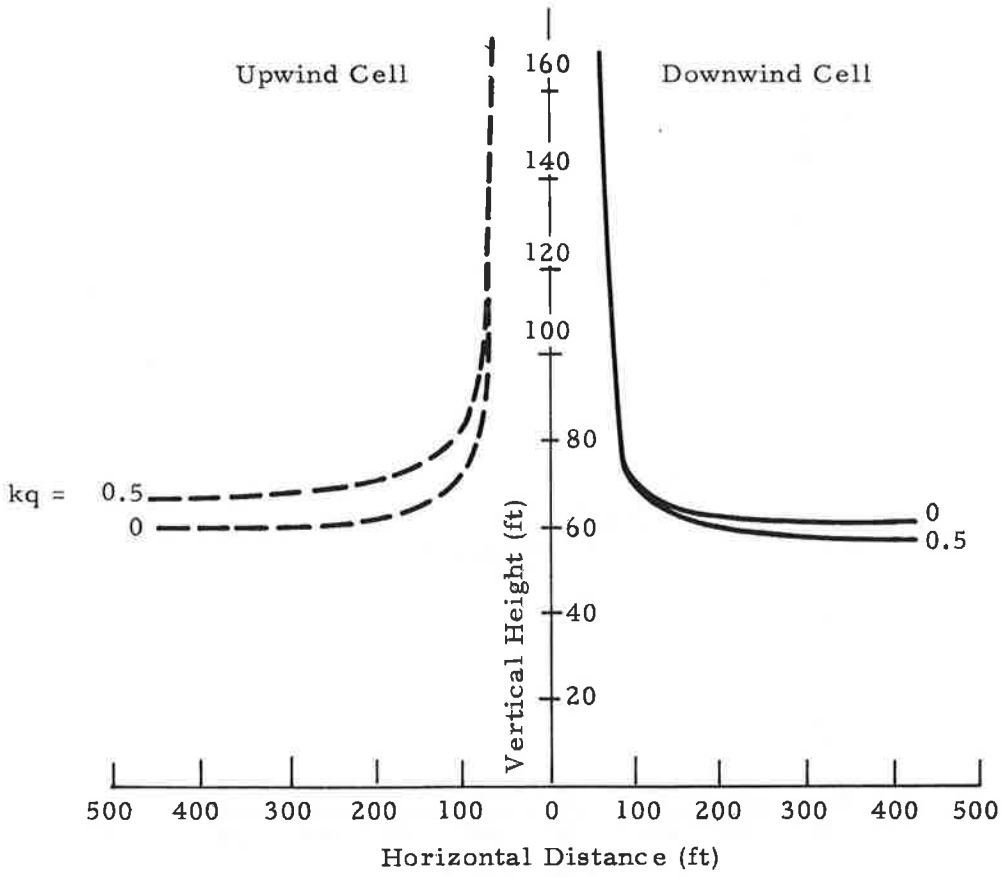

Fig. 3-17 - Influence of Vorticity Detrainment on Wake Vortex Spreading for a B-747 in Landing Configuration; $C_L = 1.21$, $K = 0.6$, $\sigma = 1.0$

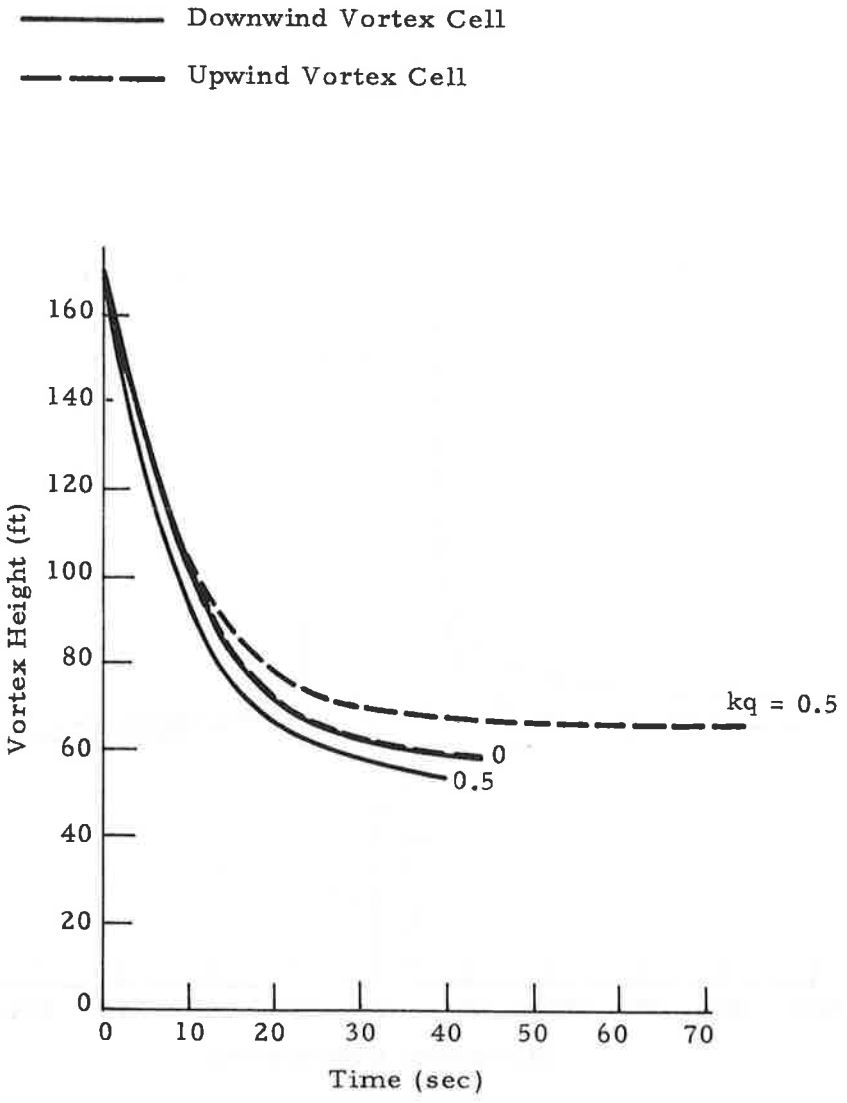

Fig. 3-18 - Influence of Vorticity Detrainment on Wake Vortex Descent for a B-747 in Landing Configuration; C_L = 1.21, K = 0.6, σ = 1.0

In addition to vorticity detrainment, the inertial mass of the vortex pair is relevant in the near ground transport process. For the trajectories in Figs. 3-16, 3-17 and 3-18 the inertial mass of both cells was set equal to a small finite value. However, if we also use the asymmetric vortex cross sections from the streamline calculations to define the inertial mass of the vortex pair, then the trajectories are somewhat different. For the corresponding B-747 landing case the wake vortex trajectory including both vorticity detrainment and inertial mass is shown in Figs. 3-19, 3-20 and 3-21.

Recognition of the virtual mass term does not change the vorticity detrainment process significantly through deformation of the cell so that Fig. 3-19 is essentially identical to Fig. 3-16. However, the vertical and lateral trajectories, Figs. 3-20 and 3-21 are different from Figs. 3-15 and 3-16. When no vorticity loss occurs, i.e., kq = 0, the upwind vortex cell sinks to a lower altitude than the downwind cell. This behavior is consistent with the larger cross-sectional area and larger inertial mass of the upwind cell. Thus, the upwind cell decelerates less rapidly than the downwind cell as it approaches the ground plane and the vortex tilts upwind (i.e., the downwind vortex is at a higher altitude). If the vorticity transport parameter is increased, kq = 0.5, a mismatch in circulation occurs since the downwind cell detrains vorticity more rapidly than the upwind cell. As a result, the upwind cell descends more slowly and the tilting effect tends to be cancelled out. For vigorous vorticity detrainment, i.e., kq > 0.5, it is possible to override the mismatch in virtual mass with a mismatch in circulation. The result is a downwind tilting trend similar to that noted earlier in the absence of the inertial mass term.

On the basis of the previous example, it is seen that asymmetric vortex cell parameters originating from wind shear, inertial mass, and vorticity detrainment effects can have a marked effect on wake vortex trajectories at terminal areas. Additional comparison between the general theoretical model and available wake vortex measurements is presented in Figs. 3-22 through 3-26.

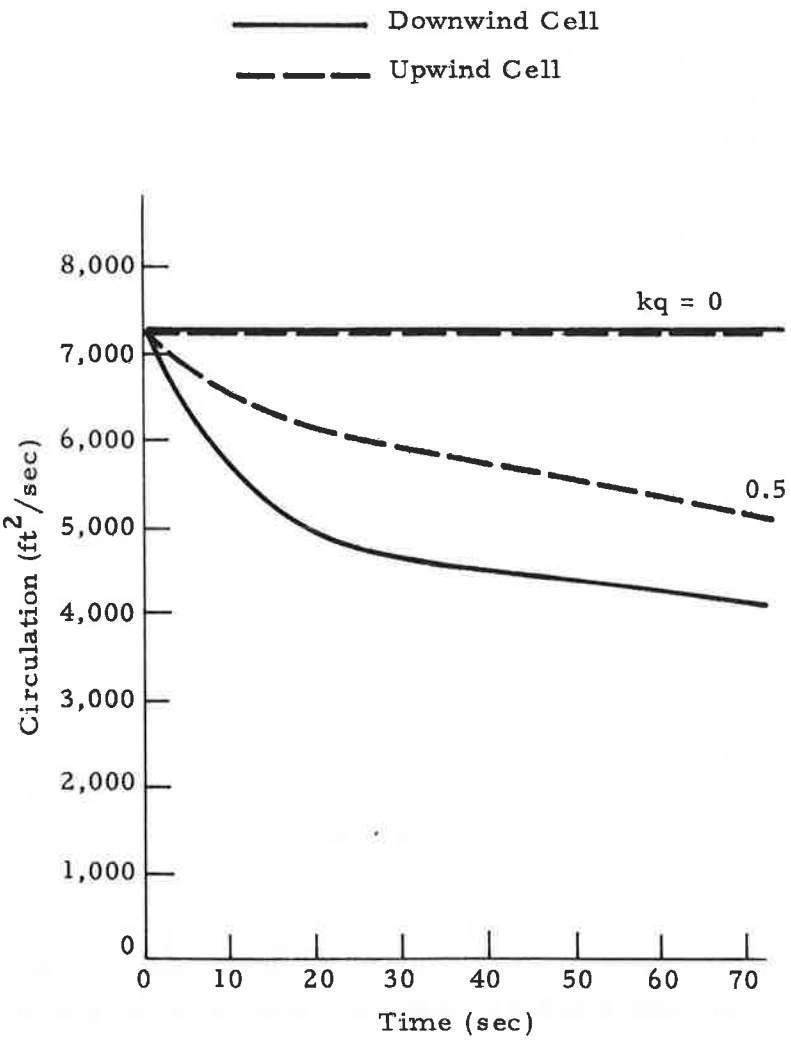

Fig. 3-19 - Influence of Vorticity Detrainment and Inertial Mass on the Circulation Strength of the Trailing Vortex Pair for a B-747 in Landing Configuration; C_L = 1.21, K = 0.6, σ = 1.0

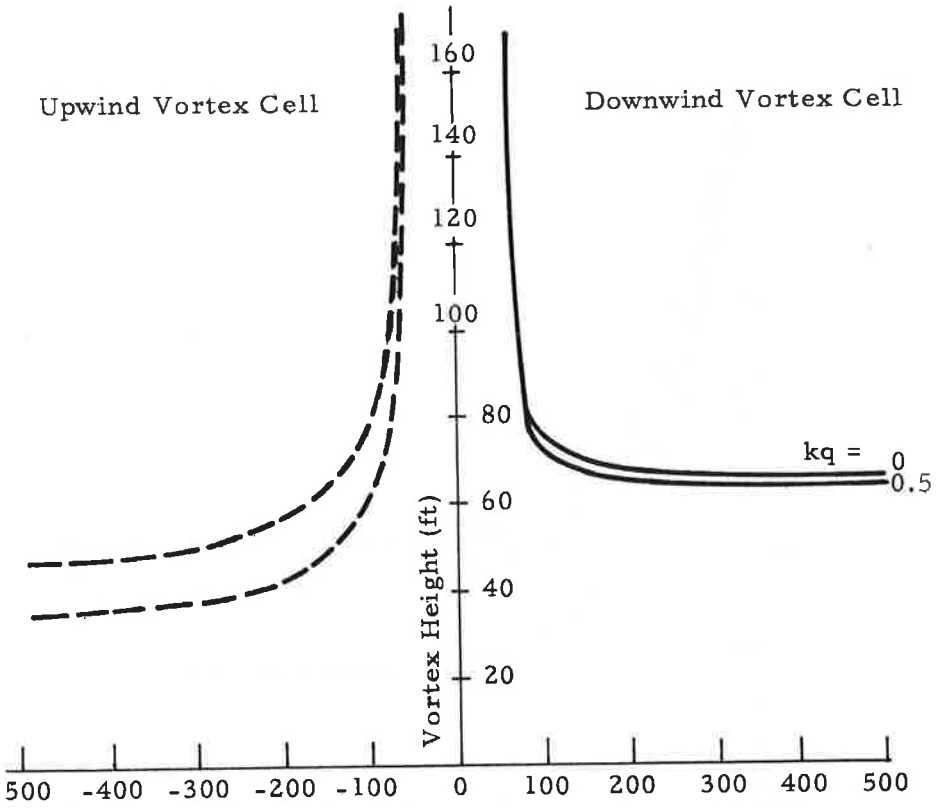

Fig. 3-20 - Influence of Vorticity Detrainment and Inertial Mass on Wake Vortex Spreading for a B-747 in Landing Configuration; C_L = 1.21, K = 0.6, σ = 1.0

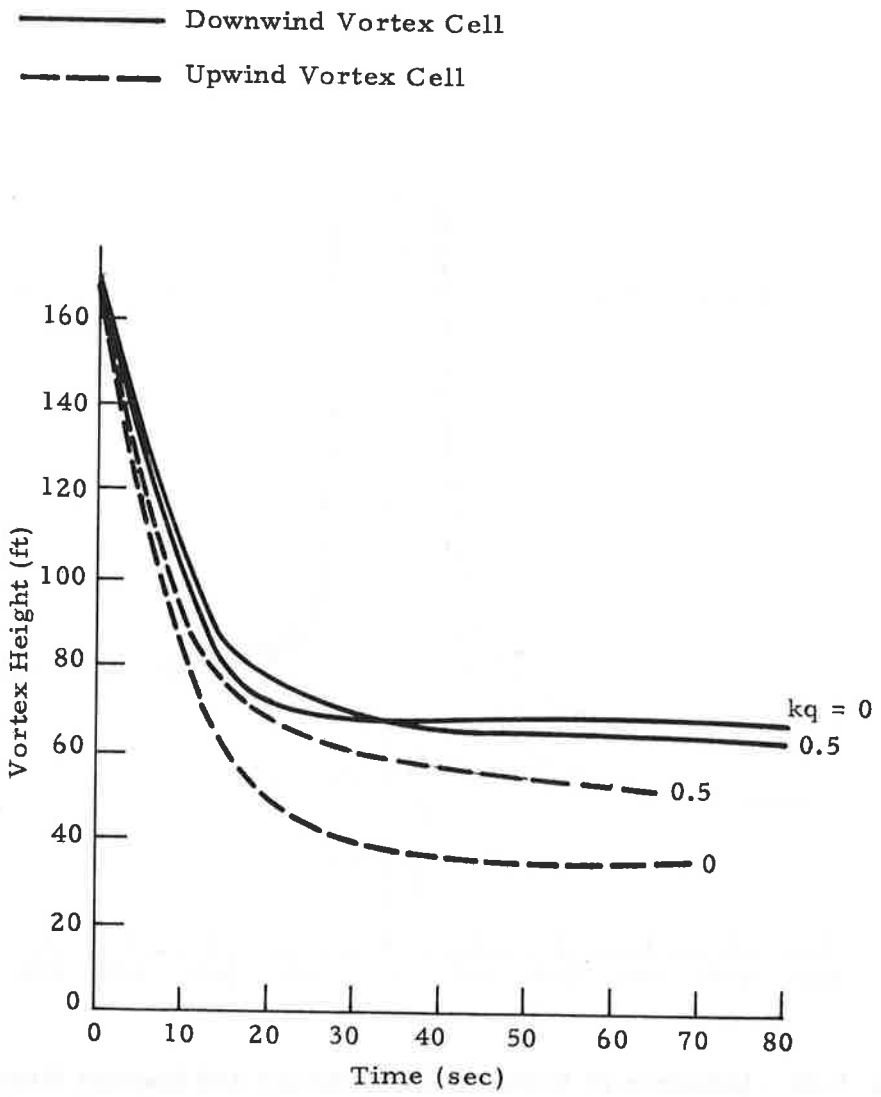

Fig. 3-21 - Influence of Vorticity Detrainment and Inertial Mass on Wake Vortex Descent for a B-747 in Landing Configuration; C_L = 1.21, K = 0.6, σ = 1.0

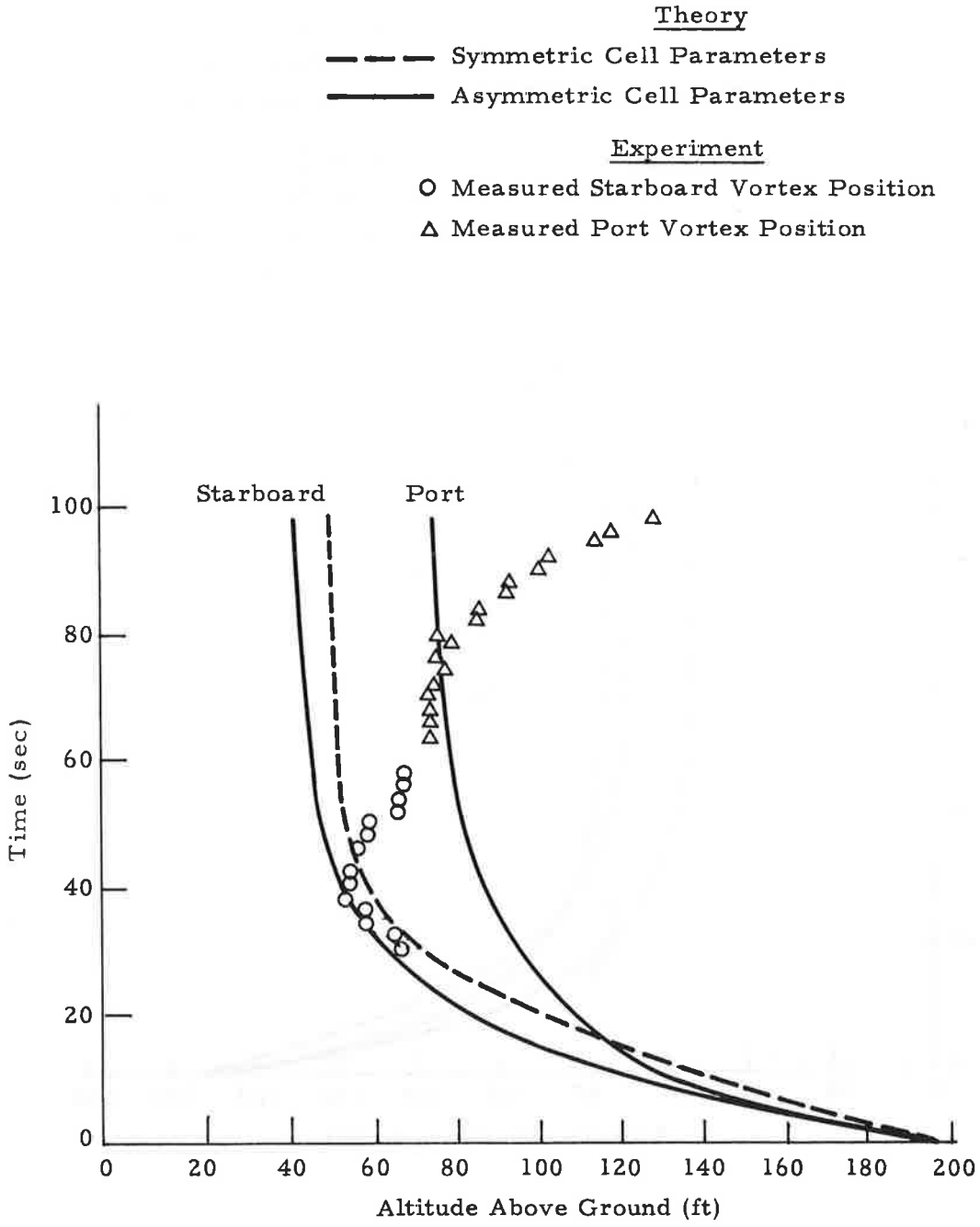

Fig. 3-22 - Predicted and Observed Wake Vortex Descent Trajectory for NAFEC B-707 Run 37

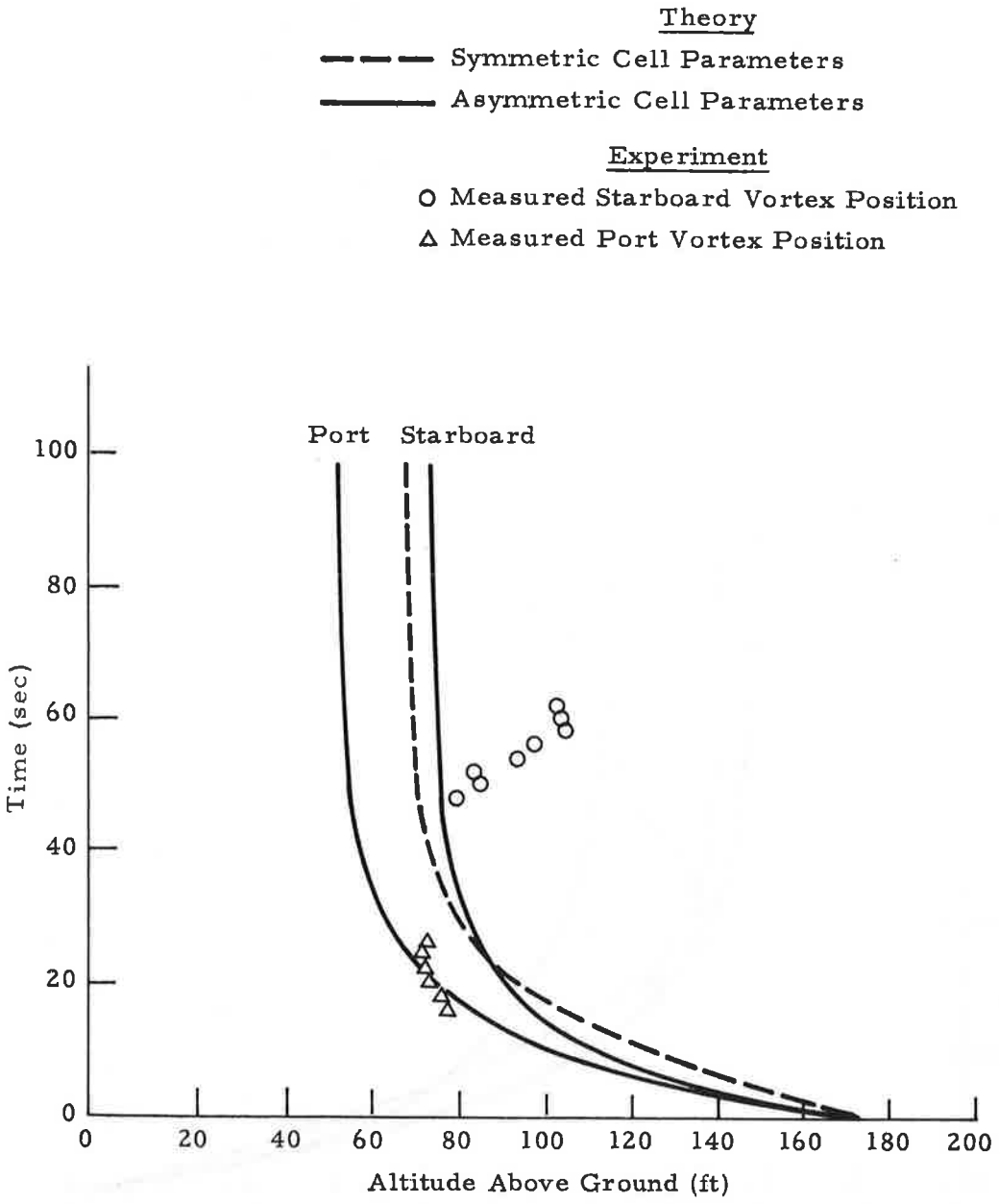

Fig. 3-23 - Predicted and Observed Wake Vortex Descent Trajectory for NAFEC B-747 Run 2

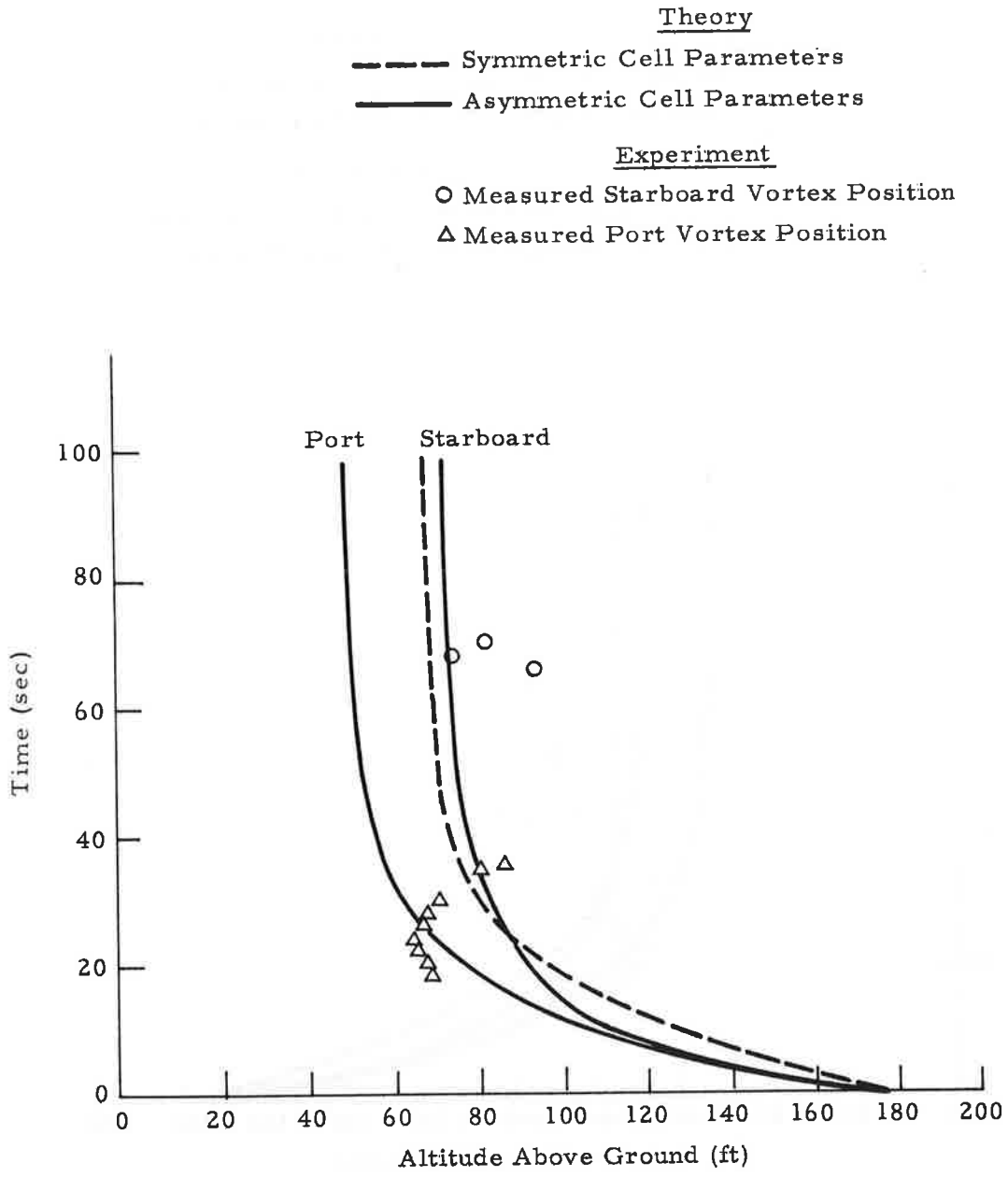

Fig. 3-24 - Predicted and Observed Wake Vortex Descent Trajectory for NAFEC B-747 Run 6

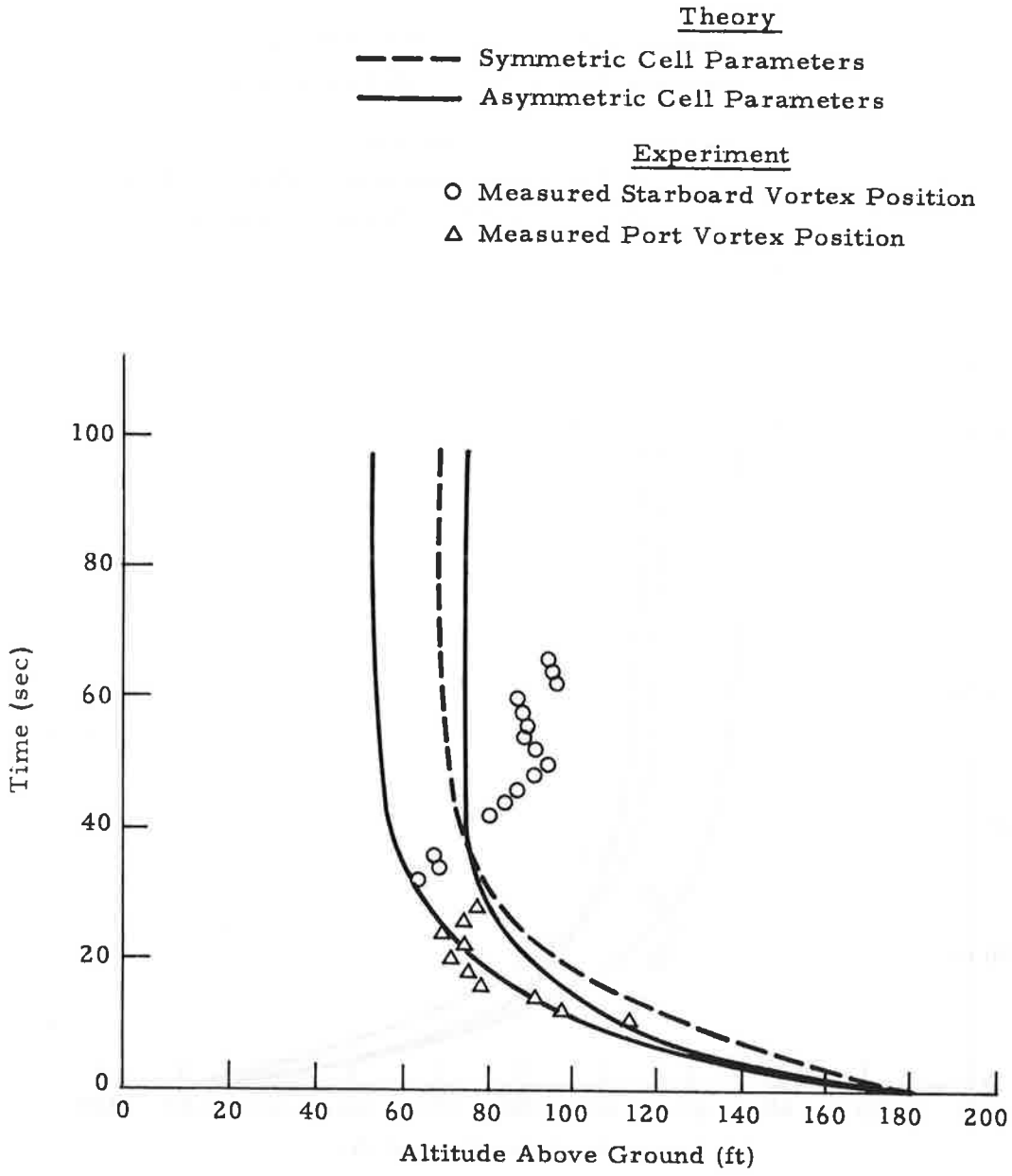

Fig. 3-25 - Predicted and Observed Wake Vortex Descent Trajectory for NAFEC B-747 Run 9

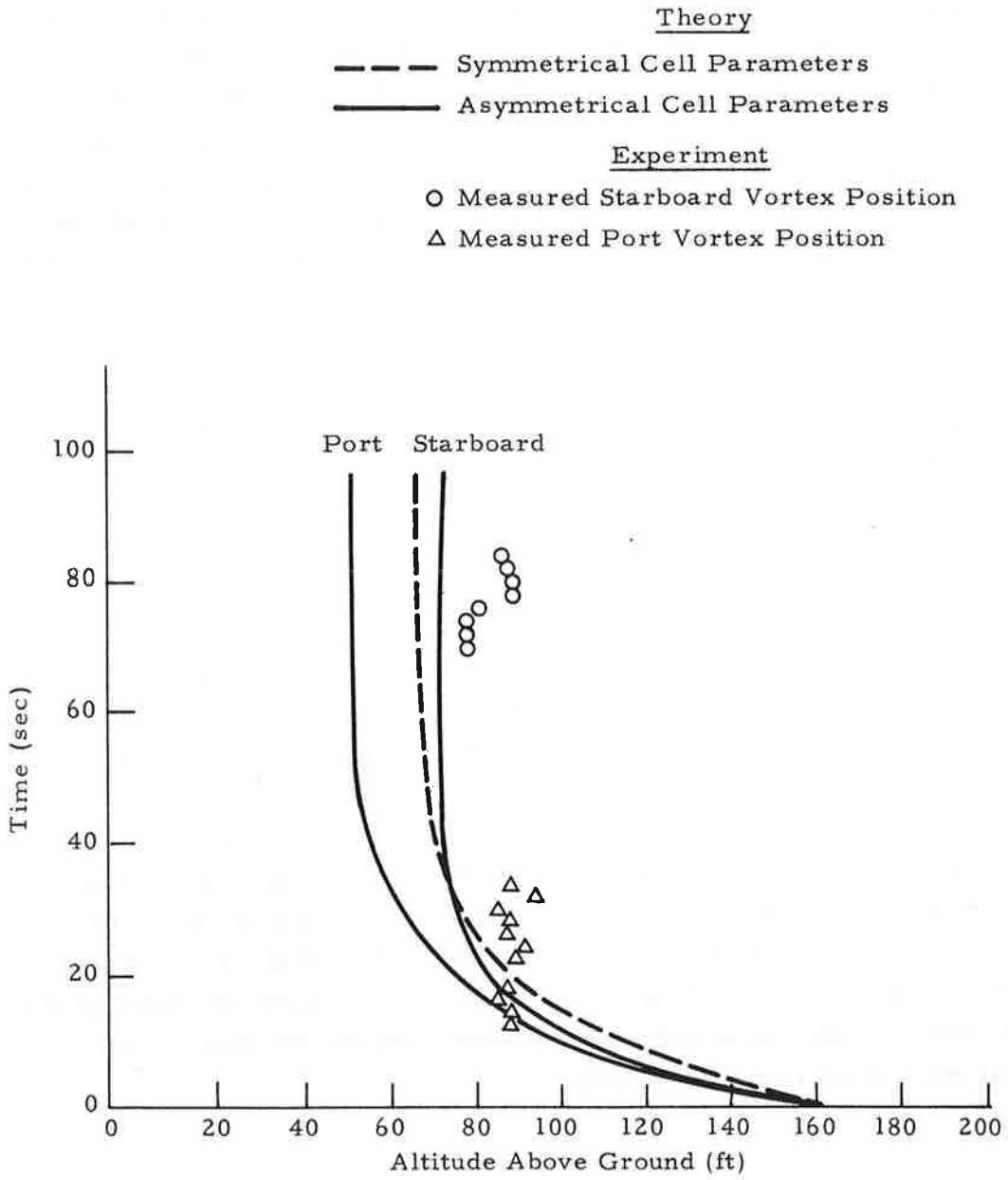

Fig. 3-26 - Predicted and Observed Wake Vortex Descent Trajectory for NAFEC B-747 Run 10

To compare the analytic wake vortex transport and decay program with observed vortex trajectories, calculations have been carried out for selected NAFEC fly-bys where the wind shear parameter is large and the buoyancy effects are minimal. The predicted and observed altitude versus time history plots are presented in Figs. 3-22 through 3-26 for representative wake vortex trajectories. Since it has been found that wind shear rather than the magnitude of the wind is important in terms of wake tilting, the altitude versus time history is an ideal method of assessing tilting effects. Previous research has already demonstrated and isolated the influence of horizontal winds on wake transport (Ref. 9) and need not be reviewed further here. Instead, the vertical wake vortex time history is considered with the understanding that an accurate altitude vs time history leads to an accurate lateral trajectory.

In each of the vortex trajectories shown in Figs. 3-22 through 3-26, the theoretical model accurately models the observed vortex tilt and vortex descent history with the turbulent mixing parameter set at $kq = 1$ and a small but finite inertial mass term. It is anticipated that these parameters can be determined more precisely from future wake vortex measurements and multiplicative coefficients can be derived to specify the complete transport and decay process.

Based on the available NAFEC measurements both upwind and downwind tilting of the wake vortex occurs which has been correlated with the dimensionless wind shear parameter. The Predictive Model demonstrates that wind shear promotes tilting through asymmetric vortex cell parameters which leads to asymmetric wake descent when vorticity detrainment and inertial mass effects are recognized.

4. CONCLUSIONS AND RECOMMENDATIONS

The wake vortex transport program has been expanded to include viscous effects and the influence of initial roll-up, atmospheric turbulence, and wind shear on the persistence and motion of wake vortices at terminal areas. Analysis of wake characteristics has shown that changes in the spanwise loading due to flaps increase the initial sink rate, decrease the separation, and initiates the circulation decay process earlier. Buoyancy due to jet exhaust entrainment and ambient stratification retards vortex spreading and increases descent. Atmospheric turbulence and shear promote a more rapid decay reducing the late-time descent and spread rates of the vortex. Vortex tilting has been related to an interaction involving the wind shear, ground plane, and vorticity detrainment process.

Recognition of the effects of tilting, spanwise loading, vorticity detrainment, burst/sink instabilities, and atmospheric conditions has resulted in an analytic wake transport and decay model with increased accuracy and improved predictive capabilities.

On the basis of this study, it is recommended that:

- A comprehensive data base be compiled and cataloged on wake vortex phenomena
- The Predictive Model developed in this study be exercised using the expanded data base
- Empirical relationships using multiplicative coefficients be utilized for expressing the dominant vortex transport and decay trends.

These recommendations are seen as a step in the implementation and use of the Predictive Model for the development of a wake vortex avoidance system.

APPENDIX A – DERIVATION OF EQUATIONS OF MOTION FOR A BUOYANT VORTEX PAIR APPROACHING THE GROUND PLANE

An exact equation for the drift of the two-dimensional inviscid buoyant vortex pair in a uniform flow subject to gravity may be derived in vector notation as (Ref. A-1)

$$(\vec{\dot{R}} - \vec{V}_\infty) \times \vec{\Gamma} - \lambda A(\vec{\ddot{R}} - \nabla\phi) = 0 \qquad (A.1)$$

where $\vec{R}$, $\vec{\dot{R}}$ and $\vec{\ddot{R}}$ are the positive velocity, and acceleration vector of the vortex centroid, $\vec{V}_\infty$ is the uniform flow velocity, ϕ is the gravitational potential, A is the buoyant vortex core area, and λ is the buoyancy index defined as $\lambda = 1 - \rho/\rho_o$ where ρ is the density of the fluid inside the vortex cell and ρ_o is the density of the surrounding atmosphere.

If the vortex pair approaches the ground plane, as sketched in Fig. 2-9, the flow is no longer uniform. The primary influence of the unsteady flow is to give rise to an inertial force resulting from the internal and virtual mass of the fluid which is transported by the vortex. For a cylindrical vortex of density ρ_o and cross sectional area πr^2 located in a uniform straining flow (which represents to lowest order the effect at the vortex of any non-uniform flow) the additional unsteady force per unit length is given by (Ref. A-2)

$$F = 2\rho_o \pi r^2 \vec{\ddot{R}} \qquad (A.2)$$

In the case of the wake vortex approaching the ground we may assume a cylindrical vortex of density ρ and cross sectional area πr^2 located in a uniform straining flow of density, ρ_o, as shown in the Critical Stage in Fig.

2-15. It follows that the additional unsteady force per unit length due to the internal and virtual mass of the vortex is given by

$$F = \rho \pi r^2 \ddot{\vec{R}} + \rho_o \pi r^2 \ddot{\vec{R}} \tag{A.3}$$

Thus, the force due to the unsteady motion is given by

$$F/\rho_o = (2 - \lambda)\pi r^2 \ddot{\vec{R}} \tag{A.4}$$

Combining the above inertial force with the Kutta-Joukowski and buoyancy forces given earlier in Eq. (A.1), the total force balance is given by

$$(\dot{\vec{R}} - \vec{V}_\infty) \times \vec{\Gamma} - \lambda A(\ddot{\vec{R}} - \nabla\phi) - (2 - \lambda)\pi r^2 \ddot{\vec{R}} = 0 \tag{A.5}$$

where A and πr^2 are the area of the buoyant vortex cell and the area of the cylindrical viscous core, respectively. For the special case when the vorticity and buoyancy carrying cross-sectional areas of the vortex are equivalent, then the equations of motion reduce to

$$(\dot{\vec{R}} - \vec{V}_\infty) \times \vec{\Gamma} - (2 - \lambda \nabla\phi)\pi r^2 \ddot{\vec{R}} = 0 \tag{A.6}$$

REFERENCES

A-1. Costen, R.C., "Drift of Buoyant Wing Tip Vortices," J. Aircraft, Vol. 9, No. 6, June 1972, pp. 406-412.

A-2. Widnall, S.A., and D. Bliss, "Slender Body Analysis of the Motion and Stability of a Vortex Filament Containing an Axial Flow," J. Fluid Mech., Vol. 50, Part 2, 1971, pp. 335-353.

APPENDIX B – COMPARISON OF PREDICTIVE MODEL USING A NON-ELLIPTICAL WING LOADING WITH OBSERVED WAKE VORTEX TRAJECTORIES

The following is a presentation of output plots generated by the Predictive Wake Vortex Transport Model for B-747 flybys using a constant non-elliptical wing loading parameter K = 0.6, and symmetric vortex cell input parameters (with no buoyancy or viscous core radius) for all cases.

Page B-3 lists aircraft information required for the transport calculation and some of the basic quantities calculated in the program for Run 1.

The display of the vortex tracks is initiated in the plot on page B-4. This plot is a cross-sectional vortex track of altitude versus lateral distance referenced to the centerline of the aircraft flight path. Each plotting symbol indicates a time as defined by the user specified time increment. Page B-5 represents a cross-sectional vortex track corresponding to the desired experimental condition. The current setup represents the NAFEC conditions with the lateral distance coordinate referenced to the NAFEC tower. The plotting characters initiating at the simulated aircraft are predicted values with the asterisks and Xs representing the starboard and port vortices, respectively. The measured vortex position as determined from the photographs are shown superimposed on the predicted tracks with the S and P corresponding to the starboard and port vortices, respectively. The solid line represents constant time lines and can be calibrated by the caption at the top of the plot.

Page B-6 is a time versus altitude track comparing predicted and photographic measurement. In the case for no wind shear, equal circulation and level flight, the starboard and port predictive tracks are identical as indicated by the double plotting character. Here again the S and P represent starboard and port vortex position obtained by measurement. Next is the

reduced ground wind track comparing predicted and measured vortex positions. The lines represent predicted vortex position versus time with the S and P referring to photographic measurement and R and L referring to ground wind measurement of the right and left vortex, respectively.

The format for the subsequent computer-generated plots is the same as the output described for Run 1.

The wake trajectories computed with K = 0.6 fit the observed vertical time histories more accurately than the previous K = $\pi/4$ calculations given in Ref. 9 for the following B-747 NAFEC runs; 4,7,8,12,15,57 and 60. For the other 16 runs the K = 0.6 calculations predict a higher sink rate than observed. It is on basis of these and previous calculations that a typical value of K, 90% of the elliptic value, was selected as most appropriate for wake descent simulations.

The influence of K on the vortex sink rate is illustrated by the figure given on page B-106.

```
                                                    RUN DATA CARD
CONFIGURATION     LANDING LEVEL FLIGHT ALL ENGINES SAME POWER
AIRCRAFT TYPE IS B747
RUN NUMBER   1
AIRCRAFT DISPLACEMENT FROM TOWER -390 FT
AIRCRAFT ALTITUDE ABREAST OF TOWER 175 FT
AIRCRAFT WEIGHT 538000. POUNDS
AIRSPEED  253.3 FT/SEC
TEMPERATURE  17 DEGREES C (NOT USED)
INITIAL WIND SPEED   8 MPH  (NOT USED)
INITIAL WIND ANGLE 250 DEGREES TRUE  (NOT USED)
FINAL WIND SPEED   6 MPH  (NOT USED)
FINAL WIND ANGLE 240 DEGREES TRUE  (NOT USED)
AIRCRAFT HEADING 105 DEGREES MAGNETIC
MONTH  9     DAY 16     HOUR  8     MINUTE 54     LOCAL TIME


$OUTPUT
SPEED   =    -.25335000E+03
WEIGHT  =     .53800000E+06
WSPAN   =     .14974400E+03

$END
$WLOG
WSPR    =     .14474060E+02
CPOWER  =     .64299051E-01
COEF    =     .25656189E+03,  -.33398911E-01,   .10540313E-02,   .16739884E+01,
              .00000000E+00,   .00000000E+00,   .00000000E+00,   .00000000E+00,
              .00000000E+00

$END
GAMMA IN FT**2/SEC =   7.83097491+03
EDDY VISCOSITY IN FT**2/SEC =   8.24884057-01
TEMPERATURE IN RANKINE =   5.29014931+02
DENSITY IN SLUGS/FT**3 =   2.30571828-03
ACOUSTIC VELOCITY IN FT/SEC =   1.12747589+03
STABILITY IN 1/SEC**2 =   0.00000000
INITIAL PARAMETER (DIMENSIONLESS) =   0.00000000
```

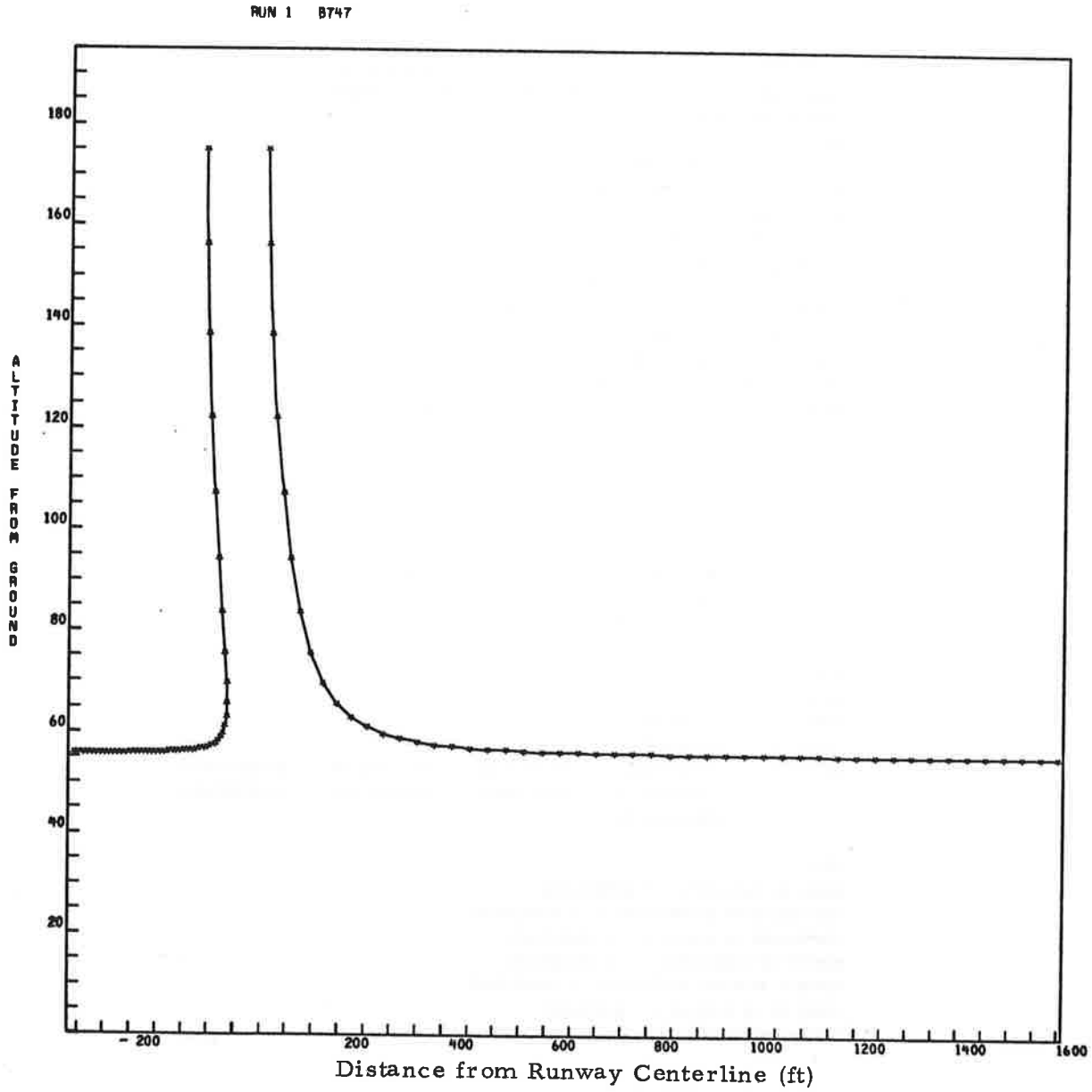
RUN 1 B747
ALTITUDE FROM GROUND
180
160
140
120
100
80
60
40
20
- 200
200
400
600
800
1000
1200
1400
1600
Distance from Runway Centerline (ft)

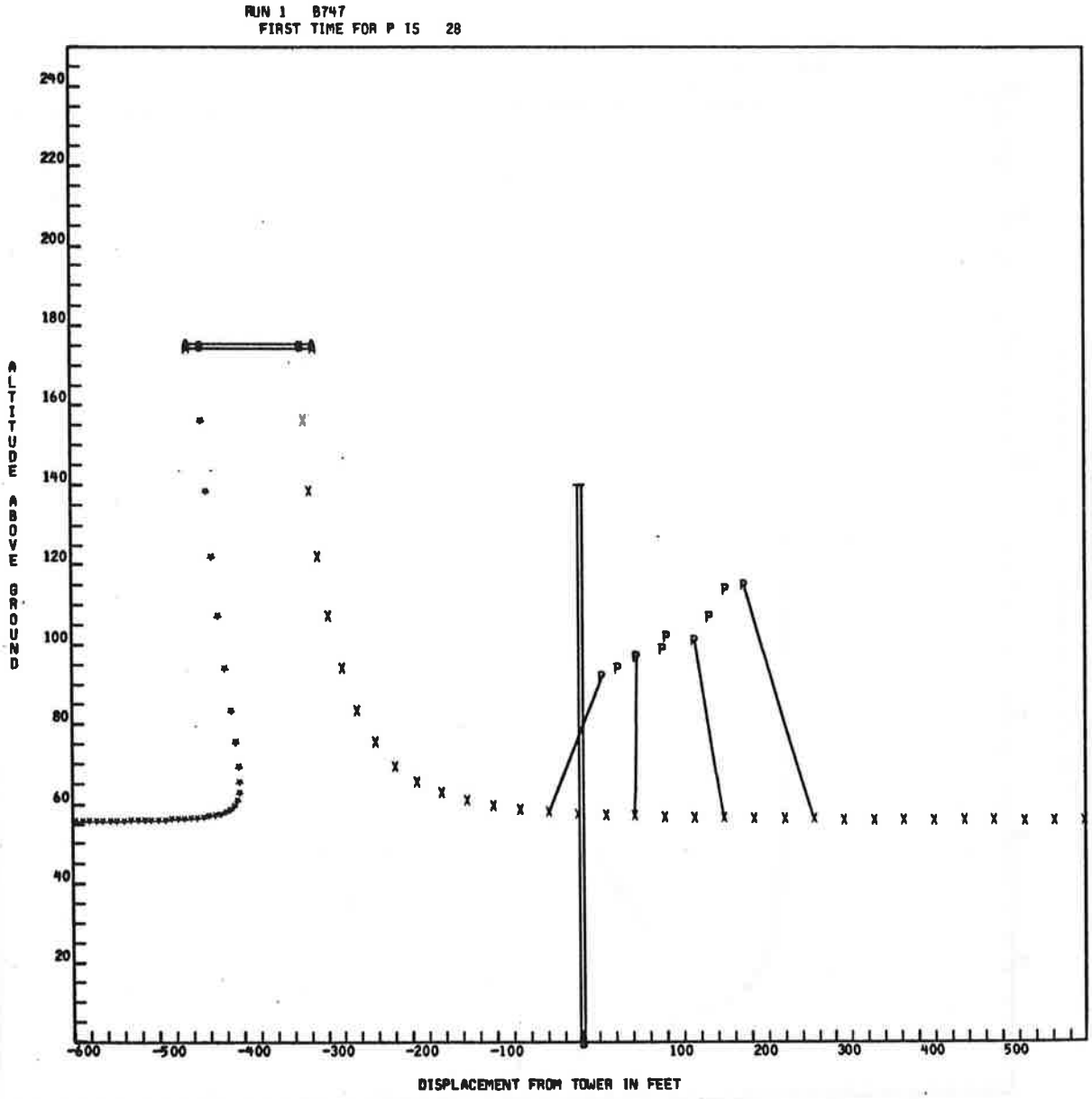
RUN 1 B747
FIRST TIME FOR P IS 28
ALTITUDE ABOVE GROUND
240
220
200
180
160
140
120
100
80
60
40
20
-600
-500
-400
-300
-200
-100
100
200
300
400
500
DISPLACEMENT FROM TOWER IN FEET

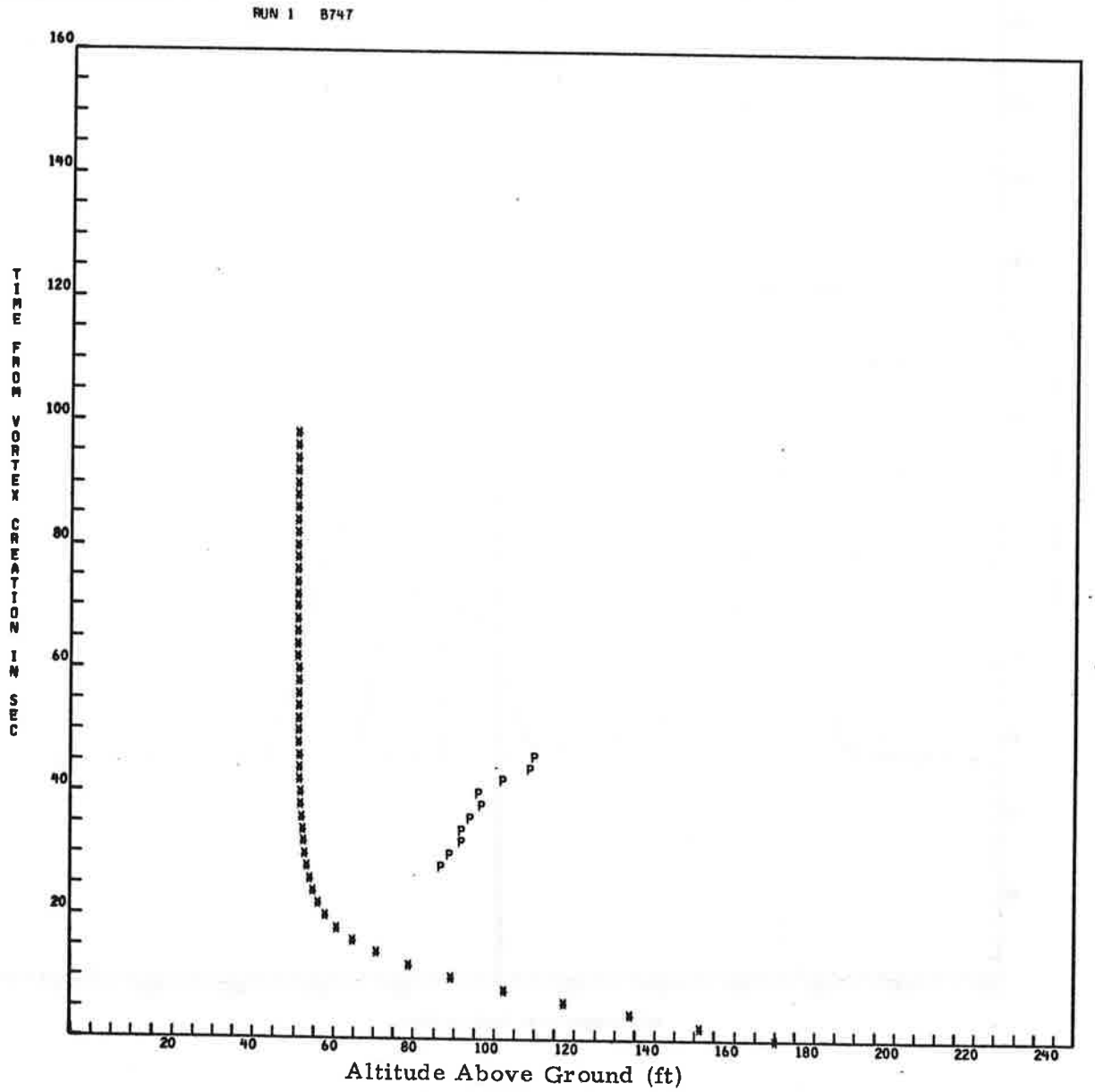
RUN 1 B747
TIME FROM VORTEX CREATION IN SEC
160
140
120
100
80
60
40
20
20
40
60
80
100
120
140
160
180
200
220
240
Altitude Above Ground (ft)

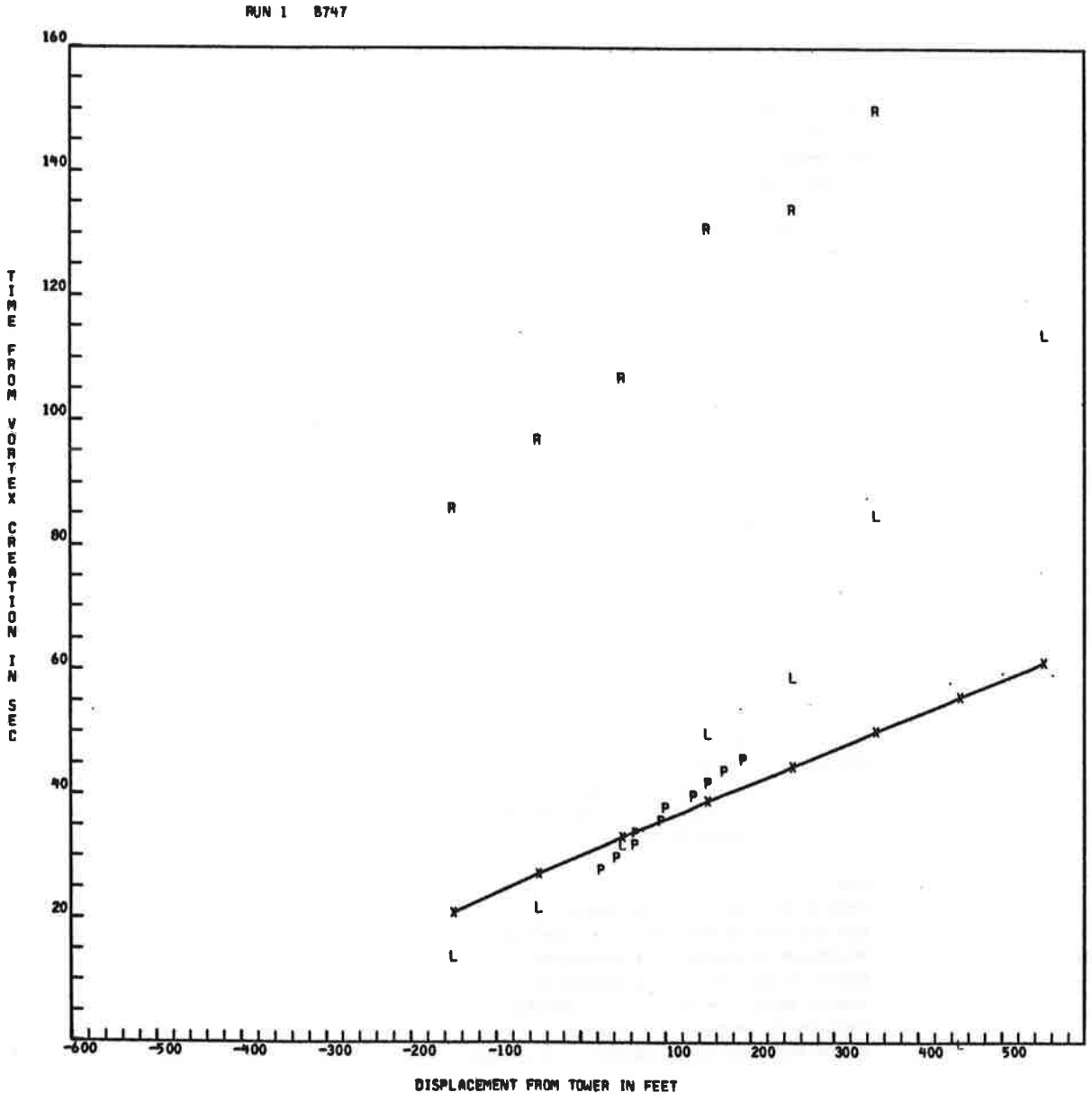
RUN 1 B747
TIME FROM VORTEX CREATION IN SEC
160
140
120
100
80
60
40
20
-600
-500
-400
-300
-200
-100
100
200
300
400
500
DISPLACEMENT FROM TOWER IN FEET
R
L
P

```
                                                    RUN DATA CARD
CONFIGURATION     LANDING LEVEL FLIGHT ALL ENGINES SAME POWER
AIRCRAFT TYPE IS B747
RUN NUMBER   2
AIRCRAFT DISPLACEMENT FROM TOWER -267 FT
AIRCRAFT ALTITUDE ABREAST OF TOWER 178 FT
AIRCRAFT WEIGHT 536000. POUNDS
AIRSPEED  256.7 FT/SEC
TEMPERATURE  17 DEGREES C (NOT USED)
INITIAL WIND SPEED   0 MPH  (NOT USED)
INITIAL WIND ANGLE   0 DEGREES TRUE  (NOT USED)
FINAL WIND SPEED   0 MPH  (NOT USED)
FINAL WIND ANGLE   0 DEGREES TRUE  (NOT USED)
AIRCRAFT HEADING 125 DEGREES MAGNETIC
MONTH  9     DAY 16     HOUR  8     MINUTE 58     LOCAL TIME



$OUTPUT
SPEED   =    -.25672800E+03
WEIGHT  =     .53600000E+06
WSPAN   =     .14974400E+03

$END
$WLOG
WSPR    =     .14993204E+02
CPOWER  =     .13012546E+00
COEF    =     .25496890E+03,   .38674871E-01,   .12020770E-02,   .11677842E+01,
              .00000000E+00,   .00000000E+00,   .00000000E+00,   .00000000E+00,
              .00000000E+00

$END
GAMMA IN FT**2/SEC =   7.72030853+03
EDDY VISCOSITY IN FT**2/SEC =   8.19124974-01
TEMPERATURE IN RANKINE =   5.30418526+02
DENSITY IN SLUGS/FT**3 =   2.29941629-03
ACOUSTIC VELOCITY IN FT/SEC =   1.12897063+03
STABILITY IN 1/SEC**2 =   0.00000000
INITIAL PARAMETER (DIMENSIONLESS) =   0.00000000
```

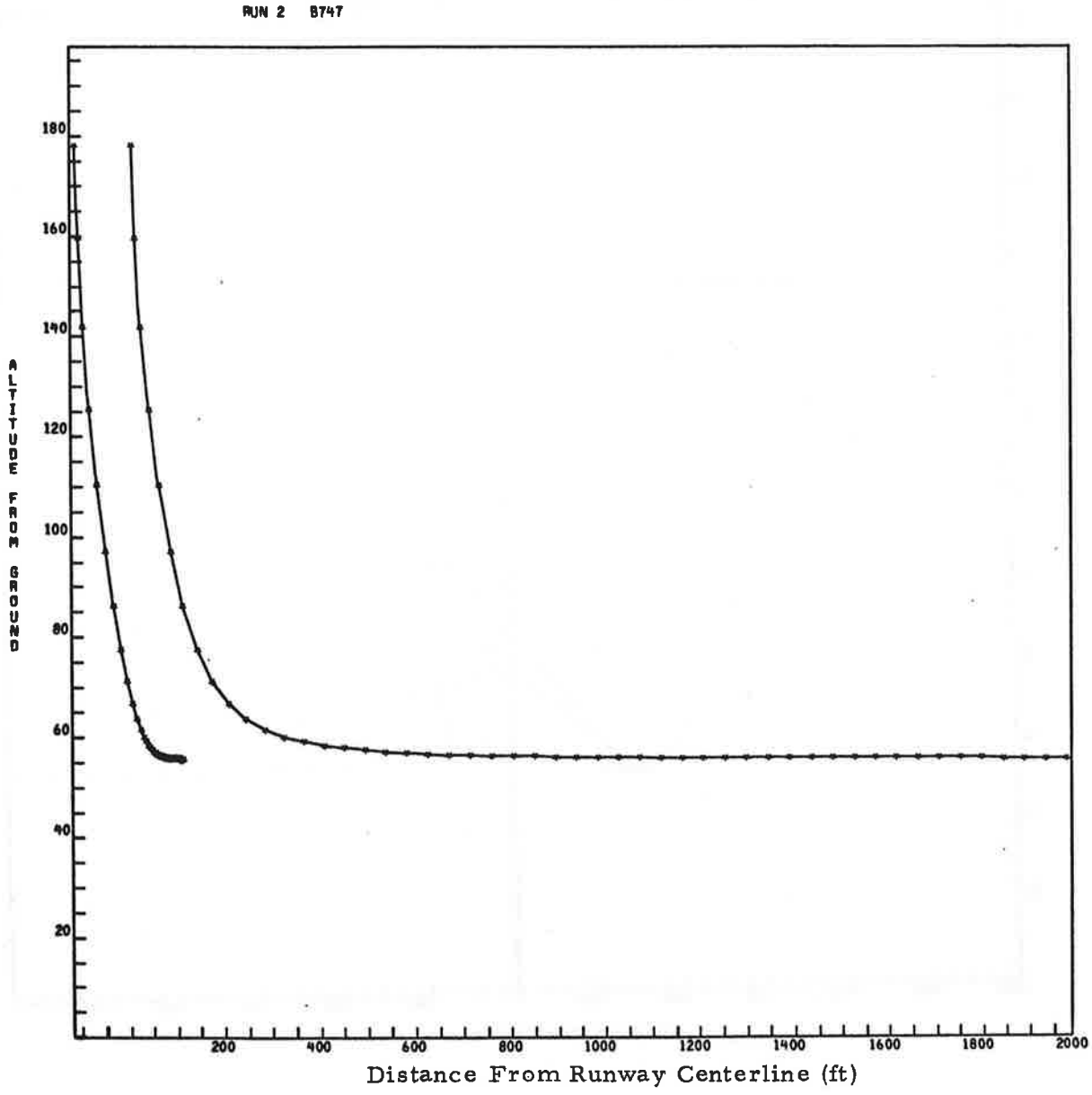
RUN 2 B747
ALTITUDE FROM GROUND
180
160
140
120
100
80
60
40
20
200
400
600
800
1000
1200
1400
1600
1800
2000
Distance From Runway Centerline (ft)

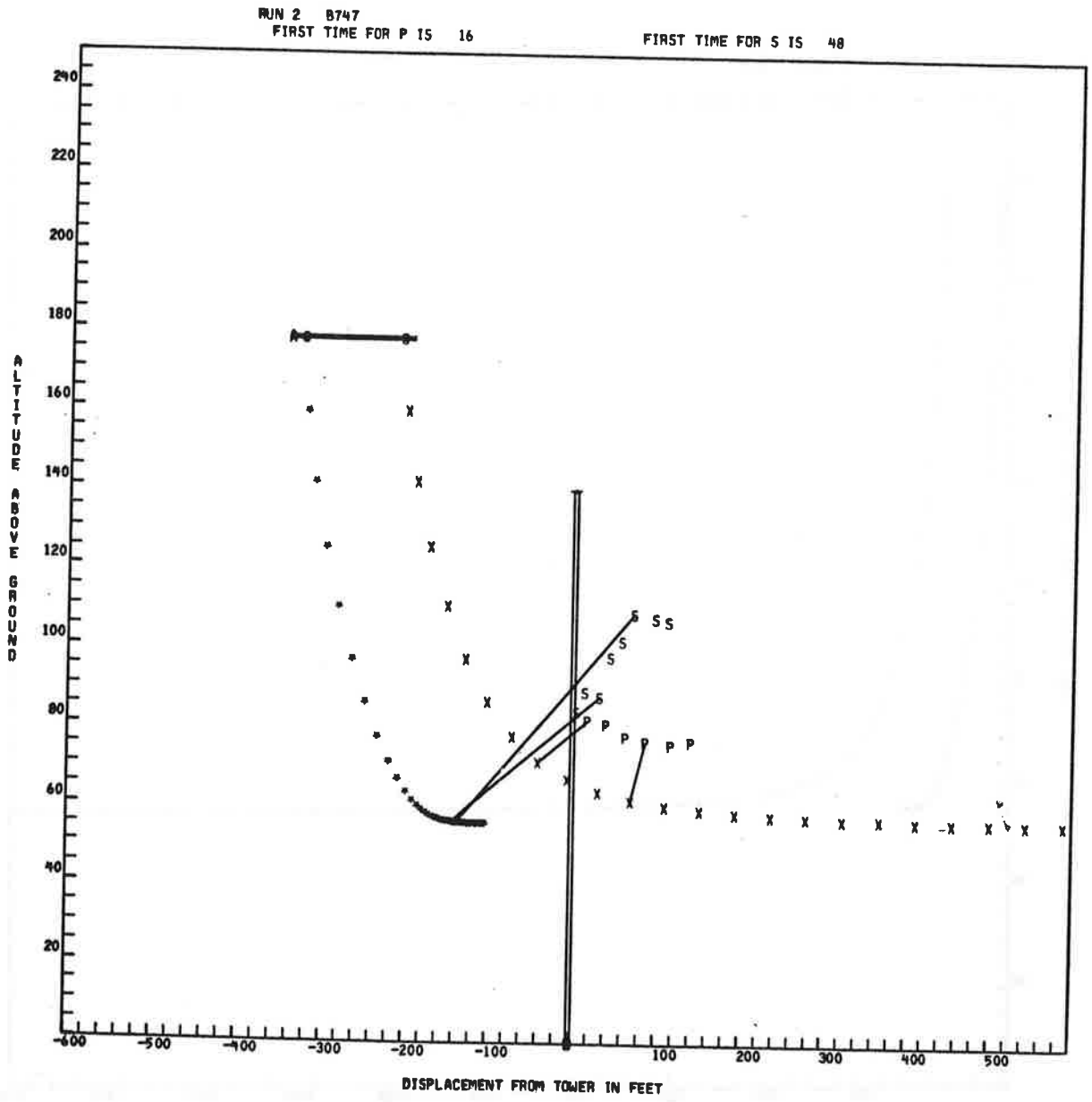
RUN 2 B747
FIRST TIME FOR P IS 16
FIRST TIME FOR S IS 48
ALTITUDE ABOVE GROUND
240
220
200
180
160
140
120
100
80
60
40
20
-600
-500
-400
-300
-200
-100
100
200
300
400
500
DISPLACEMENT FROM TOWER IN FEET

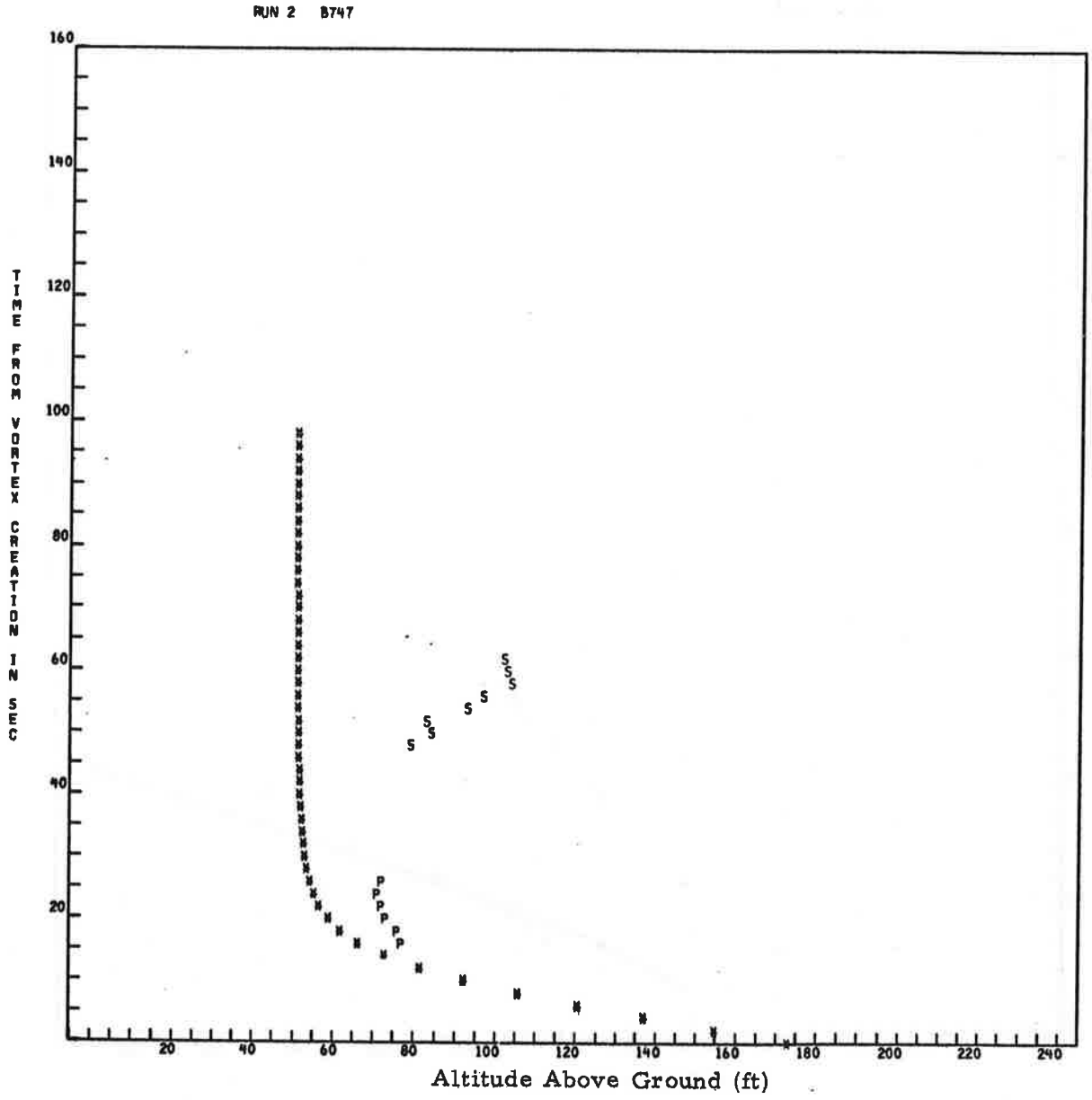
RUN 2 B747
TIME FROM VORTEX CREATION IN SEC
160
140
120
100
80
60
40
20
20
40
60
80
100
120
140
160
180
200
220
240
Altitude Above Ground (ft)

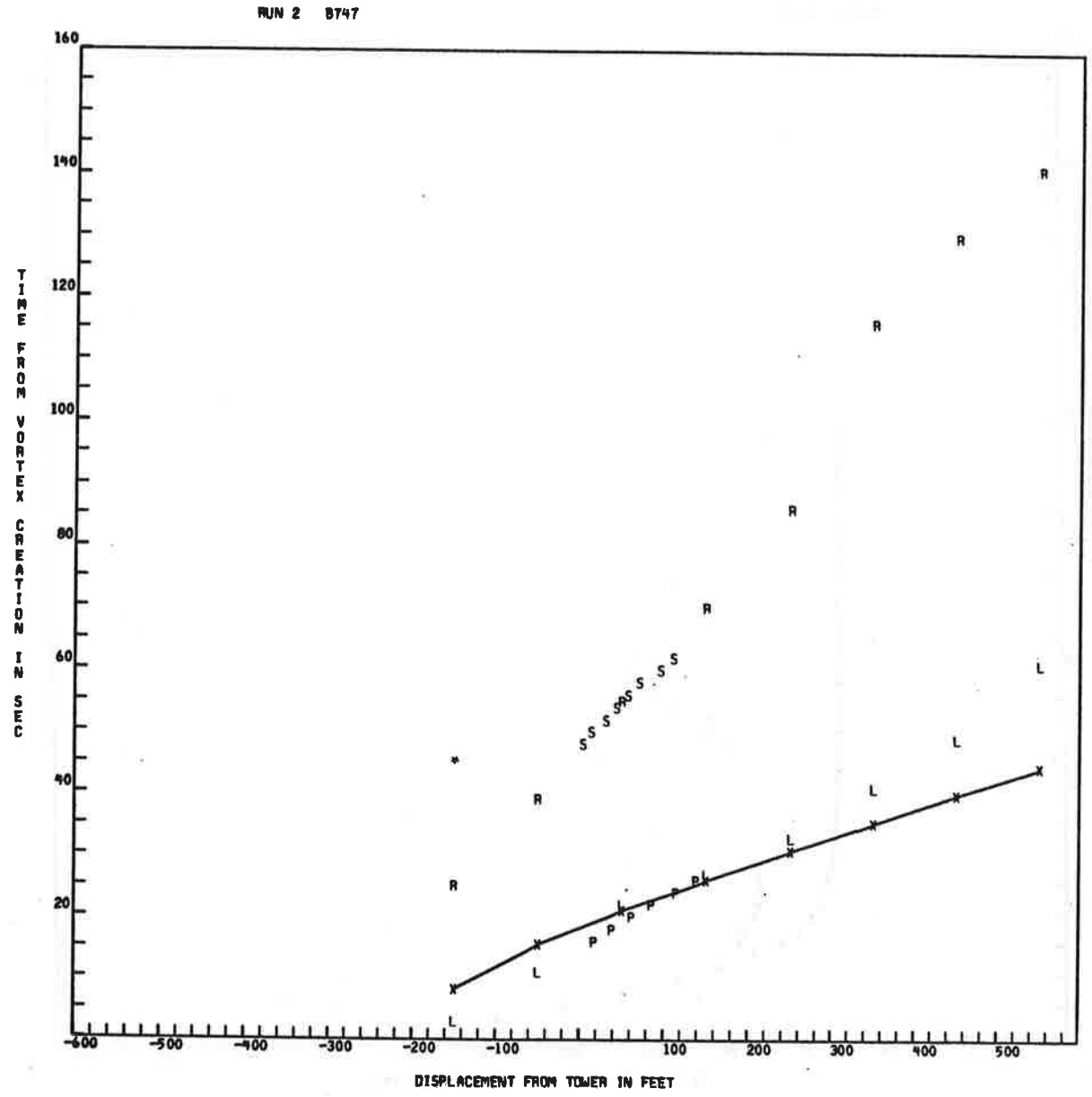
RUN 2 B747
TIME FROM VORTEX CREATION IN SEC
160
140
120
100
80
60
40
20
-600
-500
-400
-300
-200
-100
100
200
300
400
500
DISPLACEMENT FROM TOWER IN FEET

```
                                                        RUN DATA CARD
CONFIGURATION     LANDING LEVEL FLIGHT ALL ENGINES SAME POWER
AIRCRAFT TYPE IS B747
RUN NUMBER   3
AIRCRAFT DISPLACEMENT FROM TOWER -448 FT
AIRCRAFT ALTITUDE ABREAST OF TOWER 191 FT
AIRCRAFT WEIGHT 534000. POUNDS
AIRSPEED  256.7 FT/SEC
TEMPERATURE  17 DEGREES C (NOT USED)
INITIAL, WIND SPEED   5 MPH  (NOT USED)
INITIAL WIND ANGLE 250 DEGREES TRUE  (NOT USED)
FINAL WIND SPEED   8 MPH  (NOT USED)
FINAL WIND ANGLE 240 DEGREES TRUE  (NOT USED)
AIRCRAFT HEADING 125 DEGREES MAGNETIC
MONTH  9     DAY 16     HOUR  9     MINUTE  2     LOCAL TIME



$OUTPUT
SPEED   =    -.25672800E+03
WEIGHT  =     .53400000E+06
WSPAN   =     .14974400E+03

$END
$WLOG
WSPR    =     .17973364E+02
CPOWER  =     .77371543E-01
COEF    =     .26026377E+03,   .12344263E-01,   .53632256E-03,   .12937201E+01,
              .00000000E+00,   .00000000E+00,   .00000000E+00,   .00000000E+00,
              .00000000E+00

$END
GAMMA IN FT**2/SEC =   7.69683868+03
EDDY VISCOSITY IN FT**2/SEC =   8.17851804-01
TEMPERATURE IN RANKINE =   5.30542343+02
DENSITY IN SLUGS/FT**3 =   2.29782180-03
ACOUSTIC VELOCITY IN FT/SEC =   1.12910239+03
STABILITY IN 1/SEC**2 =   0.00000000
INITIAL PARAMETER (DIMENSIONLESS) =   0.00000000
```

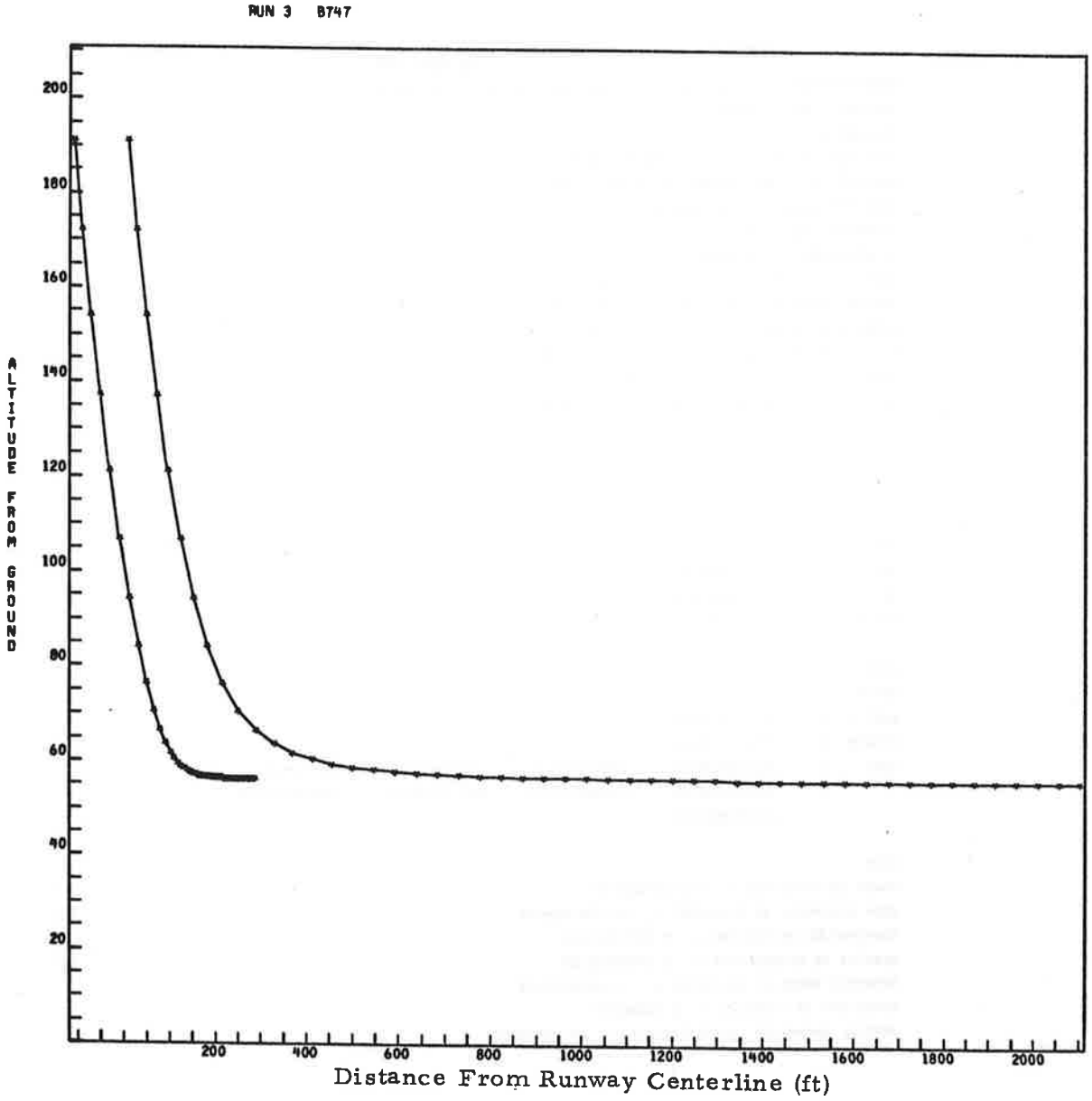
RUN 3 B747
ALTITUDE FROM GROUND
200
180
160
140
120
100
80
60
40
20
200
400
600
800
1000
1200
1400
1600
1800
2000
Distance From Runway Centerline (ft)

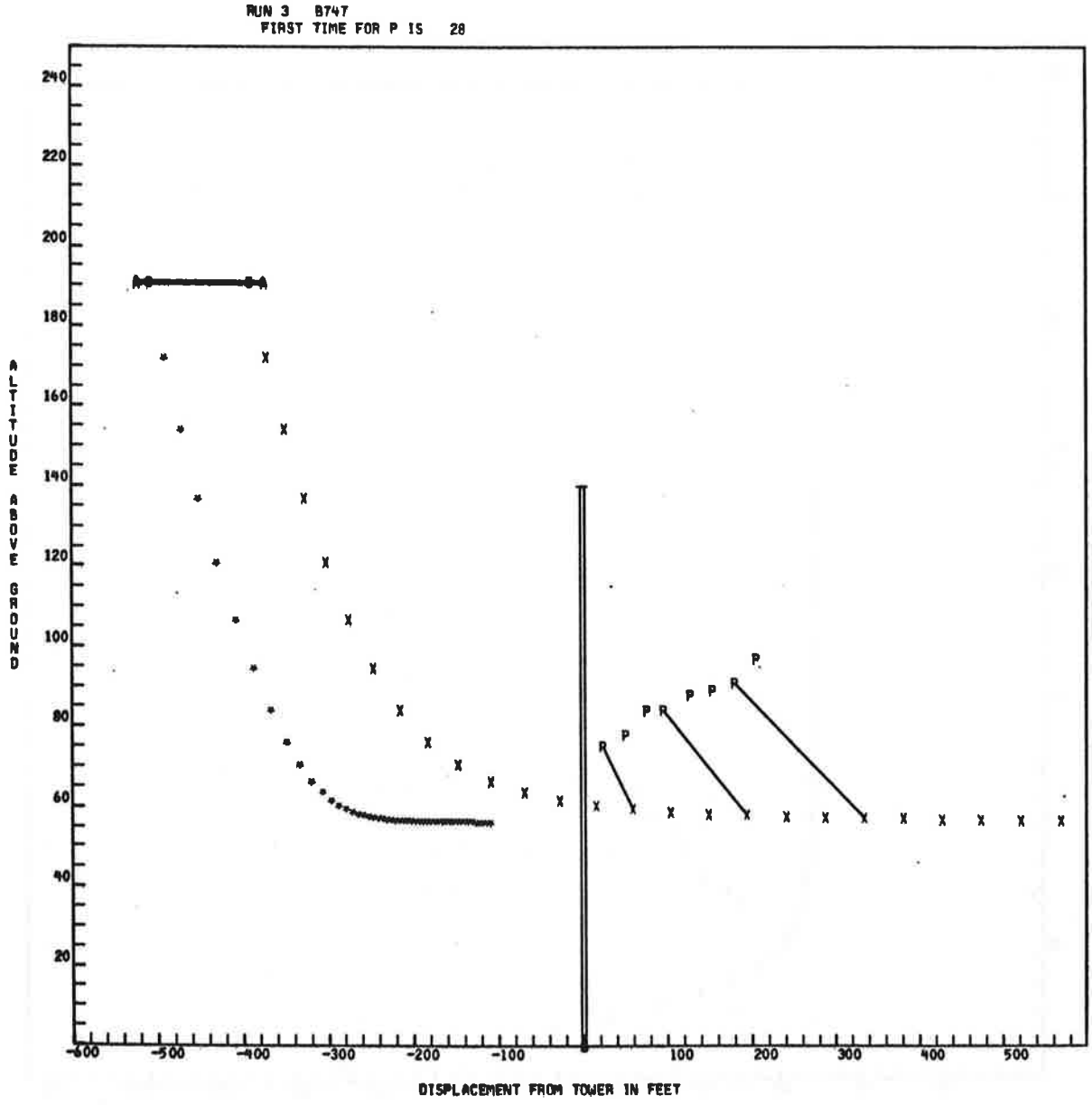
RUN 3 B747
FIRST TIME FOR P IS 28
ALTITUDE ABOVE GROUND
240
220
200
180
160
140
120
100
80
60
40
20
-600
-500
-400
-300
-200
-100
100
200
300
400
500
DISPLACEMENT FROM TOWER IN FEET

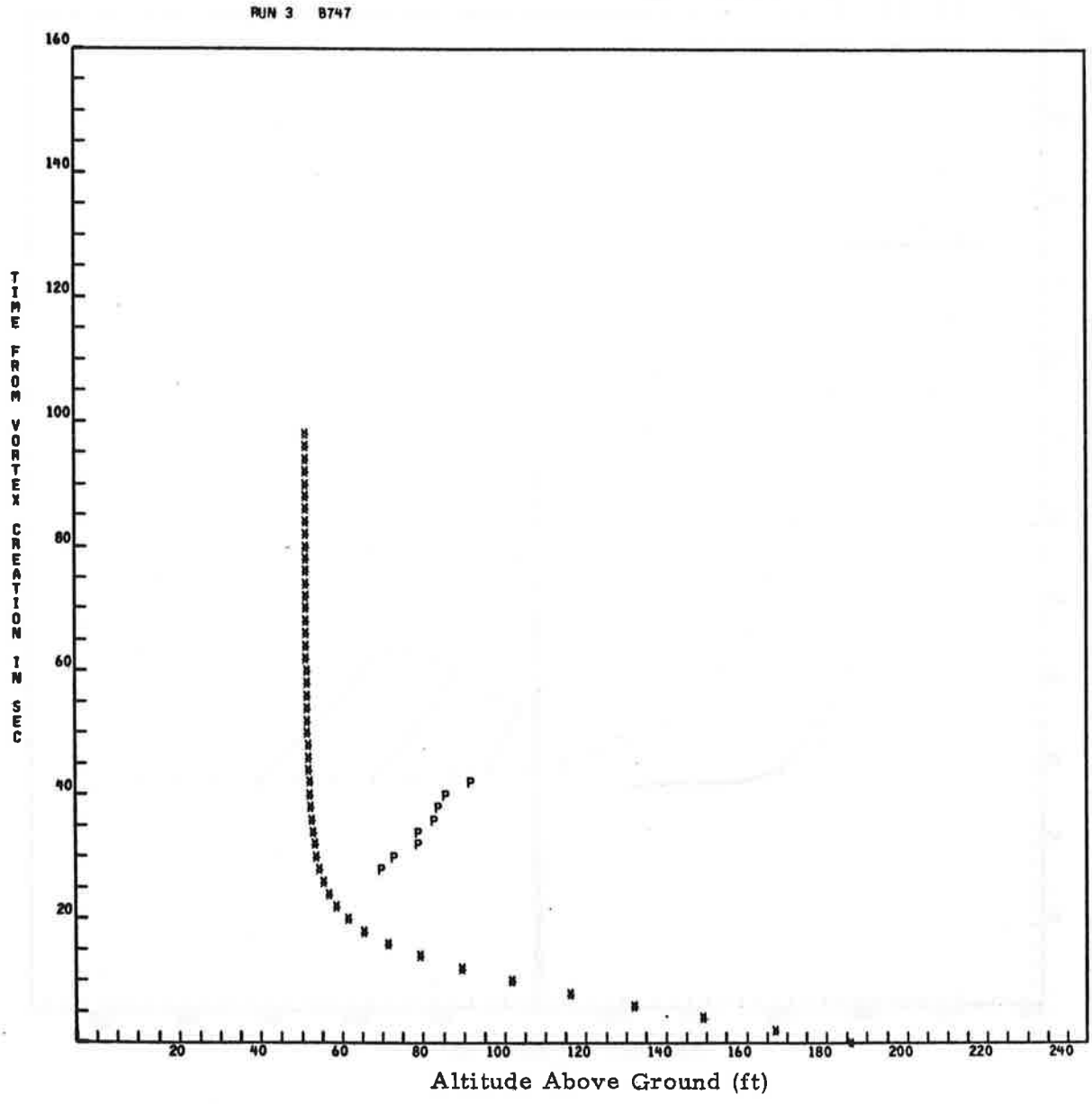
RUN 3 B747
TIME FROM VORTEX CREATION IN SEC
160
140
120
100
80
60
40
20
20
40
60
80
100
120
140
160
180
200
220
240
Altitude Above Ground (ft)

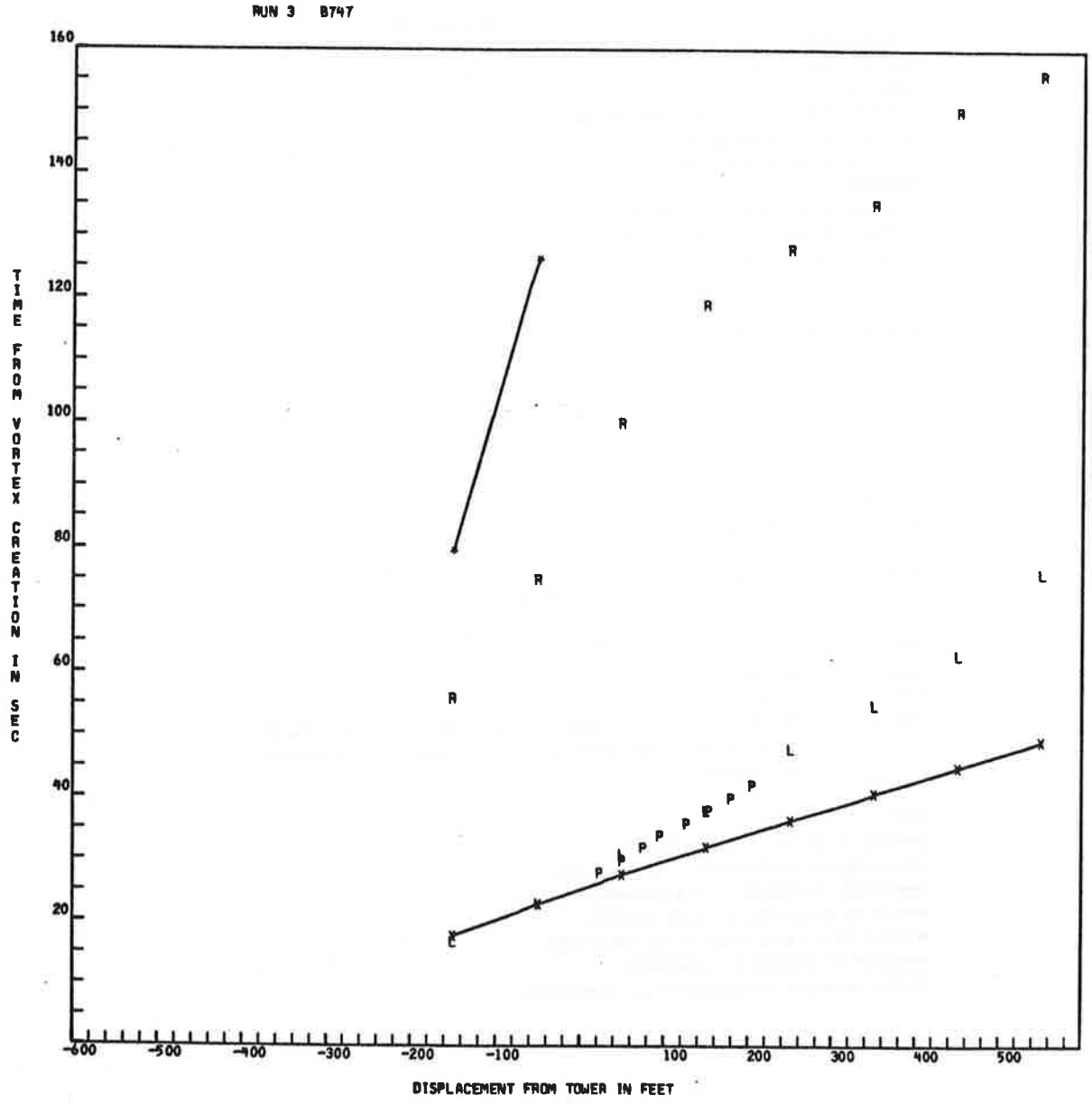
RUN 3 B747
TIME FROM VORTEX CREATION IN SEC
160
140
120
100
80
60
40
20
-600
-500
-400
-300
-200
-100
100
200
300
400
500
DISPLACEMENT FROM TOWER IN FEET
R
L
P

RUN DATA CARD

CONFIGURATION LANDING LEVEL FLIGHT ALL ENGINES SAME POWER
AIRCRAFT TYPE IS B747
RUN NUMBER 4
AIRCRAFT DISPLACEMENT FROM TOWER -291 FT
AIRCRAFT ALTITUDE ABREAST OF TOWER 197 FT
AIRCRAFT WEIGHT 532000. POUNDS
AIRSPEED 243.2 FT/SEC
TEMPERATURE 17 DEGREES C (NOT USED)
INITIAL WIND SPEED 5 MPH (NOT USED)
INITIAL WIND ANGLE 250 DEGREES TRUE (NOT USED)
FINAL WIND SPEED 8 MPH (NOT USED)
FINAL WIND ANGLE 250 DEGREES TRUE (NOT USED)
AIRCRAFT HEADING 130 DEGREES MAGNETIC
MONTH 9 DAY 16 HOUR 9 MINUTE 6 LOCAL TIME

$OUTPUT
SPEED = -.24321600E+03
WEIGHT = .53200000E+06
WSPAN = .14974400E+03

$END
$WLOG
WSPR = .13273246E+02
CPOWER = .13769303E-01
COEF = .25127995E+03, .19224443E+00, -.33775045E-03, .20989050E+01,
.00000000E+00, .00000000E+00, .00000000E+00, .00000000E+00,
.00000000E+00

$END
GAMMA IN FT**2/SEC = 0.00242206+03
EDDY VISCOSITY IN FT**2/SEC = 0.31362642-01
TEMPERATURE IN RANKINE = 5.24388458+02
DENSITY IN SLUGS/FT**3 = 2.32412107-03
ACOUSTIC VELOCITY IN FT/SEC = 1.12253494+03
STABILITY IN 1/SEC**2 = 0.00000000
INITIAL PARAMETER (DIMENSIONLESS) = 0.00000000

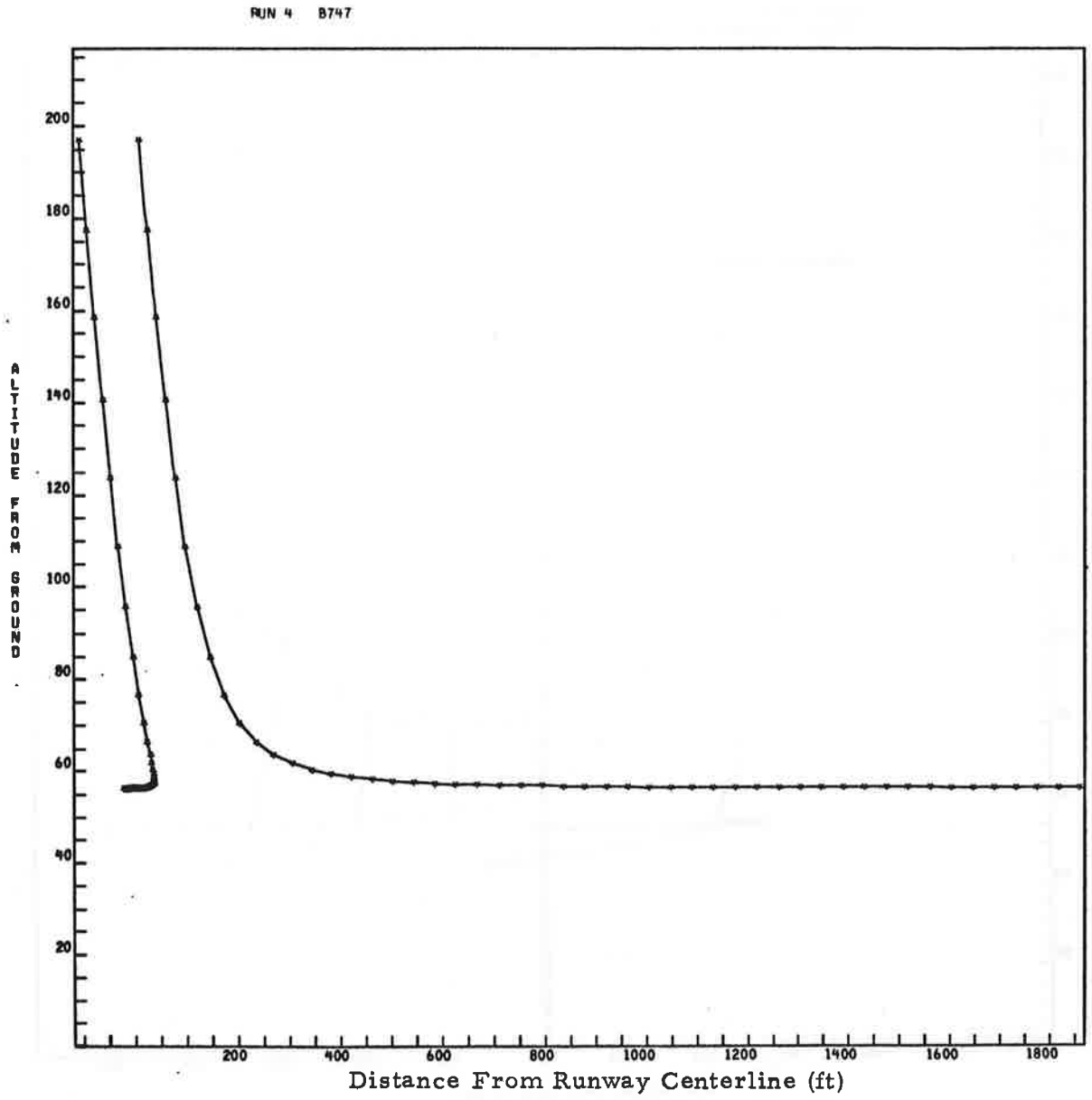
RUN 4 B747
ALTITUDE FROM GROUND
200
180
160
140
120
100
80
60
40
20
200
400
600
800
1000
1200
1400
1600
1800
Distance From Runway Centerline (ft)

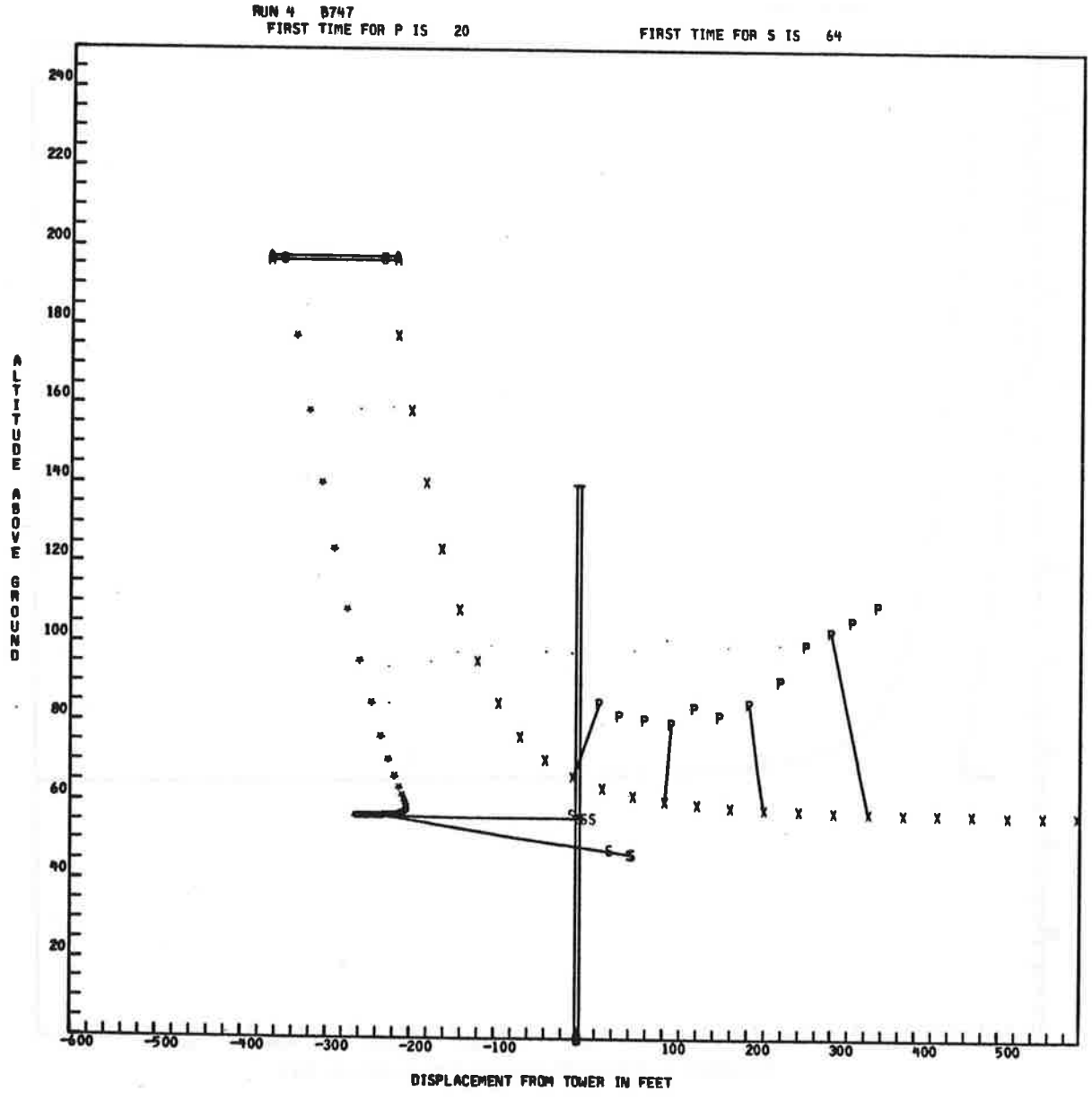
RUN 4 B747
FIRST TIME FOR P IS 20
FIRST TIME FOR S IS 64
ALTITUDE ABOVE GROUND
240
220
200
180
160
140
120
100
80
60
40
20
-600
-500
-400
-300
-200
-100
100
200
300
400
500
DISPLACEMENT FROM TOWER IN FEET

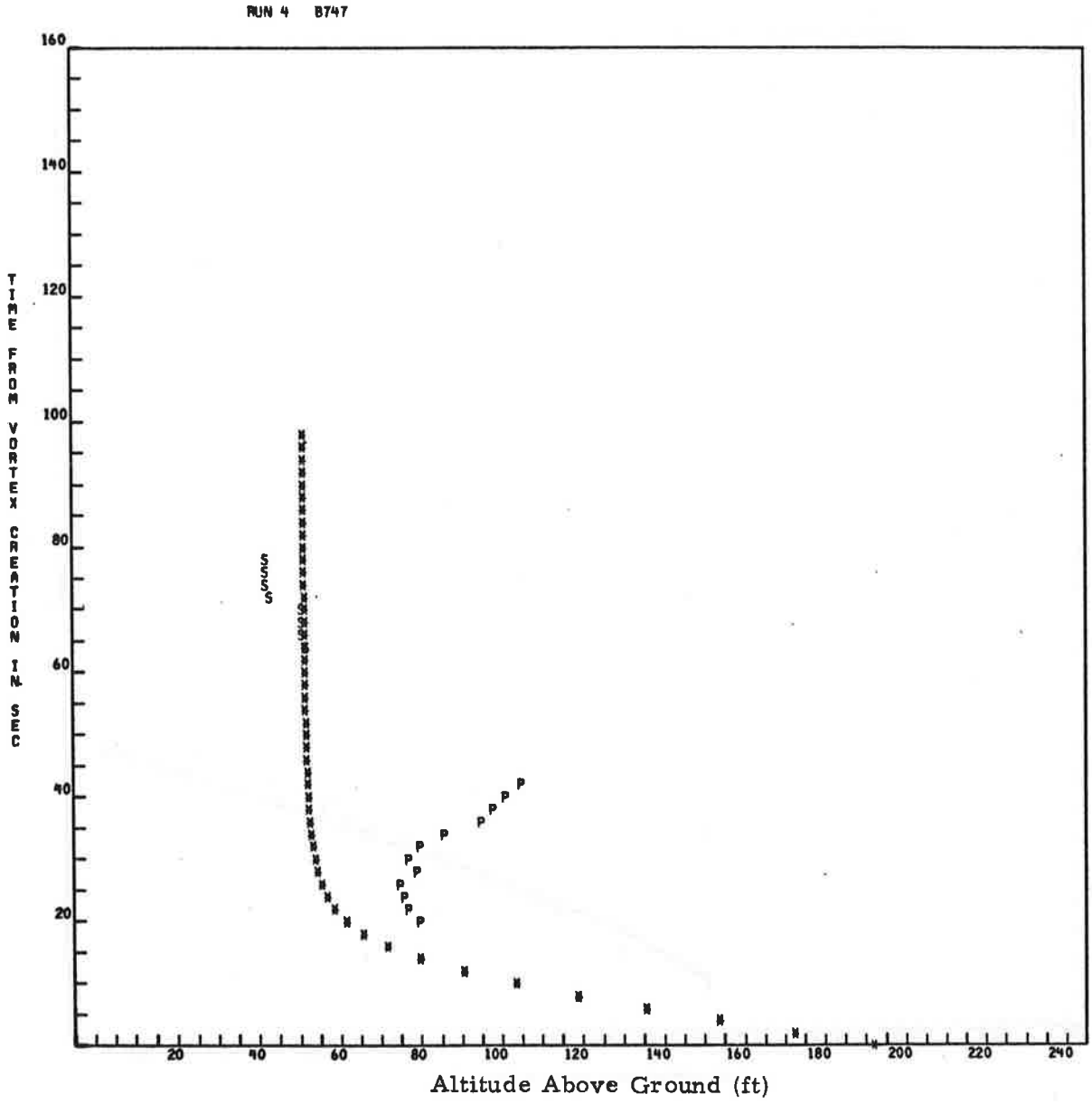
RUN 4 B747
TIME FROM VORTEX CREATION IN SEC
160
140
120
100
80
60
40
20
20
40
60
80
100
120
140
160
180
200
220
240
Altitude Above Ground (ft)

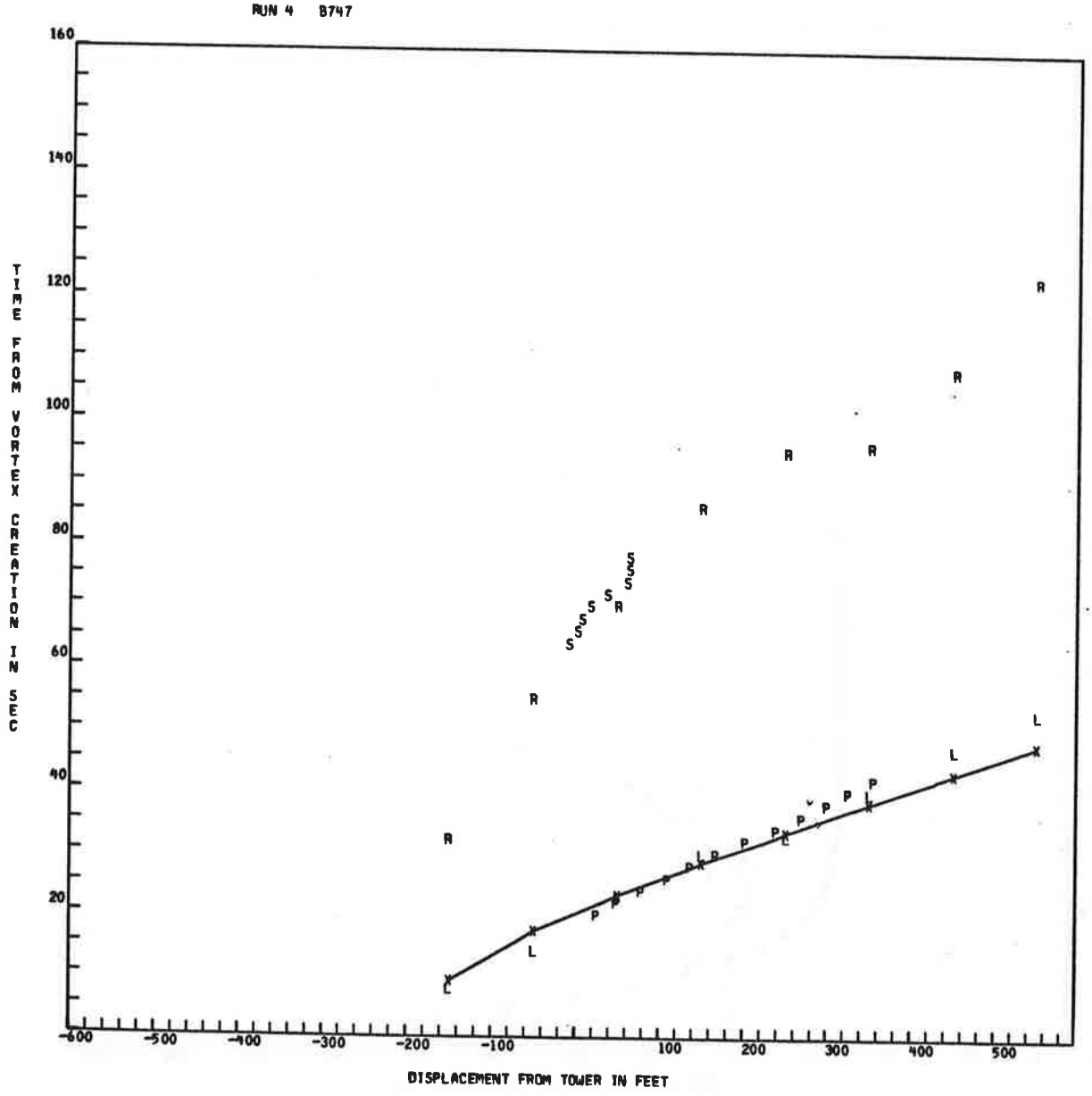
RUN 4 B747
TIME FROM VORTEX CREATION IN SEC
160
140
120
100
80
60
40
20
-600
-500
-400
-300
-200
-100
100
200
300
400
500
DISPLACEMENT FROM TOWER IN FEET

```
                                                          RUN DATA CARD
CONFIGURATION     LANDING LEVEL FLIGHT ALL ENGINES SAME POWER
AIRCRAFT TYPE IS B747
RUN NUMBER   5
AIRCRAFT DISPLACEMENT FROM TOWER -296 FT
AIRCRAFT ALTITUDE ABREAST OF TOWER 163 FT
AIRCRAFT WEIGHT 530000. POUNDS
AIRSPEED  246.6 FT/SEC
TEMPERATURE  17 DEGREES C (NOT USED)
INITIAL WIND SPEED   8 MPH  (NOT USED)
INITIAL WIND ANGLE 250 DEGREES TRUE  (NOT USED)
FINAL WIND SPEED   5 MPH  (NOT USED)
FINAL WIND ANGLE 260 DEGREES TRUE  (NOT USED)
AIRCRAFT HEADING 132 DEGREES MAGNETIC
MONTH  9     DAY 16     HOUR  9     MINUTE 10     LOCAL TIME



$OUTPUT
SPEED   =    -.24659400E+03
WEIGHT  =     .53000000E+06
WSPAN   =     .14974400E+03

$END
$WLOG
WSPR    =     .15358286E+02
CPOWER  =    -.27429159E-01
COEF    =     .26367492E+03,  -.13018556E+00,   .11804826E-02,   .30299827E+01,
              .00000000E+00,   .00000000E+00,   .00000000E+00,   .00000000E+00,
              .00000000E+00

$END
GAMMA IN FT**2/SEC =   7.87541522+03
EDDY VISCOSITY IN FT**2/SEC =   8.24321039-01
TEMPERATURE IN RANKINE =   5.25850891+02
DENSITY IN SLUGS/FT**3 =   2.32049485-03
ACOUSTIC VELOCITY IN FT/SEC =   1.12409912+03
STABILITY IN 1/SEC**2 =   0.00000000
INITIAL PARAMETER (DIMENSIONLESS) =   0.00000000
```

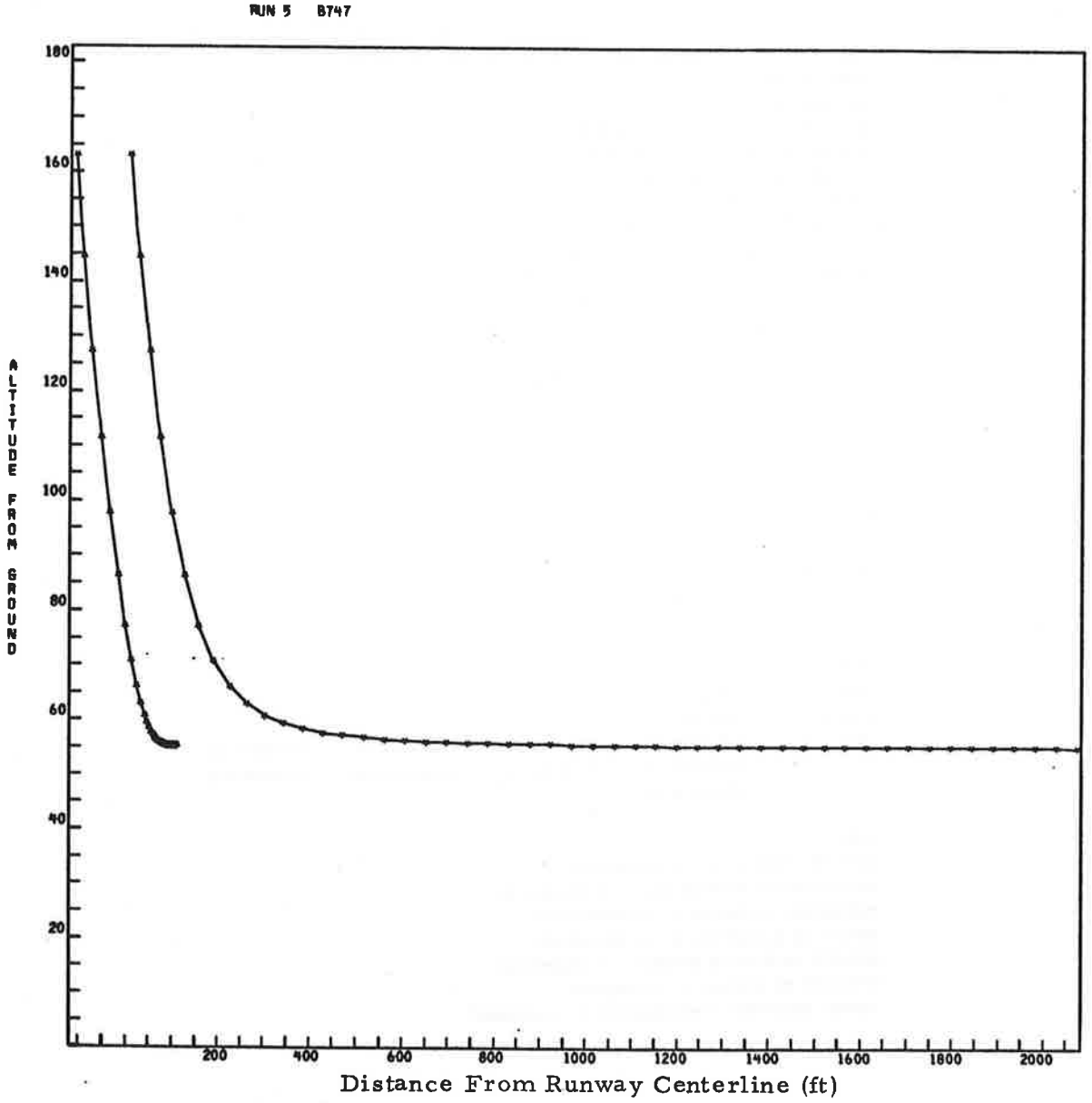
RUN 5 B747
ALTITUDE FROM GROUND
180
160
140
120
100
80
60
40
20
200
400
600
800
1000
1200
1400
1600
1800
2000
Distance From Runway Centerline (ft)

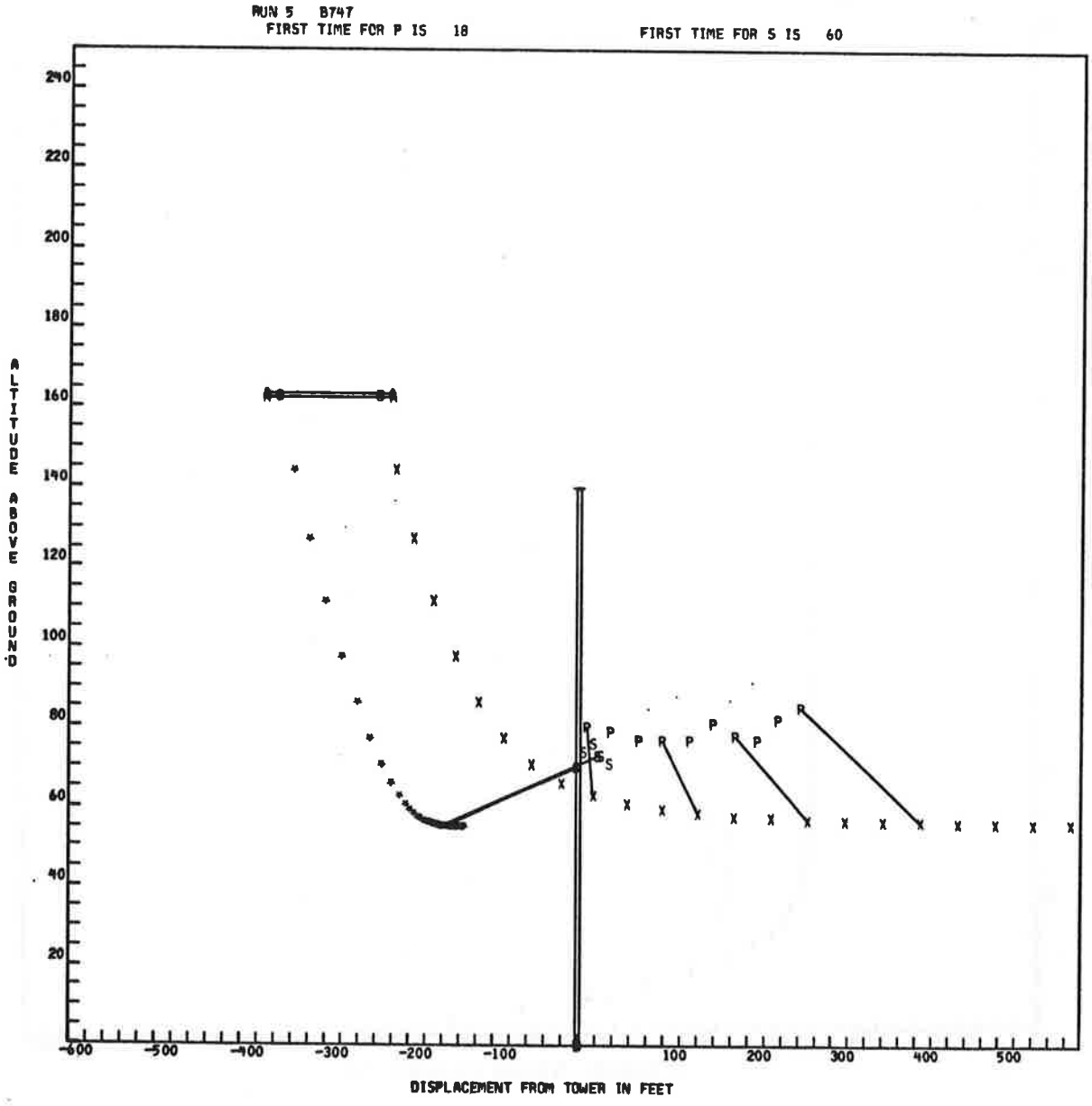
RUN 5 B747
FIRST TIME FOR P IS 18
FIRST TIME FOR S IS 60
ALTITUDE ABOVE GROUND
240
220
200
180
160
140
120
100
80
60
40
20
-600
-500
-400
-300
-200
-100
100
200
300
400
500
DISPLACEMENT FROM TOWER IN FEET

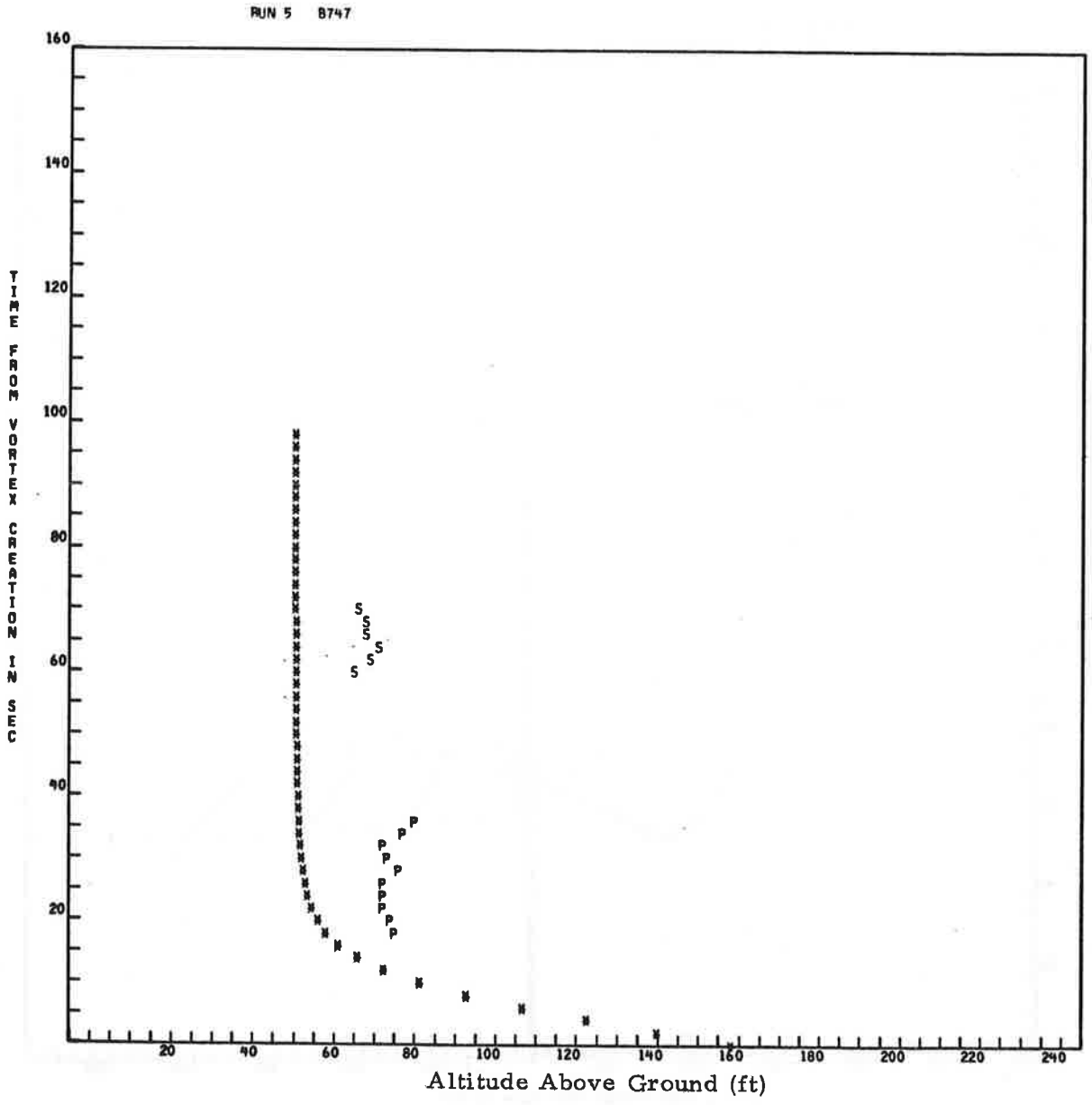
RUN 5 8747
TIME FROM VORTEX CREATION IN SEC
160
140
120
100
80
60
40
20
20
40
60
80
100
120
140
160
180
200
220
240
Altitude Above Ground (ft)

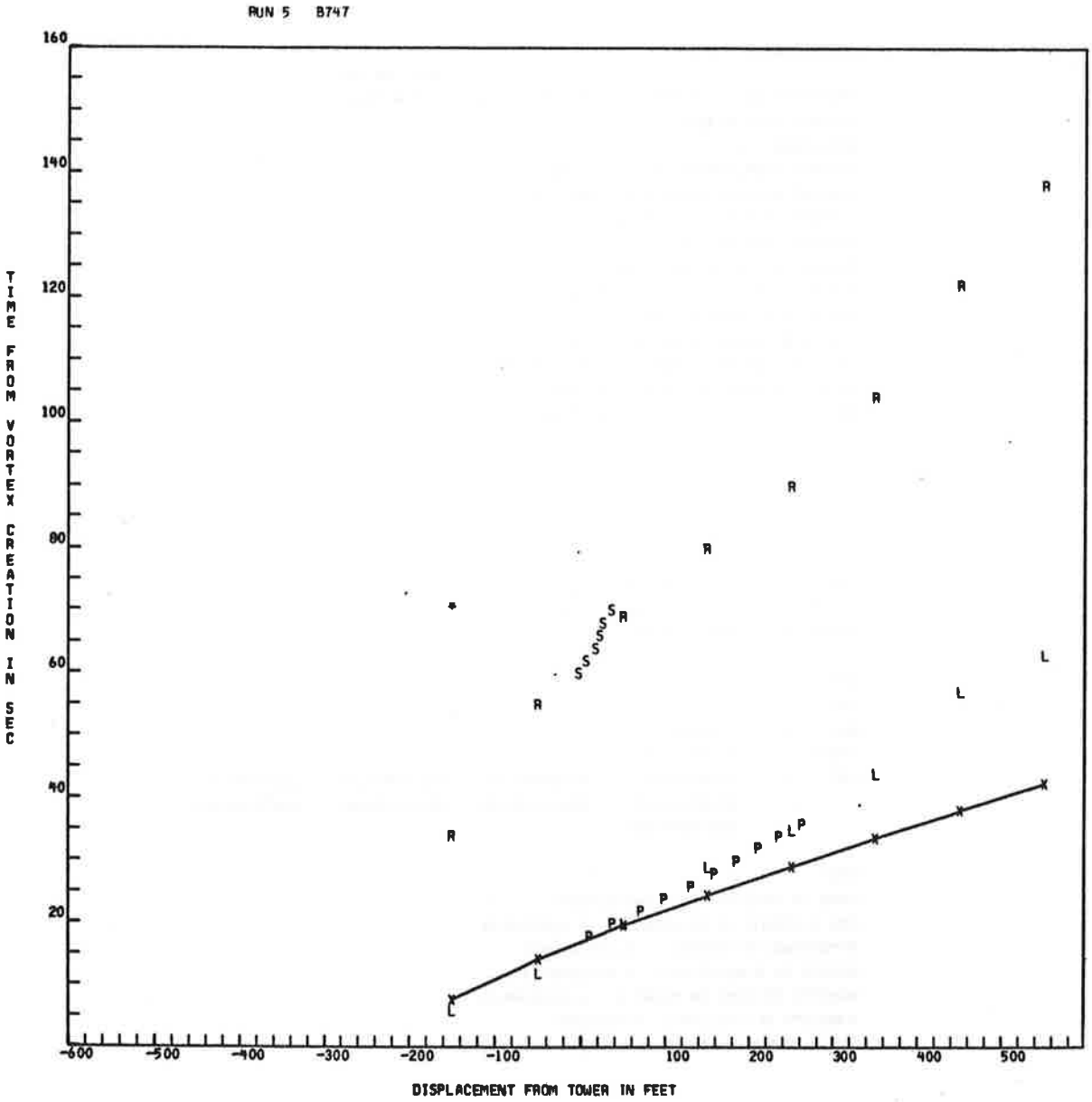
RUN 5 B747
TIME FROM VORTEX CREATION IN SEC
160
140
120
100
80
60
40
20
-600
-500
-400
-300
-200
-100
100
200
300
400
500
DISPLACEMENT FROM TOWER IN FEET

```
                                                    RUN DATA CARD
CONFIGURATION     LANDING LEVEL FLIGHT ALL ENGINES SAME POWER
AIRCRAFT TYPE IS B747
RUN NUMBER   6
AIRCRAFT DISPLACEMENT FROM TOWER -261 FT
AIRCRAFT ALTITUDE ABREAST OF TOWER 179 FT
AIRCRAFT WEIGHT 528000. POUNDS
AIRSPEED  253.3 FT/SEC
TEMPERATURE  17 DEGREES C (NOT USED)
INITIAL WIND SPEED   9 MPH  (NOT USED)
INITIAL WIND ANGLE 250 DEGREES TRUE  (NOT USED)
FINAL WIND SPEED  10 MPH  (NOT USED)
FINAL WIND ANGLE 255 DEGREES TRUE  (NOT USED)
AIRCRAFT HEADING 130 DEGREES MAGNETIC
MONTH  9     DAY 16     HOUR  9     MINUTE 14     LOCAL TIME



$OUTPUT
SPEED   =    -.25335000E+03
WEIGHT  =     .52800000E+06
WSPAN   =     .14974400E+03

$END
$WLOG
WSPR    =     .15809297E+02
CPOWER  =     .11253494E+00
COEF    =     .25224051E+03,   .33188536E+00,  -.11313155E-02,   .28082560E+01,
              .00000000E+00,   .00000000E+00,   .00000000E+00,   .00000000E+00,
              .00000000E+00

$END
GAMMA IN FT**2/SEC =   7.68212695+03
EDDY VISCOSITY IN FT**2/SEC =   8.14859048-01
TEMPERATURE IN RANKINE =   5.28714828+02
DENSITY IN SLUGS/FT**3 =   2.30670598-03
ACOUSTIC VELOCITY IN FT/SEC =   1.12715605+03
STABILITY IN 1/SEC**2 =   0.00000000
INITIAL PARAMETER (DIMENSIONLESS) =   0.00000000
```

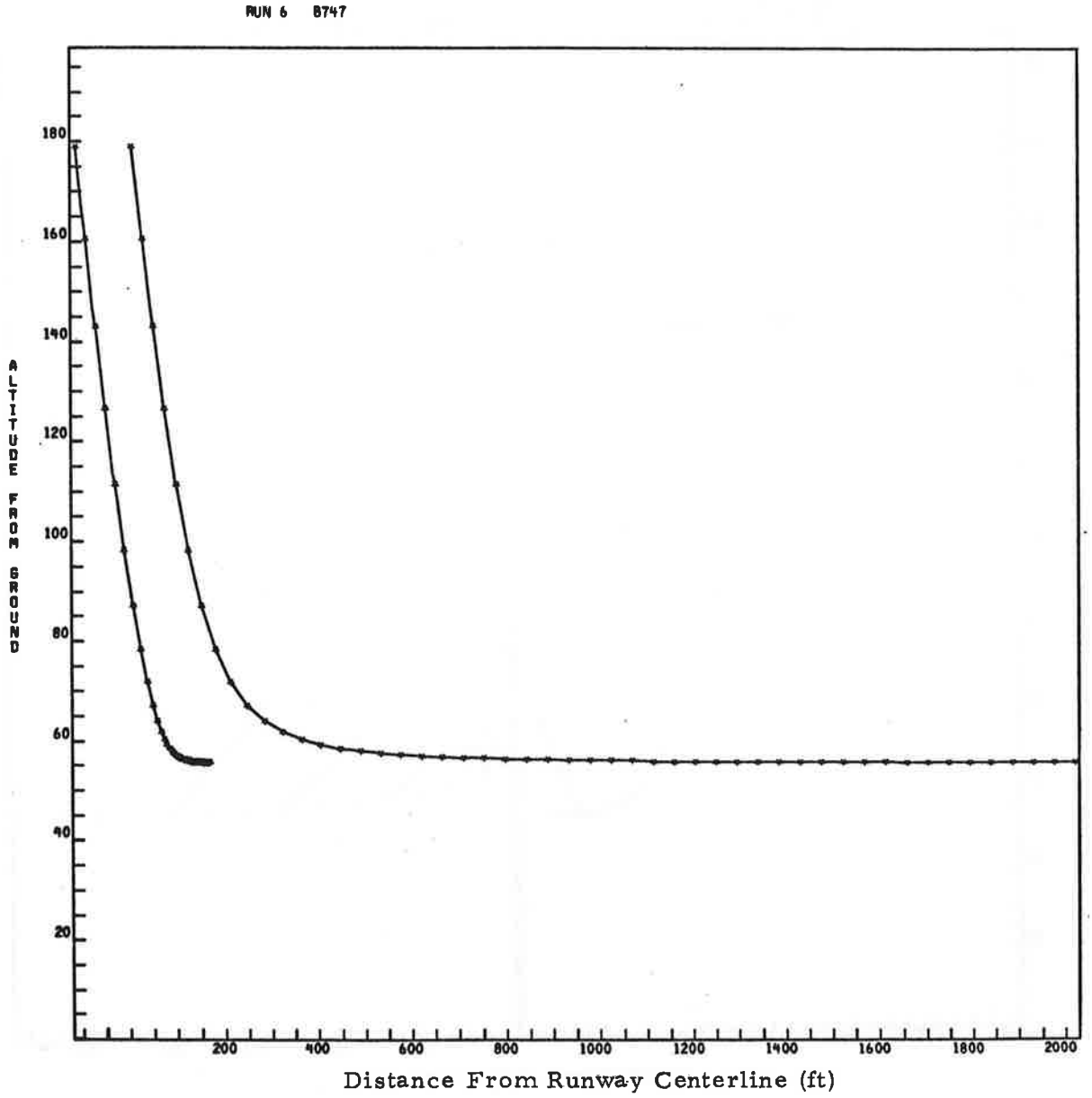
RUN 6 B747
ALTITUDE FROM GROUND
180
160
140
120
100
80
60
40
20
200
400
600
800
1000
1200
1400
1600
1800
2000
Distance From Runway Centerline (ft)

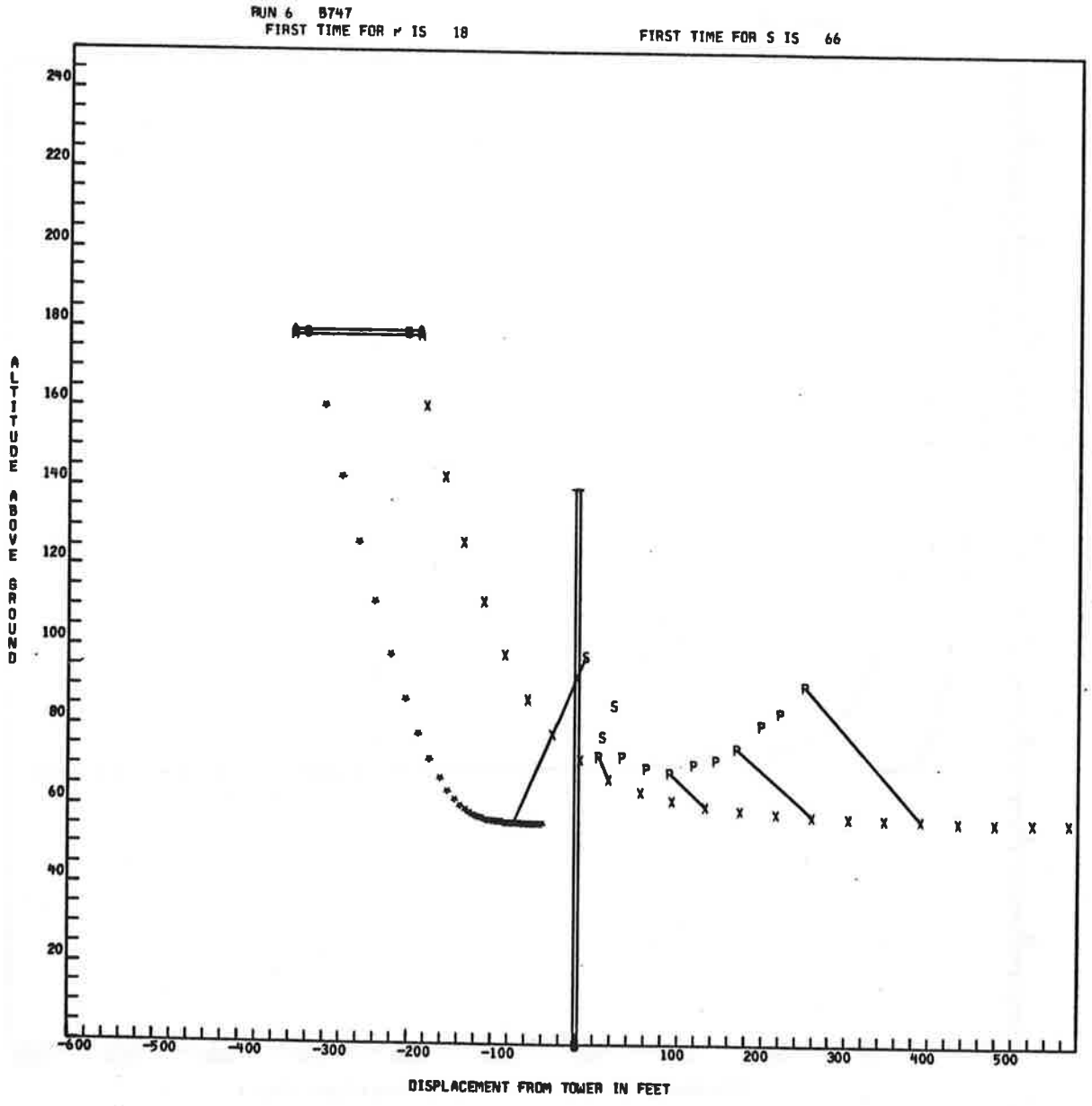
RUN 6 B747
FIRST TIME FOR P IS 18
FIRST TIME FOR S IS 66
ALTITUDE ABOVE GROUND
240
220
200
180
160
140
120
100
80
60
40
20
-600
-500
-400
-300
-200
-100
100
200
300
400
500
DISPLACEMENT FROM TOWER IN FEET

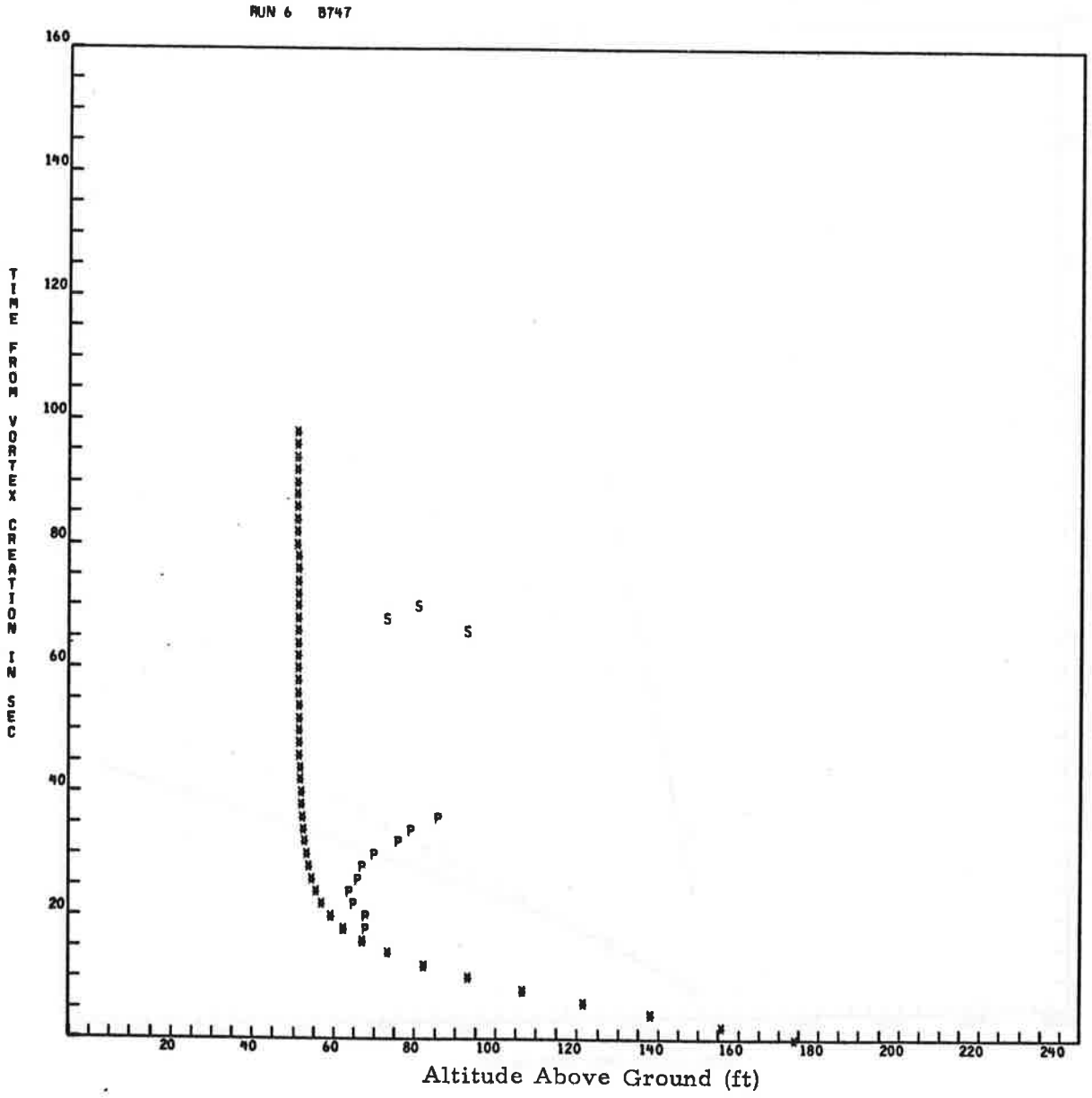
RUN 6 B747
TIME FROM VORTEX CREATION IN SEC
160
140
120
100
80
60
40
20
20
40
60
80
100
120
140
160
180
200
220
240
Altitude Above Ground (ft)

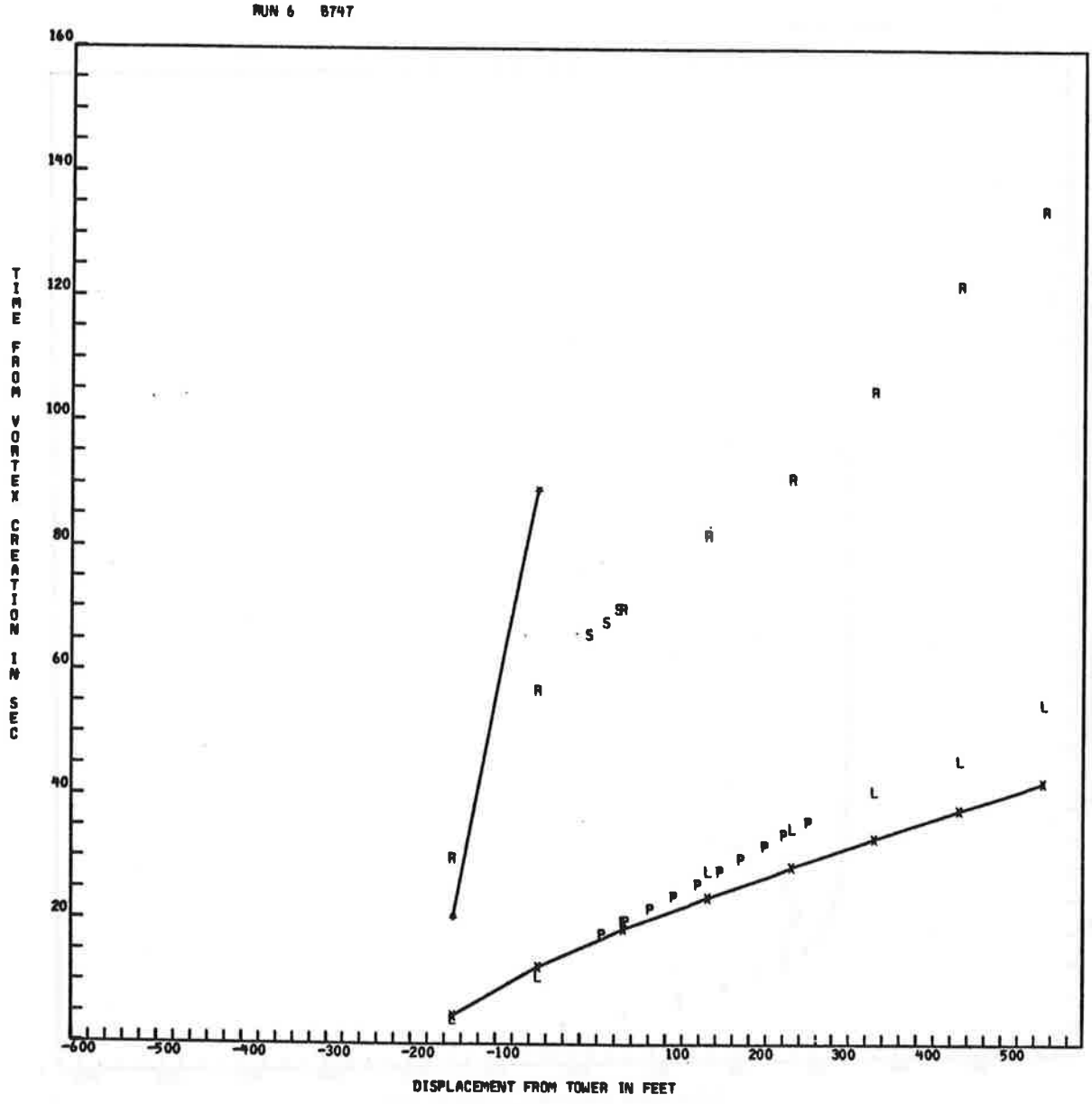
RUN 6 B747
TIME FROM VORTEX CREATION IN SEC
160
140
120
100
80
60
40
20
-600
-500
-400
-300
-200
-100
100
200
300
400
500
DISPLACEMENT FROM TOWER IN FEET

```
                                                    RUN DATA CARD
CONFIGURATION     LANDING LEVEL FLIGHT ALL ENGINES SAME POWER
AIRCRAFT TYPE IS B747
RUN NUMBER   7
AIRCRAFT DISPLACEMENT FROM TOWER -176 FT
AIRCRAFT ALTITUDE ABREAST OF TOWER 168 FT
AIRCRAFT WEIGHT 526000. POUNDS
AIRSPEED  266.9 FT/SEC
TEMPERATURE  17 DEGREES C (NOT USED)
INITIAL WIND SPEED  10 MPH  (NOT USED)
INITIAL WIND ANGLE 250 DEGREES TRUE  (NOT USED)
FINAL WIND SPEED   8 MPH  (NOT USED)
FINAL WIND ANGLE 250 DEGREES TRUE  (NOT USED)
AIRCRAFT HEADING 130 DEGREES MAGNETIC
MONTH  9     DAY 16     HOUR  9     MINUTE 18     LOCAL TIME



$OUTPUT
SPEED   =    -.26686200E+03
WEIGHT  =     .52600000E+06
WSPAN   =     .14974400E+03

$END
$WLOG
WSPR    =     .18058703E+02
CPOWER  =     .47687956E-01
COEF    =     .27052396E+03,   .20565942E+00,  -.94126377E-03,   .17132708E+01,
              .00000000E+00,   .00000000E+00,   .00000000E+00,   .00000000E+00,
              .00000000E+00

$END
GAMMA IN FT**2/SEC =   7.27117731+03
EDDY VISCOSITY IN FT**2/SEC =   7.88054414-01
TEMPERATURE IN RANKINE =   5.29333008+02
DENSITY IN SLUGS/FT**3 =   2.30491537-03
ACOUSTIC VELOCITY IN FT/SEC =   1.12781480+03
STABILITY IN 1/SEC**2 =   0.00000000
INITIAL PARAMETER (DIMENSIONLESS) =   0.00000000
```

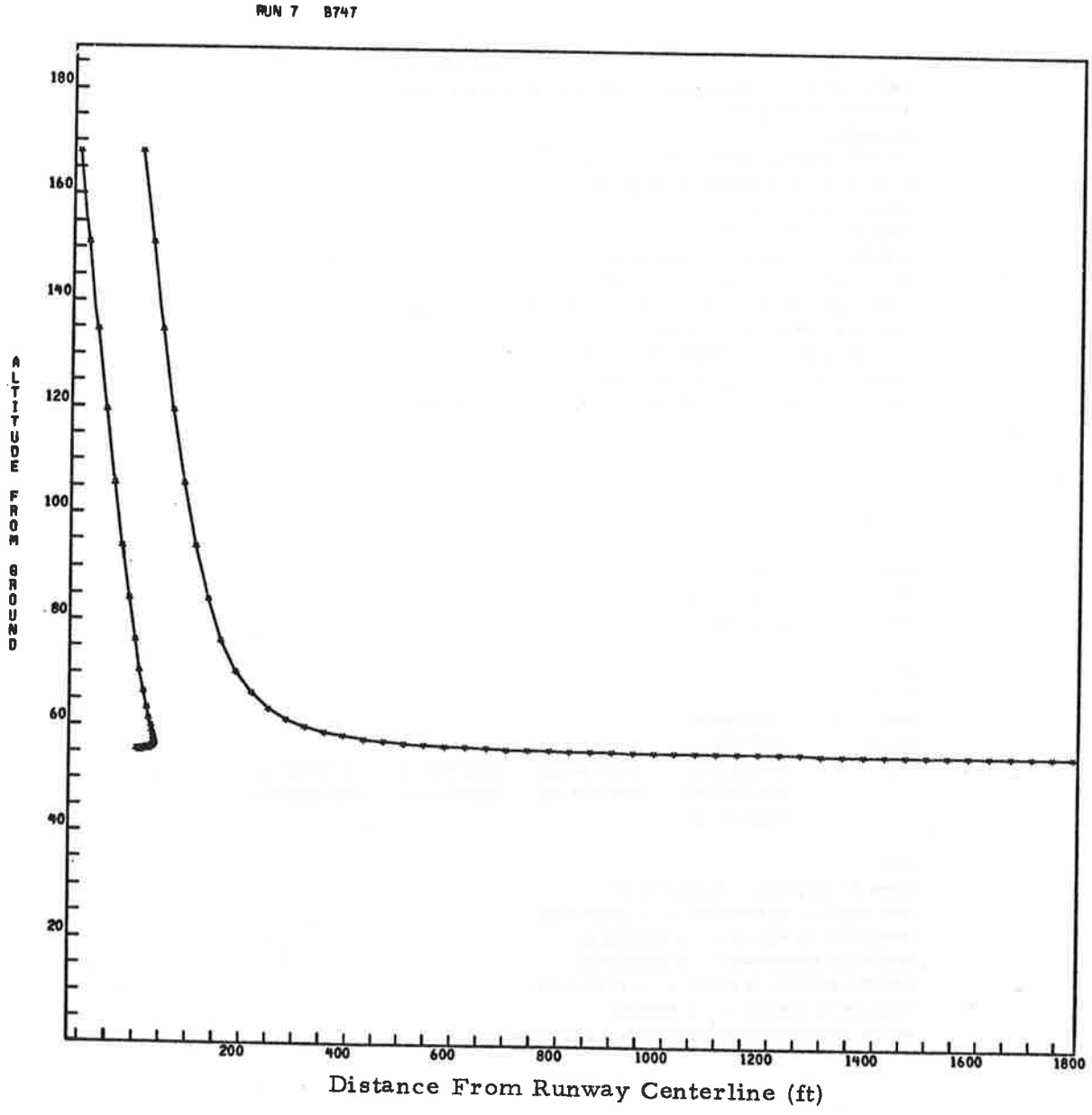
RUN 7 B747
ALTITUDE FROM GROUND
180
160
140
120
100
80
60
40
20
200
400
600
800
1000
1200
1400
1600
1800
Distance From Runway Centerline (ft)

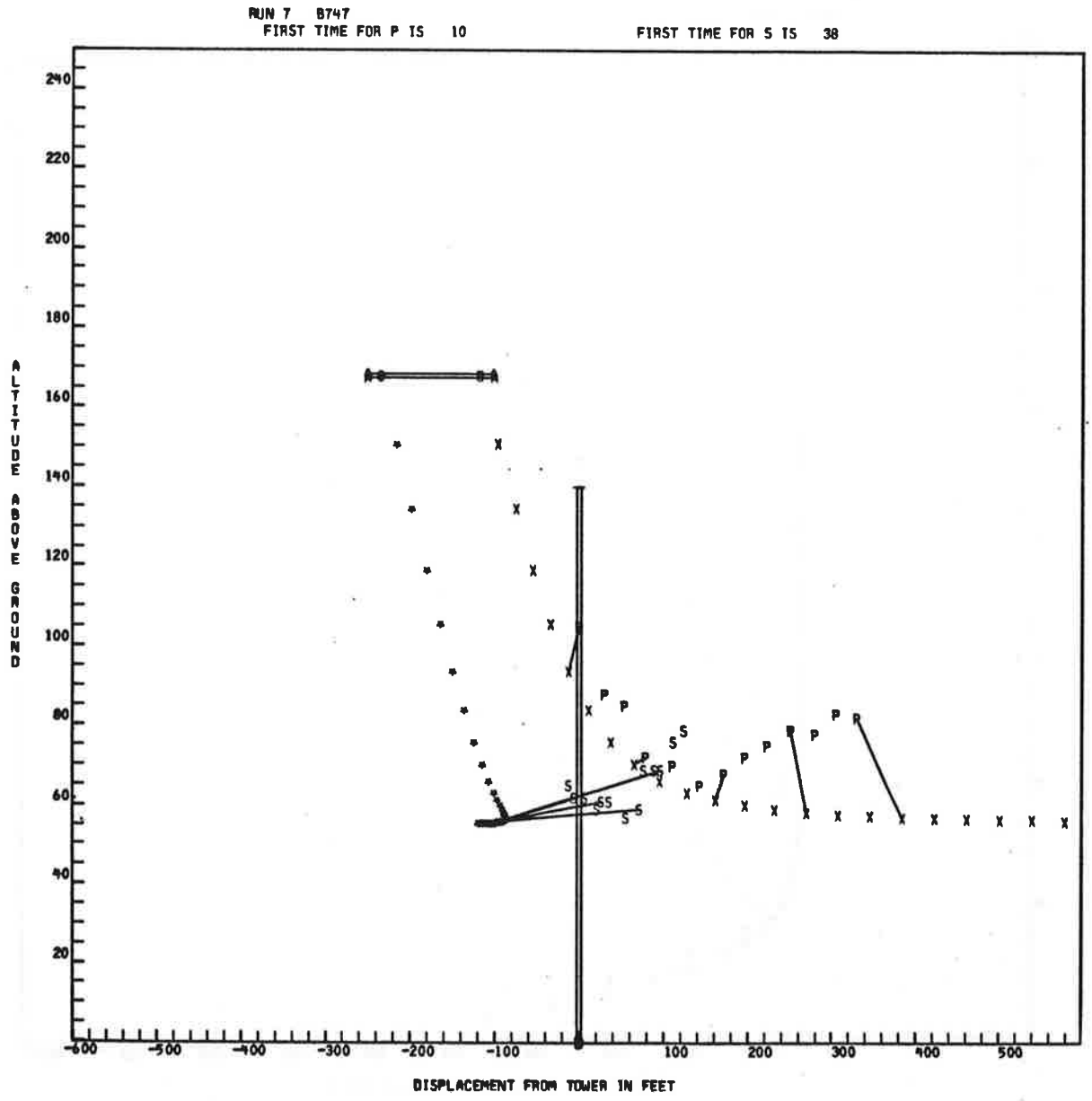
RUN 7 B747
FIRST TIME FOR P IS 10
FIRST TIME FOR S IS 38
ALTITUDE ABOVE GROUND
240
220
200
180
160
140
120
100
80
60
40
20
-600
-500
-400
-300
-200
-100
100
200
300
400
500
DISPLACEMENT FROM TOWER IN FEET

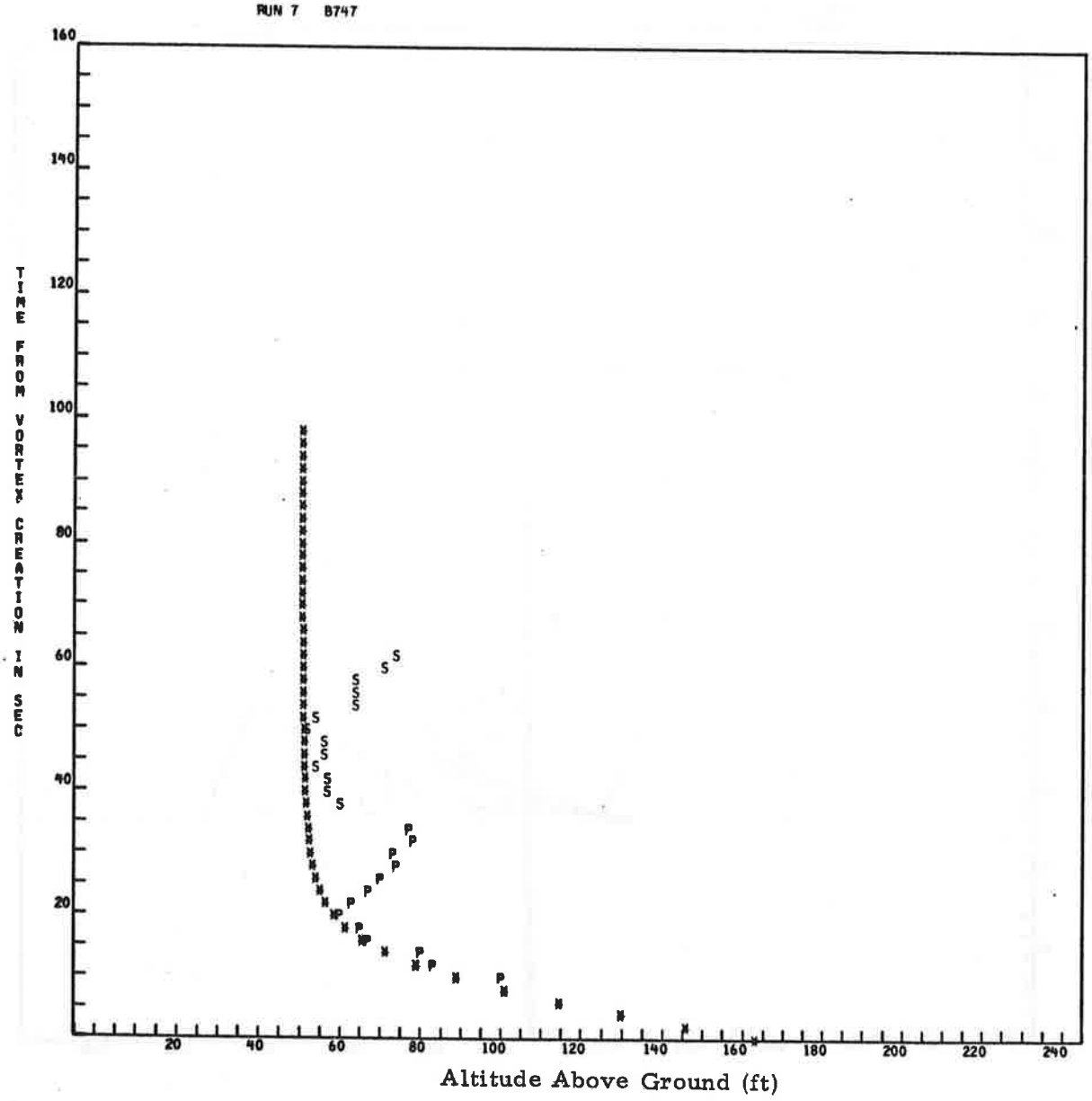
RUN 7 B747
TIME FROM VORTEX CREATION IN SEC
160
140
120
100
80
60
40
20
20
40
60
80
100
120
140
160
180
200
220
240
Altitude Above Ground (ft)

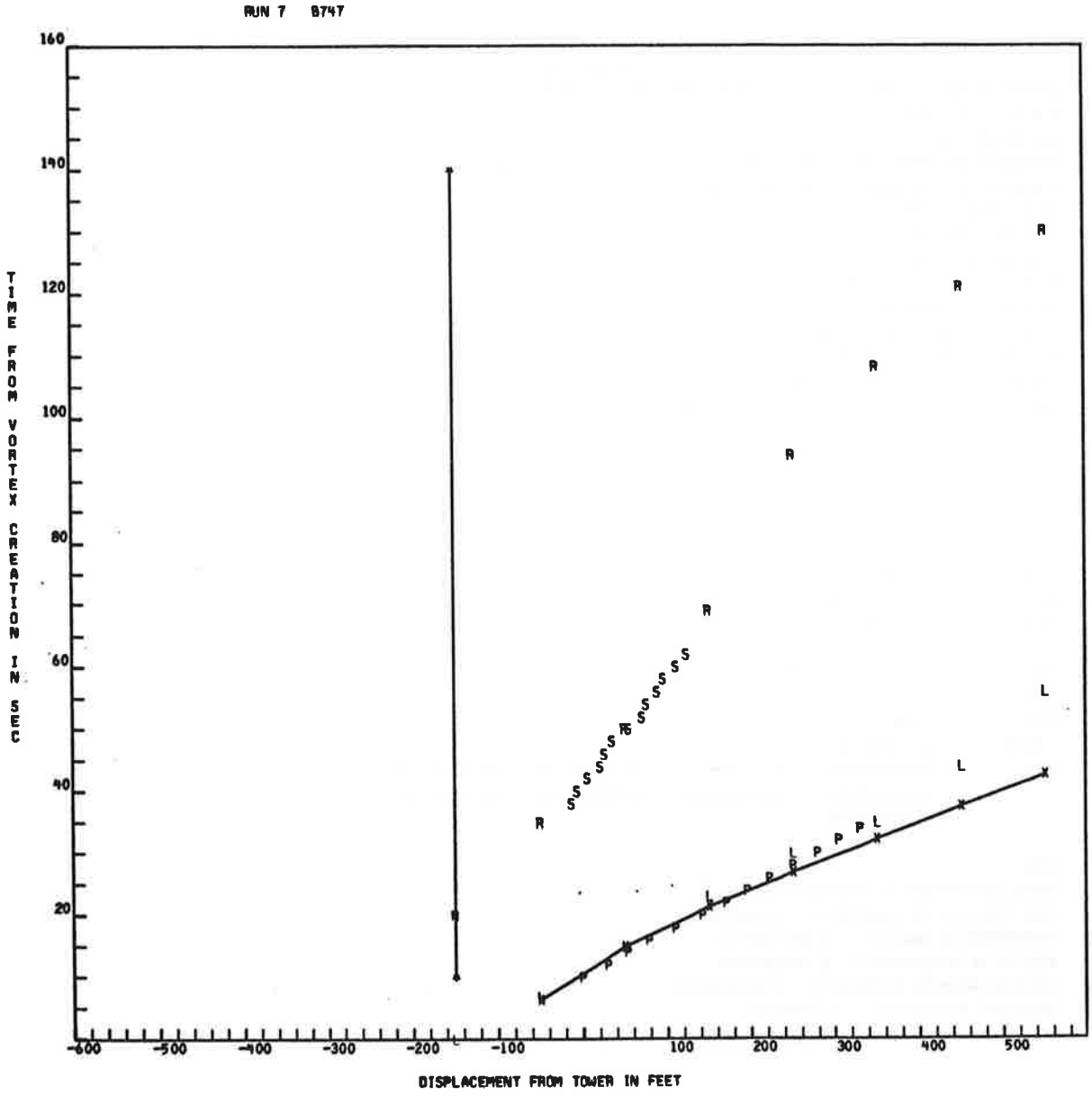
RUN 7 B747
TIME FROM VORTEX CREATION IN SEC
160
140
120
100
80
60
40
20
-600
-500
-400
-300
-200
-100
100
200
300
400
500
DISPLACEMENT FROM TOWER IN FEET

```
                                                    RUN DATA CARD
CONFIGURATION     LANDING LEVEL FLIGHT ALL ENGINES SAME POWER
AIRCRAFT TYPE IS B747
RUN NUMBER   8
AIRCRAFT DISPLACEMENT FROM TOWER -235 FT
AIRCRAFT ALTITUDE ABREAST OF TOWER 187 FT
AIRCRAFT WEIGHT 522000. POUNDS
AIRSPEED  261.8 FT/SEC
TEMPERATURE  17 DEGREES C (NOT USED)
INITIAL WIND SPEED   6 MPH  (NOT USED)
INITIAL WIND ANGLE 250 DEGREES TRUE  (NOT USED)
FINAL WIND SPEED   8 MPH  (NOT USED)
FINAL WIND ANGLE 260 DEGREES TRUE  (NOT USED)
AIRCRAFT HEADING 130 DEGREES MAGNETIC
MONTH  9     DAY 16     HOUR  9     MINUTE 22     LOCAL TIME




$OUTPUT
SPEED   =    -.26179500E+03
WEIGHT  =     .52200000E+06
WSPAN   =     .14974400E+03

$END
$WLOG
WSPR    =     .13200361E+02
CPOWER  =     .62943880E-01
COEF    =     .26260511E+03,  -.74109669E-01,   .12042854E-02,   .92333092E+00,
              .00000000E+00,   .00000000E+00,   .00000000E+00,   .00000000E+00,
              .00000000E+00

$END
GAMMA IN FT**2/SEC =   7.35647314+03
EDDY VISCOSITY IN FT**2/SEC =   7.93684281-01
TEMPERATURE IN RANKINE =   5.29044868+02
DENSITY IN SLUGS/FT**3 =   2.30462468-03
ACOUSTIC VELOCITY IN FT/SEC =   1.12750780+03
STABILITY IN 1/SEC**2 =   0.00000000
INITIAL PARAMETER (DIMENSIONLESS) =   0.00000000
```

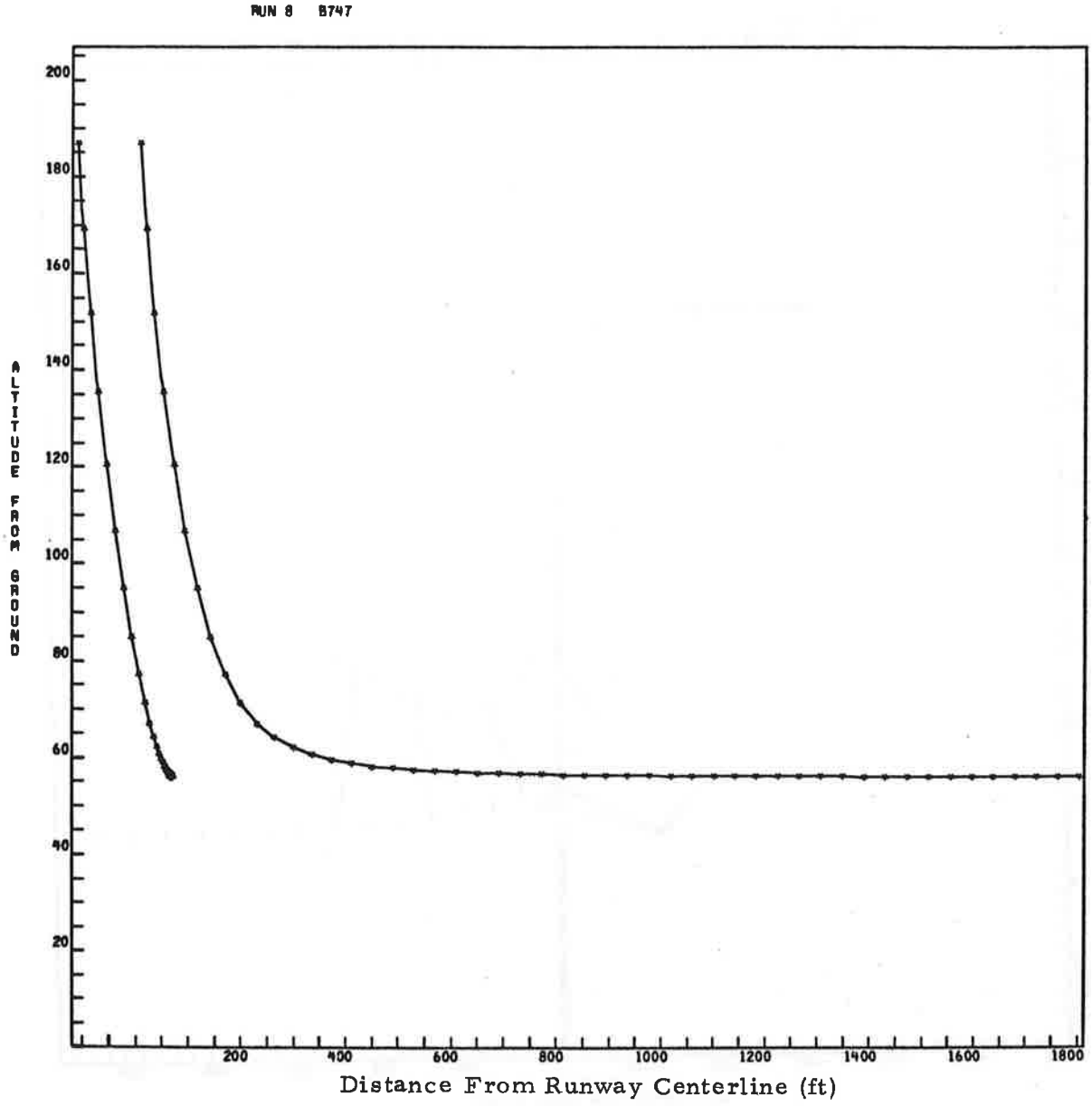
RUN 8 B747
ALTITUDE FROM GROUND
200
180
160
140
120
100
80
60
40
20
200
400
600
800
1000
1200
1400
1600
1800
Distance From Runway Centerline (ft)

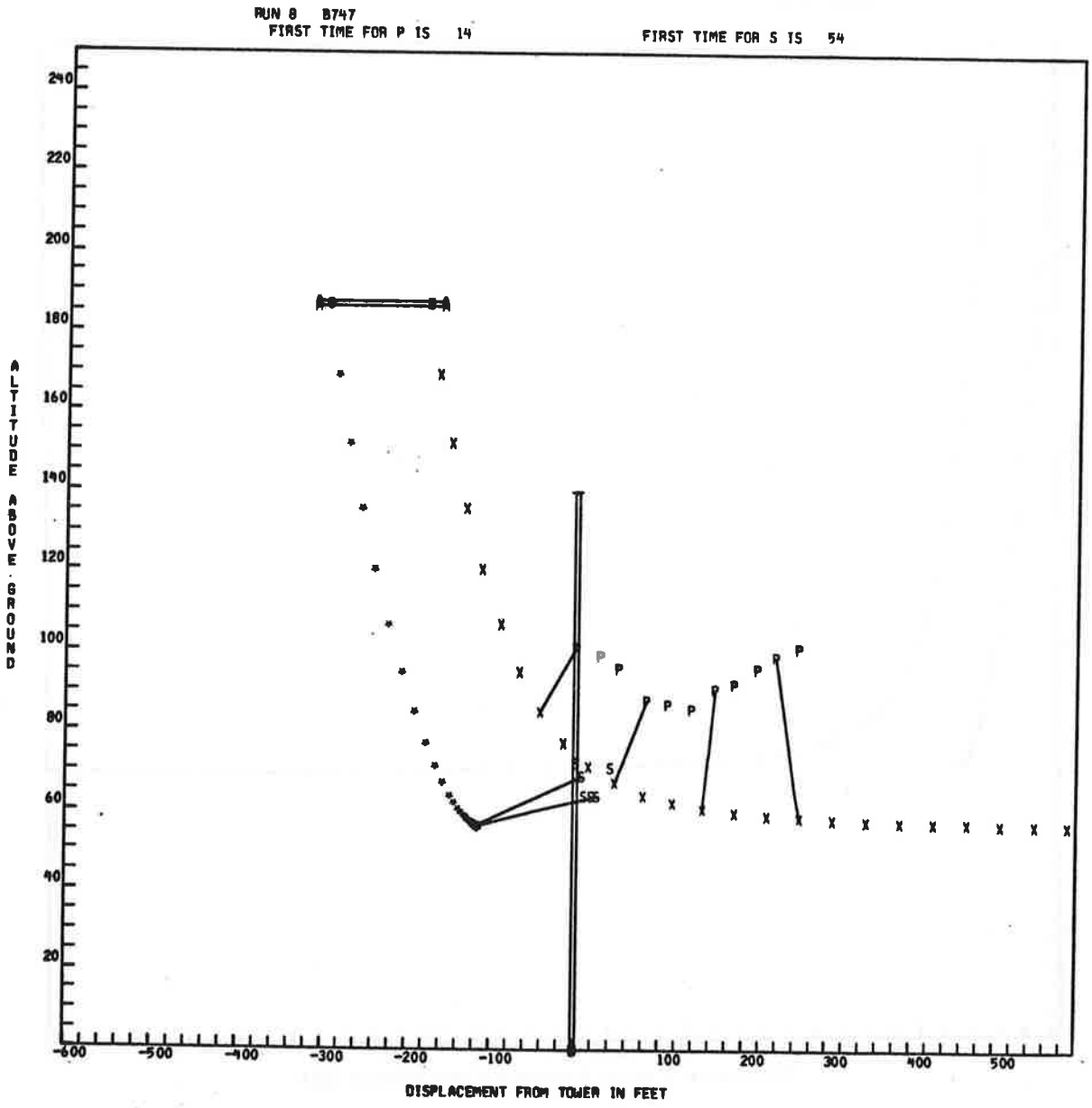
RUN 8 B747
FIRST TIME FOR P IS 14
FIRST TIME FOR S IS 54
ALTITUDE ABOVE GROUND
240
220
200
180
160
140
120
100
80
60
40
20
-600
-500
-400
-300
-200
-100
100
200
300
400
500
DISPLACEMENT FROM TOWER IN FEET

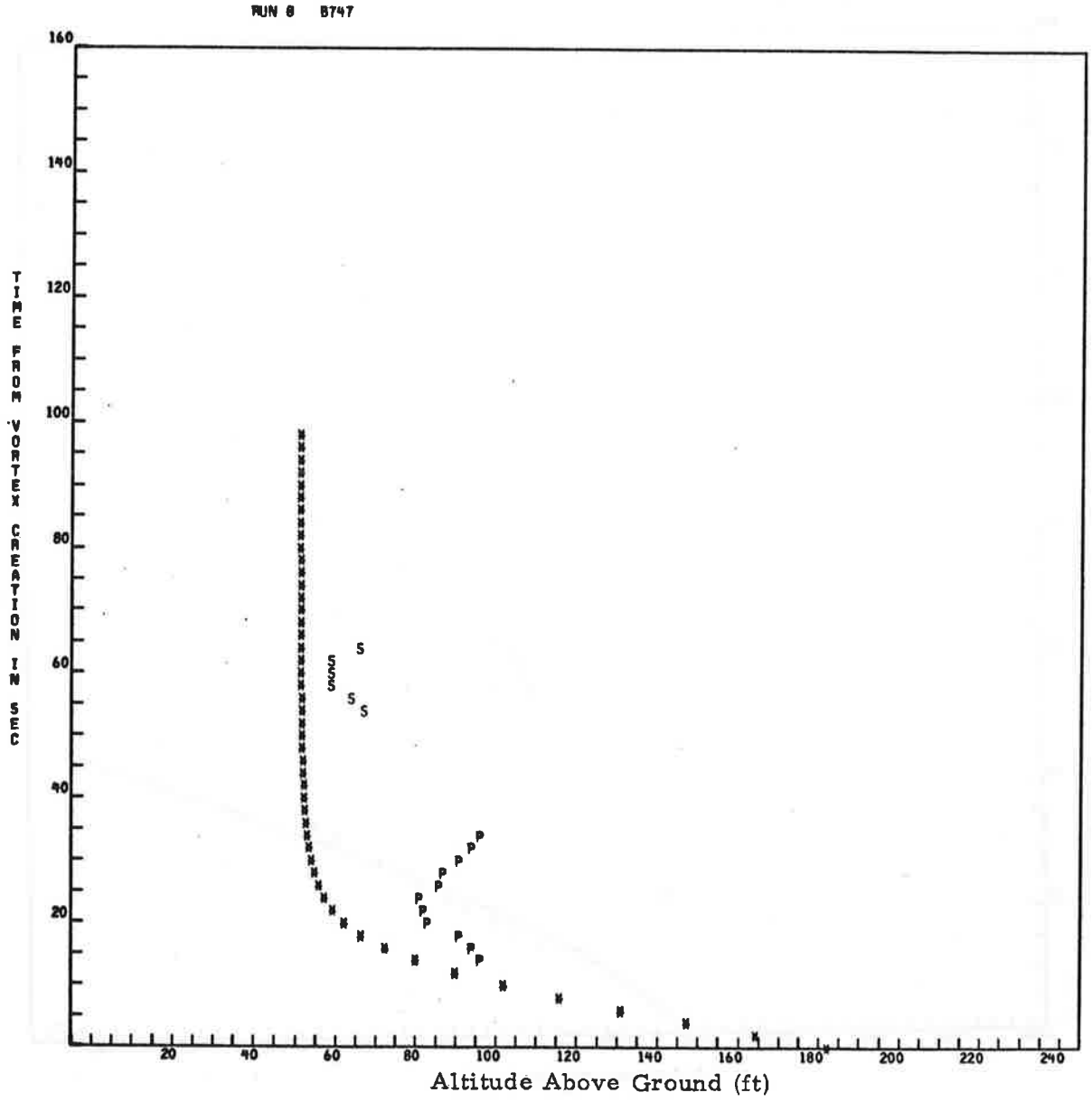
RUN 8 B747
160
140
120
100
80
60
40
20
TIME FROM VORTEX CREATION IN SEC
20
40
60
80
100
120
140
160
180
200
220
240
Altitude Above Ground (ft)

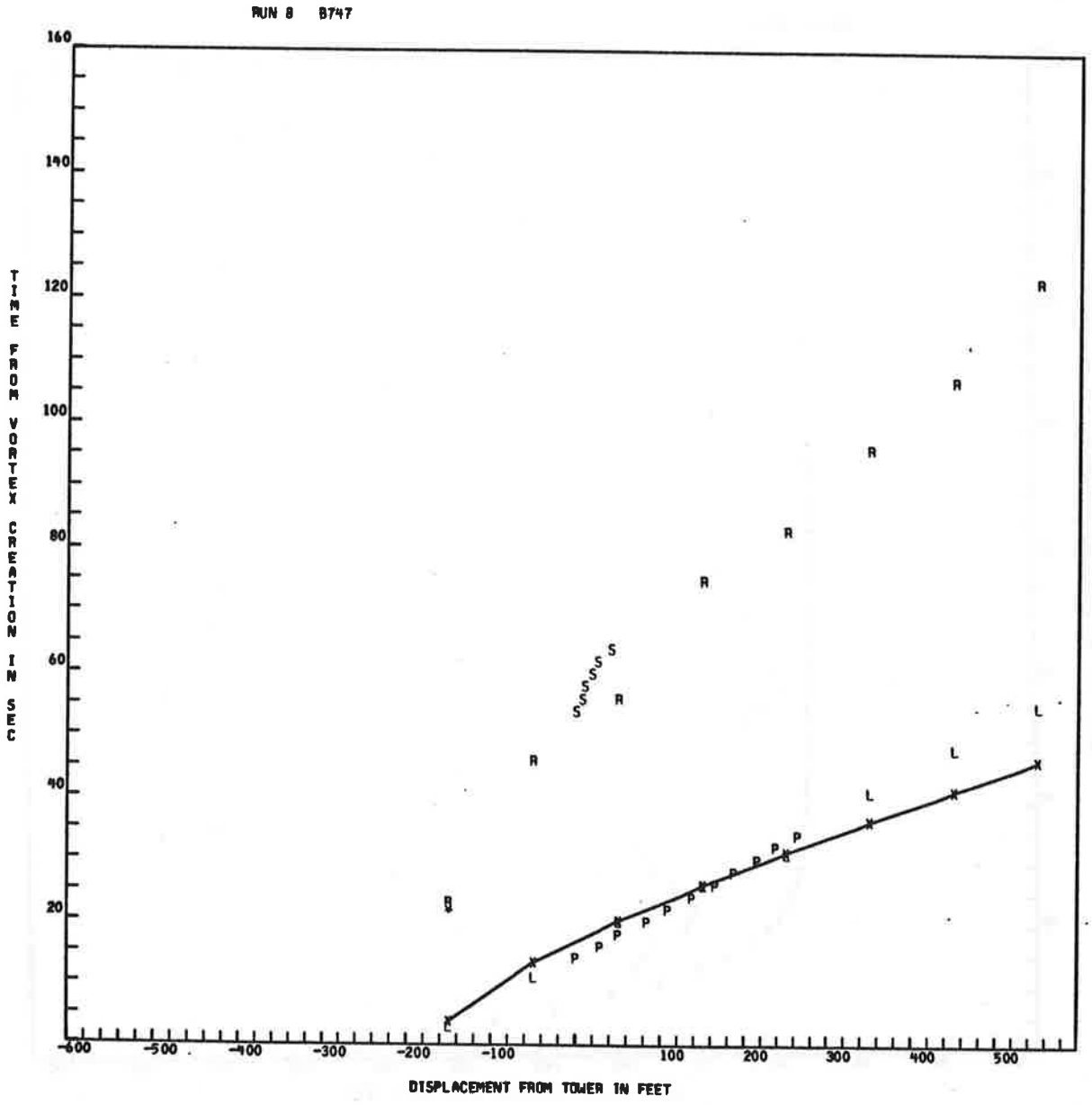
RUN 8 B747
TIME FROM VORTEX CREATION IN SEC
160
140
120
100
80
60
40
20
-600
-500
-400
-300
-200
-100
100
200
300
400
500
DISPLACEMENT FROM TOWER IN FEET

```
                                                    RUN DATA CARD
CONFIGURATION     LANDING LEVEL FLIGHT ALL ENGINES SAME POWER
AIRCRAFT TYPE IS B747
RUN NUMBER   9
AIRCRAFT DISPLACEMENT FROM TOWER -140 FT
AIRCRAFT ALTITUDE ABREAST OF TOWER 184 FT
AIRCRAFT WEIGHT 520000. POUNDS
AIRSPEED  244.9 FT/SEC
TEMPERATURE  17 DEGREES C (NOT USED)
INITIAL WIND SPEED   3 MPH  (NOT USED)
INITIAL WIND ANGLE 200 DEGREES TRUE  (NOT USED)
FINAL WIND SPEED   7 MPH  (NOT USED)
FINAL WIND ANGLE 250 DEGREES TRUE  (NOT USED)
AIRCRAFT HEADING 130 DEGREES MAGNETIC
MONTH  9     DAY 16     HOUR  9     MINUTE 26     LOCAL TIME



$OUTPUT
SPEED   =    -.24490500E+03
WEIGHT  =     .52000000E+06
WSPAN   =     .14974400E+03

$END
$WLOG
WSPR    =     .11634031E+02
CPOWER  =     .13167709E+00
COEF    =     .25291770E+03,   .14732393E+00,   .19754234E-03,   .28621755E+01,
              .00000000E+00,   .00000000E+00,   .00000000E+00,   .00000000E+00,
              .00000000E+00

$END
GAMMA IN FT**2/SEC =   7.80877820+03
EDDY VISCOSITY IN FT**2/SEC =   8.21899258-01
TEMPERATURE IN RANKINE =   5.27913626+02
DENSITY IN SLUGS/FT**3 =   2.31197593-03
ACOUSTIC VELOCITY IN FT/SEC =   1.12587492+03
STABILITY IN 1/SEC**2 =   0.00000000
INITIAL PARAMETER (DIMENSIONLESS) =   0.00000000
```

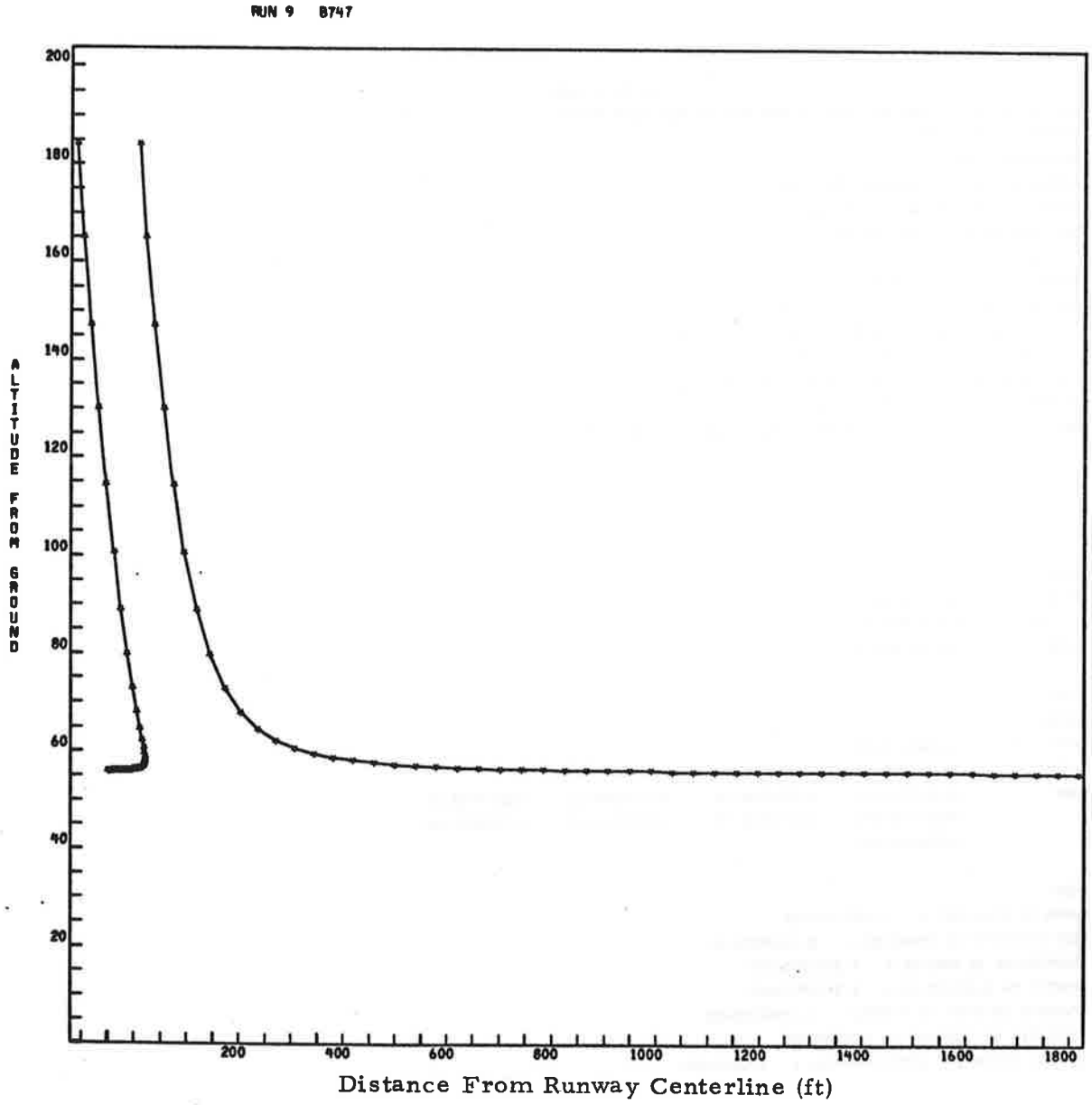
RUN 9 B747
ALTITUDE FROM GROUND
200
180
160
140
120
100
80
60
40
20
200
400
600
800
1000
1200
1400
1600
1800
Distance From Runway Centerline (ft)

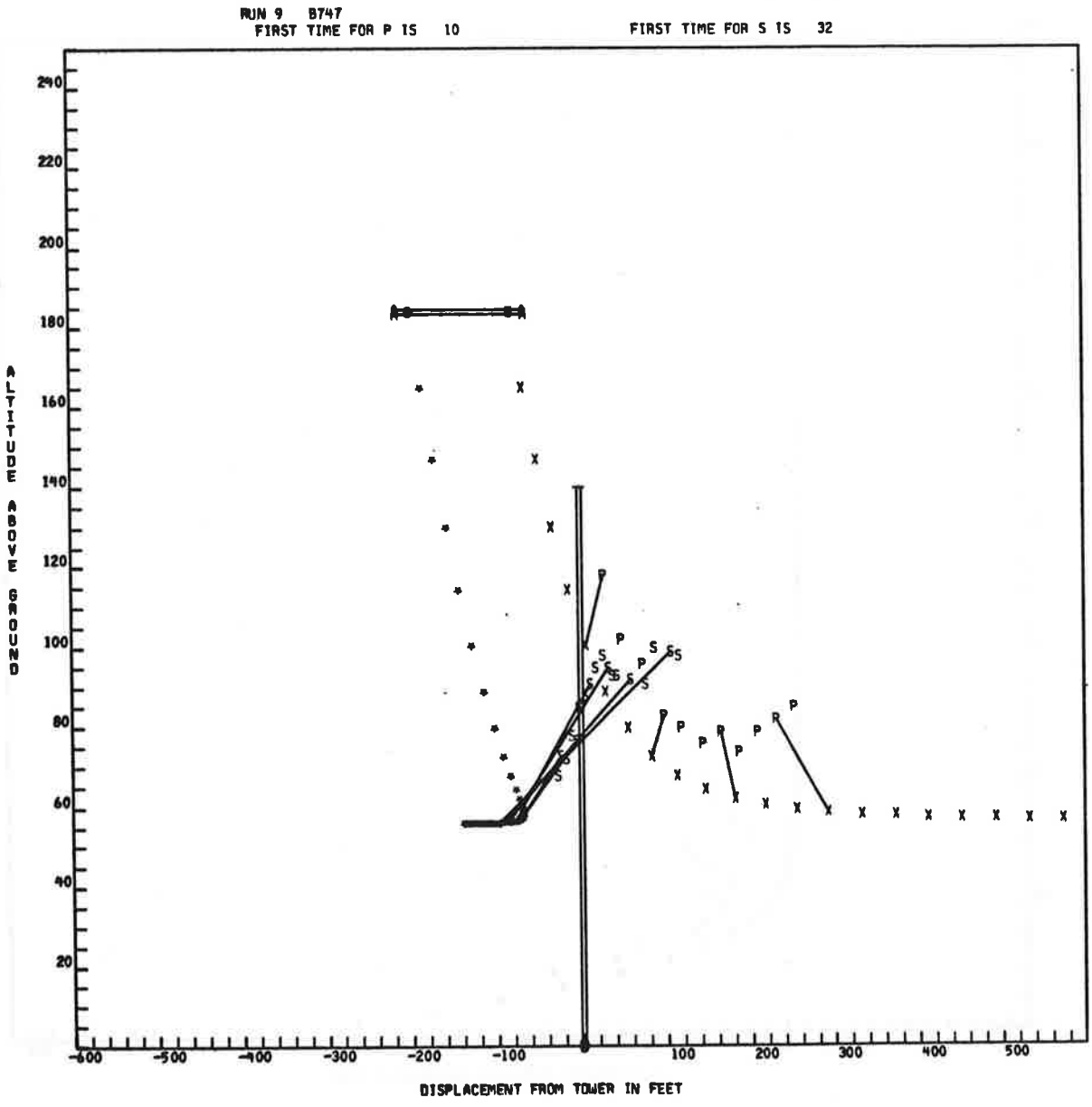
RUN 9 B747
FIRST TIME FOR P IS 10
FIRST TIME FOR S IS 32
ALTITUDE ABOVE GROUND
240
220
200
180
160
140
120
100
80
60
40
20
-600
-500
-400
-300
-200
-100
100
200
300
400
500
DISPLACEMENT FROM TOWER IN FEET

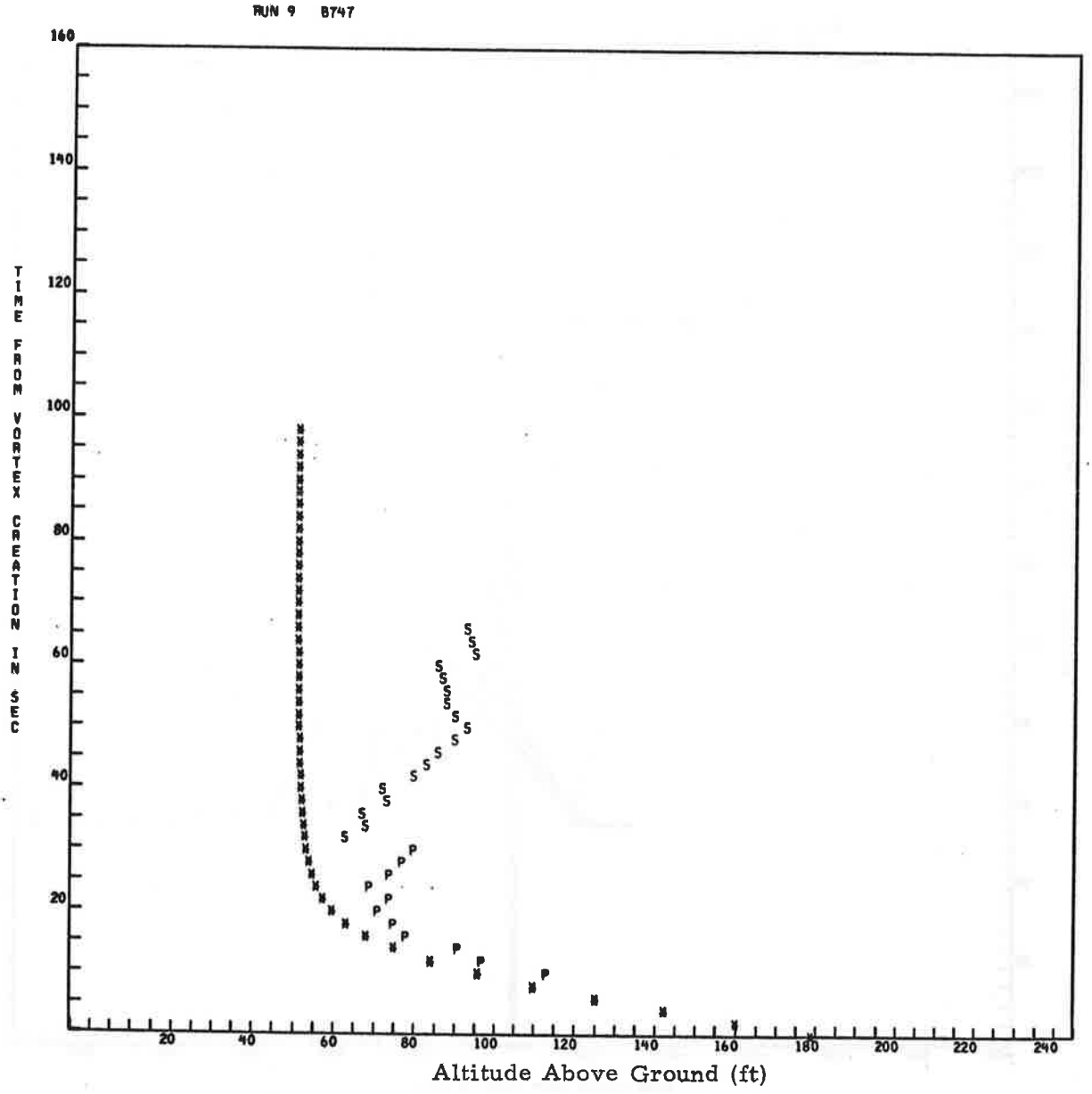
RUN 9 B747
TIME FROM VORTEX CREATION IN SEC
160
140
120
100
80
60
40
20
20
40
60
80
100
120
140
160
180
200
220
240
Altitude Above Ground (ft)

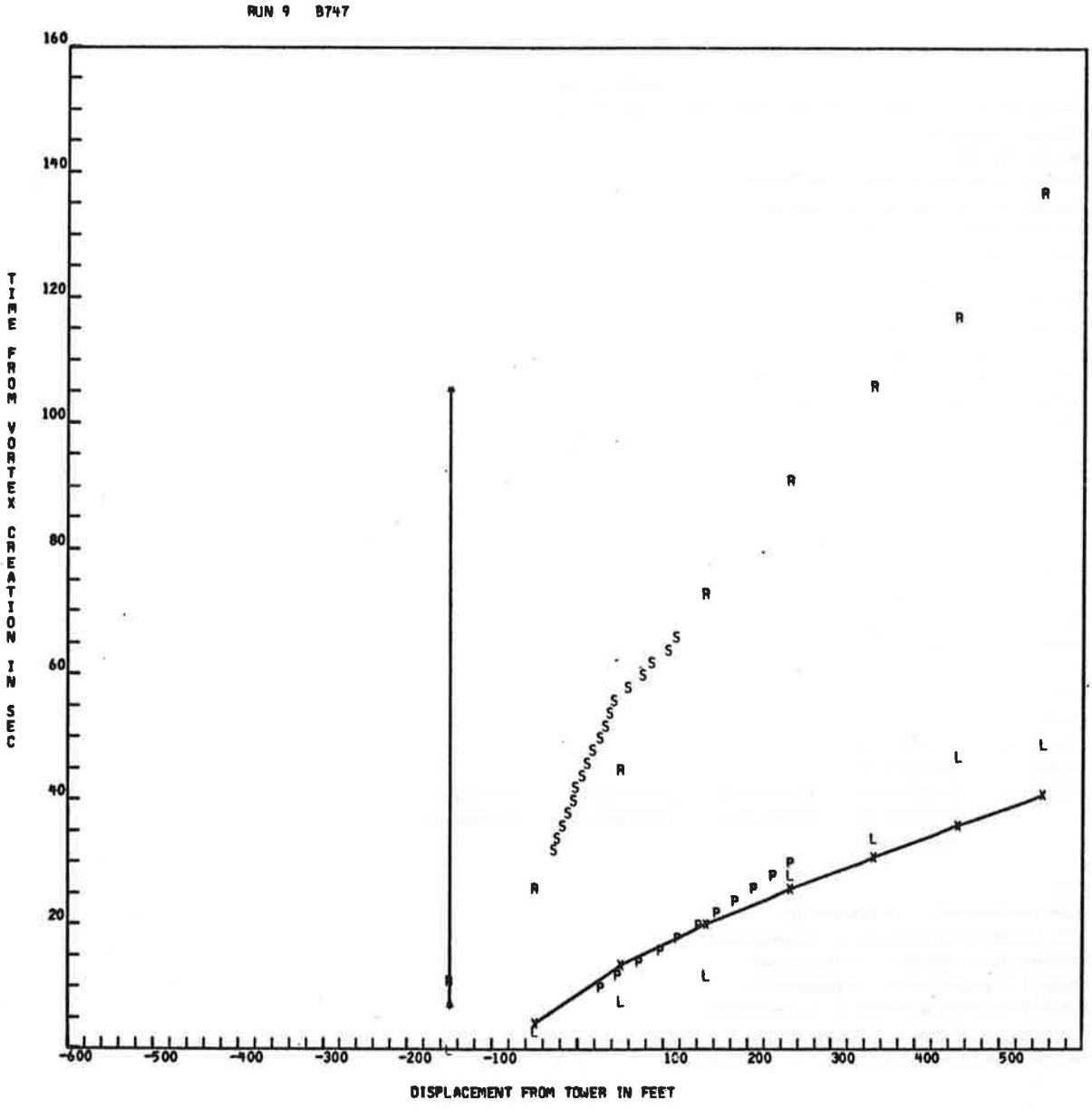
RUN 9 B747
TIME FROM VORTEX CREATION IN SEC
160
140
120
100
80
60
40
20
-600
-500
-400
-300
-200
-100
100
200
300
400
500
DISPLACEMENT FROM TOWER IN FEET

```
                                                    RUN DATA CARD
CONFIGURATION     LANDING LEVEL FLIGHT ALL ENGINES SAME POWER
AIRCRAFT TYPE IS B747
RUN NUMBER  10
AIRCRAFT DISPLACEMENT FROM TOWER -207 FT
AIRCRAFT ALTITUDE ABREAST OF TOWER 168 FT
AIRCRAFT WEIGHT 518000. POUNDS
AIRSPEED  244.9 FT/SEC
TEMPERATURE  17 DEGREES C (NOT USED)
INITIAL WIND SPEED  10 MPH  (NOT USED)
INITIAL WIND ANGLE 250 DEGREES TRUE  (NOT USED)
FINAL WIND SPEED  8 MPH  (NOT USED)
FINAL WIND ANGLE 250 DEGREES TRUE  (NOT USED)
AIRCRAFT HEADING 130 DEGREES MAGNETIC
MONTH  9     DAY 16     HOUR  9     MINUTE 31     LOCAL TIME



$OUTPUT
SPEED   =    -.24490500E+03
WEIGHT  =     .51800000E+06
WSPAN   =     .14974400E+03

$END
$WLOG
WSPA-   =     .17387810E+02
CPOWER  =    -.20043905E-01
COEF    =     .25597092E+03,   .59151629E-01,   .61012345E-03,   .24030516E+01,
              .00000000E+00,   .00000000E+00,   .00000000E+00,   .00000000E+00,
              .00000000E+00

$END
GAMMA IN FT**2/SEC =   7.82530255+03
EDDY VISCOSITY IN FT**2/SEC =   8.26439030-01
TEMPERATURE IN RANKINE =   5.30991249+02
DENSITY IN SLUGS/FT**3 =   2.29822041-03
ACOUSTIC VELOCITY IN FT/SEC =   1.12957999+03
STABILITY IN 1/SEC**2 =   0.00000000
INITIAL PARAMETER (DIMENSIONLESS) =   0.00000000
```

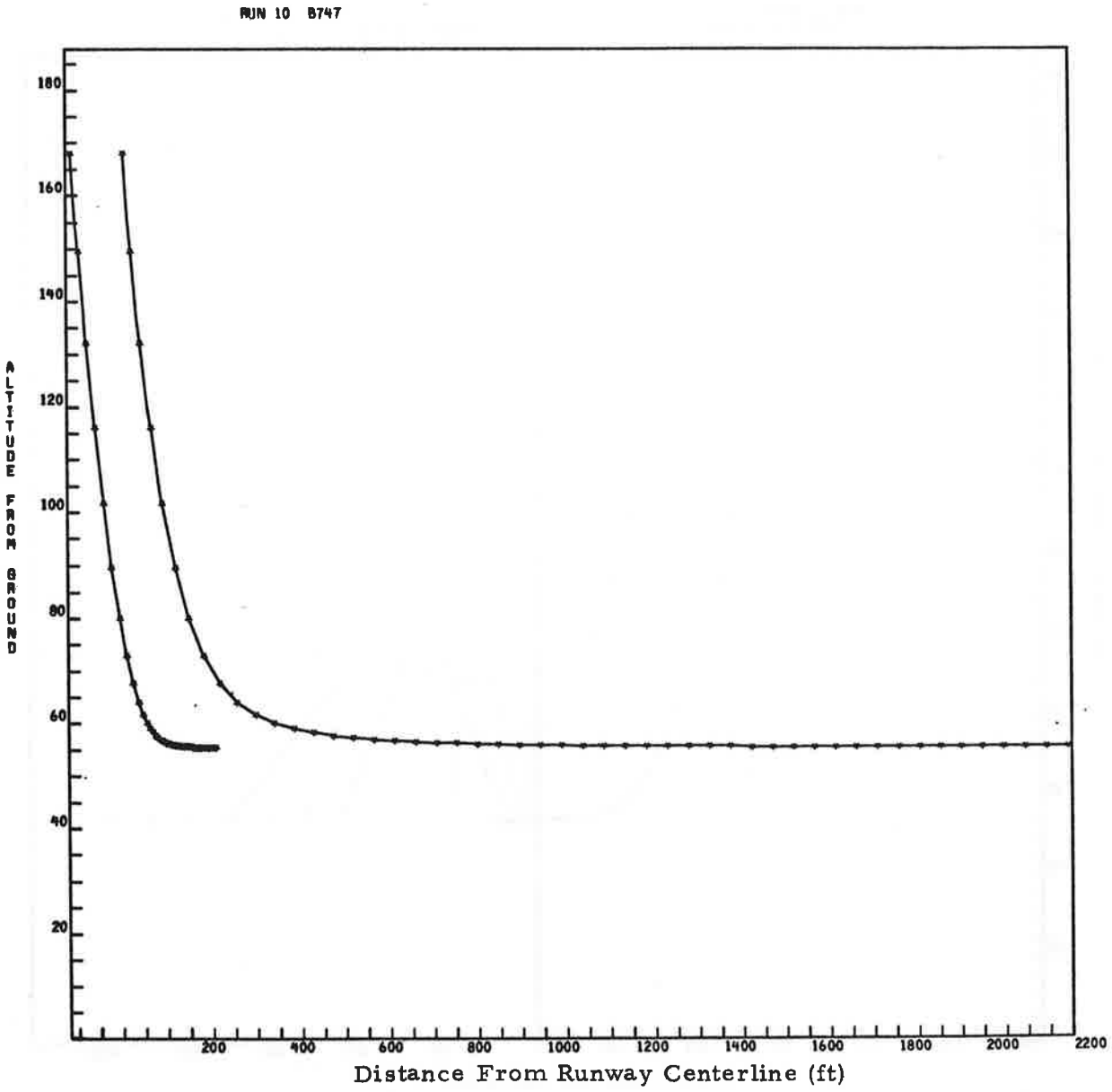
RUN 10 B747
ALTITUDE FROM GROUND
180
160
140
120
100
80
60
40
20
200
400
600
800
1000
1200
1400
1600
1800
2000
2200
Distance From Runway Centerline (ft)

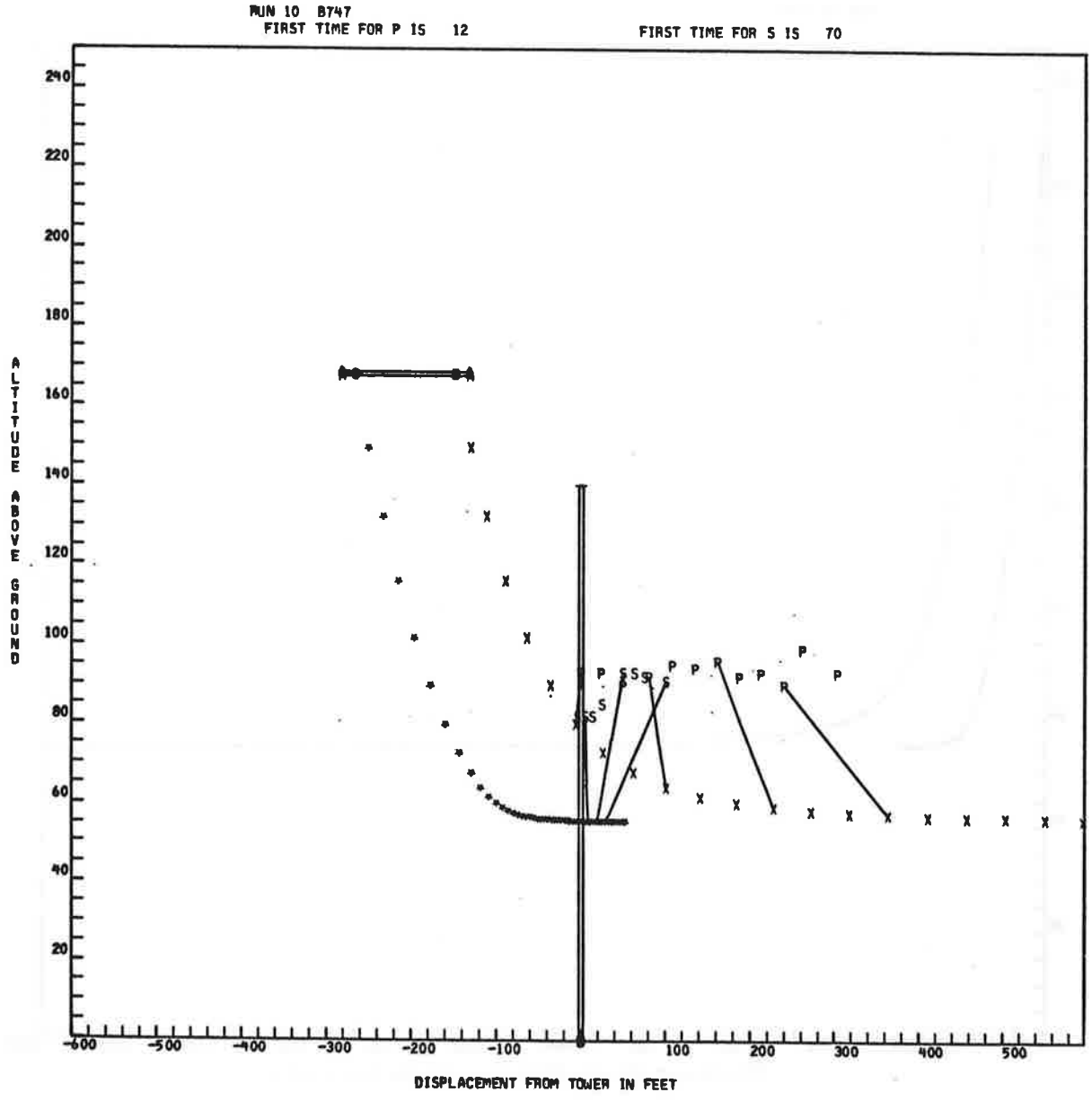
RUN 10 B747
FIRST TIME FOR P IS 12
FIRST TIME FOR S IS 70
ALTITUDE ABOVE GROUND
240
220
200
180
160
140
120
100
80
60
40
20
-600
-500
-400
-300
-200
-100
100
200
300
400
500
DISPLACEMENT FROM TOWER IN FEET

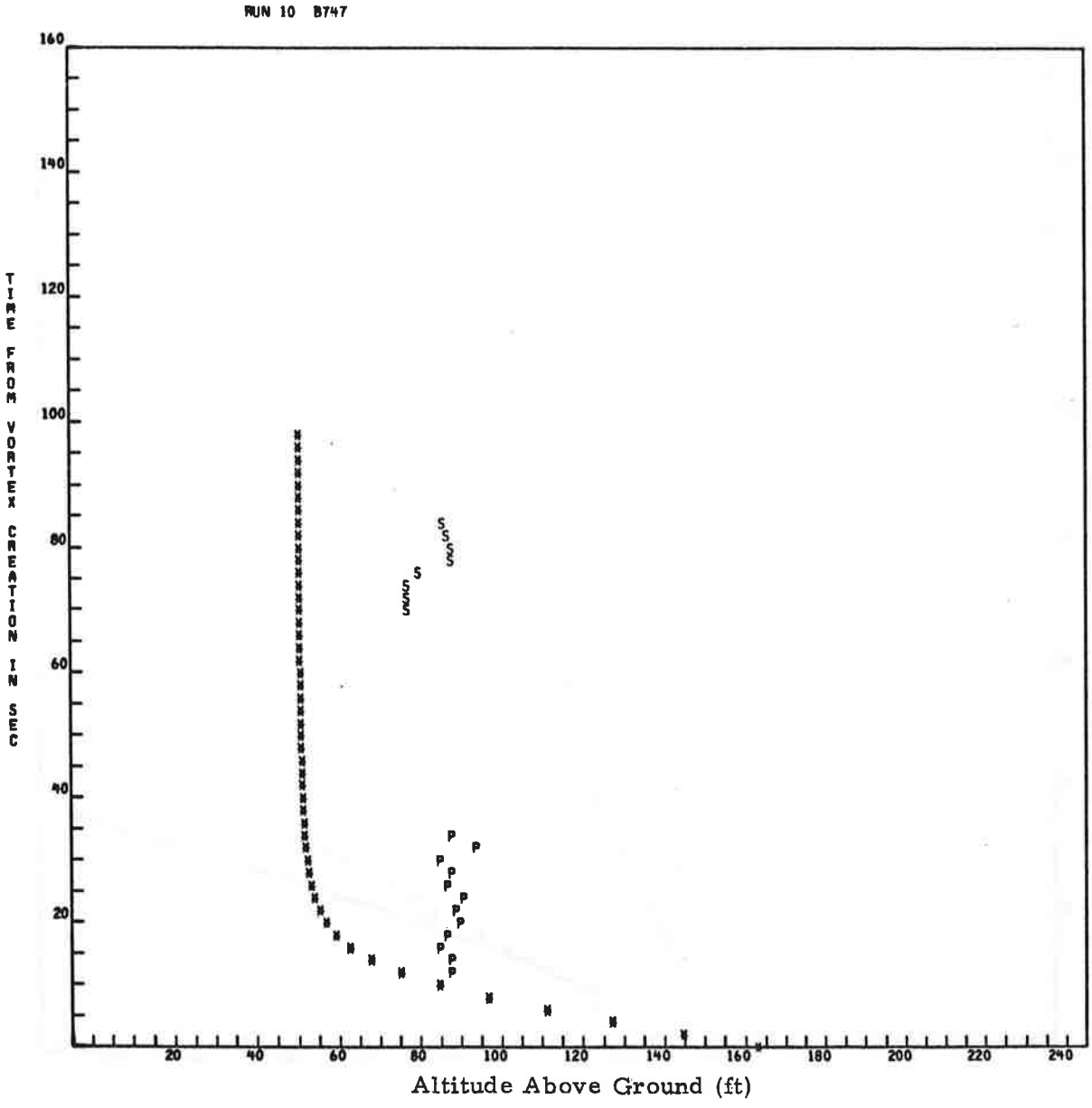
RUN 10 B747
TIME FROM VORTEX CREATION IN SEC
160
140
120
100
80
60
40
20
20
40
60
80
100
120
140
160
180
200
220
240
Altitude Above Ground (ft)

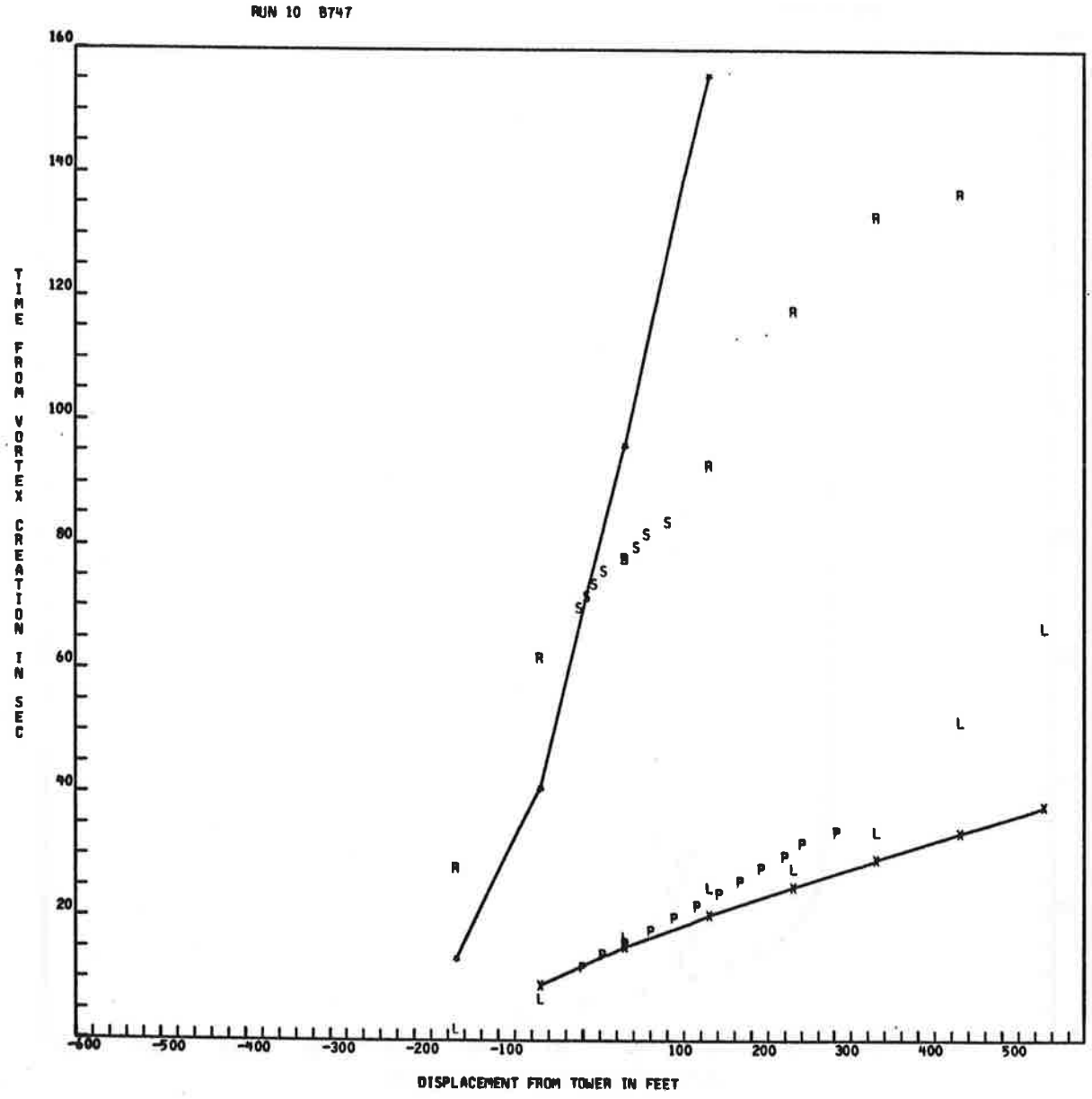
RUN 10 B747
TIME FROM VORTEX CREATION IN SEC
DISPLACEMENT FROM TOWER IN FEET
160
140
120
100
80
60
40
20
-600
-500
-400
-300
-200
-100
100
200
300
400
500

```
                                                    RUN DATA CARD
CONFIGURATION     LANDING LEVEL FLIGHT ALL ENGINES SAME POWER
AIRCRAFT TYPE IS B747
RUN NUMBER  11
AIRCRAFT DISPLACEMENT FROM TOWER -208 FT
AIRCRAFT ALTITUDE ABREAST OF TOWER 206 FT
AIRCRAFT WEIGHT 516000. POUNDS
AIRSPEED  228.0 FT/SEC
TEMPERATURE  17 DEGREES C (NOT USED)
INITIAL WIND SPEED   4 MPH  (NOT USED)
INITIAL WIND ANGLE 240 DEGREES TRUE  (NOT USED)
FINAL WIND SPEED   0 MPH  (NOT USED)
FINAL WIND ANGLE   0 DEGREES TRUE  (NOT USED)
AIRCRAFT HEADING 132 DEGREES MAGNETIC
MONTH  9     DAY 16     HOUR  9     MINUTE 35     LOCAL TIME




$OUTPUT
SPEED   =    -.22801500E+03
WEIGHT  =     .51600000E+06
WSPAN   =     .14974400E+03

$END
$WLOG
WSPR    =     .17143642E+02
CPOWER  =     .32410081E-02
COEF    =     .23873092E+03,   .14599176E+00,   .75909277E-03,   .31998366E+01,
              .00000000E+00,   .00000000E+00,   .00000000E+00,   .00000000E+00,
              .00000000E+00

$END
GAMMA IN FT**2/SEC =   8.37337292+03
EDDY VISCOSITY IN FT**2/SEC =   8.61584425-01
TEMPERATURE IN RANKINE =   5.30334900+02
DENSITY IN SLUGS/FT**3 =   2.29798164-03
ACOUSTIC VELOCITY IN FT/SEC =   1.12888164+03
STABILITY IN 1/SEC**2 =   0.00000000
INITIAL PARAMETER (DIMENSIONLESS) =   0.00000000
```

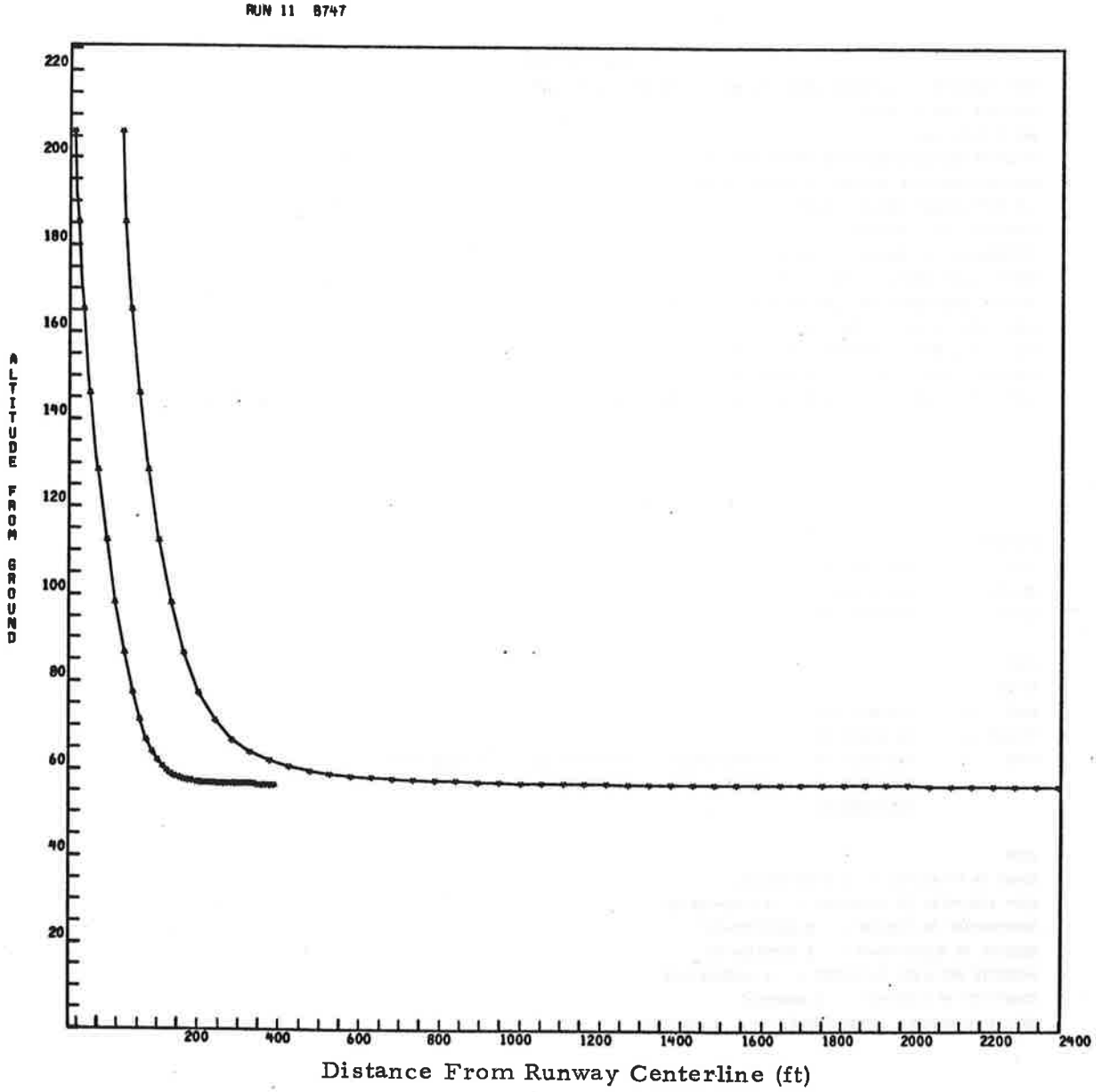
RUN 11 B747
ALTITUDE FROM GROUND
220
200
180
160
140
120
100
80
60
40
20
200
400
600
800
1000
1200
1400
1600
1800
2000
2200
2400
Distance From Runway Centerline (ft)

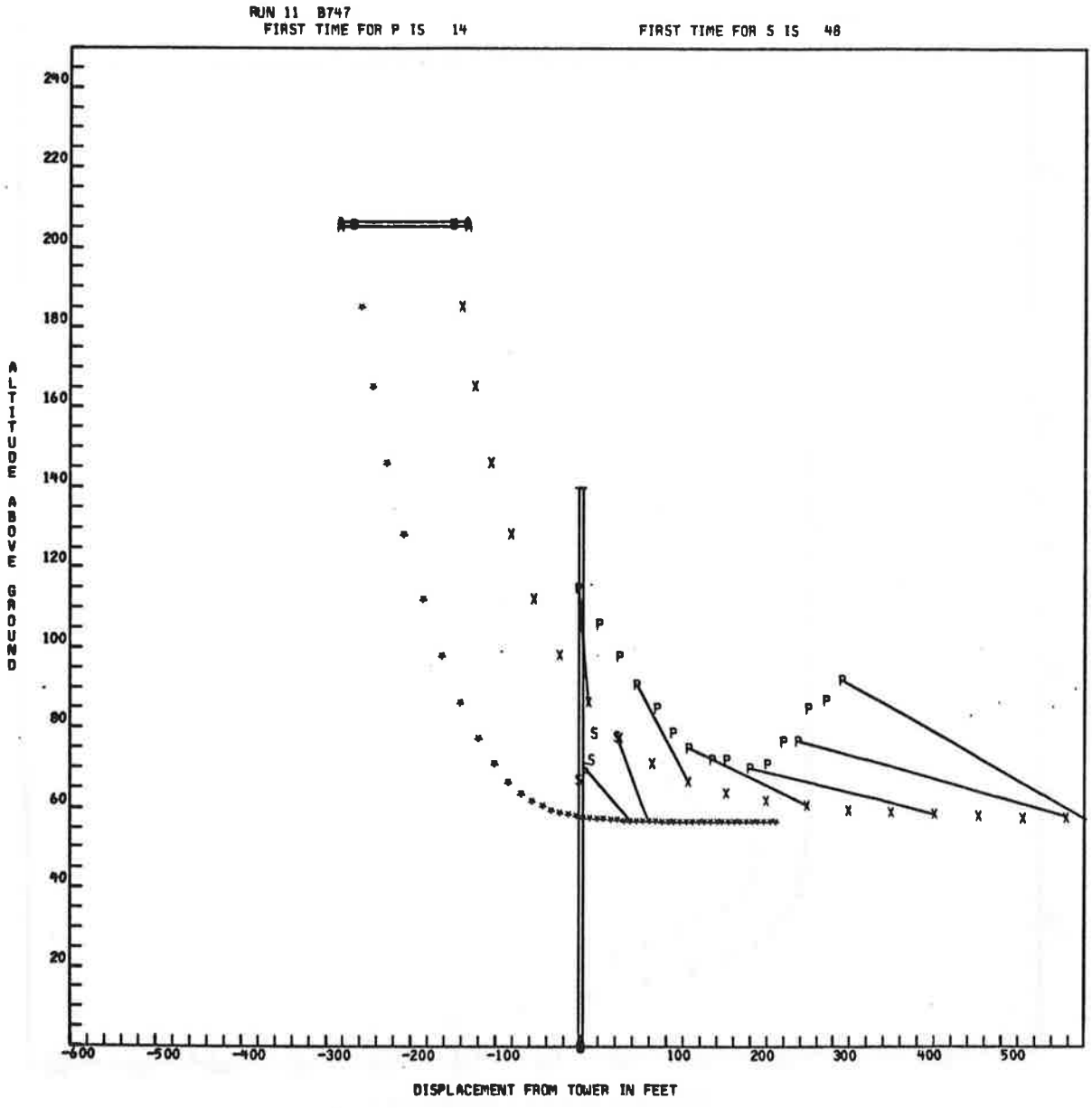
RUN 11 B747
FIRST TIME FOR P IS 14
FIRST TIME FOR S IS 48
ALTITUDE ABOVE GROUND
240
220
200
180
160
140
120
100
80
60
40
20
-600
-500
-400
-300
-200
-100
100
200
300
400
500
DISPLACEMENT FROM TOWER IN FEET

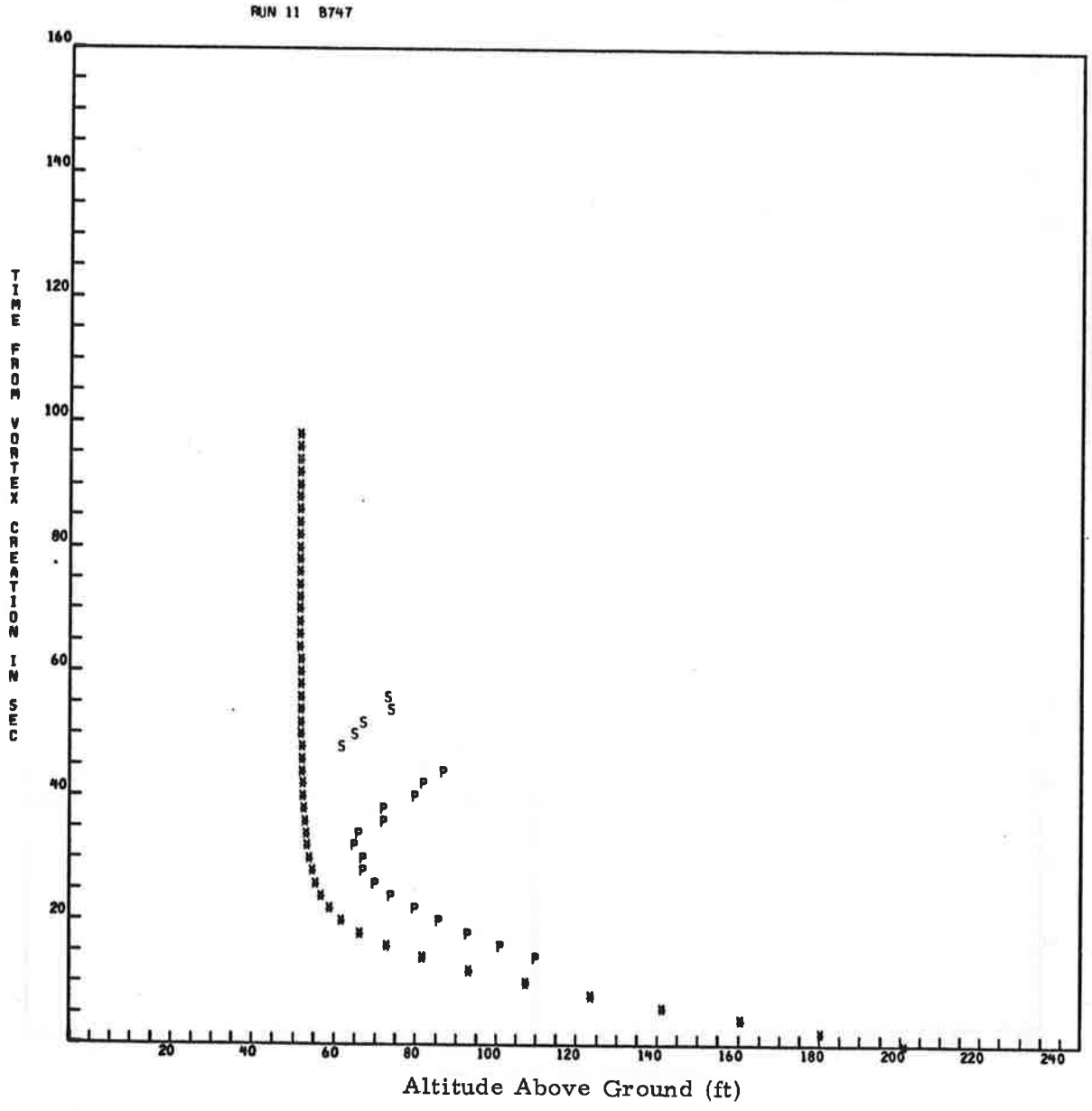
RUN 11 8747
TIME FROM VORTEX CREATION IN SEC
160
140
120
100
80
60
40
20
20
40
60
80
100
120
140
160
180
200
220
240
Altitude Above Ground (ft)

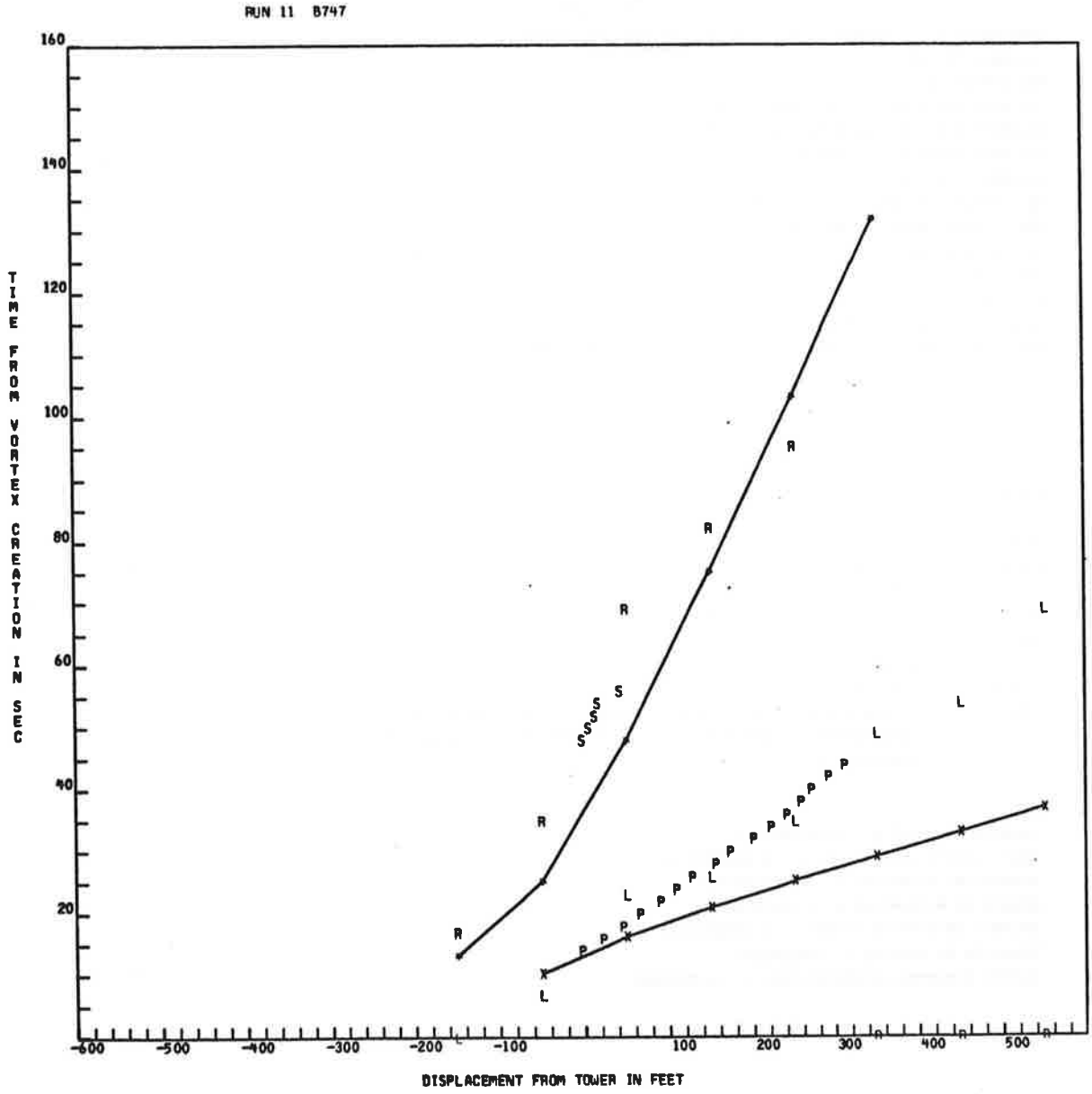
RUN 11 B747
TIME FROM VORTEX CREATION IN SEC
160
140
120
100
80
60
40
20
-600
-500
-400
-300
-200
-100
100
200
300
400
500
DISPLACEMENT FROM TOWER IN FEET

```
                                                    RUN DATA CARD
CONFIGURATION     LANDING LEVEL FLIGHT ALL ENGINES SAME POWER
AIRCRAFT TYPE IS B747
RUN NUMBER  12
AIRCRAFT DISPLACEMENT FROM TOWER -136 FT
AIRCRAFT ALTITUDE ABREAST OF TOWER 225 FT
AIRCRAFT WEIGHT 514000. POUNDS
AIRSPEED  236.5 FT/SEC
TEMPERATURE  17 DEGREES C (NOT USED)
INITIAL WIND SPEED   3 MPH  (NOT USED)
INITIAL WIND ANGLE 240 DEGREES TRUE  (NOT USED)
FINAL WIND SPEED   0 MPH  (NOT USED)
FINAL WIND ANGLE   0 DEGREES TRUE  (NOT USED)
AIRCRAFT HEADING 130 DEGREES MAGNETIC
MONTH  9     DAY 16     HOUR  9     MINUTE 39     LOCAL TIME



$OUTPUT
SPEED   =    -.23646000E+03
WEIGHT  =     .51400000E+06
WSPAN   =     .14974400E+03

$END
$WLOG
WSPR    =     .13694753E+02
CPOWER  =    -.91851767E-01
COEF    =     .23782479E+03,  -.18662135E-02,   .19427570E-02,   .29430882E+01,
              .00000000E+00,   .00000000E+00,   .00000000E+00,   .00000000E+00,
              .00000000E+00

$END
GAMMA IN FT**2/SEC =   7.97977802+03
EDDY VISCOSITY IN FT**2/SEC =   8.31627794-01
TEMPERATURE IN RANKINE =   5.25776146+02
DENSITY IN SLUGS/FT**3 =   2.31619610-03
ACOUSTIC VELOCITY IN FT/SEC =   1.12401923+03
STABILITY IN 1/SEC**2 =   0.00000000
INITIAL PARAMETER (DIMENSIONLESS) =   0.00000000
```

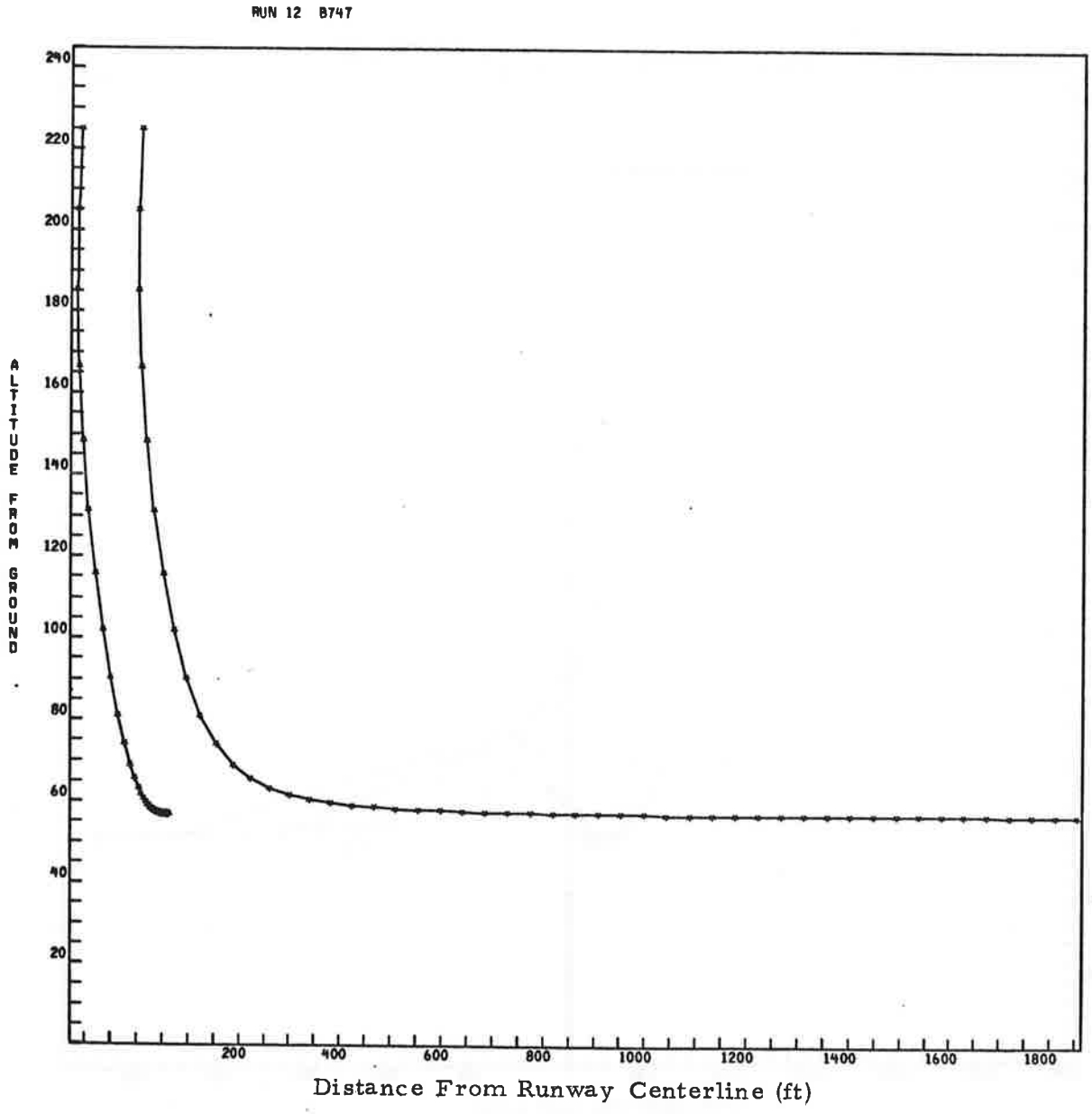
RUN 12 B747
ALTITUDE FROM GROUND
240
220
200
180
160
140
120
100
80
60
40
20
200
400
600
800
1000
1200
1400
1600
1800
Distance From Runway Centerline (ft)

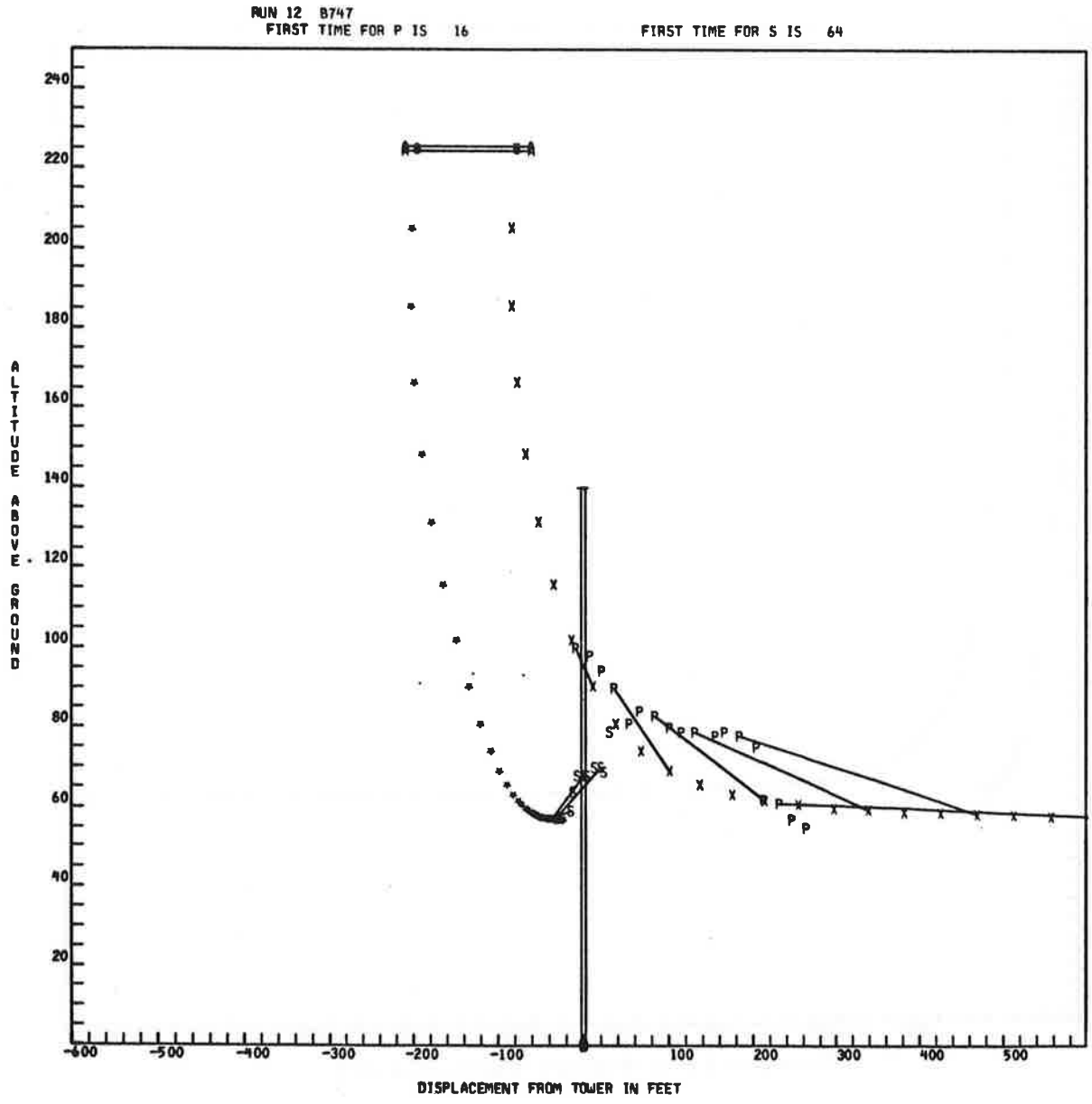
RUN 12 B747
FIRST TIME FOR P IS 16
FIRST TIME FOR S IS 64
ALTITUDE ABOVE GROUND
240
220
200
180
160
140
120
100
80
60
40
20
-600
-500
-400
-300
-200
-100
100
200
300
400
500
DISPLACEMENT FROM TOWER IN FEET

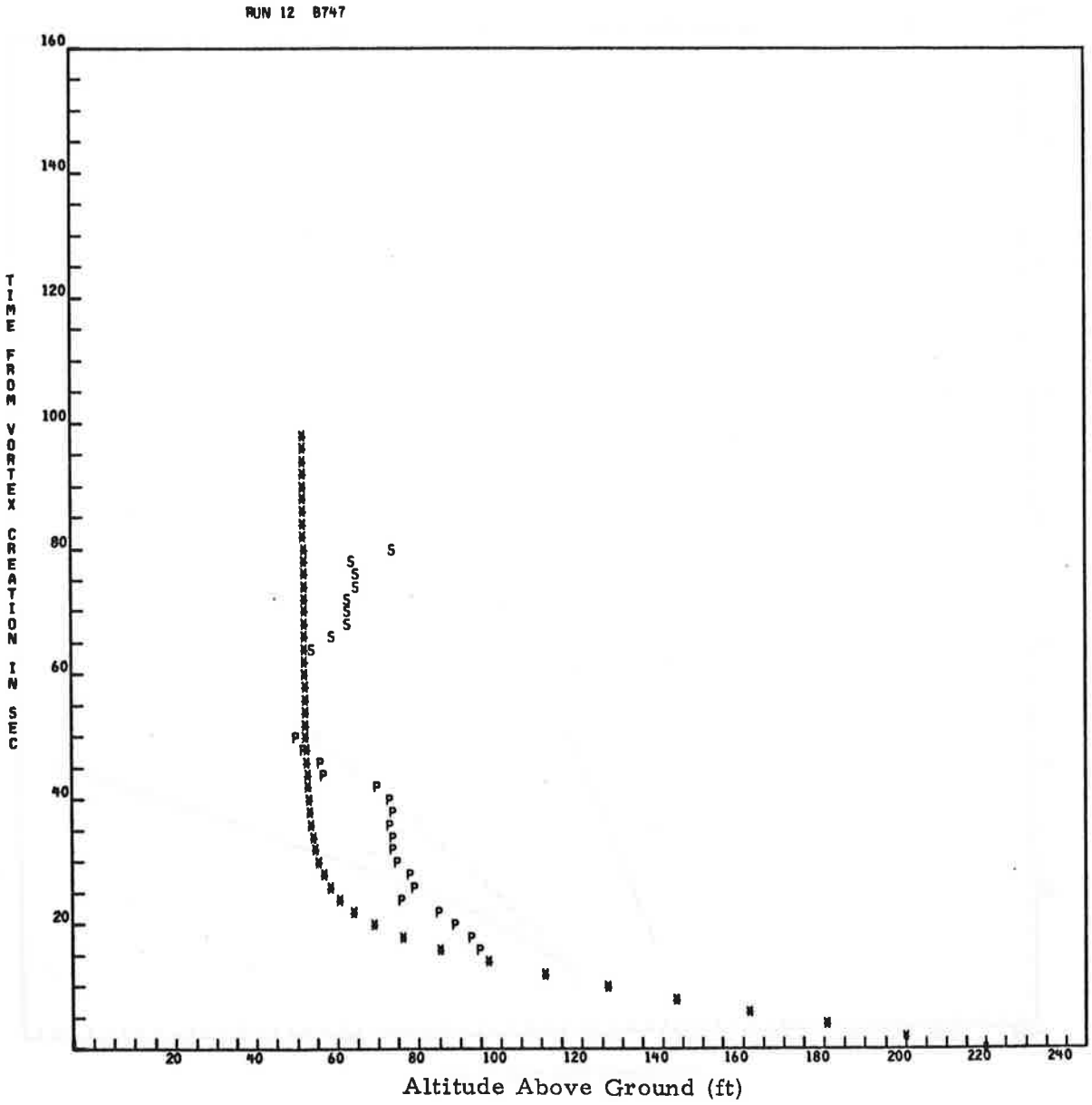
RUN 12 B747
TIME FROM VORTEX CREATION IN SEC
160
140
120
100
80
60
40
20
20
40
60
80
100
120
140
160
180
200
220
240
Altitude Above Ground (ft)

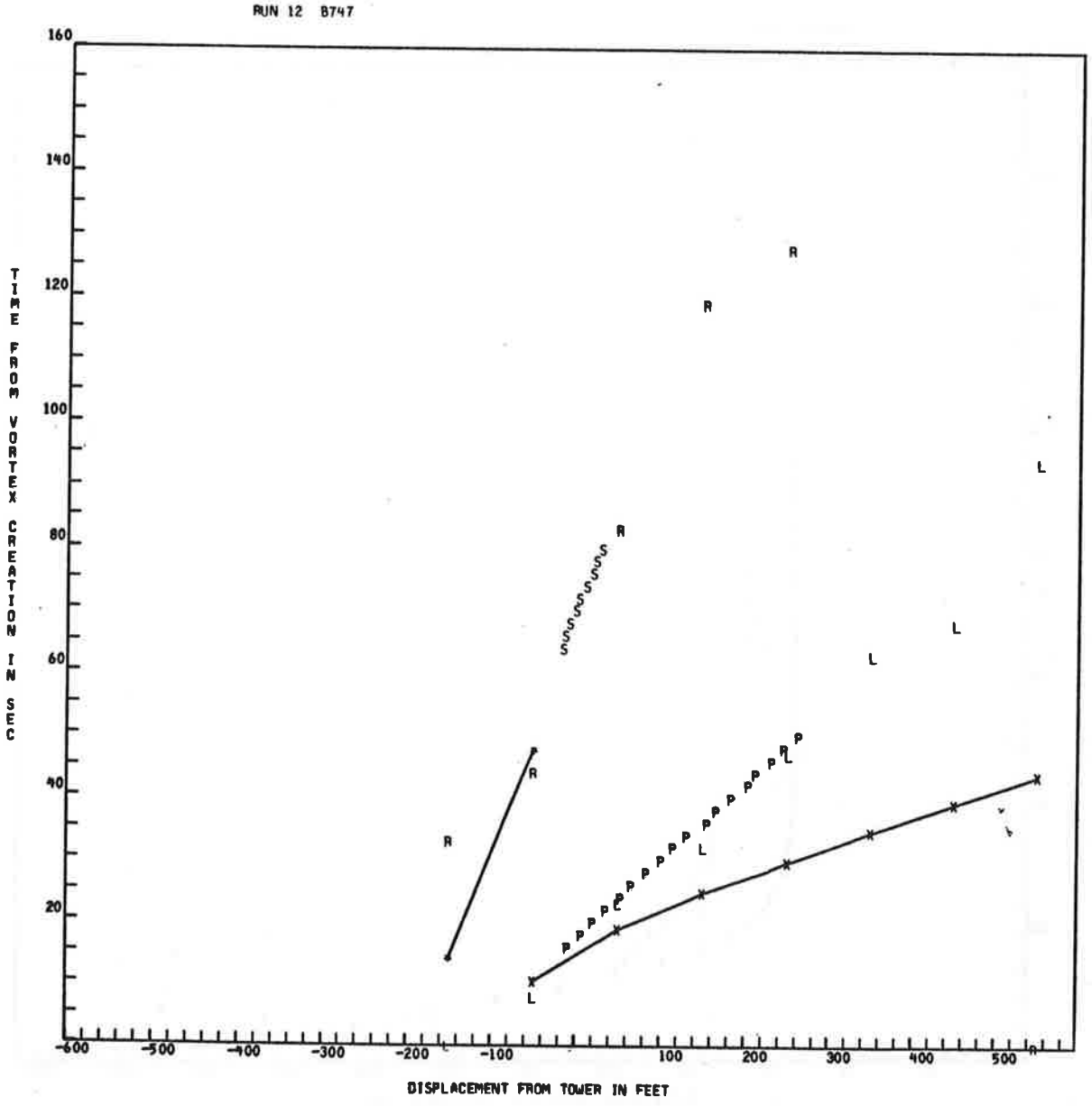
RUN 12 B747
TIME FROM VORTEX CREATION IN SEC
160
140
120
100
80
60
40
20
-600
-500
-400
-300
-200
-100
100
200
300
400
500
DISPLACEMENT FROM TOWER IN FEET

```
                                                        RUN DATA CARD
CONFIGURATION     LANDING LEVEL FLIGHT ALL ENGINES SAME POWER
AIRCRAFT TYPE IS B747
RUN NUMBER  13
AIRCRAFT DISPLACEMENT FROM TOWER -441 FT
AIRCRAFT ALTITUDE ABREAST OF TOWER 234 FT
AIRCRAFT WEIGHT 486000. POUNDS
AIRSPEED  233.1 FT/SEC
TEMPERATURE  23 DEGREES C (NOT USED)
INITIAL WIND SPEED   8 MPH  (NOT USED)
INITIAL WIND ANGLE 265 DEGREES TRUE  (NOT USED)
FINAL WIND SPEED   0 MPH  (NOT USED)
FINAL WIND ANGLE   0 DEGREES TRUE  (NOT USED)
AIRCRAFT HEADING 130 DEGREES MAGNETIC
MONTH  9     DAY 16     HOUR 10     MINUTE 35     LOCAL TIME



$OUTPUT
SPEED   =    -.23308200E+03
WEIGHT  =     .48600000E+06
WSPAN   =     .14974400E+03

$END
$WLOG
WSPR    =     .12012450E+02
CPOWER  =     .13212316E+00
COEF    =     .28746853E+03,  -.93077147E-01,   .77755151E-03,   .33643820E+01,
              .00000000E+00,   .00000000E+00,   .00000000E+00,   .00000000E+00,
              .00000000E+00

$END
GAMMA IN FT**2/SEC =   7.69681659+03
EDDY VISCOSITY IN FT**2/SEC =   8.16202186-01
TEMPERATURE IN RANKINE =   5.28578651+02
DENSITY IN SLUGS/FT**3 =   2.30344106-03
ACOUSTIC VELOCITY IN FT/SEC =   1.12701089+03
STABILITY IN 1/SEC**2 =   0.00000000
INITIAL PARAMETER (DIMENSIONLESS) =   0.00000000
```

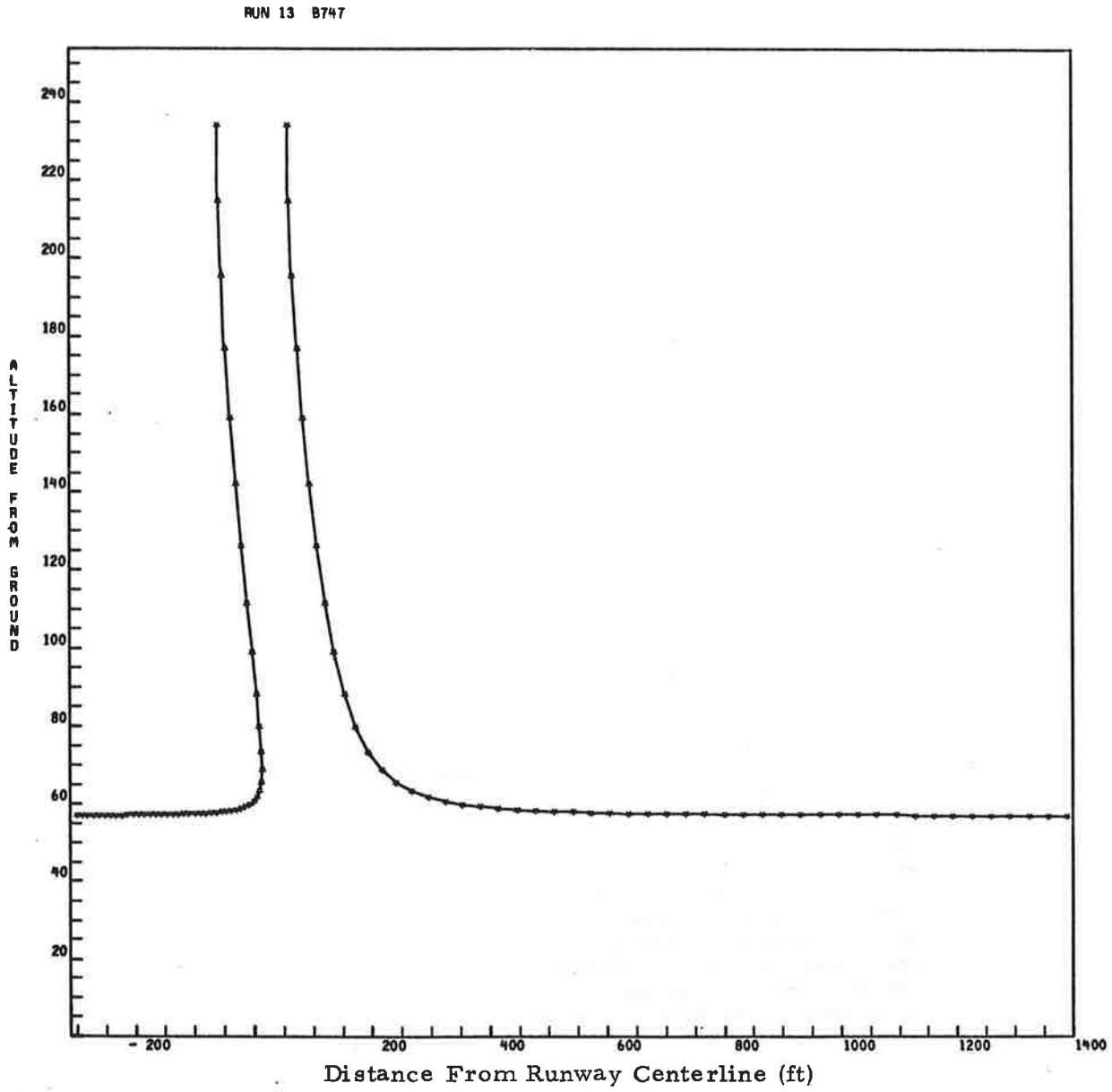
RUN 13 B747
ALTITUDE FROM GROUND
240
220
200
180
160
140
120
100
80
60
40
20
- 200
200
400
600
800
1000
1200
1400
Distance From Runway Centerline (ft)

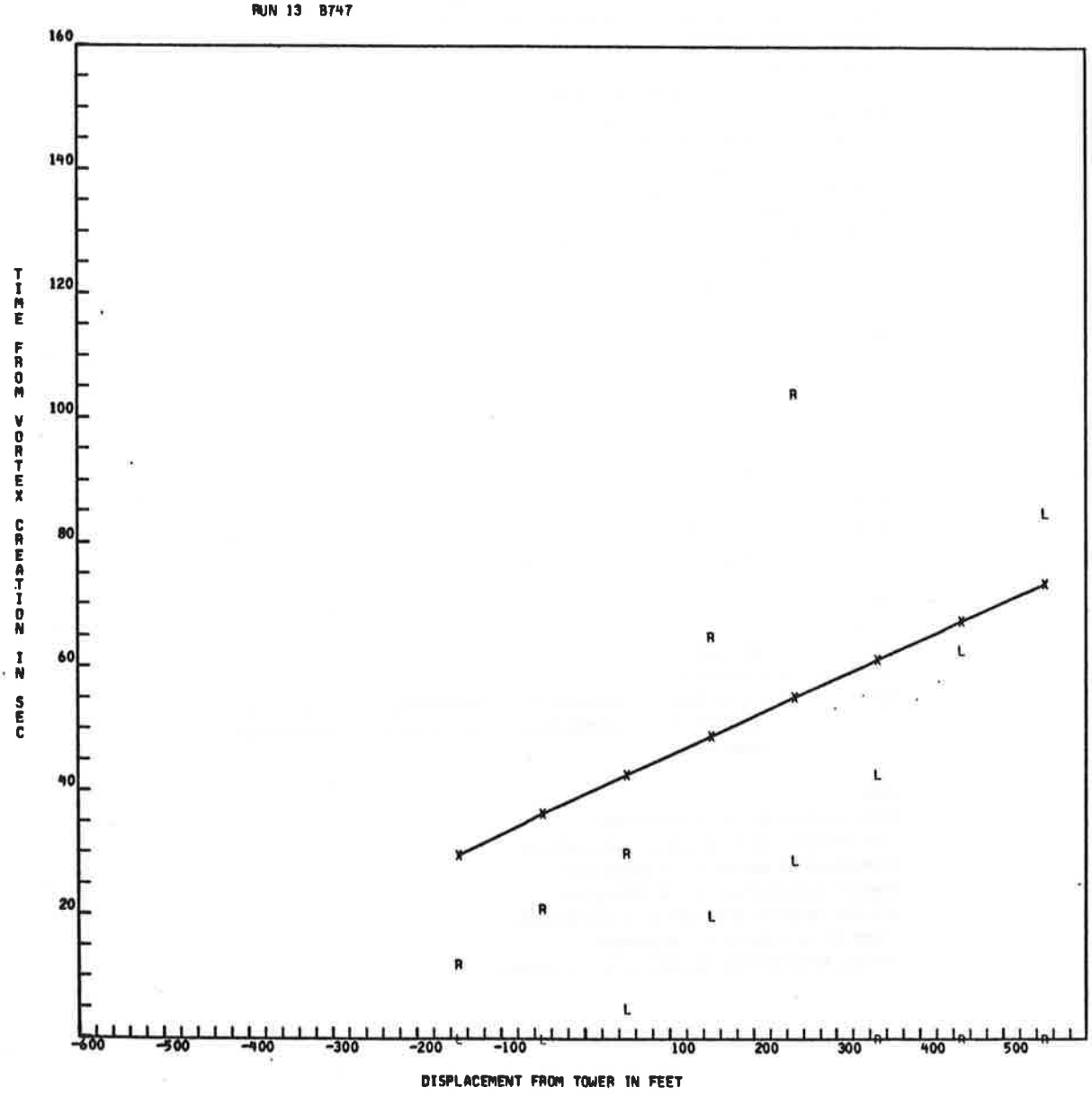
RUN 13 B747
160
140
120
100
80
60
40
20
TIME FROM VORTEX CREATION IN SEC
-600
-500
-400
-300
-200
-100
100
200
300
400
500
DISPLACEMENT FROM TOWER IN FEET
R
L

```
                                                        RUN DATA CARD
CONFIGURATION     LANDING LEVEL FLIGHT ALL ENGINES SAME POWER
AIRCRAFT TYPE IS B747
RUN NUMBER  14
AIRCRAFT DISPLACEMENT FROM TOWER -438 FT
AIRCRAFT ALTITUDE ABREAST OF TOWER 224 FT
AIRCRAFT WEIGHT 484000. POUNDS
AIRSPEED  239.8 FT/SEC
TEMPERATURE  23 DEGREES C (NOT USED)
INITIAL WIND SPEED   5 MPH  (NOT USED)
INITIAL WIND ANGLE 245 DEGREES TRUE  (NOT USED)
FINAL WIND SPEED   5 MPH  (NOT USED)
FINAL WIND ANGLE 250 DEGREES TRUE  (NOT USED)
AIRCRAFT HEADING 132 DEGREES MAGNETIC
MONTH  9     DAY 16     HOUR 10     MINUTE 39     LOCAL TIME


$OUTPUT
SPEED   =    -.23983800E+03
WEIGHT  =     .48400000E+06
WSPAN   =     .14974400E+03

$END
$WLOG
WSPR    =     .13836002E+02
CPOWER  =    -.45404010E-01
COEF    =     .28752927E+03,  -.95814819E-01,   .79920737E-03,   .34122933E+01,
              .00000000E+00,   .00000000E+00,   .00000000E+00,   .00000000E+00,
              .00000000E+00

$END
GAMMA IN FT**2/SEC =   7.46956293+03
EDDY VISCOSITY IN FT**2/SEC =   8.02723236-01
TEMPERATURE IN RANKINE =   5.30188446+02
DENSITY IN SLUGS/FT**3 =   2.29716866-03
ACOUSTIC VELOCITY IN FT/SEC =   1.12872575+03
STABILITY IN 1/SEC**2 =   0.00000000
INITIAL PARAMETER (DIMENSIONLESS) =   0.00000000
```

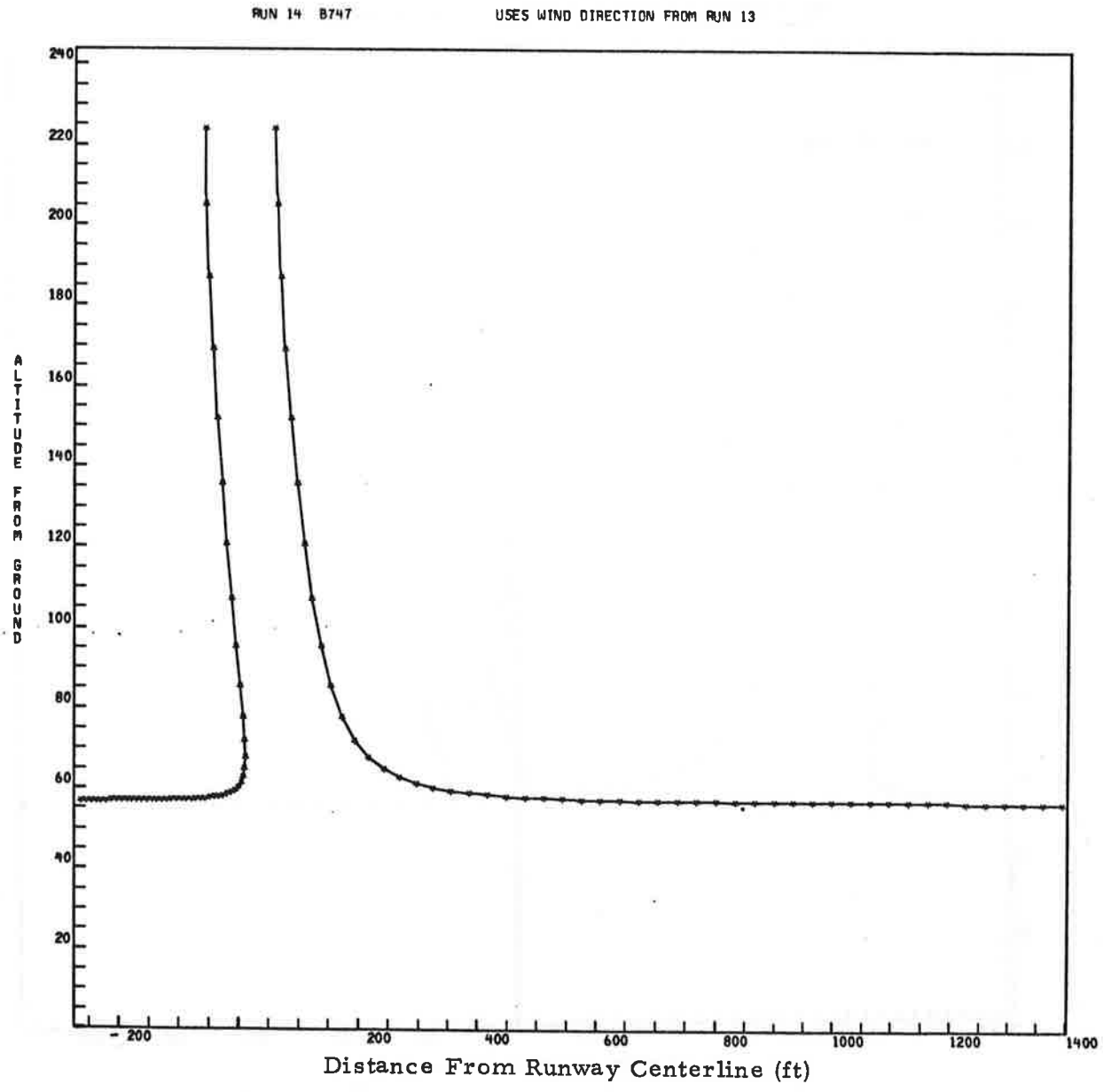
RUN 14 B747
USES WIND DIRECTION FROM RUN 13
ALTITUDE FROM GROUND
240
220
200
180
160
140
120
100
80
60
40
20
- 200
200
400
600
800
1000
1200
1400
Distance From Runway Centerline (ft)

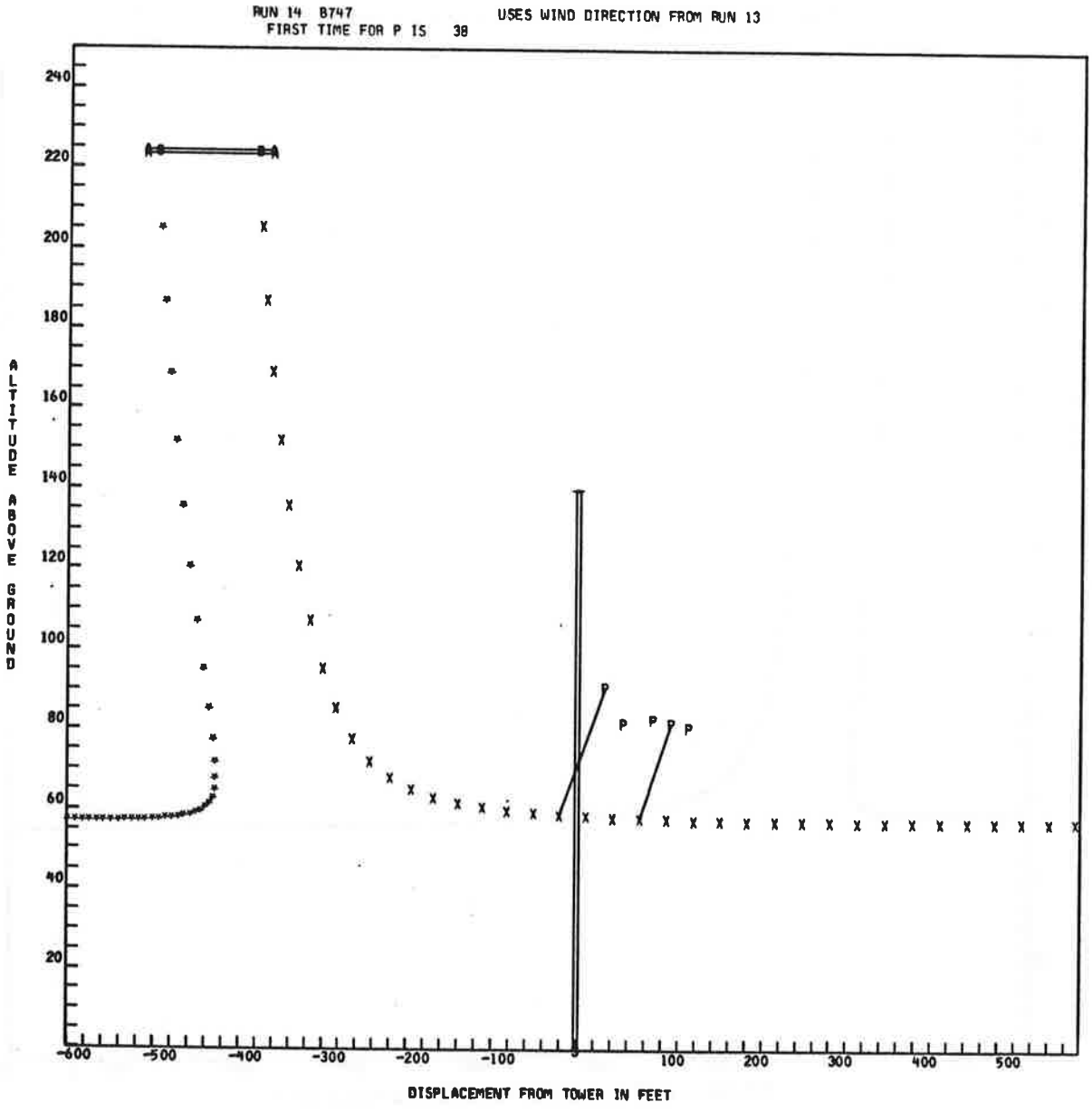
RUN 14 8747
FIRST TIME FOR P IS 38
USES WIND DIRECTION FROM RUN 13
ALTITUDE ABOVE GROUND
240
220
200
180
160
140
120
100
80
60
40
20
-600
-500
-400
-300
-200
-100
100
200
300
400
500
DISPLACEMENT FROM TOWER IN FEET

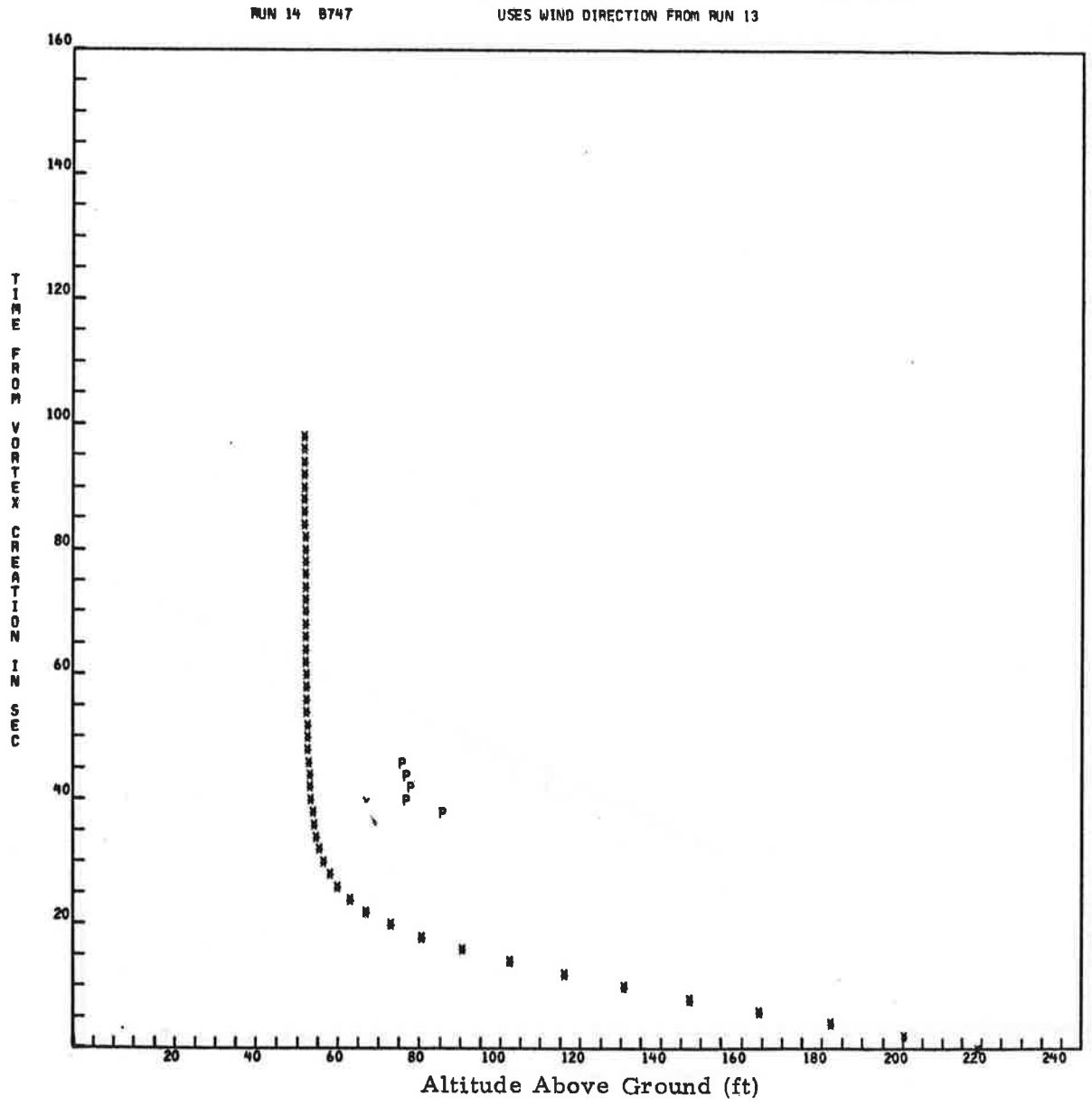
RUN 14 B747
USES WIND DIRECTION FROM RUN 13
TIME FROM VORTEX CREATION IN SEC
160
140
120
100
80
60
40
20
20
40
60
80
100
120
140
160
180
200
220
240
Altitude Above Ground (ft)

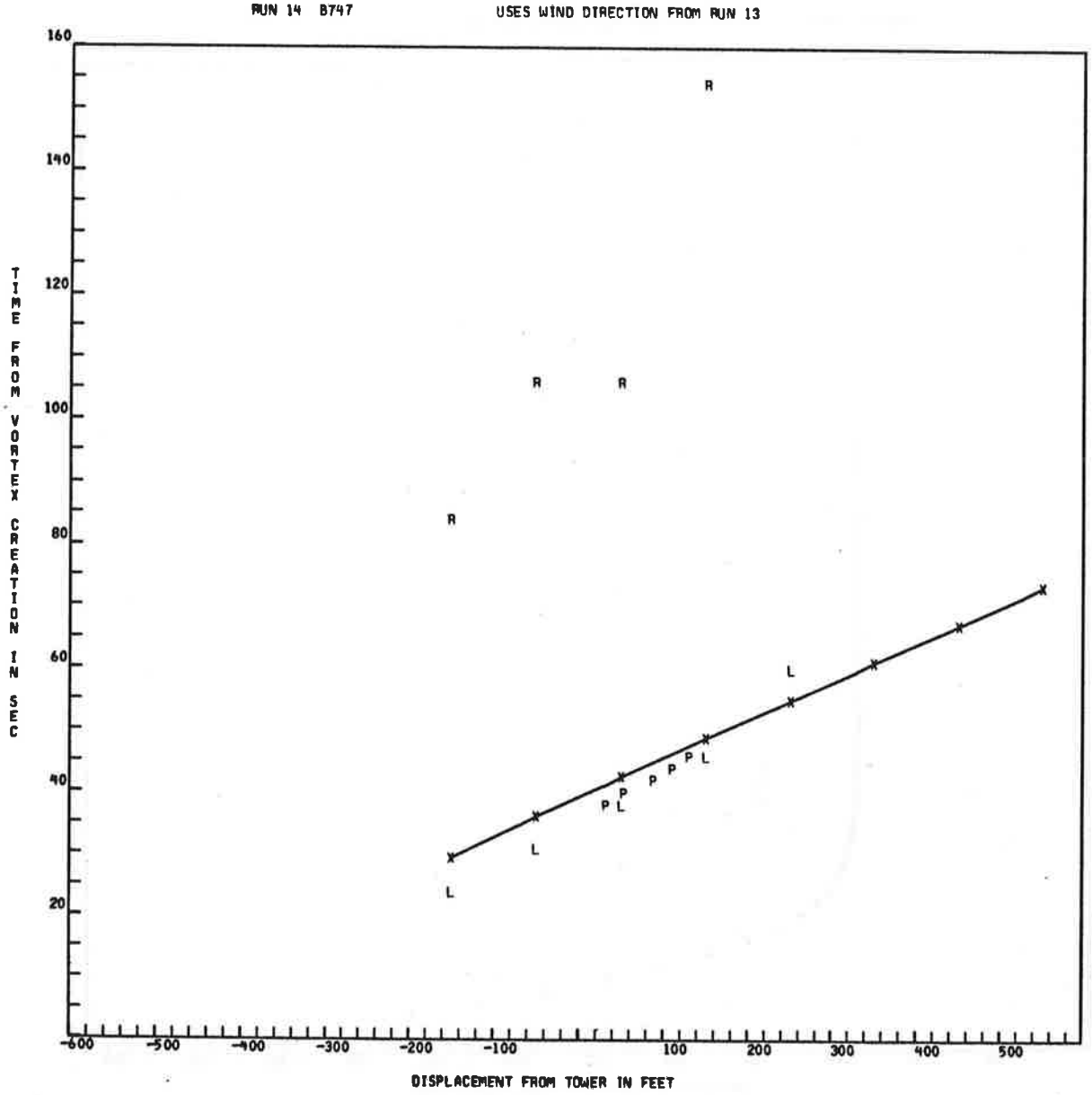
RUN 14 B747
USES WIND DIRECTION FROM RUN 13
TIME FROM VORTEX CREATION IN SEC
DISPLACEMENT FROM TOWER IN FEET
160
140
120
100
80
60
40
20
-600
-500
-400
-300
-200
-100
100
200
300
400
500
R
R
R
R
L
L
L
P
P
P
P
P
L
L

```
                                                    RUN DATA CARD
CONFIGURATION     LANDING LEVEL FLIGHT ALL ENGINES SAME POWER
AIRCRAFT TYPE IS B747
RUN NUMBER  15
AIRCRAFT DISPLACEMENT FROM TOWER -266 FT
AIRCRAFT ALTITUDE ABREAST OF TOWER 189 FT
AIRCRAFT WEIGHT 482000. POUNDS
AIRSPEED  239.8 FT/SEC
TEMPERATURE  23 DEGREES C (NOT USED)
INITIAL WIND SPEED   8 MPH  (NOT USED)
INITIAL WIND ANGLE 265 DEGREES TRUE  (NOT USED)
FINAL WIND SPEED   0 MPH  (NOT USED)
FINAL WIND ANGLE   0 DEGREES TRUE  (NOT USED)
AIRCRAFT HEADING 130 DEGREES MAGNETIC
MONTH  9     DAY 16     HOUR 10     MINUTE 44     LOCAL TIME



$OUTPUT
SPEED   =    -.23983800E+03
WEIGHT  =     .48200000E+06
WSPAN   =     .14974400E+03

$END
$WLOG
WSPR    =     .12502376E+02
CPOWER  =     .98455849E-01
COEF    =     .27531831E+03,  -.48841572E-02,   .63729851E-03,   .68184748E+00,
              .00000000E+00,   .00000000E+00,   .00000000E+00,   .00000000E+00,
              .00000000E+00

$END
GAMMA IN FT**2/SEC =   7.45568176+03
EDDY VISCOSITY IN FT**2/SEC =   8.03329870-01
TEMPERATURE IN RANKINE =   5.32074509+02
DENSITY IN SLUGS/FT**3 =   2.29193547-03
ACOUSTIC VELOCITY IN FT/SEC =   1.13073160+03
STABILITY IN 1/SEC**2 =   0.00000000
INITIAL PARAMETER (DIMENSIONLESS) =   0.00000000
```

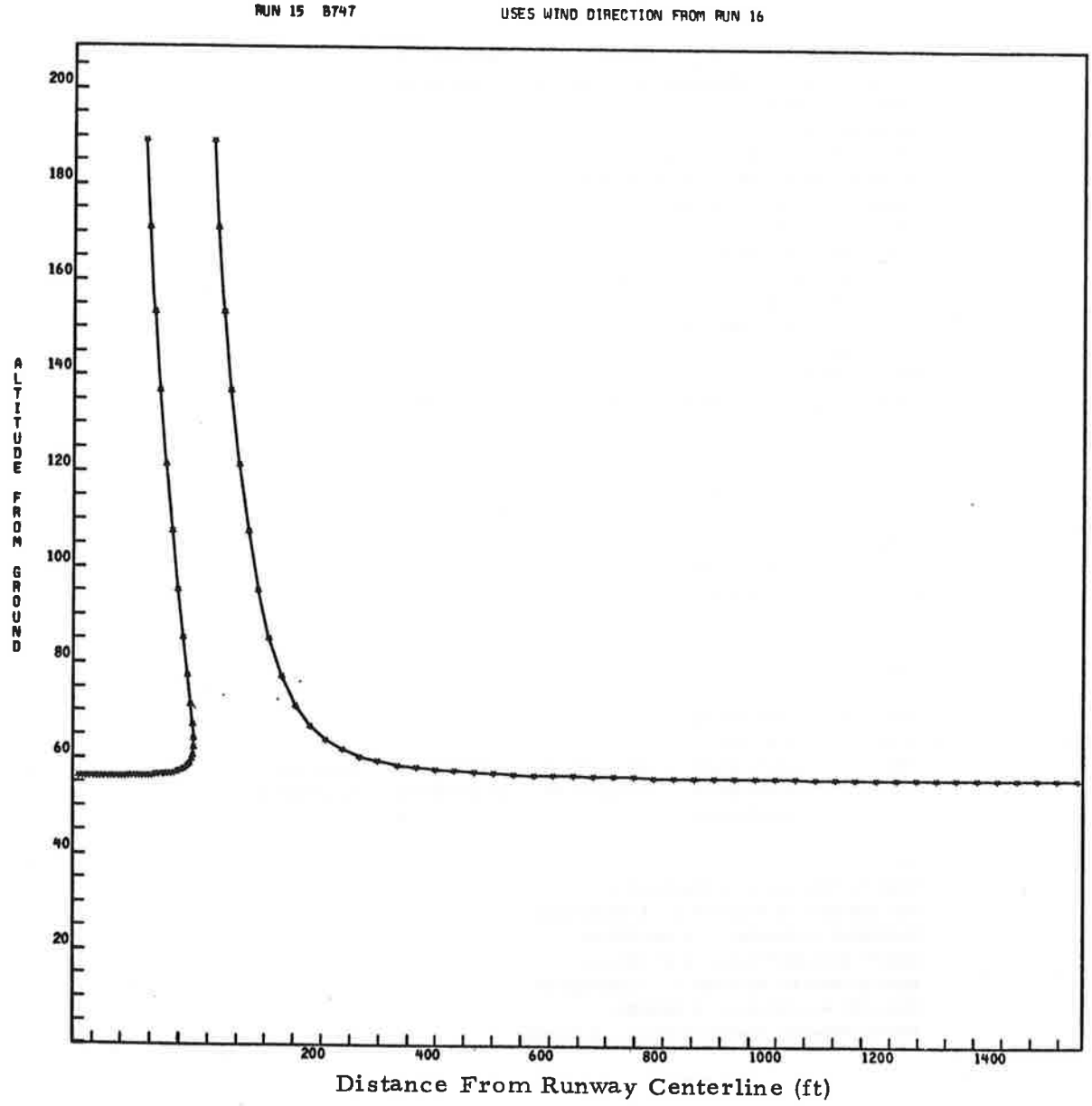
RUN 15 B747
USES WIND DIRECTION FROM RUN 16
ALTITUDE FROM GROUND
200
180
160
140
120
100
80
60
40
20
200
400
600
800
1000
1200
1400
Distance From Runway Centerline (ft)

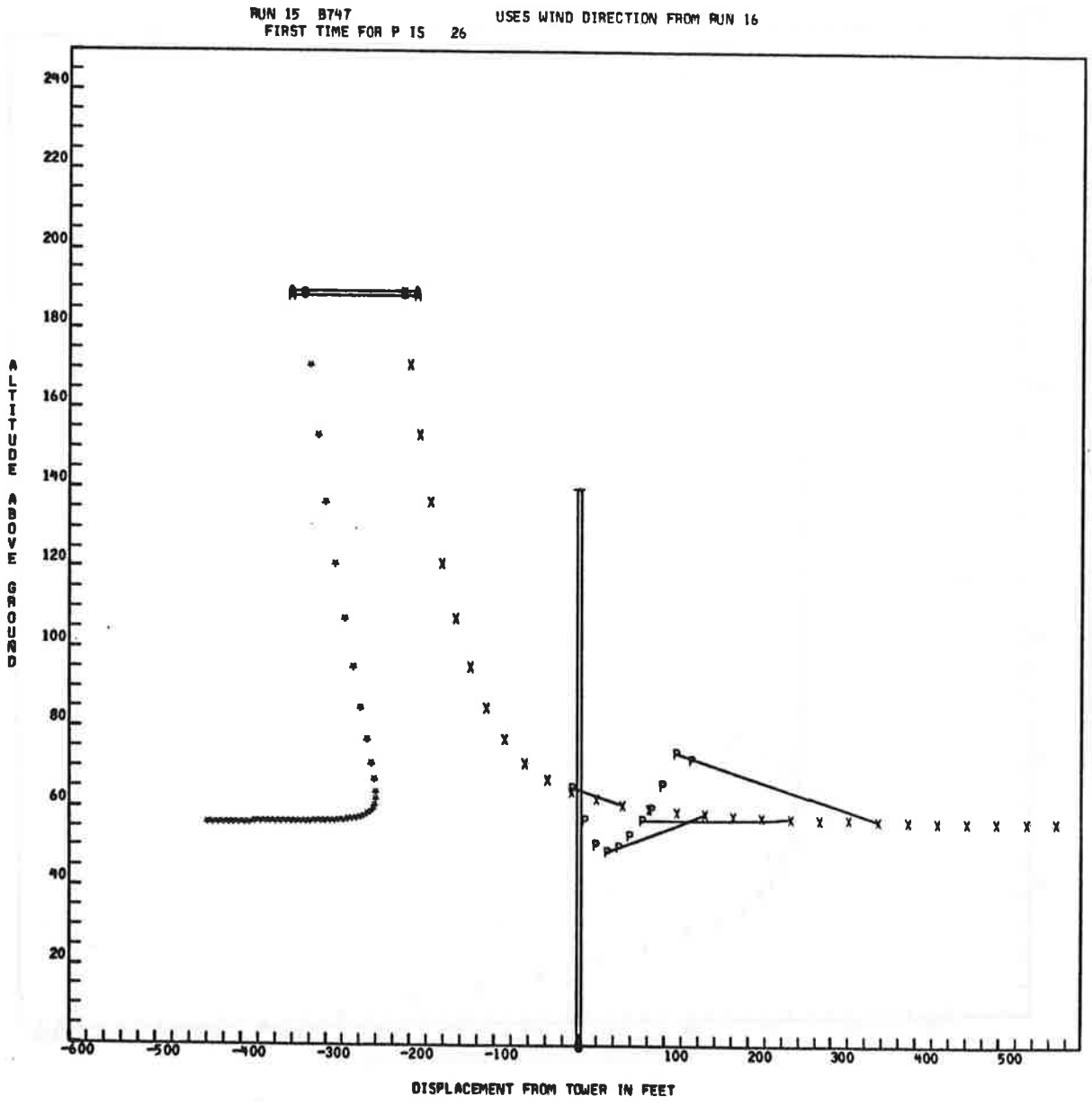
RUN 15 B747
FIRST TIME FOR P 15 26
USES WIND DIRECTION FROM RUN 16
ALTITUDE ABOVE GROUND
240
220
200
180
160
140
120
100
80
60
40
20
-600
-500
-400
-300
-200
-100
100
200
300
400
500
DISPLACEMENT FROM TOWER IN FEET

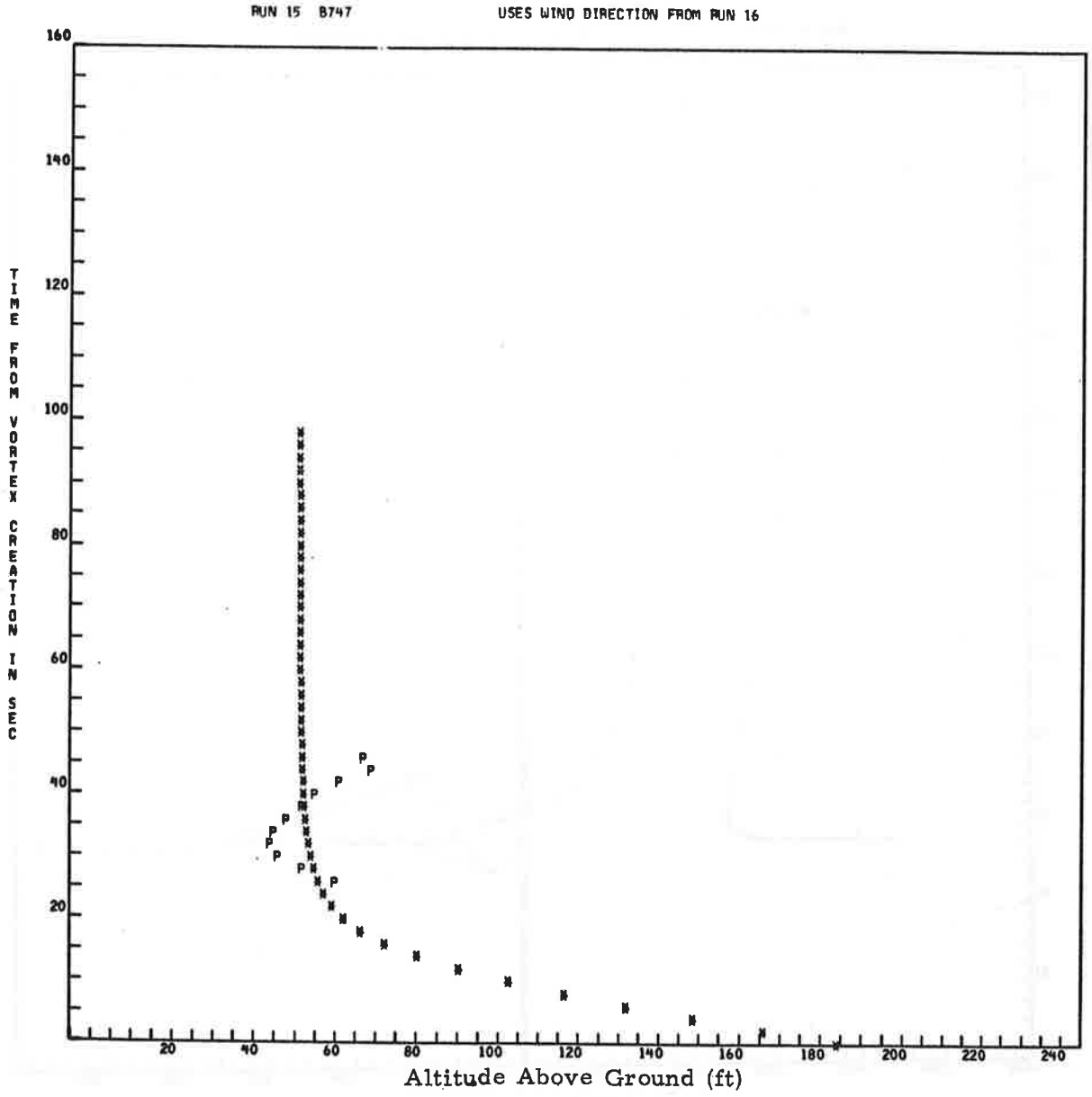
RUN 15 B747
USES WIND DIRECTION FROM RUN 16
TIME FROM VORTEX CREATION IN SEC
160
140
120
100
80
60
40
20
20
40
60
80
100
120
140
160
180
200
220
240
Altitude Above Ground (ft)

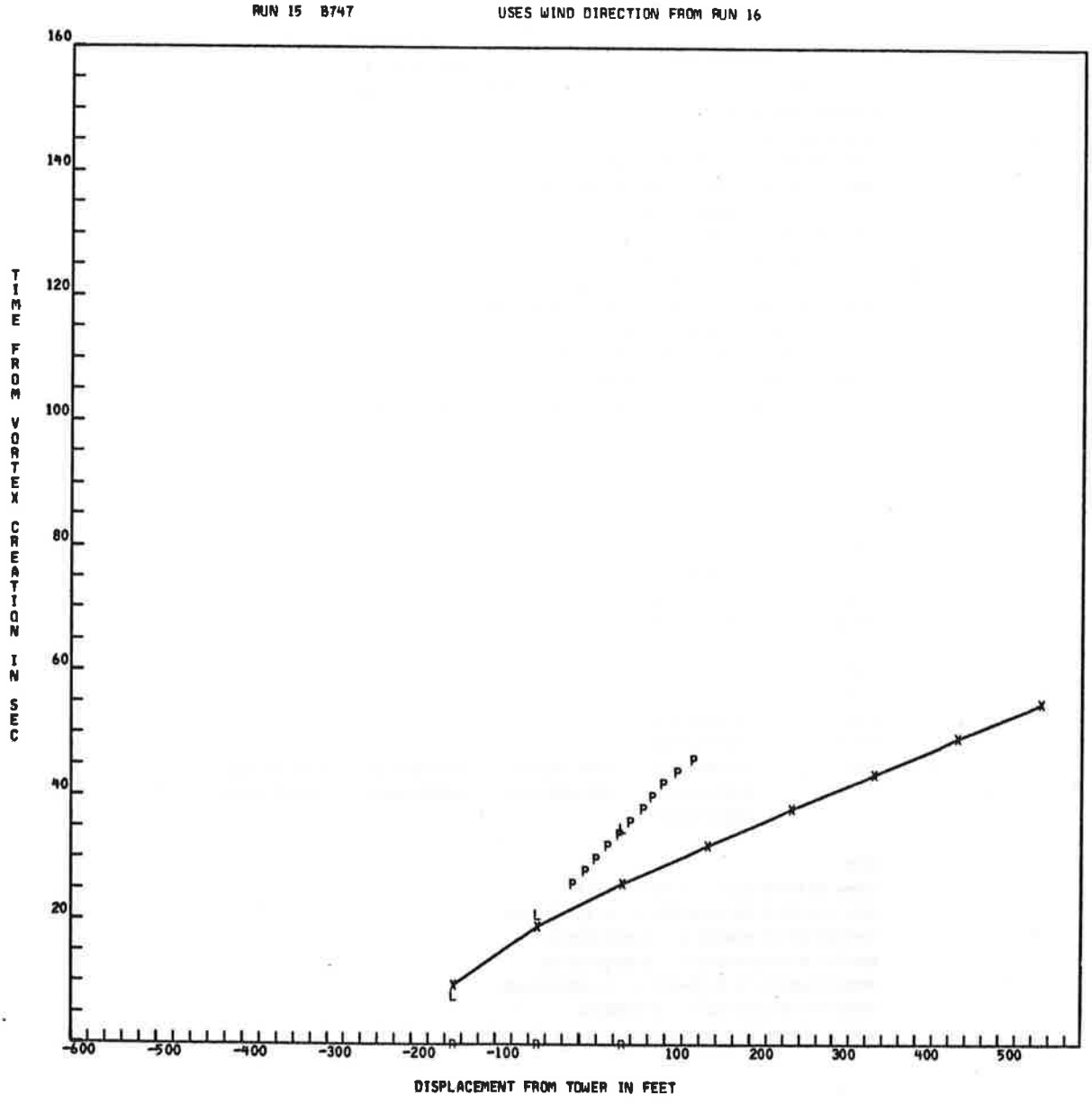
RUN 15 B747
USES WIND DIRECTION FROM RUN 16
TIME FROM VORTEX CREATION IN SEC
160
140
120
100
80
60
40
20
-600
-500
-400
-300
-200
-100
100
200
300
400
500
DISPLACEMENT FROM TOWER IN FEET

```
                                                    RUN DATA CARD
CONFIGURATION     LANDING LEVEL FLIGHT ALL ENGINES SAME POWER
AIRCRAFT TYPE IS B747
RUN NUMBER  16
AIRCRAFT DISPLACEMENT FROM TOWER -222 FT
AIRCRAFT ALTITUDE ABREAST OF TOWER 178 FT
AIRCRAFT WEIGHT 480000. POUNDS
AIRSPEED  229.7 FT/SEC
TEMPERATURE  24 DEGREES C (NOT USED)
INITIAL WIND SPEED   9 MPH  (NOT USED)
INITIAL WIND ANGLE 270 DEGREES TRUE  (NOT USED)
FINAL WIND SPEED   5 MPH  (NOT USED)
FINAL WIND ANGLE 275 DEGREES TRUE  (NOT USED)
AIRCRAFT HEADING 130 DEGREES MAGNETIC
MONTH  9     DAY 16     HOUR 10     MINUTE 47     LOCAL TIME



$OUTPUT
SPEED   =    -.22970400E+03
WEIGHT  =     .48000000E+06
WSPAN   =     .14974400E+03

$END
$WLOG
WSPR    =     .14810240E+02
CPOWER  =     .11825174E+00
COEF    =     .27562955E+03,  -.15707588E-01,   .70551987E-03,   .63196877E+00,
              .00000000E+00,   .00000000E+00,   .00000000E+00,   .00000000E+00,
              .00000000E+00

$END
GAMMA IN FT**2/SEC =   7.75211176+03
EDDY VISCOSITY IN FT**2/SEC =   8.23063850-01
TEMPERATURE IN RANKINE =   5.32264832+02
DENSITY IN SLUGS/FT**3 =   2.29199338-03
ACOUSTIC VELOCITY IN FT/SEC =   1.13093381+03
STABILITY IN 1/SEC**2 =   0.00000000
INITIAL PARAMETER (DIMENSIONLESS) =   0.00000000
```

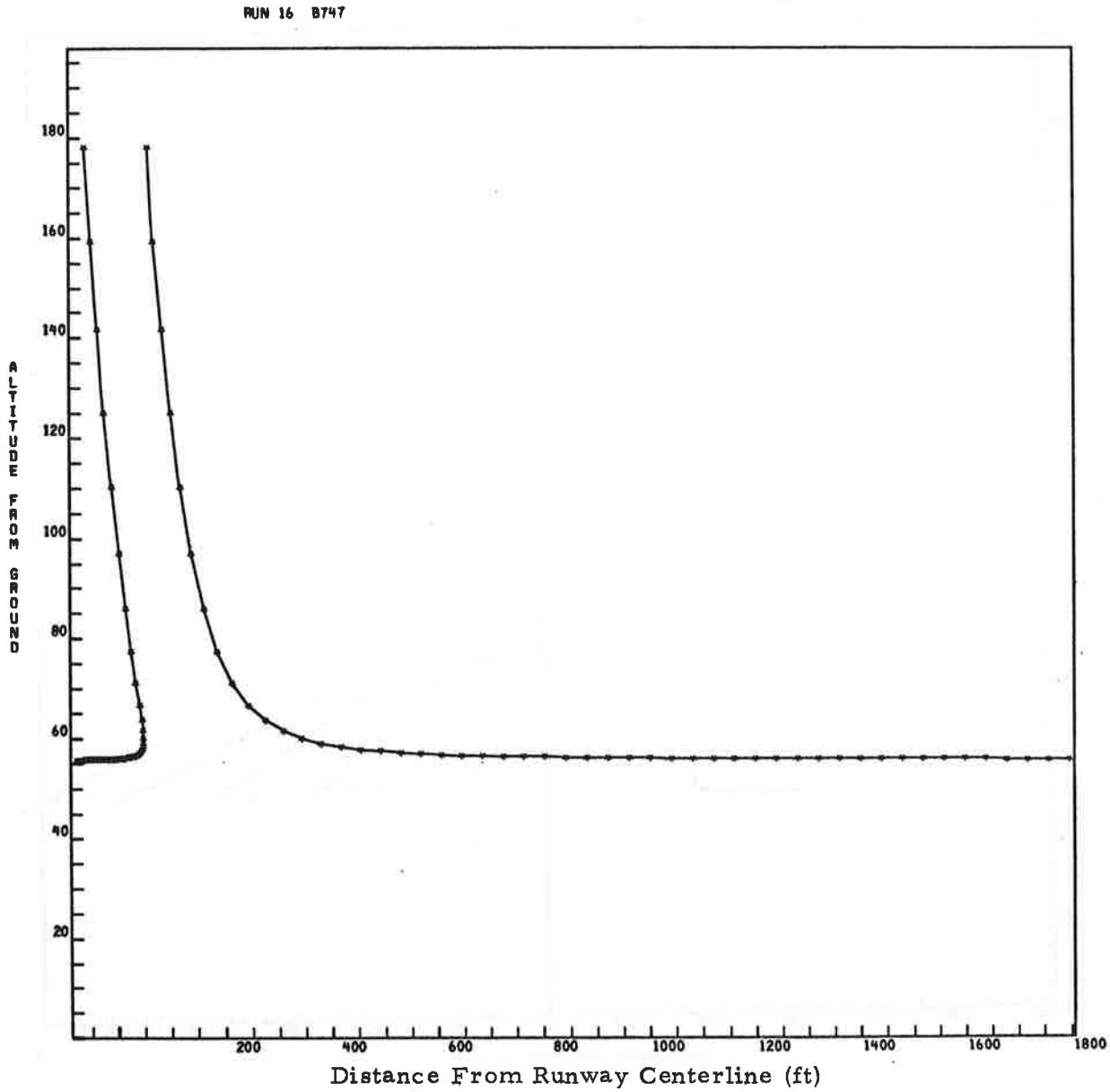
RUN 16 B747
ALTITUDE FROM GROUND
180
160
140
120
100
80
60
40
20
200
400
600
800
1000
1200
1400
1600
1800
Distance From Runway Centerline (ft)

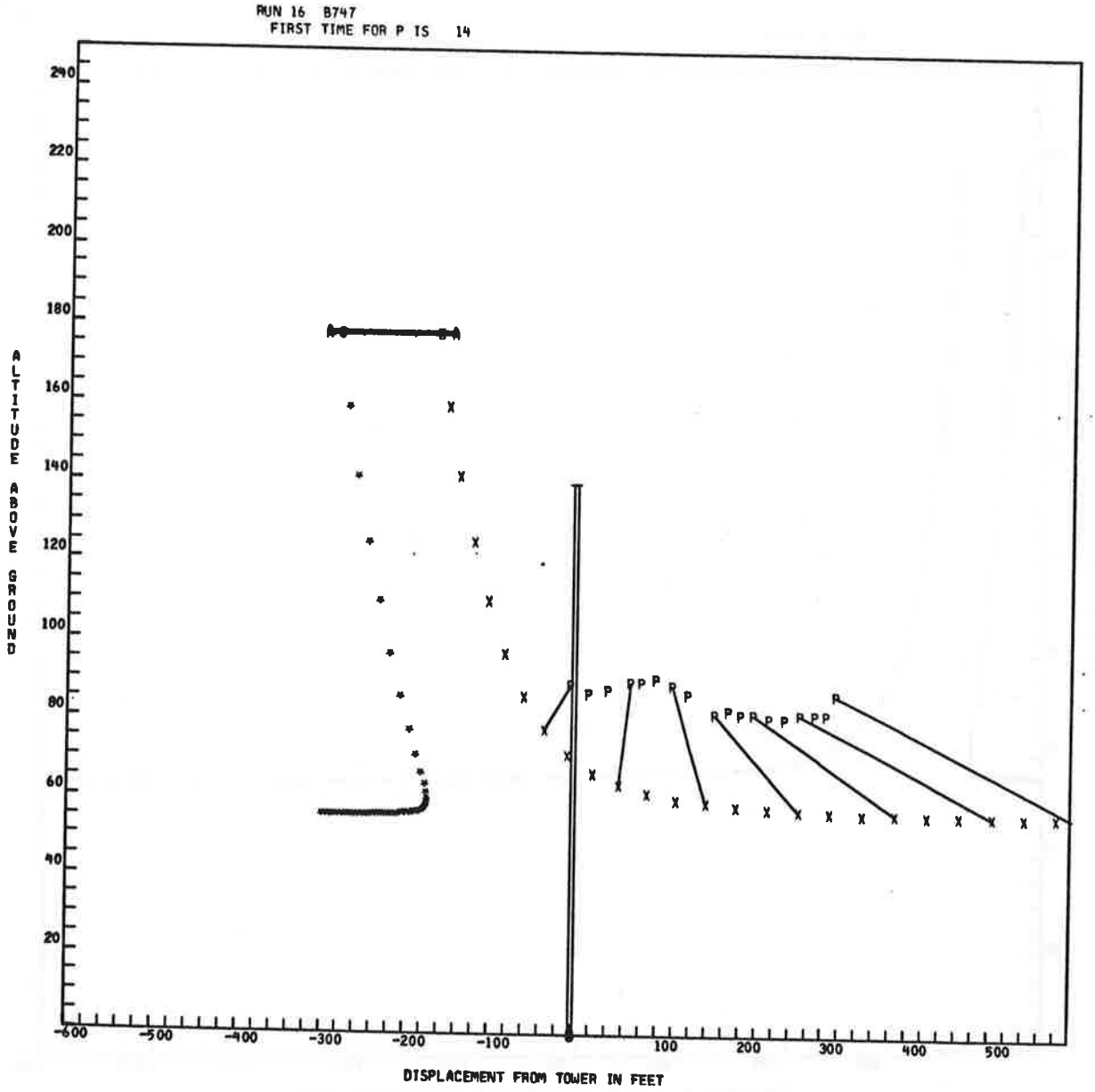
RUN 16 B747
FIRST TIME FOR P IS 14
ALTITUDE ABOVE GROUND
240
220
200
180
160
140
120
100
80
60
40
20
-600
-500
-400
-300
-200
-100
100
200
300
400
500
DISPLACEMENT FROM TOWER IN FEET

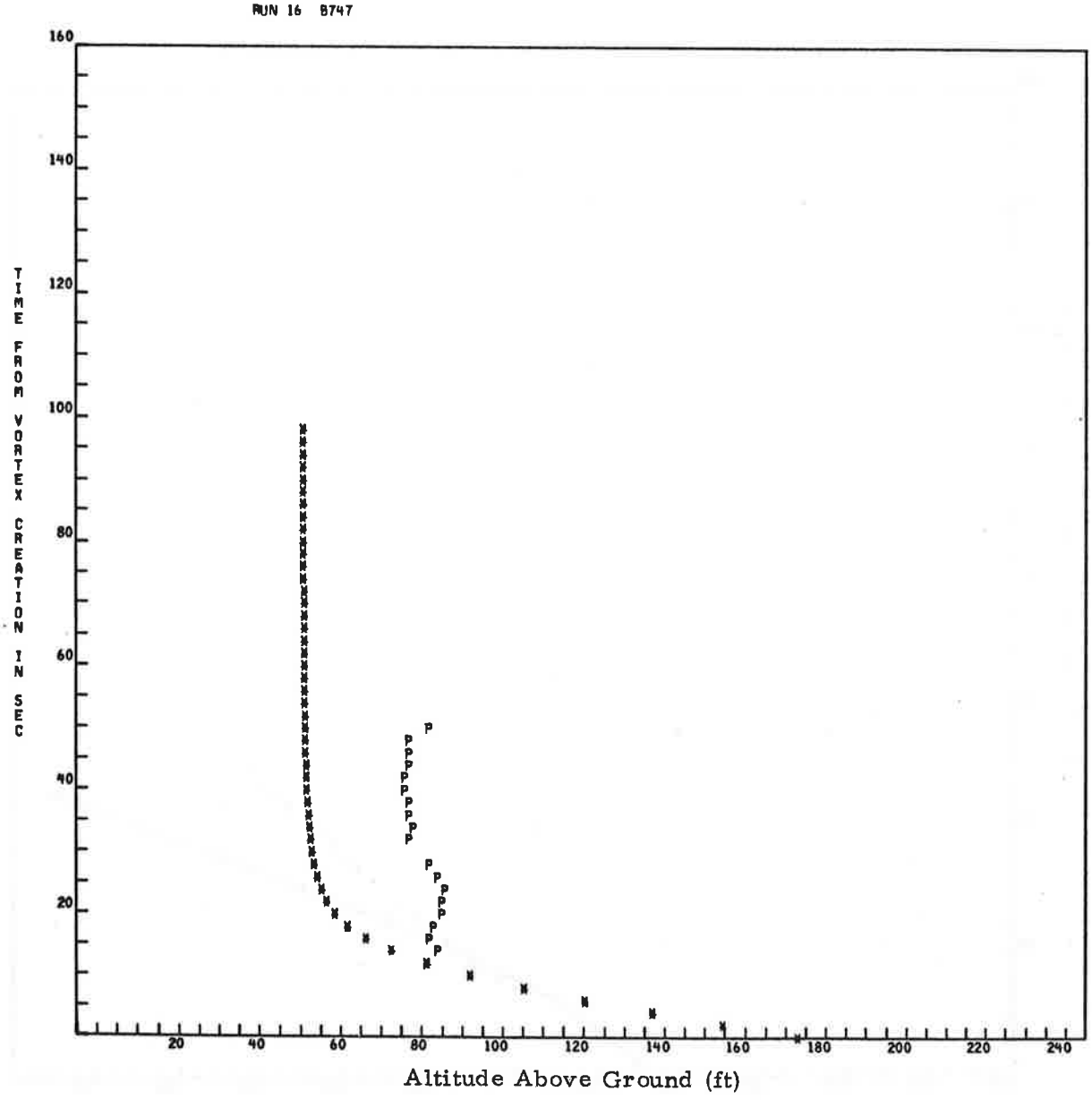
RUN 16 8747
TIME FROM VORTEX CREATION IN SEC
160
140
120
100
80
60
40
20
20
40
60
80
100
120
140
160
180
200
220
240
Altitude Above Ground (ft)

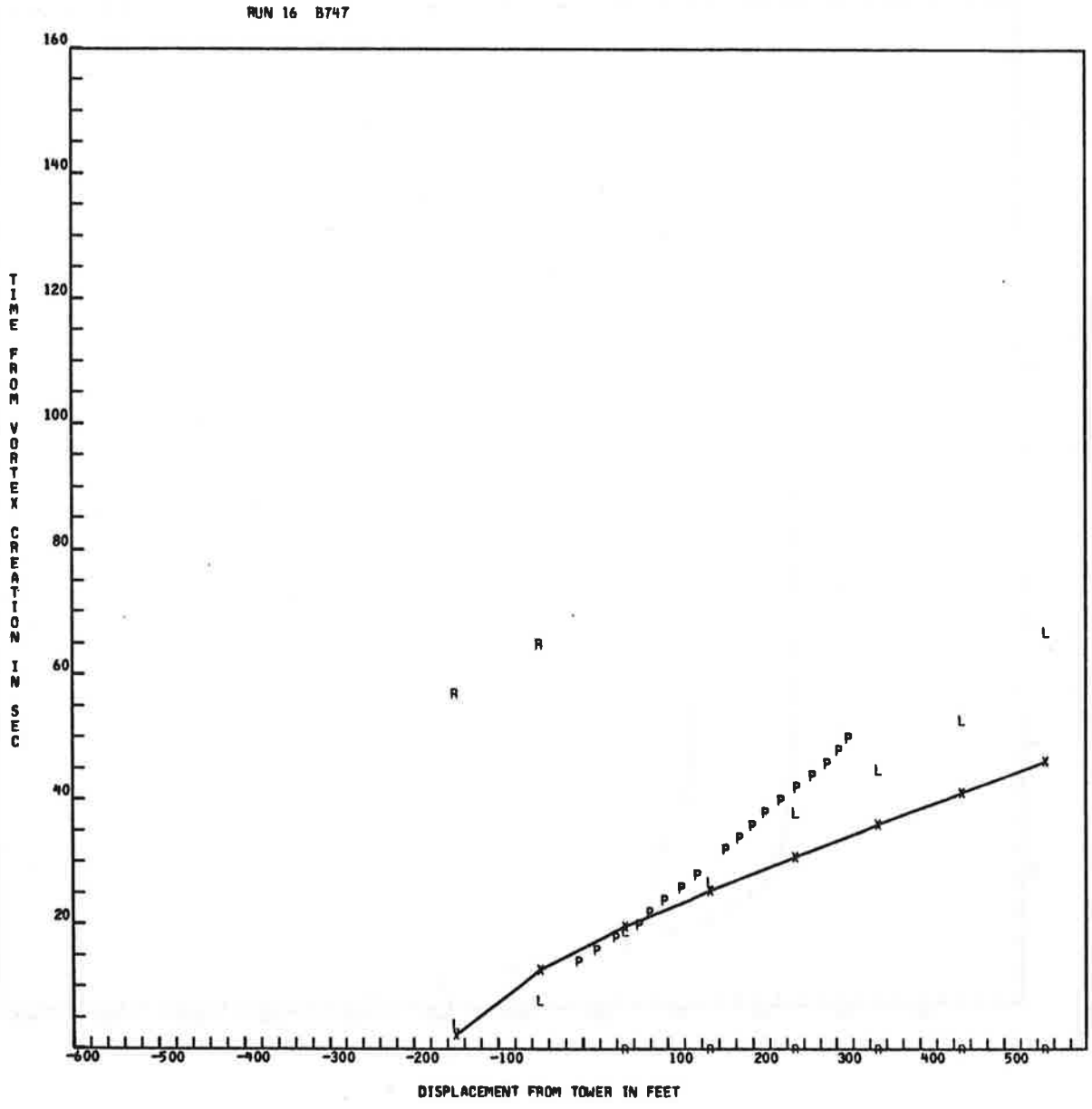
RUN 16 B747
160
140
120
100
80
60
40
20
TIME FROM VORTEX CREATION IN SEC
-600
-500
-400
-300
-200
-100
100
200
300
400
500
DISPLACEMENT FROM TOWER IN FEET

```
                                                        RUN DATA CARD
CONFIGURATION     LANDING LEVEL FLIGHT ALL ENGINES SAME POWER
AIRCRAFT TYPE IS B747
RUN NUMBER  17
AIRCRAFT DISPLACEMENT FROM TOWER -229 FT
AIRCRAFT ALTITUDE ABREAST OF TOWER 187 FT
AIRCRAFT WEIGHT 478000. POUNDS
AIRSPEED  228.0 FT/SEC
TEMPERATURE  24 DEGREES C (NOT USED)
INITIAL WIND SPEED   9 MPH  (NOT USED)
INITIAL WIND ANGLE 280 DEGREES TRUE  (NOT USED)
FINAL WIND SPEED   0 MPH  (NOT USED)
FINAL WIND ANGLE   0 DEGREES TRUE  (NOT USED)
AIRCRAFT HEADING 132 DEGREES MAGNETIC
MONTH  9     DAY 16     HOUR 10     MINUTE 52     LOCAL TIME



$OUTPUT
SPEED   =    -.22801500E+03
WEIGHT  =     .47800000E+06
WSPAN   =     .14974400E+03

$END
$WLOG
WSPR    =     .15211066E+02
CPOWER  =     .33544965E-01
COEF    =     .25938473E+03,   .16776454E+00,   .44287454E-03,   .18463949E+01,
              .00000000E+00,   .00000000E+00,   .00000000E+00,   .00000000E+00,
              .00000000E+00

$END
GAMMA IN FT**2/SEC =   7.77590912+03
EDDY VISCOSITY IN FT**2/SEC =   8.24473R36-01
TEMPERATURE IN RANKINE =   5.32018623+02
DENSITY IN SLUGS/FT**3 =   2.29231347-03
ACOUSTIC VELOCITY IN FT/SEC =   1.13067221+03
STABILITY IN 1/SEC**2 =   0.00000000
INITIAL PARAMETER (DIMENSIONLESS) =   0.00000000
```

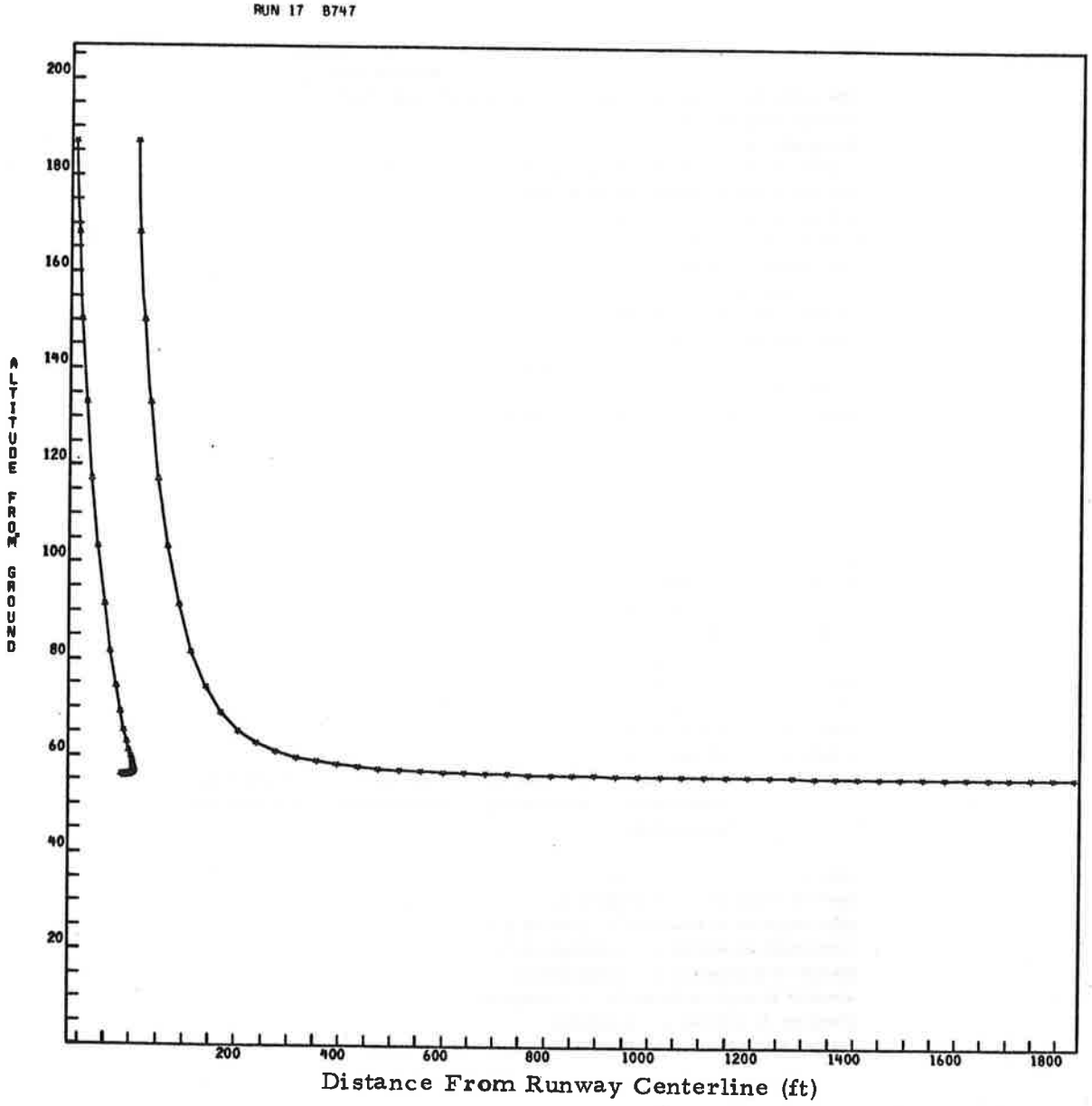
RUN 17 B747
ALTITUDE FROM GROUND
200
180
160
140
120
100
80
60
40
20
200
400
600
800
1000
1200
1400
1600
1800
Distance From Runway Centerline (ft)

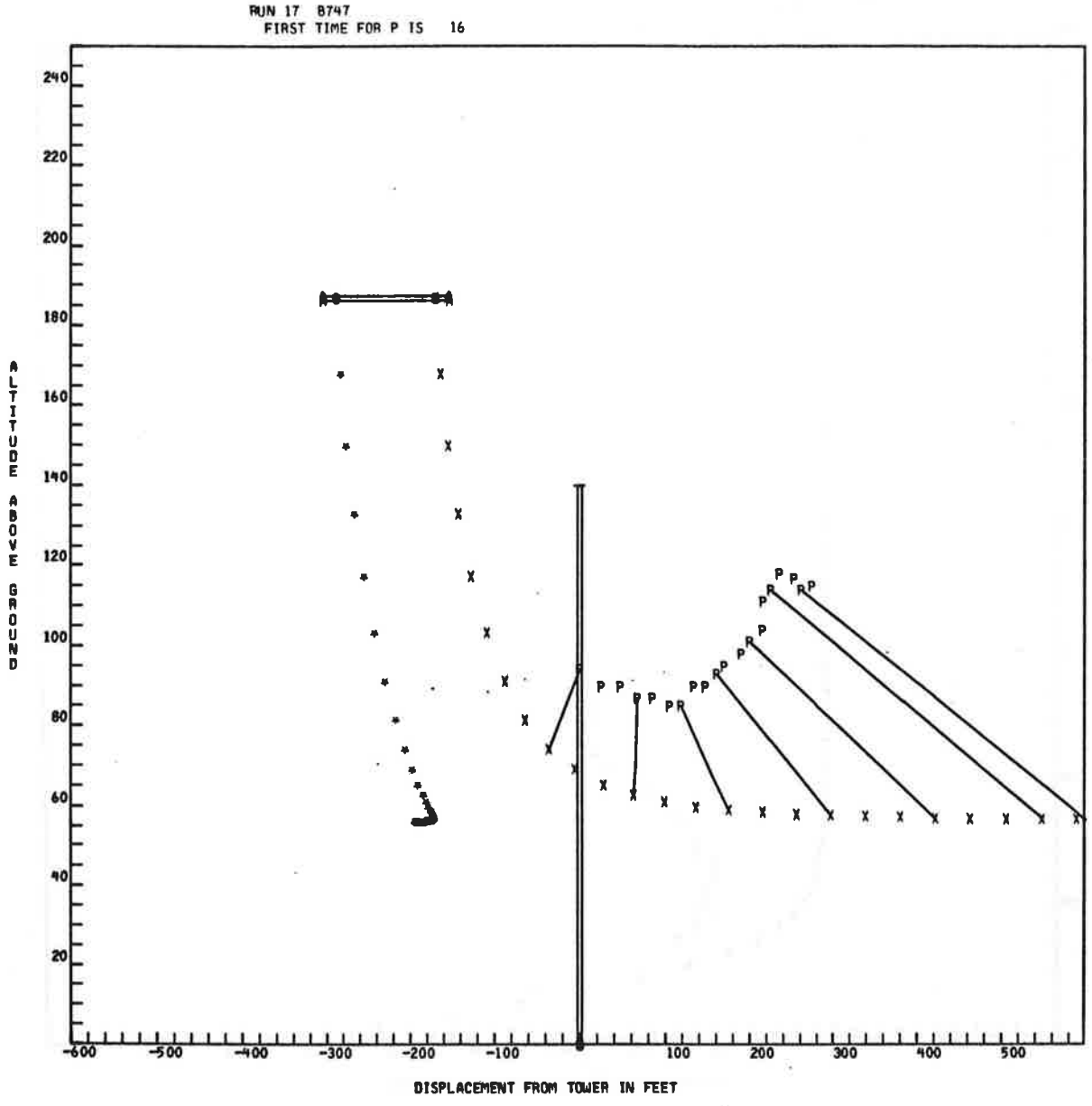
RUN 17 B747
FIRST TIME FOR P IS 16
ALTITUDE ABOVE GROUND
240
220
200
180
160
140
120
100
80
60
40
20
-600
-500
-400
-300
-200
-100
100
200
300
400
500
DISPLACEMENT FROM TOWER IN FEET

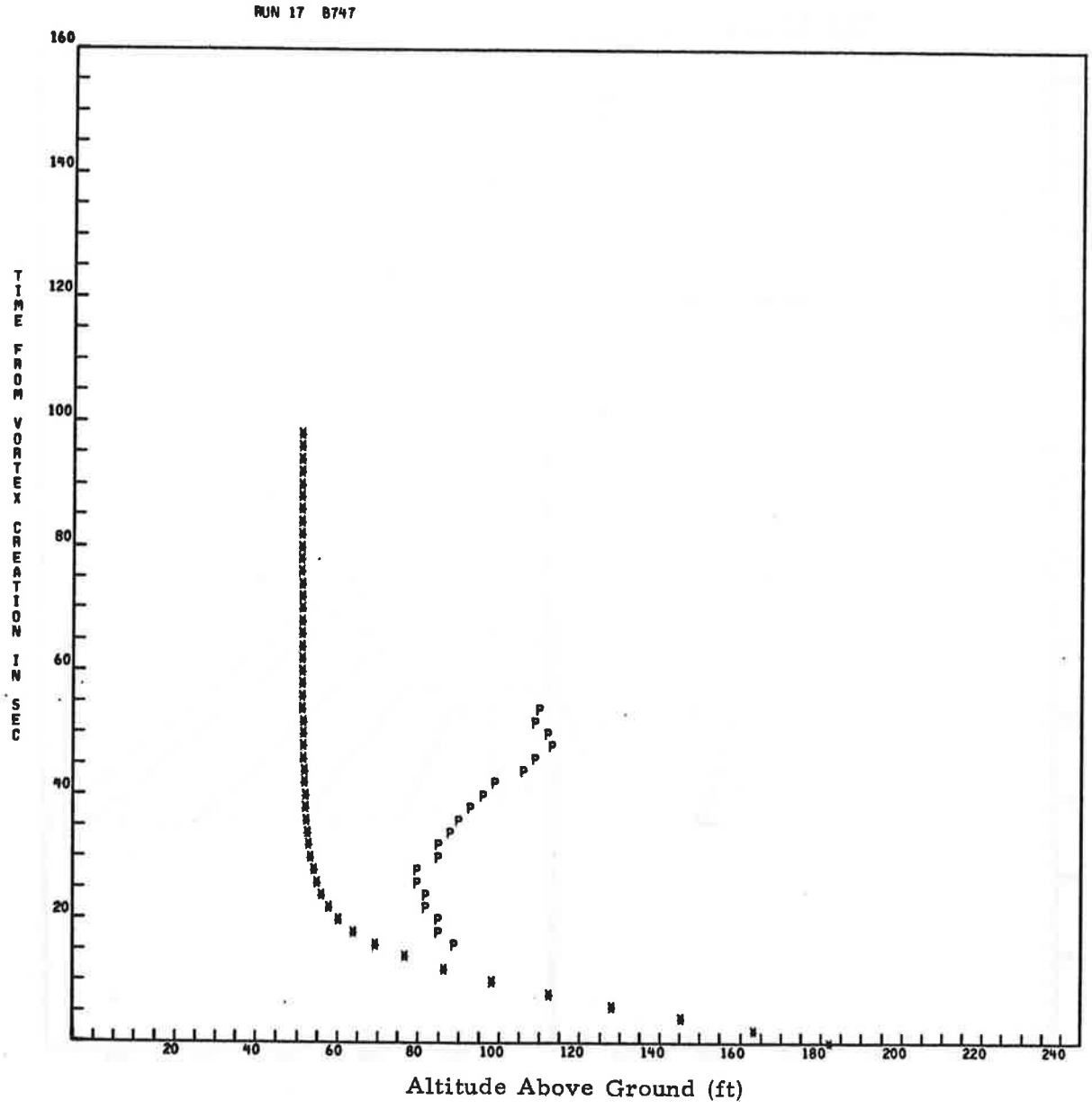
RUN 17 B747
160
140
120
100
80
60
40
20
TIME FROM VORTEX CREATION IN SEC
20
40
60
80
100
120
140
160
180
200
220
240
Altitude Above Ground (ft)

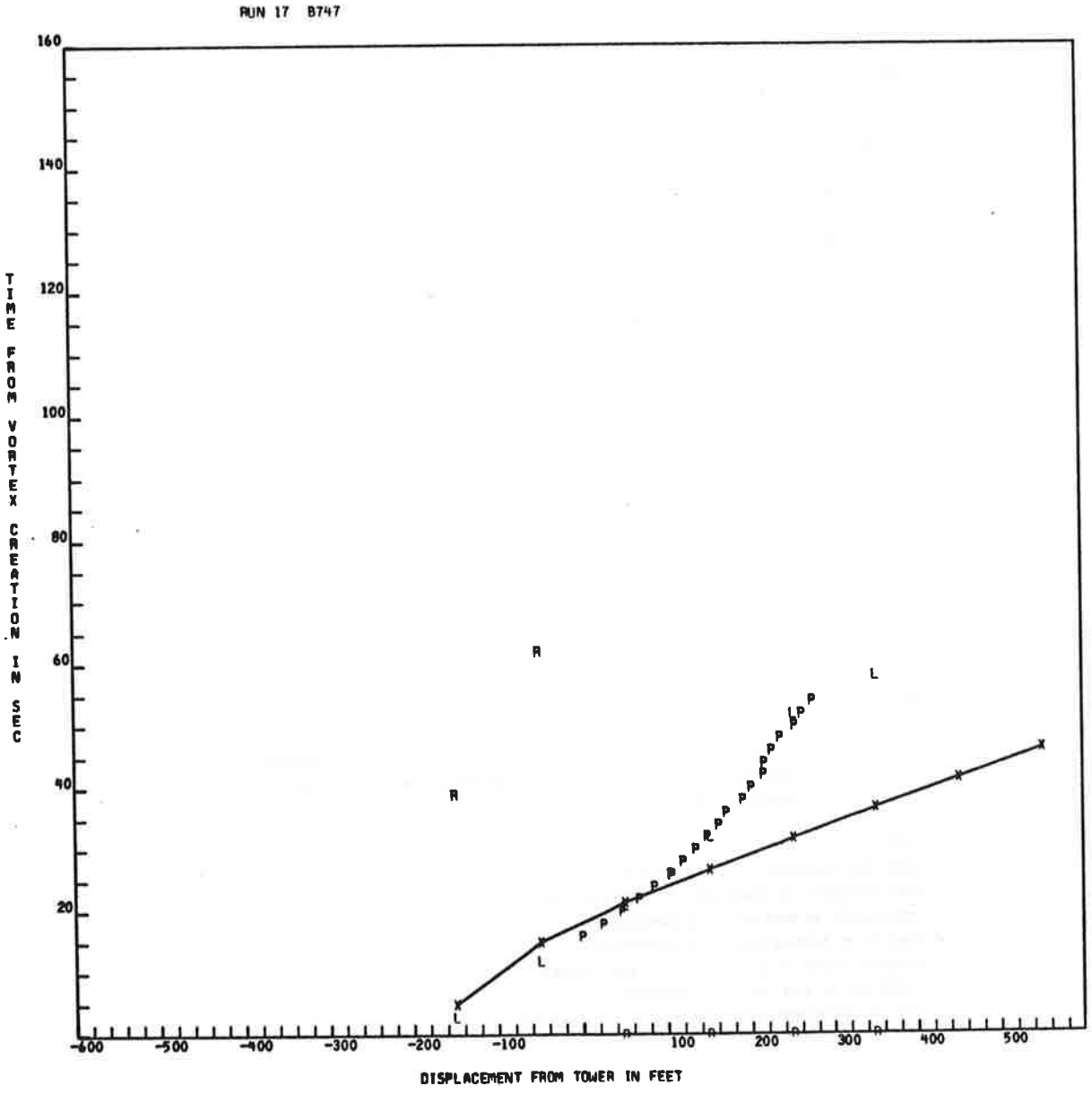
RUN 17 B747
160
140
120
100
80
60
40
20
TIME FROM VORTEX CREATION IN SEC
-600
-500
-400
-300
-200
-100
100
200
300
400
500
DISPLACEMENT FROM TOWER IN FEET
R
R
L
L
L
P

```
                                                    RUN DATA CARD
CONFIGURATION     HOLDING LEVEL FLIGHT ALL ENGINES SAME POWER
AIRCRAFT TYPE IS B747
RUN NUMBER  55
AIRCRAFT DISPLACEMENT FROM TOWER -171 FT
AIRCRAFT ALTITUDE ABREAST OF TOWER 177 FT
AIRCRAFT WEIGHT 593000. POUNDS
AIRSPEED  337.8 FT/SEC
TEMPERATURE  14 DEGREES C (NOT USED)
INITIAL WIND SPEED  13 MPH  (NOT USED)
INITIAL WIND ANGLE 220 DEGREES TRUE  (NOT USED)
FINAL WIND SPEED  10 MPH  (NOT USED)
FINAL WIND ANGLE 220 DEGREES TRUE  (NOT USED)
AIRCRAFT HEADING 132 DEGREES MAGNETIC
MONTH 10     DAY 17     HOUR  8     MINUTE 36     LOCAL TIME



$OUTPUT
SPEED   =    -.33780000E+03
WEIGHT  =     .59300000E+06
WSPAN   =     .14974400E+03

$END
$WLOG
WSPR    =     .15607715E+02
CPOWER  =     .19504493E+00
COEF    =     .22126596E+03,   .48117681E+00,  -.23942564E-02,   .15834953E+01,
              .00000000E+00,   .00000000E+00,   .00000000E+00,   .00000000E+00,
              .00000000E+00

$END
GAMMA IN FT**2/SEC =   6.42231653+03
EDDY VISCOSITY IN FT**2/SEC =   7.23777741-01
TEMPERATURE IN RANKINE =   5.20491028+02
DENSITY IN SLUGS/FT**3 =   2.32414945-03
ACOUSTIC VELOCITY IN FT/SEC =   1.11835562+03
STABILITY IN 1/SEC**2 =   0.00000000
INITIAL PARAMETER (DIMENSIONLESS) =   0.00000000
```

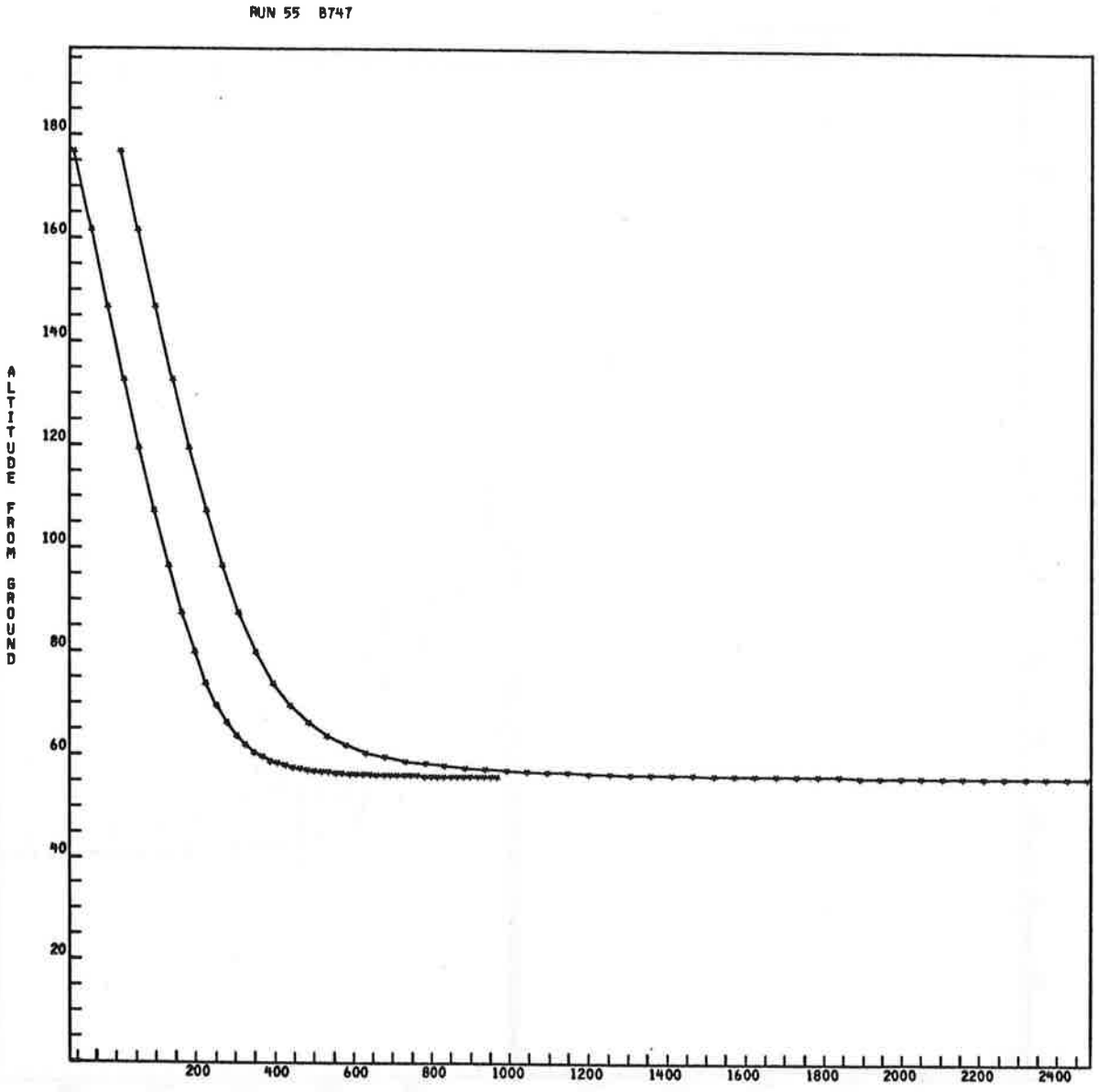
RUN 55 B747
ALTITUDE FROM GROUND
180
160
140
120
100
80
60
40
20
200
400
600
800
1000
1200
1400
1600
1800
2000
2200
2400
Distance From Runway Centerline (ft)

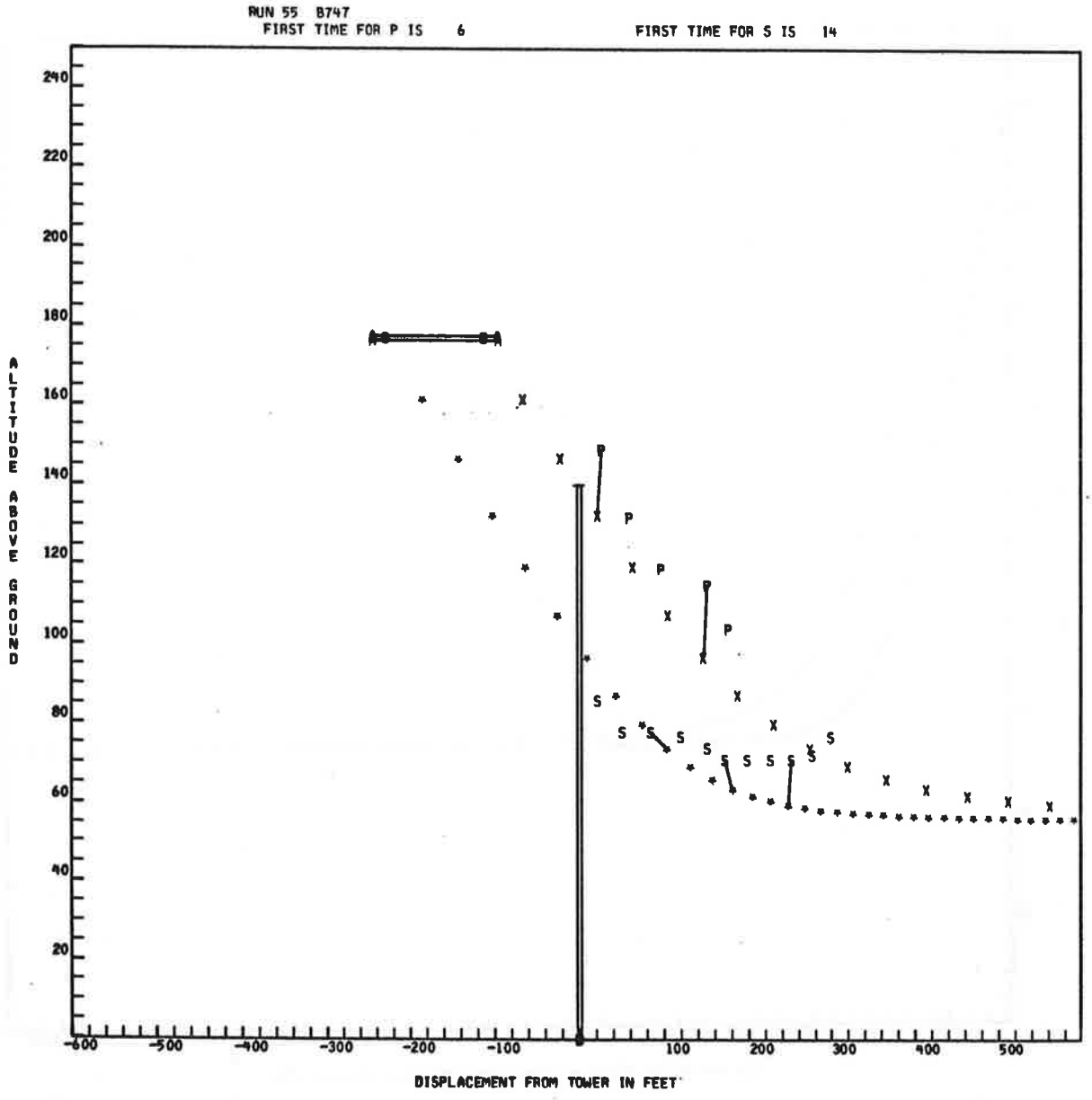
RUN 55 B747
FIRST TIME FOR P IS 6
FIRST TIME FOR S IS 14
ALTITUDE ABOVE GROUND
240
220
200
180
160
140
120
100
80
60
40
20
-600
-500
-400
-300
-200
-100
100
200
300
400
500
DISPLACEMENT FROM TOWER IN FEET

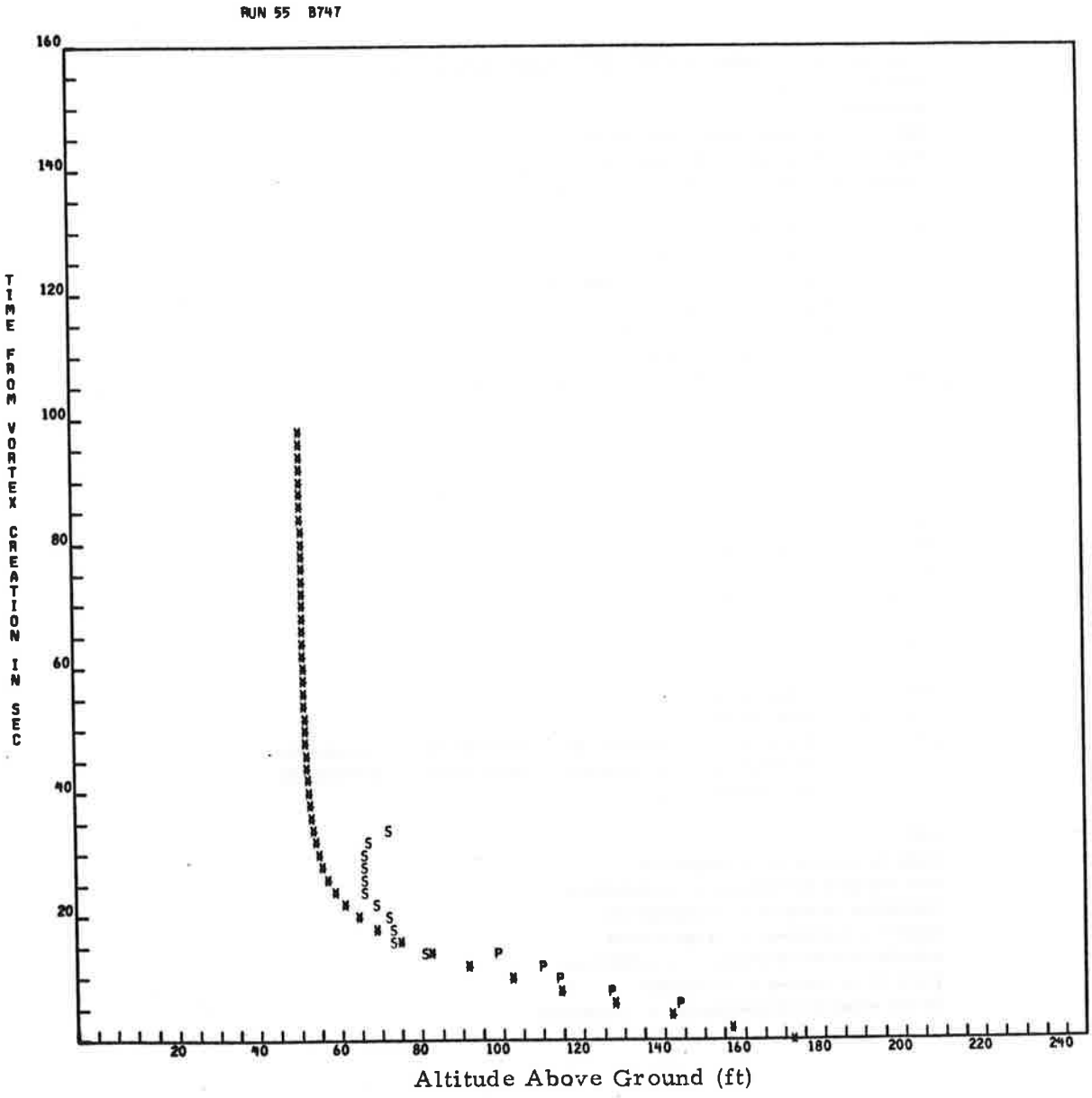
RUN 55 B747
TIME FROM VORTEX CREATION IN SEC
160
140
120
100
80
60
40
20
20
40
60
80
100
120
140
160
180
200
220
240
Altitude Above Ground (ft)

RUN DATA CARD

CONFIGURATION LANDING, OUTBOARD ENGINE TOWARD TOWER AT IDLE
AIRCRAFT TYPE IS B747
RUN NUMBER 56
AIRCRAFT DISPLACEMENT FROM TOWER -185 FT
AIRCRAFT ALTITUDE ABREAST OF TOWER 184 FT
AIRCRAFT WEIGHT 591000. POUNDS
AIRSPEED 270.2 FT/SEC
TEMPERATURE 14 DEGREES C (NOT USED)
INITIAL WIND SPEED 13 MPH (NOT USED)
INITIAL WIND ANGLE 220 DEGREES TRUE (NOT USED)
FINAL WIND SPEED 13 MPH (NOT USED)
FINAL WIND ANGLE 220 DEGREES TRUE (NOT USED)
AIRCRAFT HEADING 132 DEGREES MAGNETIC
MONTH 10 DAY 17 HOUR 8 MINUTE 40 LOCAL TIME

$OUTPUT
SPEED = -.27024000E+03
WEIGHT = .59100000E+06
WSPAN = .14974400E+03

$END
$WLOG
WSPR = .16021747E+02
CPOWER = .19094699E+00
COEF = .22209777E+03, .46868644E+00, -.23092432E-02, .18196846E+01,
.00000000E+00, .00000000E+00, .00000000E+00, .00000000E+00,
.00000000E+00

$END
GAMMA IN FT**2/SEC = 7.99530859+03
EDDY VISCOSITY IN FT**2/SEC = 8.28628853-01
TEMPERATURE IN RANKINE = 5.20002090+02
DENSITY IN SLUGS/FT**3 = 2.32575159-03
ACOUSTIC VELOCITY IN FT/SEC = 1.11783023+03
STABILITY IN 1/SEC**2 = 0.00000000
INITIAL PARAMETER (DIMENSIONLESS) = 0.00000000

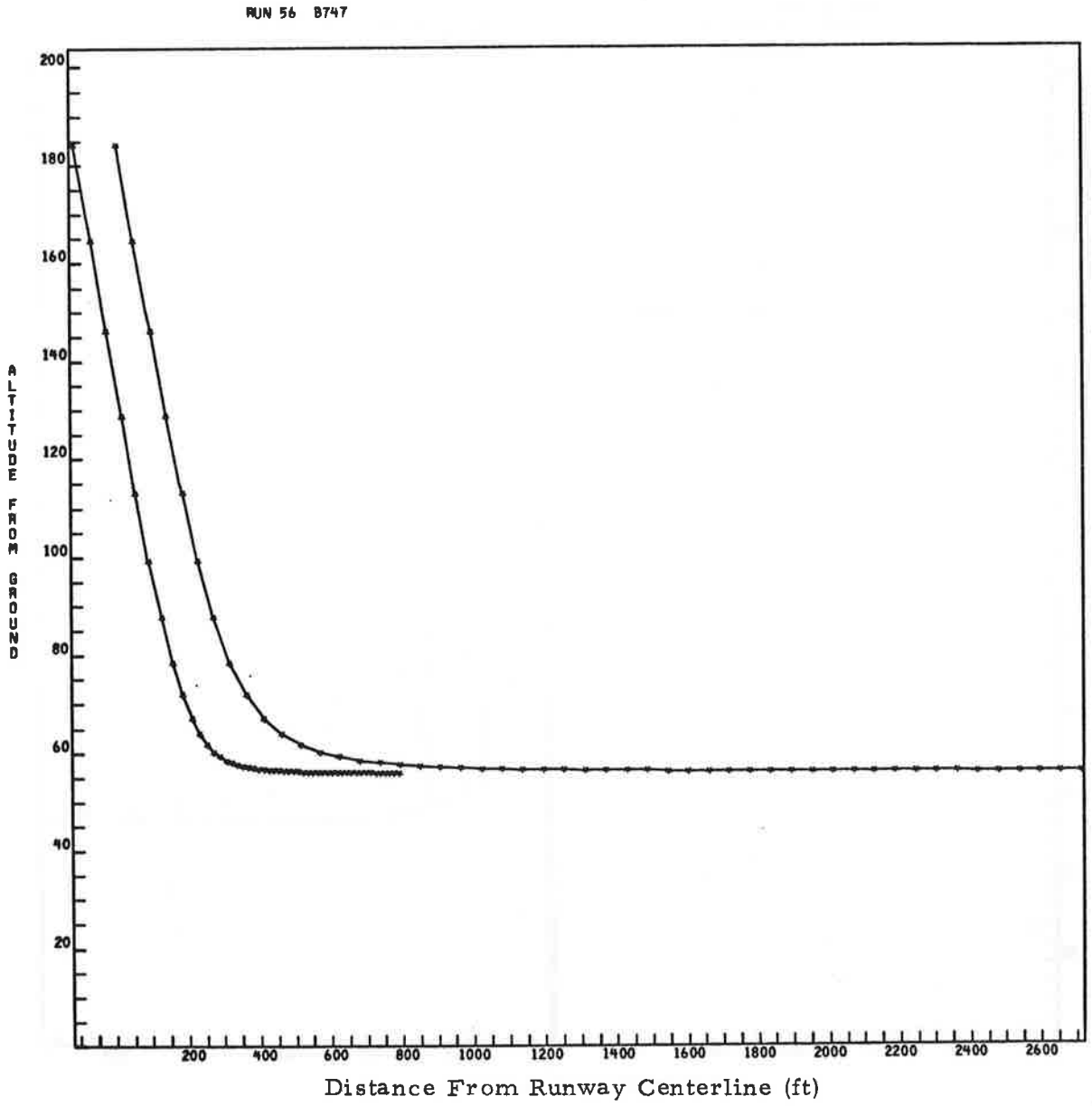
RUN 56 B747
ALTITUDE FROM GROUND
200
180
160
140
120
100
80
60
40
20
200
400
600
800
1000
1200
1400
1600
1800
2000
2200
2400
2600
Distance From Runway Centerline (ft)

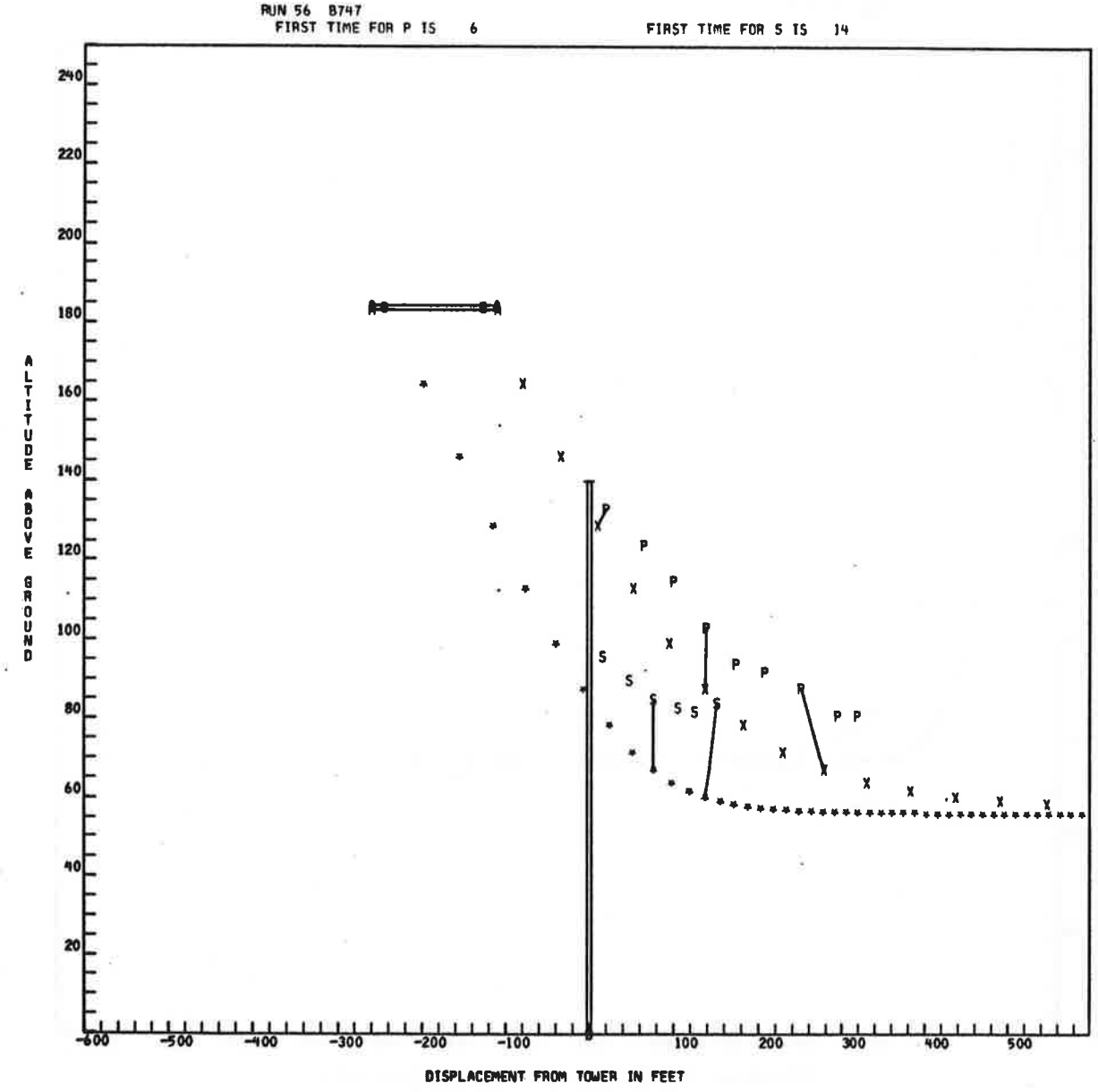
RUN 56 B747
FIRST TIME FOR P IS 6
FIRST TIME FOR S IS 14
ALTITUDE ABOVE GROUND
240
220
200
180
160
140
120
100
80
60
40
20
-600
-500
-400
-300
-200
-100
100
200
300
400
500
DISPLACEMENT FROM TOWER IN FEET

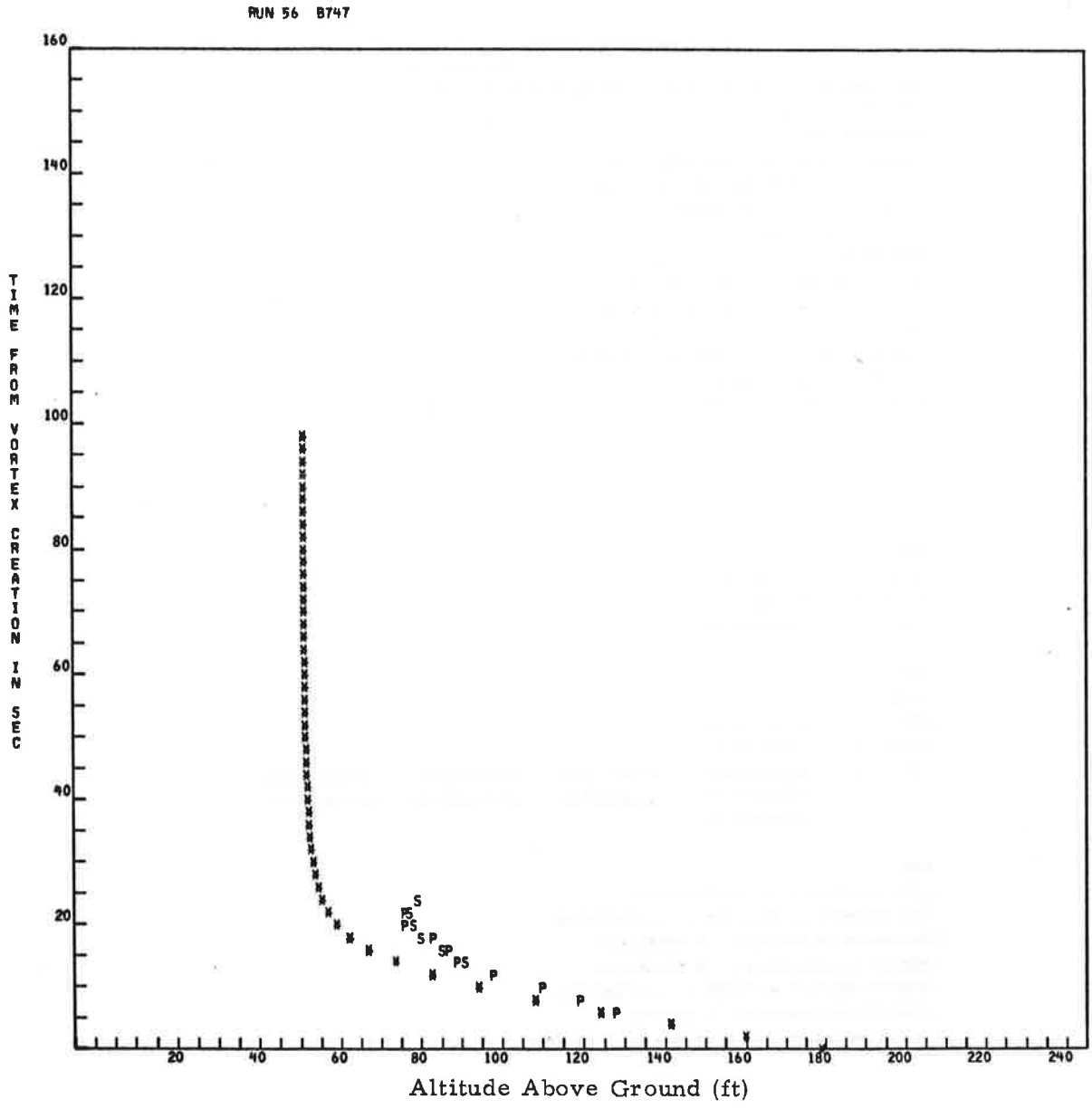
RUN 56 B747
TIME FROM VORTEX CREATION IN SEC
160
140
120
100
80
60
40
20
20
40
60
80
100
120
140
160
180
200
220
240
Altitude Above Ground (ft)

```
                                                    RUN DATA CARD
CONFIGURATION     LANDING, OUTBOARD ENGINE TOWARD TOWER AT IDLE
AIRCRAFT TYPE IS B747
RUN NUMBER  57
AIRCRAFT DISPLACEMENT FROM TOWER -170 FT
AIRCRAFT ALTITUDE ABREAST OF TOWER 170 FT
AIRCRAFT WEIGHT 589000. POUNDS
AIRSPEED  263.5 FT/SEC
TEMPERATURE  14 DEGREES C (NOT USED)
INITIAL WIND SPEED  10 MPH  (NOT USED)
INITIAL WIND ANGLE 230 DEGREES TRUE  (NOT USED)
FINAL WIND SPEED  11 MPH  (NOT USED)
FINAL WIND ANGLE 235 DEGREES TRUE  (NOT USED)
AIRCRAFT HEADING 130 DEGREES MAGNETIC
MONTH 10.    DAY 17     HOUR  8     MINUTE 45     LOCAL TIME



$OUTPUT
SPEED   =    -.26348400E+03
WEIGHT  =     .58900000E+06
WSPAN   =     .14974400E+03

$END
$WLOG
WSPR    =     .18905415E+02
CPOWER  =     .13961404E+00
COEF    =     .22656558E+03,   .30137775E+00,  -.13505396E-02,   .10731229E+01,
              .00000000E+00,   .00000000E+00,   .00000000E+00,   .00000000E+00,
              .00000000E+00

$END
GAMMA IN FT**2/SEC =   8.16841791+03
EDDY VISCOSITY IN FT**2/SEC =   8.39543842-01
TEMPERATURE IN RANKINE =   5.19999641+02
DENSITY IN SLUGS/FT**3 =   2.32693262-03
ACOUSTIC VELOCITY IN FT/SEC =   1.11782759+03
STABILITY IN 1/SEC**2 =   0.00000000
INITIAL PARAMETER (DIMENSIONLESS) =   0.00000000
```

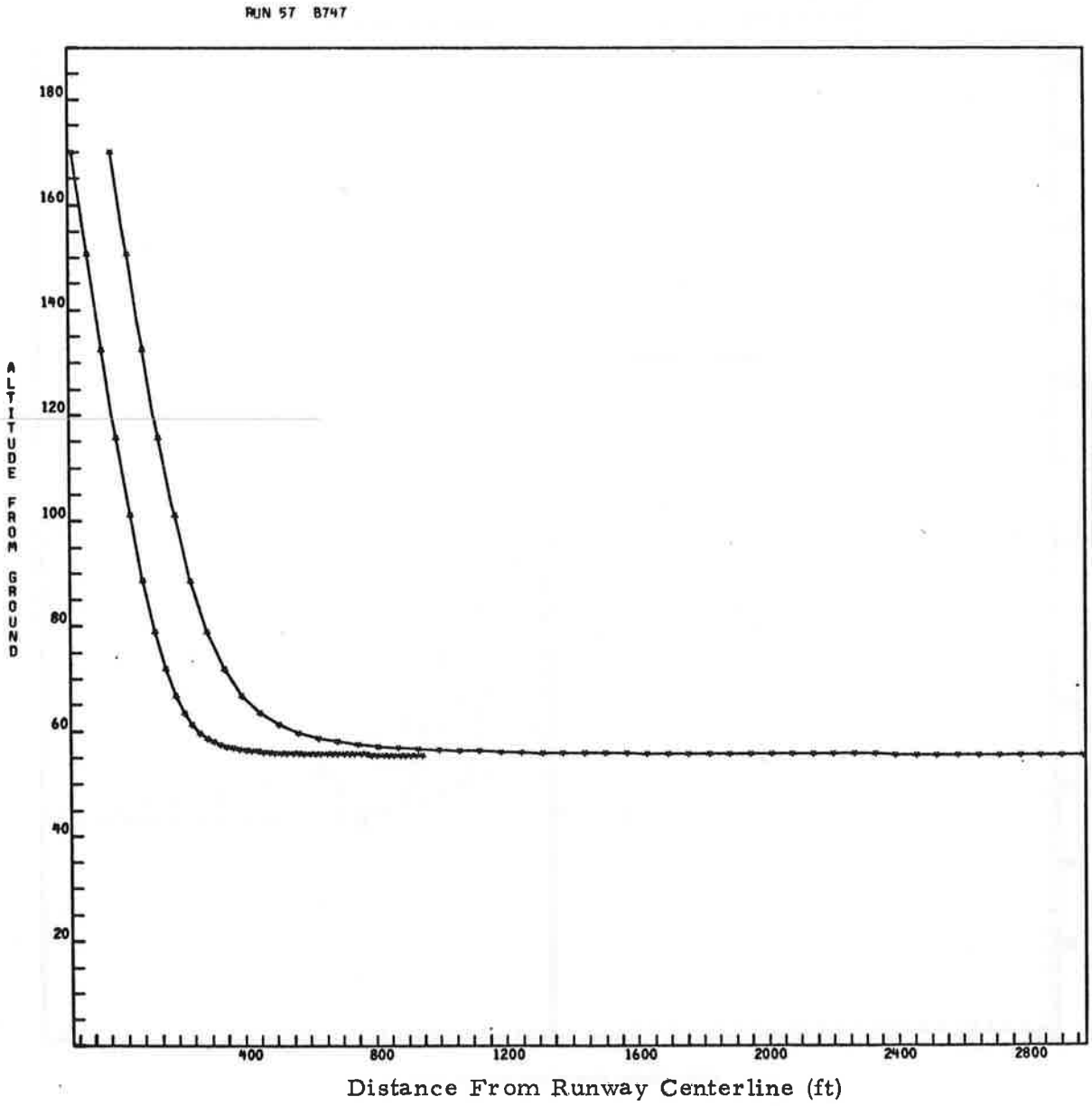
RUN 57 B747
ALTITUDE FROM GROUND
180
160
140
120
100
80
60
40
20
400
800
1200
1600
2000
2400
2800
Distance From Runway Centerline (ft)

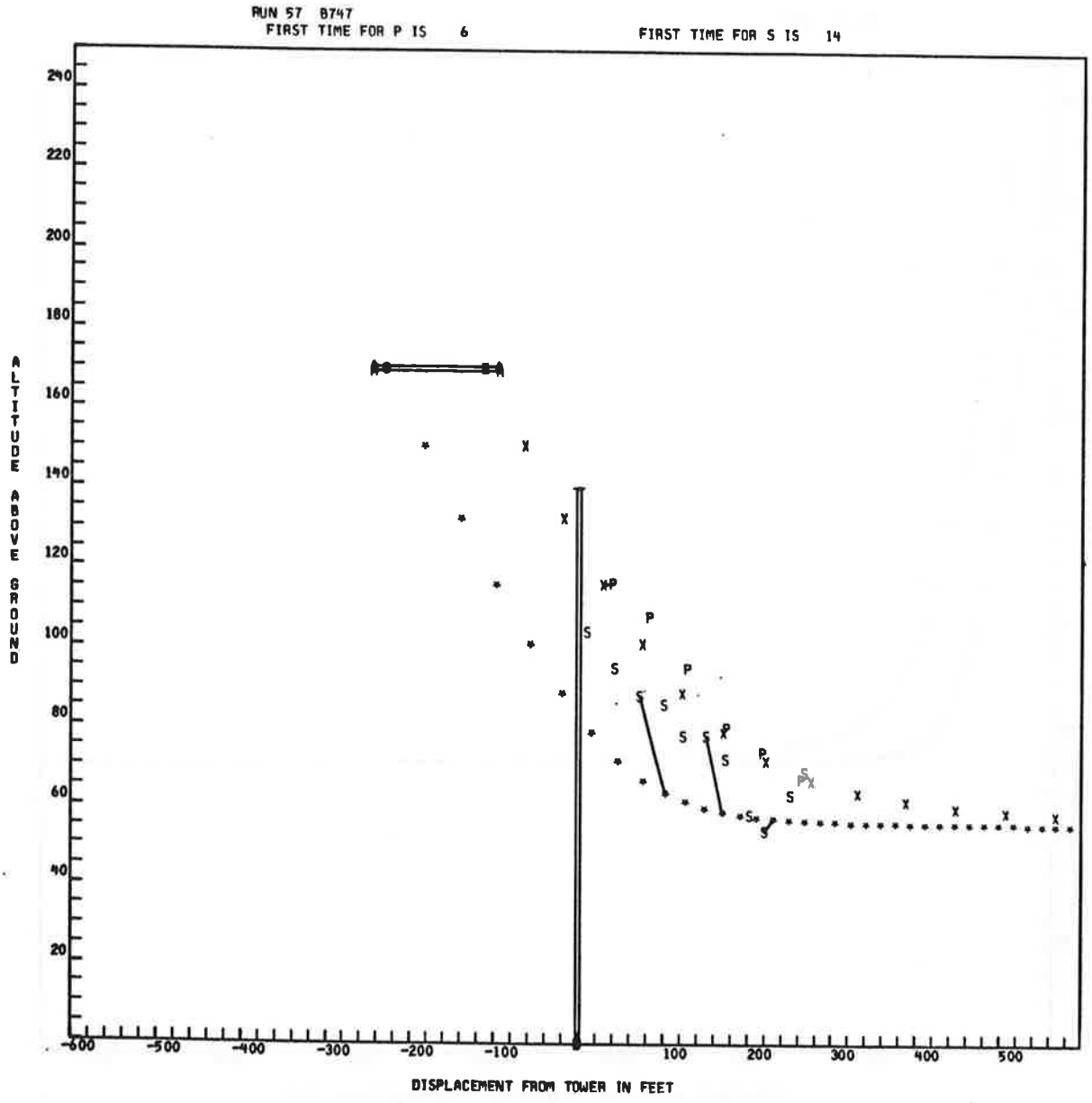
RUN 57 8747
FIRST TIME FOR P IS 6
FIRST TIME FOR S IS 14
ALTITUDE ABOVE GROUND
240
220
200
180
160
140
120
100
80
60
40
20
-600
-500
-400
-300
-200
-100
100
200
300
400
500
DISPLACEMENT FROM TOWER IN FEET

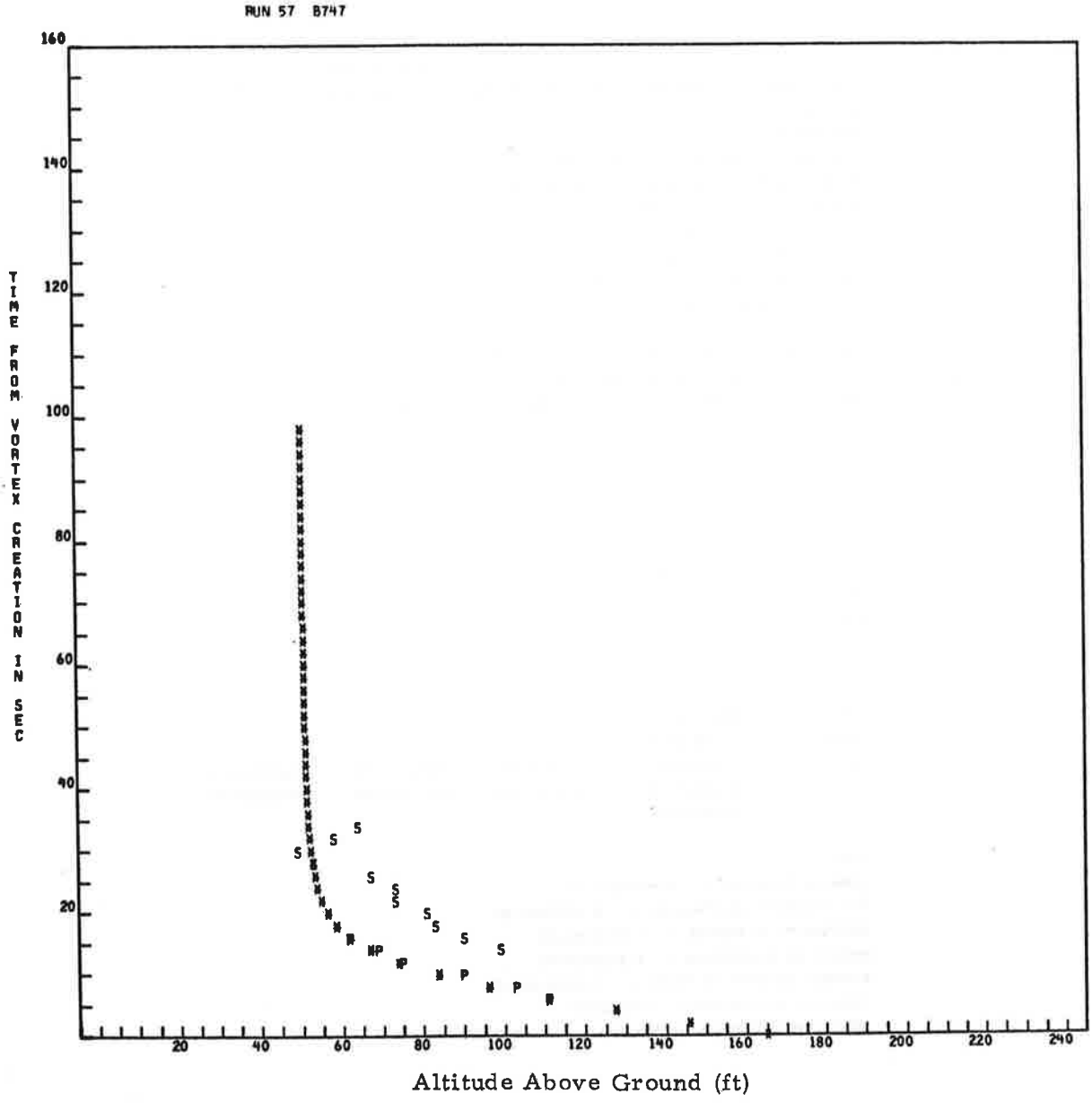
RUN 57 B747
TIME FROM VORTEX CREATION IN SEC
160
140
120
100
80
60
40
20
20
40
60
80
100
120
140
160
180
200
220
240
Altitude Above Ground (ft)

```
                                                    RUN DATA CARD
CONFIGURATION     LANDING, OUTBOARD ENGINE AWAY FROM TOWER AT IDLE
AIRCRAFT TYPE IS B747
RUN NUMBER  59
AIRCRAFT DISPLACEMENT FROM TOWER -215 FT
AIRCRAFT ALTITUDE ABREAST OF TOWER 166 FT
AIRCRAFT WEIGHT 585000. POUNDS
AIRSPEED  270.2 FT/SEC
TEMPERATURE  15 DEGREES C (NOT USED)
INITIAL WIND SPEED  15 MPH  (NOT USED)
INITIAL WIND ANGLE 240 DEGREES TRUE  (NOT USED)
FINAL WIND SPEED  13 MPH  (NOT USED)
FINAL WIND ANGLE 240 DEGREES TRUE  (NOT USED)
AIRCRAFT HEADING 128 DEGREES MAGNETIC
MONTH 10     DAY 17     HOUR  8     MINUTE 56     LOCAL TIME



$OUTPUT
SPEED   =     -.27024000E+03
WEIGHT  =      .58500000E+06
WSPAN   =      .14974400E+03

$END
$WLOG
WSPR    =      .19889850E+02
CPOWER  =      .12073464E+00
COEF    =      .25751830E+03,   .19390340E+00,  -.79025289E-03,   .27330451E+01,
               .00000000E+00,   .00000000E+00,   .00000000E+00,   .00000000E+00,
               .00000000E+00

$END
GAMMA IN FT**2/SEC =   7.94543213+03
EDDY VISCOSITY IN FT**2/SEC =   8.27784039-01
TEMPERATURE IN RANKINE =   5.22406166+02
DENSITY IN SLUGS/FT**3 =   2.31659127-03
ACOUSTIC VELOCITY IN FT/SEC =   1.12041122+03
STABILITY IN 1/SEC**2 =   0.00000000
INITIAL PARAMETER (DIMENSIONLESS) =   0.00000000
```

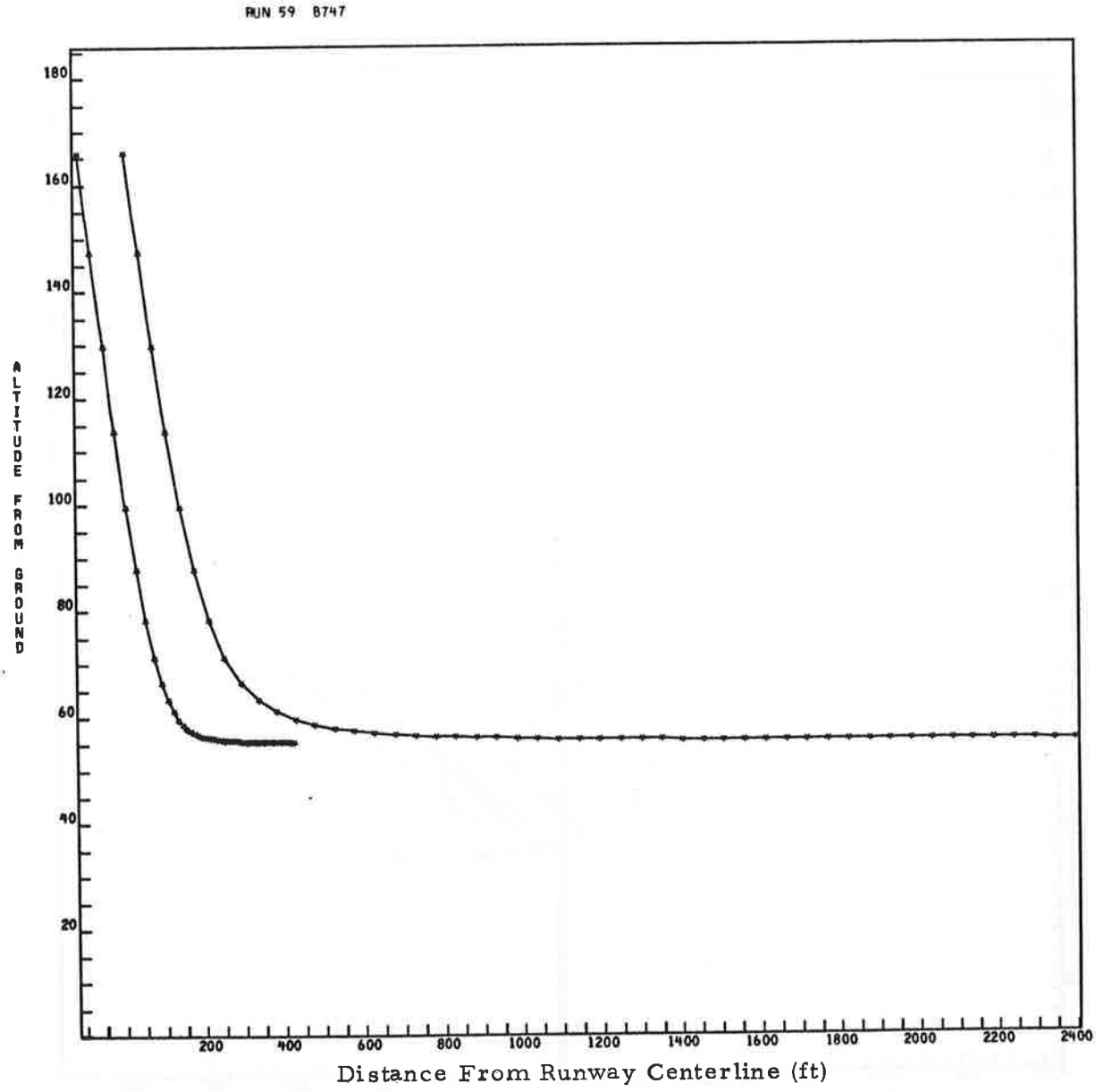
RUN 59 8747
ALTITUDE FROM GROUND
180
160
140
120
100
80
60
40
20
200
400
600
800
1000
1200
1400
1600
1800
2000
2200
2400
Distance From Runway Centerline (ft)

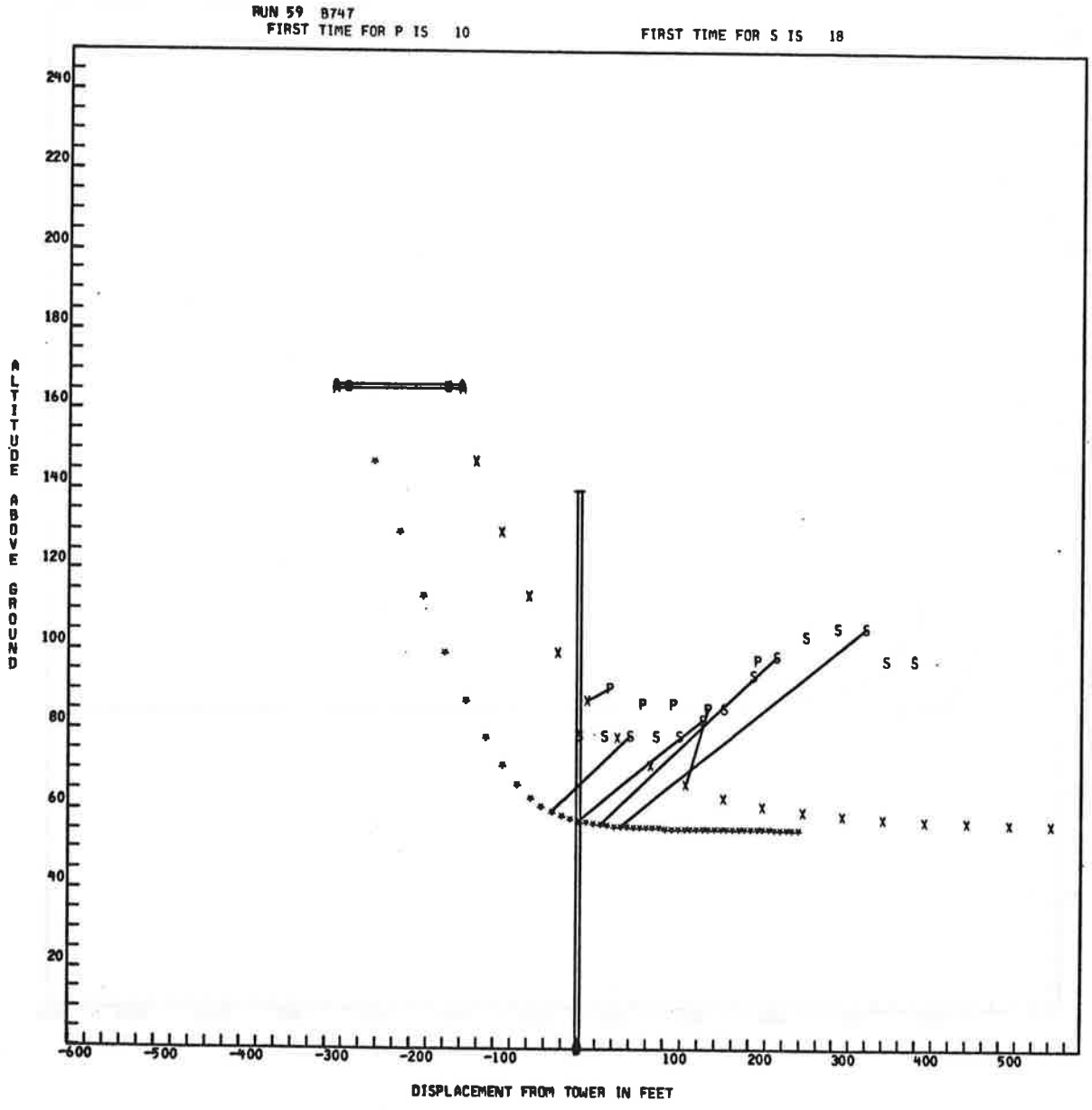
RUN 59 B747
FIRST TIME FOR P IS 10
FIRST TIME FOR S IS 18
ALTITUDE ABOVE GROUND
240
220
200
180
160
140
120
100
80
60
40
20
-600
-500
-400
-300
-200
-100
100
200
300
400
500
DISPLACEMENT FROM TOWER IN FEET

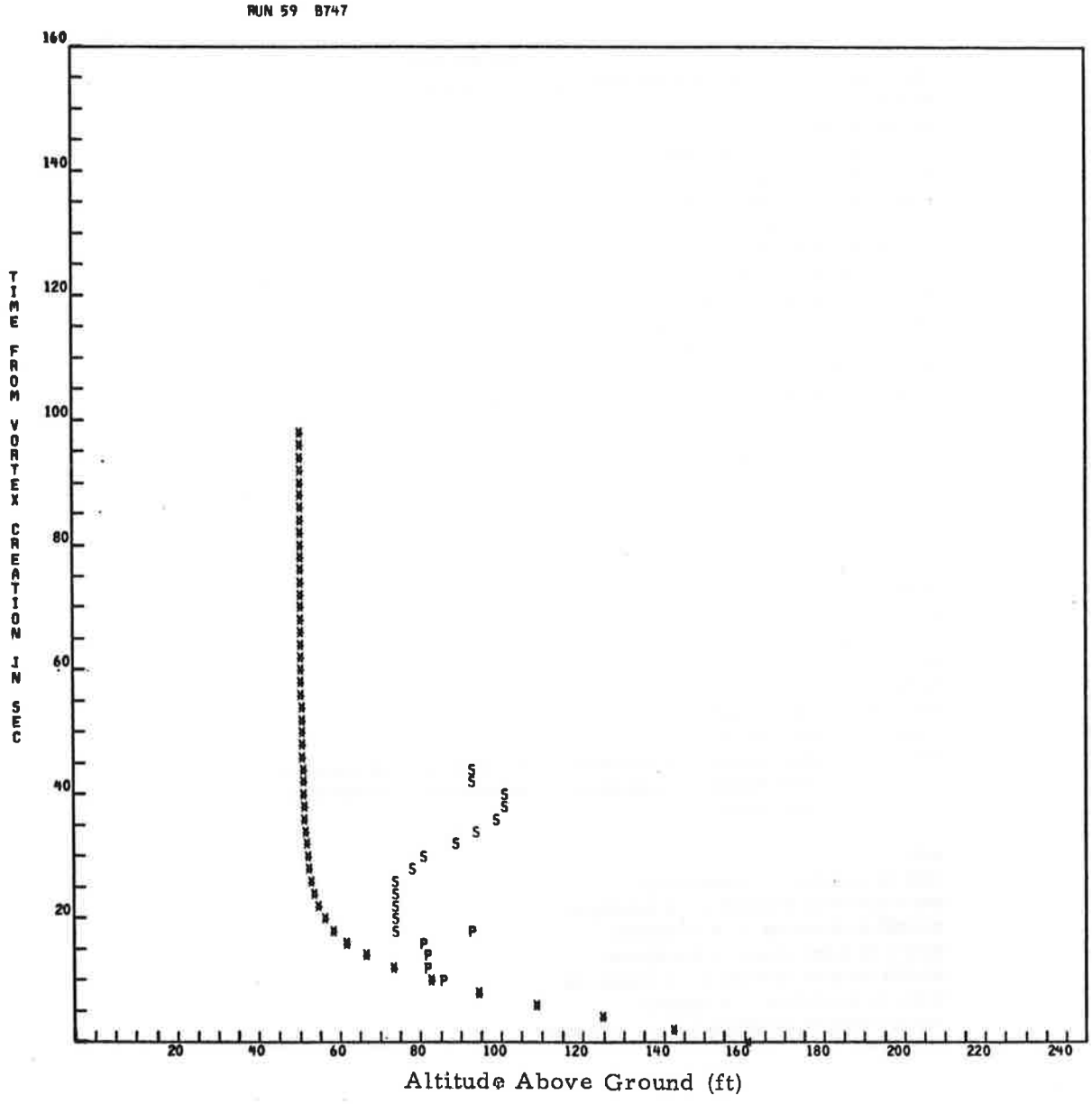
RUN 59 B747
TIME FROM VORTEX CREATION IN SEC
160
140
120
100
80
60
40
20
20
40
60
80
100
120
140
160
180
200
220
240
Altitude Above Ground (ft)

```
                                                    RUN DATA CARD
CONFIGURATION     LANDING, OUTBOARD ENGINE AWAY FROM TOWER AT IDLE
AIRCRAFT TYPE IS B747
RUN NUMBER  60
AIRCRAFT DISPLACEMENT FROM TOWER -207 FT
AIRCRAFT ALTITUDE ABREAST OF TOWER 158 FT
AIRCRAFT WEIGHT 581000. POUNDS
AIRSPEED  270.2 FT/SEC
TEMPERATURE  15 DEGREES C (NOT USED)
INITIAL WIND SPEED   0 MPH  (NOT USED)
INITIAL WIND ANGLE   0 DEGREES TRUE  (NOT USED)
FINAL WIND SPEED   8 MPH  (NOT USED)
FINAL WIND ANGLE 260 DEGREES TRUE  (NOT USED)
AIRCRAFT HEADING 128 DEGREES MAGNETIC
MONTH 10     DAY 17     HOUR  9     MINUTE  1     LOCAL TIME



$OUTPUT
SPEED   =    -.27024000E+03
WEIGHT  =     .58100000E+06
WSPAN   =     .14974400E+03

$END
$WLOG
WSPR    =     .21082094E+02
CPOWER  =     .12186378E+00
COEF    =     .25818710E+03,   .24415519E+00,  -.11243473E-02,   .21300692E+01,
              .00000000E+00,   .00000000E+00,   .00000000E+00,   .00000000E+00,
              .00000000E+00

$END
GAMMA IN FT**2/SEC =   7.89080664+03
EDDY VISCOSITY IN FT**2/SEC =   8.24299976-01
TEMPERATURE IN RANKINE =   5.22536919+02
DENSITY IN SLUGS/FT**3 =   2.31667870-03
ACOUSTIC VELOCITY IN FT/SEC =   1.12055144+03
STABILITY IN 1/SEC**2 =   0.00000000
INITIAL PARAMETER (DIMENSIONLESS) =   0.00000000
```

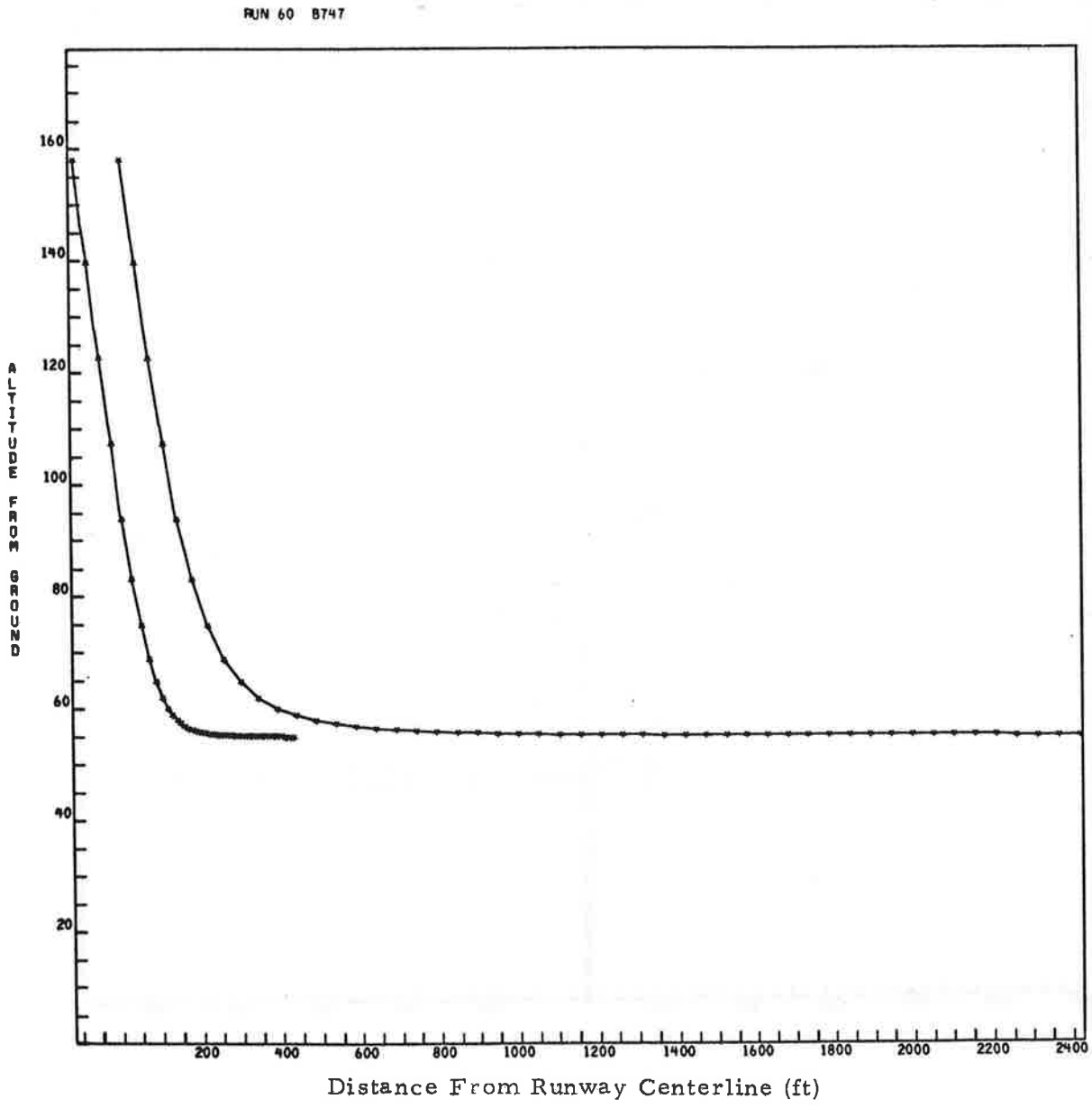
RUN 60 B747
ALTITUDE FROM GROUND
160
140
120
100
80
60
40
20
200
400
600
800
1000
1200
1400
1600
1800
2000
2200
2400
Distance From Runway Centerline (ft)

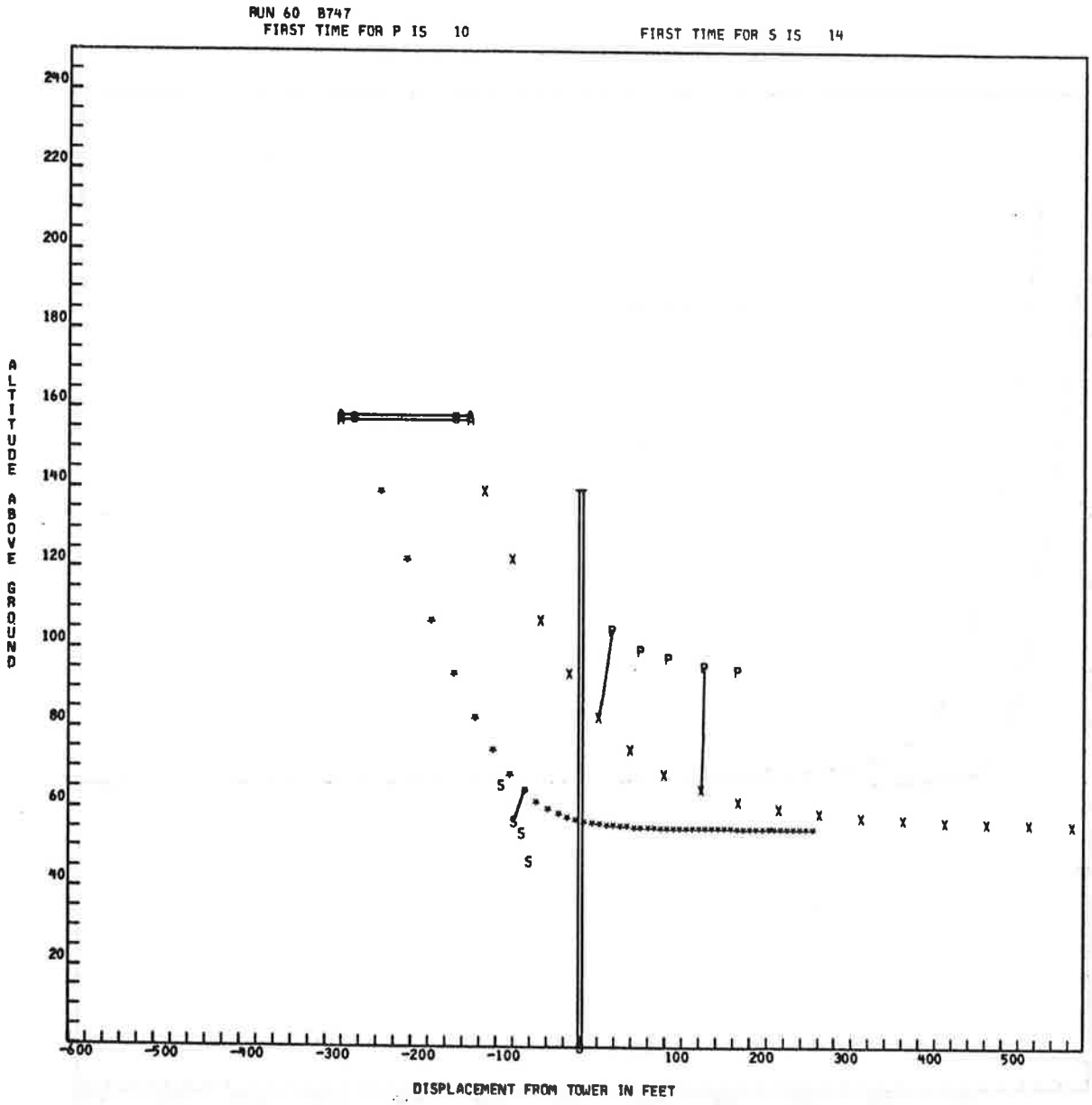
RUN 60 B747
FIRST TIME FOR P IS 10
FIRST TIME FOR S IS 14
ALTITUDE ABOVE GROUND
240
220
200
180
160
140
120
100
80
60
40
20
-600
-500
-400
-300
-200
-100
100
200
300
400
500
DISPLACEMENT FROM TOWER IN FEET

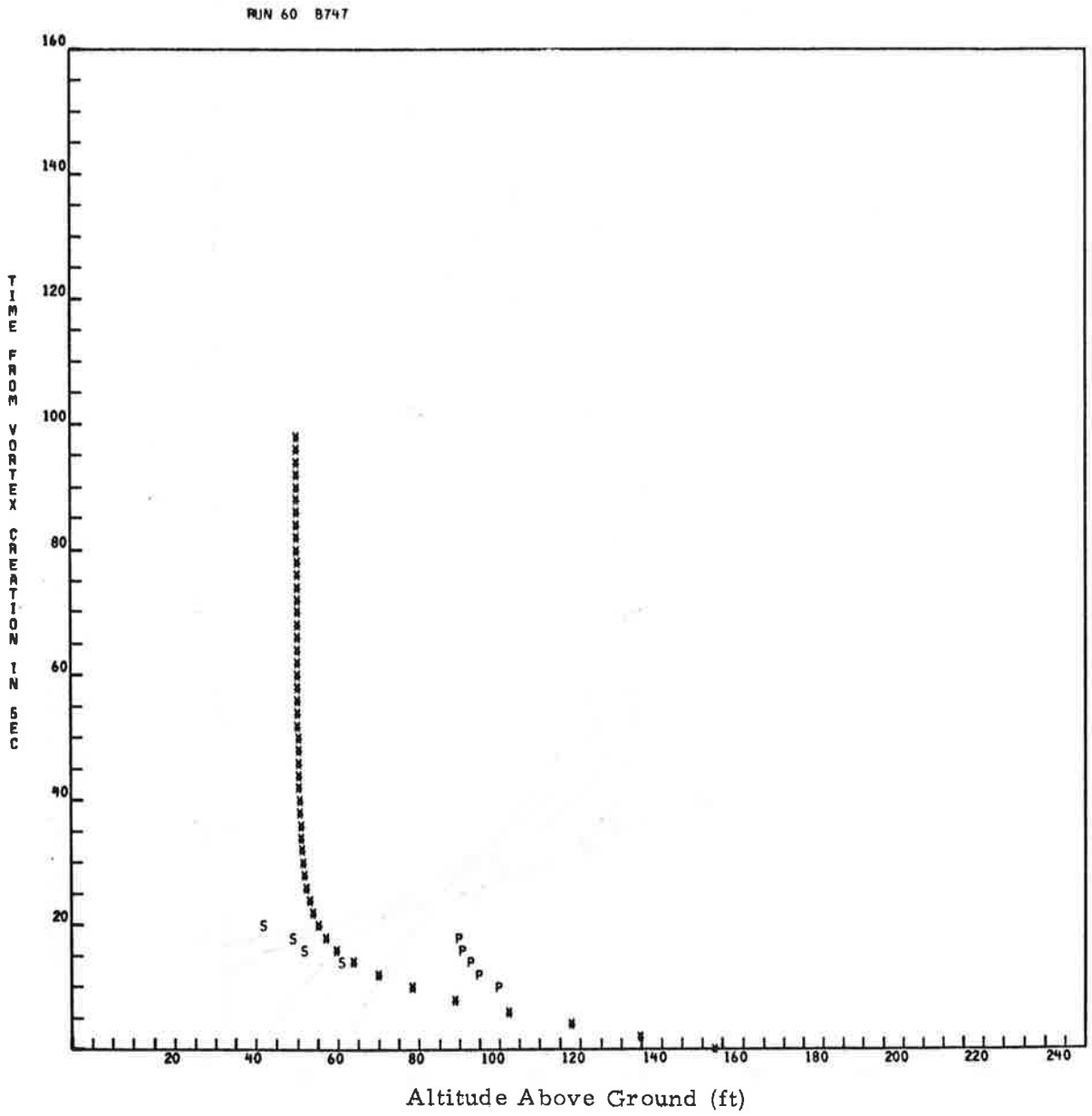
RUN 60 B747
TIME FROM VORTEX CREATION IN SEC
160
140
120
100
80
60
40
20
20
40
60
80
100
120
140
160
180
200
220
240
Altitude Above Ground (ft)

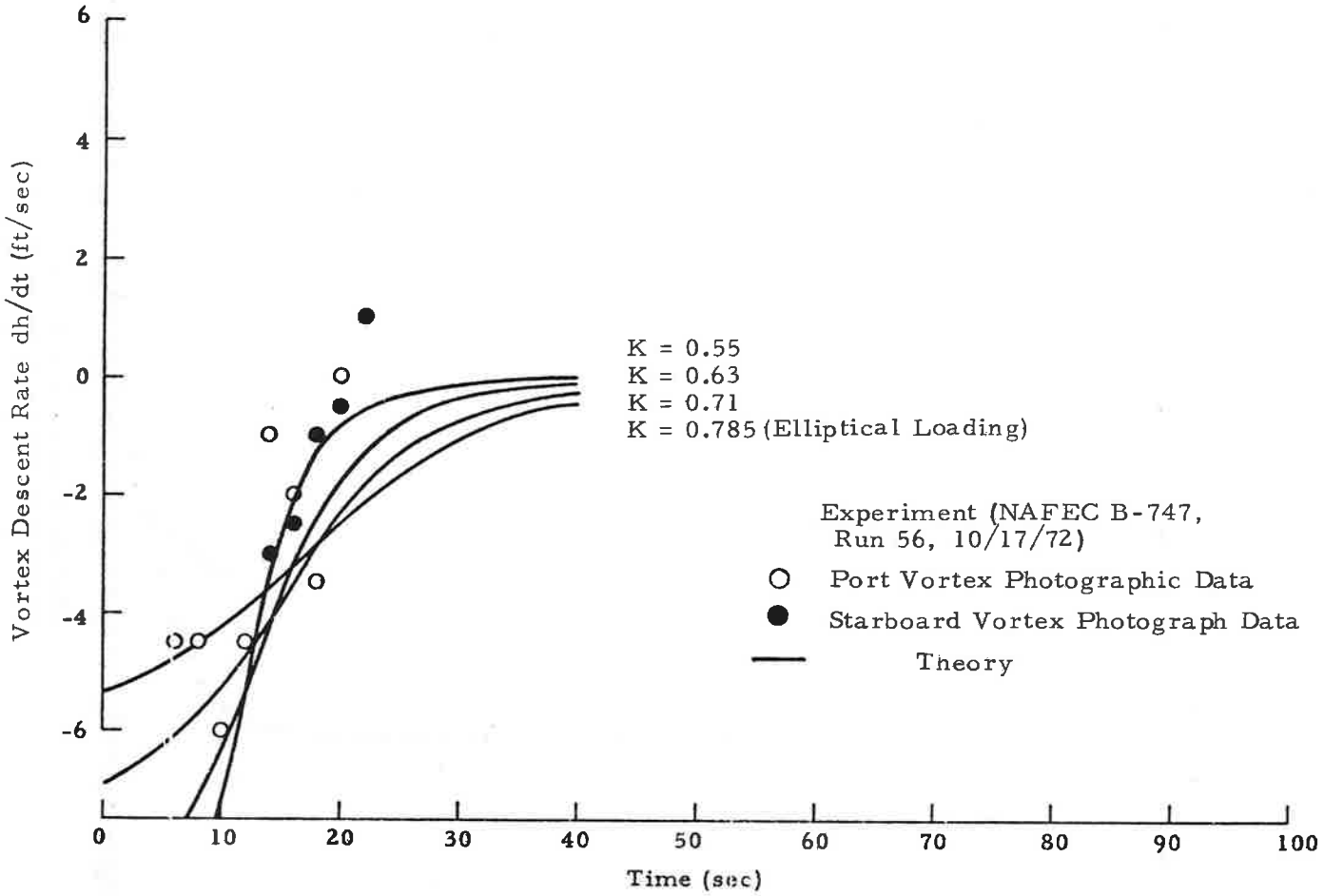

Comparison of Measured and Predicted Vortex Sink Rate as a Function of Time for a B-747 in Landing Configuration

APPENDIX C – INFLUENCE OF BUOYANCY ON VORTEX MOTION

The influence of buoyancy on vortex wake transport can be illustrated on the basis of elementary momentum conservation principles. For a vortex pair of circulation, Γ, and separation, b', in a fluid of density, ρ_o, the momentum per unit length is

$$M = \rho_o \Gamma b' \tag{C.1}$$

In order to cancel the downward momentum of the vortex pair, an opposing force, F, must be applied so that

$$\int F \, dt = M \tag{C.2}$$

The opposing force can be an upward buoyancy force per unit length, $F = \Delta\rho g A$, where $\Delta\rho$ is the buoyancy deficit of the vortex of cross-sectional area A. Assuming a constant buoyancy force and circulation for the vortex pair, that is, $\Delta\rho$, A, and Γ are independent of time, then the characteristic time required for the buoyancy force to cancel the downward momentum of the vortex becomes

$$t = \frac{\rho_o \Gamma b'}{\Delta\rho g A} \tag{C.3}$$

The density ratio above can be further reduced from the definition $\Delta\rho = \rho_o - \rho$ and $\lambda = 1 - \rho/\rho_o$ with the result that

$$t = \frac{\Gamma b'}{g A \lambda} \tag{C.4}$$

where C_P is the heat capacity of air at constant pressure. The parameter $\dot{M}$ is the mass of air which is enclosed by the vortex per second which is defined as

$$\dot{M} = \rho A U_\infty \tag{D.6}$$

where ρ, A, and U_∞ are the air density, vortex cross-sectional area, and aircraft flight speed, respectively. Substituting Eqs. (D.4) and (D.6) into (D.5), the temperature rise of the vortex is given by

$$\Delta T = \frac{qW\,(TSFC)}{3600\,g\,\tau\rho A U_\infty C_P} \tag{D.7}$$

If the aircraft weight is expressed in terms of lift parameters, $W = L = 1/2\rho U_\infty^2 C_L \bar{c} b$, the temperature rise due to engine exhaust ingestion can be summarized in terms of the primary aircraft parameters as follows:

$$\Delta T = \frac{b\bar{c}\,(TSFC)q U_\infty C_L}{7200\,\tau A C_P g} \tag{D.8}$$

APPENDIX E – REPORT OF INVENTIONS

Under this contract an improved analytic model has been formulated for predicting wake vortex transport in the terminal area environment. While the objectives of the contract have been successfully fulfilled, no innovation, discovery, or invention was made.

REFERENCES

1. Gupta, V. A., "Vortex Related Accidents over the Ten-Year Period 1964-1973," FAA EM-75-6, April 1975.

2. Air Force Inspection and Safety Center (AFISC), 1975, "Accidents/Incidents 1965 – 12 February 1975 When Winds, Turbulence, Prop/Jet Wake was a Factor During Takeoff, Landing, or Go-Around."

3. Wilson, D. J., M. R. Brashears, E. A. Carter, and K. R. Shrider, "Wake Vortex Avoidance System," Lockheed Missiles & Space Co., Inc., Report FAA-RD-72-108 (also LMSC-HREC D306226), December 1972.

4. Brashears, M. R., and J. N. Hallock, "Aircraft Wake Vortex Transport Model," AIAA Paper 73-679, AIAA 6th Fluid and Plasma Dynamics Conference, Palm Springs, Calif., July 1973.

5. Brashears, M. R., and J. N. Hallock, "Aircraft Wake Vortex Transport Model," J. Aircraft, Vol. 11, 1974, p. 265.

6. Brashears, M. R., J. N. Hallock and N. A. Logan, "Analysis of Predicted Aircraft Wake Vortex Transport and Comparison with Experiment," AIAA Paper 74-506, AIAA 7th Fluid and Plasma Dynamics Conference, Palo Alto, Calif., 1974.

7. Brashears, M. R., S. J. Robertson, B. C. Johnson, C. Fan, and K. R. Shrider, "Wake Vortex Transport Considerations and Meteorological Data Analysis," LMSC-HREC TR D390424, Lockheed Missiles & Space Company, Huntsville, Ala., November 1974.

8. Brashears, M. R., and J. N. Hallock, "A Predictive Model of Wake Vortex Transport," Proceedings of AMS/AIAA Sixth Conference on Aerospace and Aeronautical Meteorology, El Paso, Texas, November 1974.

9. Brashears, M. R., N. A. Logan, S. J. Robertson, K. R. Shrider and C. D. Walters, "Analysis of Predicted Aircraft Wake Vortex Transport and Comparison with Experiment," Report No. FAA-RD-74-74, Vols. I and II, April 1974.

10. Lanchester, F. W., Aerodynamics, 2nd Ed., London, Constable & Company, Ltd., 1909, p. 178.

11. Durand, W. F., editor, Aerodynamic Theory, Vol. II, Div. E, Dover Publications, New York, 1934, pp. 328-330.

12. Ibid., Vol. IV, Div. J, pp. 72-84.

13. Spreiter, J. R., and A. H. Sacks, "The Rolling Up of the Trailing Vortex Sheet and Its Effect on the Downwash Behind Wings, J. Aero. Sci., Vol. 18, No. 1, January 1951, pp. 21-72.

14. Westwater, F. L., "Rolling Up of the Surface of Discontinuity Behind an Aerofoil of Finite Span," A.R.C. R&M 1962, 1935.

15. Takami, H., "A Numerical Experiment with Discrete Vortex Approximation with Reference to the Rolling Up of a Vortex Sheet," Stanford University Department of Aeronautics and Astronautics Report No. 202, 1964.

16. Hackett, J. E., and M. R. Evans, "Vortex Wakes Behind High Lift Wings," J. Aircraft, Vol. 8, No. 5, May 1975, pp. 334-340.

17. Chorin, A. J., and P. S. Bernard, "Discretization of a Vortex Sheet with an Example of Roll-Up," J. Comp. Phys., 13, 1973, pp. 423-429.

18. Moore, D. W., "A Numerical Study of the Roll-Up of a Finite Vortex Sheet," J. Fluid Mech., Vol. 63, No. 2, August 1974, pp. 225-235.

19. Bloom, A. M., and H. Jen, "Roll-Up of Aircraft Trailing Vortices Using Artificial Viscosity, J. Aircraft, Vol. 11, No. 11, November 1974, pp. 714-716.

20. Betz, A., "Behavior of Vortex Systems," NACA TM 713 (trans. from ZAMM, Vol. XII,3, 1932.

21. Howard, L. N., "Divergence Formulas Involving Vorticity," Arch. Rational Mech. Anal., Vol. 1, No. 1, May 1957, pp. 113-123.

22. Donaldson, C. duP., R. S. Snedeker and R. D. Sullivan, "A Method of Calculating Aircraft Wake Velocity Profiles and Comparison with Full-Scale Experimental Measurements," J. Aircraft, Vol. 11, No. 9, September 1974, pp. 547-555.

23. Rossow, V., "On the Inviscid Rolled-Up Structure of Lift-Generated Vortices," J. Aircraft, Vol. 10, No. 11, November 1973, pp. 647-650.

24. Jordan, P., "Structure of Betz Vortex Cores," J. Aircraft, Vol. 10, No. 11, November 1973, pp. 691-693.

25. Yates, J. E., "Calculation of Initial Vortex Roll-Up in Aircraft Wakes," J. Aircraft, Vol. 11, No. 7, July 1974, pp. 397-400.

26. Brown, C. E., "Aerodynamics of Wake Vortices," AIAA J., No. 11, No. 4, April 1973, pp. 531-536.

27. Rossow, V. J., "Theoretical Study of Lift-Generated Vortex Sheets Designed to Avoid Roll-Up," NASA TM X-62, 304, September 1973.

28. Bilanin, A. J., C. duP. Donaldson, and R. S. Snedeker, "An Analytic and Experimental Investigation of the Wakes Behind Flapped and Unflapped Wings., AFFDL-TR-74-90, Wright-Patterson AFB, Ohio, May 1974.

29. Snedeker, A. J., and A. J. Bilanin, "Analysis of the Vortex Wakes of the B-727, L-1011, DC-10 and B-747 Aircraft," ARAP Report No. 245, July 1975.

30. Donaldson, C. duP., and A. J. Bilanin, "Vortex Wakes of Conventional Aircraft," AGARDograph 204, May 1975.

31. Costen, R. C., "Drift of Buoyant Wing Tip Vortices," J. Aircraft, Vol. 9, No. 6, June 1972, pp. 406-412.

32. Lissaman, P. B. S., S. C. Crow, P. B. MacCready, Jr., I. H. Tombach, and E. R. Bate, Jr., "Aircraft Vortex Wake Descent and Decay Under Real Atmospheric Effects," FAA-RD-73-120, 1973.

33. Hallock, J. N., "Wake Vortex Decay near the Ground," AIAA Paper 75-882, June 1975.

34. Lezius, D. K., "Water Tank Study of the Decay of Trailing Vortices," AIAA J., Vol. 12, No. 8, August 1974, pp. 1065-1071.

35. Baldwin, B. S., Y. S. Sheaffer and N. A. Chigier, "Prediction of Far Flow Field in Trailing Vortices," AIAA Paper 72-989, September 1972.

36. Fohl, T., S. Kahalas, A. D. Zalay and R. Zalosh, "Entrainment in Buoyant Releases During Initial Acceleration," Bull. Am. Phys. Soc., Vol. 17, No. 2, November 1972, p. 1081.

37. Tennekes, H., and J. L. Lumley, A First Course in Turbulence, MIT Press, Cambridge, Mass., 1972.

38. Crow, S. C., "The Stability Theory for a Pair of Trailing Vortices," TR-D1-82-0918, Boeing Sci. Res. Lab., Seattle, 1969 (Also AIAA Journal, Vol. 8, No. 12, December 1970, pp. 2172-2179.)

39. Crow, S. C., and E. R. Bate, "Lifespan of Trailing Vortices in a Turbulent Atmosphere," Poseidon Research Report No. 2, December 1974.

40. Barr, N. M., D. Gangaas and D. R. Schaeffer, "Wind Models for Flight Simulator Certifications of Landing and Approach Guidance and Control Systems," FAA-RD-74-206, December 1974.

41. Etkin, Bernard, Dynamics of Atmospheric Flight, Wiley, New York, 1958.

42. Lumley, J. L., and H. A. Panofsky, The Structure of Atmospheric Turbulence, Interscience Publishers, 1964.

43. Munn, R.E., Descriptive Micrometeorology, Academic Press, New York, 1966.

44. Tombach, I.H., "Observations of Atmospheric Effects of Vortex Wake Behavior," J. Aircraft, Vol. 10, No. 11, November 1973.

45. Hoshizaki, H., R. J. Conti, L.B. Anderson, K.O. Redler, J.W. Meyer, W. J. McLean and P.E. Cassady, "Study of High-Altitude Aircraft Wake Dynamics," DOT-TST-90-3, December 1972.

46. Crow, S.C., "Motion of a Vortex Pair in a Stably Stratified Fluid," Poseidon Research Report 1, May 1974.

47. Zalay, A.D., R.P. White and J.C. Balcerak, "Investigation of Viscous Line Vortices with and without the Injection of Core Turbulence," RASA Report 74-01, February 1974.

48. Verstynen, H.A., and R.E. Dunham, Jr., "A Flight Investigation of the Trailing Vortices Generated by a Jumbo Jet Transport," NASA TN D7172, April 1973.

49. Garodz, L.J., D. Lawrence and N. Miller, "The Measurement of the McDonnell-Douglas DC-9 Trailing Vortex System Using the Tower Flyby Technique," FAA-NA-74-28, May 1972.

50. Ciffone, D.L., "Correlation for Estimating Vortex Rotational Velocity Downstream Dependence," J. Aircraft, Vol. 11, No. 11, November 1974, pp. 716-717.

51. Bilanin, A.J., Private communication, July 1975.

52. McGowan, W.A., "Trailing Vortex Hazard," Paper presented 3-5 April 1968, Business Aircraft Meeting, Wichita, Kansas, SAE-680220.

53. Burnham, D.C., "Effect of Ground Wind Shear on Aircraft Trailing Vortices," AIAA J., Vol. 10, August 1972, pp. 1114-1115.

54. Lamb, H., Hydrodynamics, Dover Publications, Dover, N.Y., 1945, p. 221.

55. Widnall, S.A., and D. Bliss, "Slender Body Analysis of the Motion and Stability of a Vortex Filament Containing an Axial Flow," J. Fluid Mech., Vol. 50, Part 2, 1971, pp. 335-353.